Fisheries and Oceans Canada | Pêches et Océans Canada
Ecosystems and Oceans Science | Sciences des écosystèmes et des océans

Canadian Science Advisory Secretariat (CSAS)

Research Document 2023/083

Quebec Region

Results of Comparative Fishing Between the CCGS *Teleost* Fishing the Western IIA Trawl and CCGS *Capt. Jacques Cartier* Fishing the NEST Trawl in the Southern Gulf of St. Lawrence in 2021 and 2022

Hugues P. Benoît[1] and Yihao Yin[2]

[1]Fisheries and Oceans Canada
Maurice Lamontagne Institute
Mont Joli, QC G5H 3Z4

[2] Fisheries and Oceans Canada
Bedford Institute of Oceanography
Dartmouth, NS B2Y 4A2

December 2023

Foreword

This series documents the scientific basis for the evaluation of aquatic resources and ecosystems in Canada. As such, it addresses the issues of the day in the time frames required and the documents it contains are not intended as definitive statements on the subjects addressed but rather as progress reports on ongoing investigations.

Published by:

Fisheries and Oceans Canada
Canadian Science Advisory Secretariat
200 Kent Street
Ottawa ON K1A 0E6

http://www.dfo-mpo.gc.ca/csas-sccs/
csas-sccs@dfo-mpo.gc.ca

ISSN 1919-5044
ISBN 978-0-660-68850-3 Cat. No. Fs70-5/2023-083E-PDF

Correct citation for this publication:

Benoît, H.P., and Yin, Y. 2023. Results of Comparative Fishing Between the CCGS *Teleost* Fishing the Western IIA Trawl and CCGS *Capt. Jacques Cartier* Fishing the NEST Trawl in the Southern Gulf of St. Lawrence in 2021 and 2022. DFO Can. Sci. Advis. Sec. Res. Doc. 2023/083. xiii + 183 p.

Aussi disponible en français :

Benoît, H.P., et Yin, Y. 2023. Résultats des pêches comparatives entre le NGCC Teleost *pêchant le chalut Western IIA et le NGCC* Capt. Jacques Cartier *pêchant le chalut NEST dans le sud du golfe du Saint-Laurent en 2021 et 2022. Secr. can. des avis sci. du MPO. Doc. de rech. 2023/083. xiv + 187 p.*

TABLE OF CONTENTS

LIST OF TABLES

LIST OF FIGURES

ABSTRACT

Bottom-trawl surveys provide key inputs to stock assessments for groundfish stocks and other taxa, for ecosystem monitoring and reporting, and for research. These surveys can produce annual indices of abundance that are proportional to stock size, provided that the proportionality constant, typically called catchability, does not change over time. This is typically achieved through the use of standardized survey design and procedures. Periodically it becomes necessary or desirable to change one or more aspects of the protocol, and calibration experiments are typically required to estimate adjustments for possible changes in catchability. From 2004 to 2022, the CCGS *Teleost* fishing a Western IIA bottom-trawl was used for the annual survey of the southern Gulf of St. Lawrence (sGSL). This vessel will soon be retired and is being replaced by the CCGS *Capt. Jacques Cartier*, fishing a different trawl. Paired-trawl comparative fishing experiments involving these two vessels and gear pairs were conducted in September in 2021 and 2022 to obtain data for catch required to estimate their relative fishing efficiency for a large number of fish and invertebrate taxa that are routinely sampled in this survey. In this document we briefly describe these comparative fishing experiments and report on analyses of the resulting data for 116 fish and invertebrate taxa routinely sampled by the sGSL survey. The analyses employed a suite of contemporary statistical models used previously in extended comparative fishing analyses in the eastern United States and which were recently extensively tested using simulations. Relative catchability as a function of individual lengths (fish, lobster and squid) or carapace width (crabs) was evaluated and estimated for 38 taxa, whereas size-aggregated estimates were derived for the others. Given considerable differences between the old and replacement survey protocols, which include a substantial change in the fishing gear and tow length, important differences in length-dependent and independent relative catchability were expected for this comparative fishing experiment and were estimated for a number of taxa. Recommendations for the application of the conversion factors are provided. Use of these conversion factors will maintain the integrity of the over five decade long time series for various southern Gulf marine taxa.

1. INTRODUCTION

Worldwide, bottom-trawl surveys provide key inputs to stock assessments for groundfish stocks and other taxa, for ecosystem monitoring and reporting, and for research. These surveys can produce annual indices of abundance that are proportional to stock size, provided that the proportionality constant, typically called catchability, does not change over time. Failure to achieve this consistency via proper sampling design and standardization increases the risk of confounding changes in abundance with changes in catchability. Maintaining consistency in survey protocols, and the survey vessel and gear (hereafter, simply the protocol) is key to maintaining a constant catchability. However, periodically it becomes necessary or desirable to change one or more aspects of the protocol, and calibration experiments are typically required to estimate adjustments for possible changes in catchability. The most common and effective form of these experiments is comparative fishing, which usually involves paired trawling of vessels constituting the former and replacement protocol as close together as safety permits. This design minimizes the difference in fish densities sampled by the trawls, such that differences in catches over replicates of paired-trawl sampling will reflect the difference in catchability.

Fisheries and Oceans Canada (DFO) is undertaking comparative fishing in each of its six Atlantic bottom-trawl surveys from 2021 to 2023 to calibrate two new offshore fisheries survey vessels that will replace two retiring longstanding vessels. In some surveys, the change in vessel will also be accompanied by a change in survey trawl and survey procedures (e.g., tow duration), and the joint effect of all of these factors on relative catchability should be reflected in results of the comparative fishing experiments. In the survey of the southern Gulf of St. Lawrence (sGSL), which has taken place annually in September since 1971, the CCGS Capt. Jacques Cartier (63.4 m; 2 975 t gross tonnage) will replace the CCGS Teleost (63 m; 2 405 gross tonnage), which has been used to conduct the survey since 2004. During the sGSL survey, the CCGS Teleost has fished the Western IIA trawl (Hurlbut and Clay 1990), while the CCGS Capt. Jacques Cartier will be using the a slightly modified version of the Northeast Fisheries Science Center Ecosystem Survey Trawl, NEST (trawl details in Denton 2020; modifications outlined in Ricard et al. 2023). A standard tow aboard the CCGS Capt. Jacques Cartier is fished at 3.0 knots for 20 min, in contrast to a standard CCGS Teleost tow of 3.5 knots for 30 min. In addition, tow duration aboard the CCGS Capt. Jacques Cartier is measured from trawl touch-down to lift off, whereas aboard the Teleost it is measured from the time the winches stop deploying warp, to when haul-back is initiated (Ricard et al. 2023). Comparative fishing between the two vessels, with their respective trawls, took place during the regular survey of the sGSL in 2021, and in 2022. The design employed, sometimes termed a shadow survey design (Thiess et al. 2018), involved paired trawling at sites selected as part of the routine stratified random design for the survey (Fig. 1). Such a design best ensures that comparative fishing results will reflect the environmental conditions of the survey area, principally depths and bottom substrate, which can affect catchability. It also ensures that data will be available to estimate relative catchability adjustment factors for as many as possible of the taxa that are sampled by the survey and for which standardization is required for ongoing research and reporting.

In this document we briefly describe the 2021-2022 comparative fishing experiments for the sGSL (see Ricard et al. 2023 for a more detailed description) and report on analyses of the resulting data for 116 fish and invertebrate taxa routinely sampled by the sGSL survey. The analyses employed contemporary statistical models used previously in extended comparative fishing analyses in the eastern United States (Miller et al. 2010; Miller 2013), and applied recently to analyses of past comparative fishing data for some stocks in the Gulf of St. Lawrence (Yin and Benoît 2022a; Benoît et al. 2022). These models were extensively tested in a simulation context and were confirmed appropriate for analyses such as those employed in the present case (Yin and Benoît 2022b). As part of the analyses, estimates of relative catchability as a function of individual lengths (fish, lobster and squid) or carapace width (crabs) were derived for 38 taxa, whereas size-aggregated estimates were derived for the others. Given considerable differences between the old and replacement survey protocols, which include a substantial change in the fishing gear and tow length, important differences in length-dependent and independent relative catchability were expected for this comparative fishing experiment.

2. METHODS

2.1. COMPARATIVE FISHING

Comparative fishing between the CCGS Teleost and the CCGS Capt. Jacques Cartier took place between August 31 and September 26 in 2021, and between September 17 and 30 in 2022 (Table 1). The initiation of comparative fishing in 2022 was delayed to allow completion of comparative fishing experiments in the survey of the Estuary and northern Gulf of St. Lawrence, which also involved the CCGS Teleost. A total of 127 and 53 paired sets considered as valid comparative pairs were completed in 2021 and 2022 respectively and retained for analysis. Of the set pairs from 2022, the catch for hauls 53 and 54 was accidentally physically combined prior to catch sorting aboard the CCGS Capt. Jacques Cartier (Ricard et al. 2023). These data were included in subsequent analyses by matching them to the combined data for the same hauls for the CCGS Teleost, and assuming a trawl swept area for each vessel that was the sum of swept areas for the individual hauls.

Details of the comparative fishing experiments are presented in Ricard et al. (2023) and are therefore only briefly summarized here. At pre-selected stations, the CCGS Capt. Jacques Cartier and the CCGS Teleost fished as close together in space and in time as was safe and practical. The majority of paired sets were done side-by-side along parallel tracks. Across stations, the vessels alternated between having the other vessel on their port or starboard side. Efforts were made to ensure similar depths between the two locations fished at a station. The distance separating the vessels was typically no more than 0.5 nautical miles. In some instance in which the difference in depths between potential parallel tracks was too great (> 10 m), the vessels fished along the same track, separated by 1.5 miles.

The CCGS Teleost fished standard tows targeting a tow time of 30 minutes at 3.5 knots, while the CCGS Capt. Jacques Cartier fished standard tows of 20 minutes at 3.0 knots. Tow durations of at least 2/3 the target time were considered acceptable. Both vessels employed an auto-trawl system using Scanmar sensors in which trawl geometry is dynamically adjusted during the tow to keep the trawl square to the trawl path. The data from the Scanmar sensors were additionally used to monitor trawl performance and to potentially invalidate a tow, but were not used to calculate the swept area of each tow for use in the data analyses. Instead, tow distance was used as the sole standardizing factor for swept area.

Standard procedure in the sGSL survey is to obtain a total catch weight for each taxon in each haul. Additionally, a representative length frequency is obtained in each survey haul for all fish taxa, all crab taxa excluding hermit crabs, and for lobster and squid. Catch counts are also produced for each measured taxon.

Further details on the comparative fishing experiments are available in Ricard et al. (2023).

2.2. COMPARATIVE FISHING DATA ANALYSIS

2.2.1. Binomial models

In the analysis of comparative fishing data, the goal is to estimate the relative fishing efficiency between a pair of vessel-gear combinations (referred to as vessel in this section for simplicity). We assume the expected catch from vessel v ($v \in \{A, B\}$) at length l and at station i is

$$E[C_{vi}(l)] = q_{vi}(l)D_{vi}(l)f_{vi}$$

where, $q_{vi}(l)$ is the catchability of vessel v, D_{vi} is the underlying population density sampled by vessel v, and f_{vi} is a standardization term which usually includes the swept area of a tow, and if applicable, the proportion of sub-sampling for size measurement on-board. In a binomial model (e.g., Miller 2013), the catch from vessel A at station i, conditioning on the combined catch from both vessels at this station, $C_i(l) = C_{Ai}(l) + C_{Bi}(l)$, is binomial-distributed

$$C_{Ai}(l) \sim BI(C_i(l), p_{Ai}(l))$$

where $p_{Ai}(l)$ is the expected proportion of catch from vessel A. Tows in a pair are generally assumed to fish the same underlying densities at the station, as the paired vessels typically fish within a small distance of each other: $D_{Ai}(l) = D_{Bi}(l) = D_i(l)$. Then the logit-probability of catch by vessel A is

$$logit(p_{Ai}(l)) = log(\frac{E[C_{Ai}(l)]}{E[C_{Bi}(l)]}) = log(\rho_i(l)) + o_i$$

Where $\rho_i(l)$ is the ratio of catchabilities between vessels A and B at length l and at station i, or the conversion factor, the quantity of interest,

$$\rho_i(l) = q_{Ai}(l)/q_{Bi}(l)$$

and $o_i = log(f_{Ai}/f_{Bi})$ is an offset term derived from known standardization terms for tow length relative to the standard tow lengths and for subsampling..

For a length-based conversion factor, we consider a smooth length effect based on a general additive smooth function,

$$log(\rho(l)) = \sum_{k=0}^{K} \beta_k X_k(l) = \mathbf{X}^T\boldsymbol{\beta},$$

where $\boldsymbol{\beta}$ are the coefficient parameters and are estimated, $\mathbf{X}$, or $\{X_k(l), k = 0,1, \cdots, K\}$, are a set of smoothing basis functions, and K is the dimension of the basis that controls the number of coefficient parameters and is usually pre-defined. Here a cubic spline smoother was used (Hastie et al. 2009), with the basis functions and penalty matrices generated by the R package mgcv for R (Wood 2011; R core team 2021).

The estimation of a cubic spline smoother is based on the penalized sum of squares smoothing objective, but in practice, this is usually replaced by a penalized likelihood objective (Green and Silverman 1993):

$$\mathcal{L}(\boldsymbol{\beta}, \lambda) = f(\mathbf{Y}|\mathbf{X}, \boldsymbol{\beta})e^{-\frac{\lambda}{2}\boldsymbol{\beta}^T\mathbf{S}\boldsymbol{\beta}}$$

$\mathcal{L}$ denotes the likelihood objective function. $f(\mathbf{Y}|\mathbf{X}, \boldsymbol{\beta})$ is the joint probability function of the survey data $\mathbf{Y}$ conditional on the basis functions and coefficient parameters. $\mathbf{S}$ is the penalty matrix defined by the smoother and the dimension of the basis, and λ is the smoothness parameter. This smoothness parameter is estimated by maximum likelihood along with other model parameters but may be sensitive to the data. In such cases, it can be determined by other criteria such as generalized cross-validation (Wood 2000).

The penalized maximum likelihood smoother can also be re-parameterized into a mixed effects model (Verbyla et al. 1999; Wood 2017) to facilitate implementation as well as incorporation of additional random effects:

$$log(\rho_i(l)) = \mathbf{X}_f^T \boldsymbol{\beta}_f + \mathbf{X}_r^T \mathbf{b}$$

where $\boldsymbol{\beta}_f$ are fixed effects and $\mathbf{b}$ are random effects. $\mathbf{X}_f$ and $\mathbf{X}_r$ are transformed from the basis functions $\mathbf{X}$ and an eigen-decomposition of the penalty matrix $\mathbf{S}$, $\mathbf{X}_f = \mathbf{U}_f^T \mathbf{X}$ and $\mathbf{X}_r = \mathbf{U}_r^T \mathbf{X}$, where $\mathbf{U}_f$ and $\mathbf{U}_r$ are the eigenvectors that correspond to the zero and positive eigenvalues of $\mathbf{S}$. The random effects $b \sim \mathrm{N}(0, \mathbf{D}_+^{-\mathbf{1}}/\boldsymbol{\lambda})$ where D_+ is the diagonal matrix of the positive eigenvalues of S. In the mixed effects model representation of the cubic spline smoother, the number of fixed effects is 2 and the number of random effects is bounded by $K-2$. Smoothing effects are transformed into shrinkage of random effects in the fitting of random deviations, and can be integrated into complex mixed effects models commonly used in fisheries science (Thorson and Minto 2015).

Additional random effects can be incorporated into the mixed effects model to address variations in the relative catch efficiency related to each station,

$$log(\rho_i(l)) = \mathbf{X}_f^T(\boldsymbol{\beta}_f + \boldsymbol{\delta}_i) + \mathbf{X}_r^T(\mathbf{b} + \boldsymbol{\epsilon}_i).$$

where $\boldsymbol{\delta}_i \sim \mathrm{N}(\mathbf{0}, \boldsymbol{\Sigma})$ and $\boldsymbol{\epsilon}_i \sim \mathrm{N}(\mathbf{0}, \mathbf{D}_+^{-1}/\xi)$. From a similar re-parameterization of the cubic spline smoother, these random effects allow for deviations of the length-based conversion at each station. $\boldsymbol{\Sigma}$ is the covariance matrix of the random effects corresponding to the random deviations and contains three parameters. ξ controls the degree of smoothness of the random smoothers and the smoother at each station can differ.

A summary of the above binomial mixed model is as follows,

$$C_i(l) = C_{Ai}(l) + C_{Bi}(l)$$

$$C_{Ai}(l) \sim BI(C_i(l), p_{Ai}(l))$$

$$logit(p_{Ai}(l)) = log(\rho_i(l)) + o_i$$

$$log(\rho_i(l)) = \mathbf{X}_f^T(\boldsymbol{\beta}_f + \boldsymbol{\delta}_i) + \mathbf{X}_r^T(\mathbf{b} + \boldsymbol{\epsilon}_i)$$

The model is estimated via maximum likelihood and the marginal likelihood integrating out random effects is

$$\mathcal{L}(\boldsymbol{\beta}_f, \boldsymbol{\Sigma}, \lambda, \xi) = \int \left(\prod_{i=1}^{m} \int \int f(\mathbf{Y}_i | \mathbf{X}_f, \mathbf{X}_r, \boldsymbol{\beta}_f, \mathbf{b}, \boldsymbol{\delta}_i, \boldsymbol{\epsilon}_i) f(\boldsymbol{\delta}_i | \boldsymbol{\Sigma}) f(\boldsymbol{\epsilon}_i | \xi) \mathrm{d}\boldsymbol{\delta}_i \mathrm{d}\boldsymbol{\epsilon}_i \right) f(\mathbf{b} | \lambda) \mathrm{d}\mathbf{b}$$

The binomial mixed model can be adapted for various assumptions on the smoother and potential station variation to accommodate different underlying density of a species and data limitations especially in length measurements. A set of binomial models considered in the present analyses is provided in Table 2.

2.2.2. Beta-binomial models

The binomial assumption of the catch can be extended to a beta-binomial distribution to account for over-dispersion at the stations (Miller 2013):

$$C_{A,i}(l) \sim BB(C_i(l), p_{A,i}(l), \phi_i(l)).$$

The beta-binomial distribution is a compound of the binomial distribution and a prior beta distribution. More specifically, it assumes a beta-distributed random effect in the expected proportion of catch from vessel A across stations. As a result, the expected catch by vessel A has a variance of

$$var(C_{A,i}) = C_i p_i (1 - p_i) \frac{\phi_i + C_i}{\phi_i + 1}$$

where ϕ is the over-dispersion parameter that captures the extra-binomial variation.

The same smoothing length effect can be applied to the over-dispersion parameter,

$$log(\phi_i(l)) = \mathbf{X}_f^T \boldsymbol{\gamma} + \mathbf{X}_r^T \mathbf{g}$$

where $\boldsymbol{\gamma}$ are fixed effects and $\mathbf{g}$ are random effects, $\mathbf{g} \sim \mathrm{N}(0, \mathbf{D}_+^{-1}/\tau)$. This length effect models the variance heterogeneity and is particularly useful for projecting uncertainty to poorly sampled lengths. However, estimation of a length-based variance parameter typically requires sufficient catch at length data, which is usually not available for less abundant species.

A summary of the beta-binomial mixed model is as follows,

$$C_i(l) = C_{Ai}(l) + C_{Bi}(l)$$

$$C_{Ai}(l) \sim BB(C_i(l), p_{Ai}(l), \phi_i(l))$$

$$logit(p_{Ai}(l)) = log(\rho_i(l)) + o_i$$

$$log(\rho_i(l)) = \mathbf{X}_f^T(\boldsymbol{\beta}_f + \boldsymbol{\delta}_i) + \mathbf{X}_r^T(\mathbf{b} + \boldsymbol{\epsilon}_i)$$

$$log(\phi_i(l)) = \mathbf{X}_f^T \boldsymbol{\gamma} + \mathbf{X}_r^T \mathbf{g}$$

The marginal likelihood is

$$\mathcal{L}(\boldsymbol{\beta}_f, \boldsymbol{\gamma}, \boldsymbol{\Sigma}, \lambda, \xi, \tau)$$

$$= \int \int \left(\prod_{i=1}^{m} \int \int f(\mathbf{Y}_i | \mathbf{X}_f, \mathbf{X}_r, \boldsymbol{\beta}_f, \mathbf{b}, \boldsymbol{\gamma}, \mathbf{g}, \boldsymbol{\delta}_i, \boldsymbol{\epsilon}_i) f(\boldsymbol{\delta}_i | \boldsymbol{\Sigma}) f(\boldsymbol{\epsilon}_i | \xi) \mathrm{d}\boldsymbol{\delta}_i \mathrm{d}\boldsymbol{\epsilon}_i \right) f(\mathbf{b}|\lambda) f(\mathbf{g}|\tau) \mathrm{d}\mathbf{b} \mathrm{d}\mathbf{g}$$

Likewise, various smoothing assumptions can be applied to the variance parameter. Table 3 presents a set of beta-binomial mixed models.

2.2.3. Tweedie model for biomass data

The binomial and beta-binomial models are appropriate for data constituted of catch counts, but are not appropriate for catch weight or biomass. Biomass indices are routinely derived from survey data for population trend monitoring. For taxa that are measured, biomass values adjusted for the change in relative catchability are most reliably derived by applying the results of the analyses described above to length specific catch numbers and employing a length-weight conversion. However, individual measurements are not made for numerous invertebrate taxa, and were not made for some years or some specific survey hauls for many of the remaining taxa. Estimates of relative catchabilities were therefore required for size-aggregated catch weights for all taxa.

The analysis of catch weights required a probability distribution with a mass at zero, but that is otherwise continuous and can accommodate some overdispersion in catch weights. Unlike the models for catch counts, it was not possible to condition model estimates on the total catch. We employed the following model, which assumed that catch weights were a Tweedie (TW) distributed random variable:

$$W_{i,v} \sim TW(\mu_{i,v}, \varphi, \tau)$$
$$E[W_{i,v}] = \mu_{i,v} = \exp(v + S_i + o_{i,v})$$
$$Var[W_{i,v}] = \varphi(\mu_{i,v})^{\tau}$$

where $W_{i,v}$ is the catch weight at station *i* by vessel *v*, $\mu_{i,v}$ is the expected catch weight at station *i* for vessel *v*, φ is the dispersion parameter of the Tweedie distribution, τ is a power parameter, restricted to the interval 1< τ <2 (Dunn and Smyth 2005), *v* is the fixed vessel effect, where *exp*(*v*) = ρ, S_i is a fixed effect that accounts for the biomass at station *i*, and $o_{i,v}$ is the offset. Unlike the model for catch numbers in which the offset term was the log of the ratio of sampling efforts (tow distance and catch sampling fraction), the offset term in the Tweedie model is the log of sampling effort at station *i* for vessel *v*, relative to the standard effort for that vessel.

A version of the model in which the station effect was treated as a random effect of the following form was initially investigated:

$$E[W_{i,v}] = \mu_{i,v} = \exp(v + \delta_i + o_{i,v})$$
$$\delta_i \sim N(0, \sigma^2)$$

However, the assumed normal distribution for the random effect in the linear predictor was found to be inappropriate in the application to the data.

2.2.4. Model fitting, selection and validation

The binomial and beta-binomial models in Tables 2 and 3 for analyses of length-disaggregated catches were implemented using the Template Model Builder (TMB) package for R (Kristensen et al. 2016). TMB uses the Laplace approximation to integrate the joint negative loglikelihood (nll) over the random effects to calculate the marginal nll (mnll). Optimization of the mnll is then undertaken in R using the *nlminb()* function. The basis functions for the cubic smoothing spline and the corresponding penalty matrices were generated using the R package mgcv (Wood 2011) based on 10 equally-spaced knots ($K = 9$) within the pre-specified length range depending on the range of lengths observed proper to each taxon. TMB automatically calculates a standard error for the maximum likelihood estimation of the conversion factor via the delta method (Kristensen et al. 2016).

Analyses were also undertaken for length-aggregated catch numbers, for those taxa or instances where length-aggregated conversion factors are required. Contrary to the analyses described above that treat the catch of a taxon at a station and in a length class as the basic datum, these length-aggregated analyses modelled the total catch numbers at each station. For simplicity, these analyses were implemented using the glmmTMB function from the homonymous R package (Brooks et al. 2017). Models BI0, BI1, BB0 and BB1 (Tables 2 and 3) were fitted by specifying family=binomial(link = "logit") or family=betabinomial(link = "logit"), as appropriate, maintaining the same assumptions as the length-disaggregated models. Note that conversion factor estimates for these four models obtained from the length-aggregated analyses are likely to differ from those obtained from the length-disaggregated analyses when there is strong underlying length-dependency in relative catchability between the two vessels. Furthermore, because sample sizes are greater in the length-disaggregated analyses, standard errors on the conversion factors are generally expected to be smaller.

The analyses of catch weights were also implemented using the glmmTMB function. The option family = tweedie was specified.

Length-disaggregated models were fitted only for taxa for which there were data for at least 25 relevant set pairs (pairs with catch by at least one vessel). Size-aggregated model were only fitted for taxa for which there were data for at least 15 relevant set pairs. While these thresholds are somewhat arbitrary, they are reasonable in light of the complexity of the models (number of fixed and random parameters estimated) and are consistent with minimum requirements evident from the simulation study of Yin and Benoît (2022b).

There were in total 13 candidate models of length-disaggregated catches for estimating the conversion factors, although convergence could not be attained for any of the taxa for the most complex model, BB7. There were four candidate models for length-aggregated catch numbers. The best model for each set of analyses was selected by BIC (Bayesian information criterion) to maximize model fitting, while avoiding over-fitting of more complicated models, especially in cases without adequate data. We also examined values for Akaike information criterion (AIC), which tends to select slightly more complex models compared to BIC (Hastie et al. 2009), but which in the present applications, largely supported decisions based on BIC.

In each length-disaggregated analysis, the estimated μ function (length-dependent expected proportion of catch by vessel A) from all converged models were compared along with the sample proportions (aggregated by stations and averaged for each length) to provide a more rigorous interpretation of the results. The estimated $\rho(l)$ (expected relative catch efficiency, or conversion factor function) and associated approximate 95% confidence interval from the best model is then shown over the range of lengths contained in the input data. Normalized quantile model residuals (Dunn and Smyth 1996) were produced and plotted using boxplots against length and survey station to visually assess the adequacy of model fit. Given the potentially large number of stations for some species, which would otherwise generate a crowded boxplot, we plotted only the residuals for the first 60 tows to provide an indication of possible lack of fit. Finally, we plotted model residuals against depth and the time at which a station was fished, two factors known to affect catchability (e.g., Benoît and Swain 2003), to evaluate whether these effects might interact with the vessel effect under study. To flag possible cases where these effects may have been influential we also fit the following gaussian models (presented using pseudo equations) to the normalized quantile model residuals (NQR):

1. NQR ~ s(depth) + (1|station)
2. NQR ~ s(time) + (1|station)
3. NQR ~ factor(day) + (1|station)

where s(*x*) denotes a smooth function of variable *x*, (1|station) denotes a random effect for the station and factor(day) is a factor delineating day and night, where day = 7:00 < time ≤ 19:00, consistent with Benoît and Swain (2003). Both smoothed and discrete effects of time were considered to flag cases of a possible diel effect on relative catchability (e.g., Benoît and Swain 2003). We examined the p-values associated with the effects of depth, time and day, and further investigated the residuals patterns in cases with $p < 0.01$.

The fit of catch-aggregated analyses for counts and weights was assessed by plotting the conversion factor and associated approximate 95% confidence interval in biplots of the catch of one vessel over the other. Additionally, we examined the scaled quantile residuals obtained using the R package DHARMa (Hartig 2021). Unlike the normalized quantile residuals used in the length-disaggregated analyses above, which have an expected Gaussian distribution when model fit is adequate, the quantile residuals from DHARMa have an expected uniform distribution. The choice was dictated in part by the fact that it was easier to examine residuals using boxplots in the former case, which has more residual values. Residuals for the catch-aggregated analyses were examined for uniformity and possible overdispersion, and plotted as a function of the fitted values, station depth and time. The evaluation of residuals was in size-aggregated analyses was limited to a visual inspection.

2.2.5. Data treatment prior to analysis

Data for some taxa were grouped prior to analysis due to perceived inconsistencies in identification during the surveys or due to small sample sizes amongst related and morphologically similar taxa. *Gadus sp*. (code 251) individuals ≤ 20 cm are processed separately during catch sampling because of difficulties in distinguishing *G. morhua* and *G. ogac* at these sizes in the field. Normally samples are brought back to the laboratory for identification; however, such lab-based identification was not available in time for the comparative fishing data analyses. Given the relative prevalence of Atlantic cod in the ecosystem, the fact that confirmed catches of *G. ogac* were not sufficiently frequent to include in any of the analyses, and the assumption that the catchability of small *Gadus sp*. should be the same as that of same-sized individuals of the specific species, we combined these data with the catches for *G. morhua*. This and the other taxonomic groupings are outlined in Table 4.

In a very small number of instances, the catch of one or two individuals at the very smallest or very largest lengths had undue influence on the shape of the length-dependent conversion factor function at and around those lengths. This results from the flexibility inherent in the cubic spline functions and is a known problem for these models (Cadigan et al. 2022). Although Cadigan et al. (2022) present an alternative and likely more robust approach, it is only applicable to monotonic length-dependent relative catchability functions and was not appropriate for the results of the sGSL comparative fishing where more complex, non-monotonic, functions were prevalent. Instead we excluded the catches for these extreme lengths from the analysis. These cases are summarized in Table 5.

2.2.6. Interpretation of analysis results and application of conversion factors

Two general patterns observed in the model selection and model results motivated the adoption of additional screening criteria in determining whether a conversion factor (function) should be applied, and which should be chosen for application in future analyses of the survey data. First, there were four taxa for which the 95% confidence intervals for a length-dependent conversion factor function overlapped with a value of one across all lengths, indicating no significant statistical difference with the case of equivalent vessel catchability, despite a length-dependent model being selected. This likely resulted from the use of marginal AIC and BIC values, for which the effective number of parameters may not be correctly calculated for the model random effects, causing more complex models with smoothed length effects to be favoured. We therefore recommend not adopting conversion factor functions for which the confidence interval overlaps unity over the range of length. In these cases, we examined the results for non-length dependent analyses but found that these were typically not statistically significant either.

As noted above, the estimation of length-specific conversion factor functions can be sensitive to the sparseness of data in the tails of the length frequencies. Despite eliminating some extreme lengths, there were still cases were conversion factor values diverged considerably from the overall length-dependent trend as lengths tended toward the smallest and largest lengths. We therefore adopted the following procedure. We first identified the lengths that constituted the 0.5^{th} and 99.5^{th} percentiles of the taxon-specific total length frequency distribution for the 2021-2022 experiment for taxa with at least 20 length classes, and used the 2.5^{th} and 97.5^{th} percentiles for taxa with fewer classes. We then identified the conversions factor function values at these percentiles for each taxon, and assumed these values as constants for lengths below and above these percentiles, respectively. These constant values were projected respectively to the taxon-specific smallest and largest lengths observed since 1971 in the survey.

3. RESULTS

The results of the various analyses for the numerous taxa covered in this report are simply too voluminous to interpret in detail. Instead we aimed to provide detailed figures and tables that describe the results and support decisions for the application of conversion factors, and provide some interpretation of results only for key harvested species and species of conservation concern. These species are ones for which reporting on survey results is likely to be most consequential and frequent, and therefore where the need for careful examination and interpretation of comparative fishing results is arguably greatest. We begin by explaining the structure for the presentation of results, and then address results for these specific species, as well as other cases involving notable results.

3.1. PRESENTATION OF RESULTS

The following tables and figures provide taxon-specific results.

Table 6 provides the total number of relevant set pairs (i.e., pairs in which the taxon was caught by at least one of the two vessels), the number of pairs for which only the CCGS Capt. Jacques Cartier caught the taxon, and the number of pairs for which only the CCGS Teleost caught the taxon. Notably, the table provides a reference to the number for the figure(s) in which the results are presented for that taxon. Taxa for which length-disaggregated analyses were supported are presented first, followed by those for which size-aggregated analyses were employed.

Table 7 provides details of the model evidence and selection (ΔAIC and ΔBIC values) for the length-disaggregated analyses.

Table 8 presents the p-values for the smooth effect of depth, the smooth effect of time and the fixed effect of day on the normalized quantile residuals from the best length-disaggregated model. Values < 0.01 are indicated in bold.

Table 9 provides details of the model evidence and selection (AIC and BIC values) for the length-aggregated analyses of catch numbers, and the estimated conversion factors (rho) and 95% confidence intervals for the analyses of catch numbers and of catch weights for taxa that were otherwise also considered in length-disaggregated analyses.

Table 10 provides the same types of results as Table 9, but for those taxa that were not considered in length-disaggregated analyses, either because representative length sampling was not undertaken or because the total number of relevant set pairs was $15 \le n < 25$.

Plots for the results of the length-disaggregated analyses are presented in multiple panels across three pages for each taxon. Figs. 3-5 provide an explanation of the content of each page. Briefly, the first page (labelled a.) provides a summary of the data from a spatial, size-aggregated and length-specific perspective (details in Fig. 3). Results for the size-aggregated analyses are plotted in one of the panels in an effort to reduce the total number of figures contained in this report. The second page (labelled b.) provides a plot of the fit of all converged models and a plot of the selected conversion factor function and 95% confidence interval, along with the projected constant values we propose for the smallest and largest lengths (details in Fig. 4). Finally, the third page (labelled c.) provides various boxplots for the normalized quantile residual values for the selected model (details in Fig. 5).

Plots for the results of the length-aggregated analyses, including the fitted model and model quantile residuals, are presented on a single page for each taxon for the analyses of catch counts (left column) and catch weights (right column) for measured taxa, and catch weights only (single column) for taxa that aren't measured (details in Fig. 6). Figures are presented only for taxa that were not subjected to length-disaggregated analyses to reduce the total number of figures in this report. Nonetheless, fits of the selected length-aggregated model for catch for the remaining taxa are presented in the plots for length-disaggregated analyses and the estimated conversion factor values are in Table 9. Detailed residual plots were created and examined even though they are not formally presented here.

3.2. SOME SPECIFIC RESULTS

3.2.1. Atlantic cod (*Gadus morhua*)

With the exception of the very smallest sizes (< 8 cm) and larger sizes (> 45 cm), standardized catches by the CCGS Capt. Jacques Cartier were consistently larger than those by the CCGS Teleost (Fig. 7a). Model BB5 provided the best fit to the data and predicted an asymmetric concave relative catch efficiency function that declined steeply for sizes up to about 10 cm, reaching levels below 0.2, before rising more or less continually to a level consistent with equivalent catchability around 50 cm (Fig. 7b). The plots of normalized quantile residuals indicate that the model fit was adequate (Fig. 7c).

3.2.2. White hake (*Urophycis tenuis*)

White hake were mainly captured in the eastern Northumberland Strait and off northern Cape Breton, and to a lesser extent along the Laurentian channel (Fig. 8a). Standardized catches by the CCGS Capt. Jacques Cartier were greater in almost all instances. While model BB1 was selected by BIC, models BB4 and BB5 were favored by AIC. The latter two models estimate a nearly identical catchability function (Fig. 8b), which also corresponds roughly with the function estimated for cod (Fig. 7b), a related species for which a similar relative catchability might be expected and for which there were considerably more observations with which to produce estimates. Given these results and the fact that BB4 was the second most likely model according to BIC, with a delta value suggesting the model is not implausible, we recommend using the estimate from that model. Specifically, BB4 predicted a slight curvilinear relative catchability function that fluctuated around a value of around 0.6 across most lengths, but with higher values at small lengths (Fig. 8b). Model fit appeared to be adequate (Fig. 8c).

3.2.3. Redfish (*Sebastes sp.*)

Overall standardized catches of redfish were largely similar between vessels and were characterized by a strong mode in the catches that peaked at 24 to 25 cm (Fig. 9a). Redfish at sizes below the mode were more prevalent in standardized catches by the CCGS Capt. Jacques Cartier, and those above the mode in catches by the CCGS Teleost. Model BB4 was selected and predicted a sigmoidal monotonically increasing relative catch efficiency function for which equal efficiency (a value of 1) was predicted at 30 cm, with increasingly large confidence intervals thereafter (Fig. 9b). Model fit appeared to be adequate (Fig. 9c).

3.2.4. Atlantic halibut (*Hippoglossus hippoglossus*)

Atlantic halibut were captured infrequently and only in small numbers during the comparative fishing experiments (Fig. 10a). Length-aggregated analyses resulted in no significant difference in relative efficiency between the two vessel, and confidence intervals for the length-disaggregated analyses were very close to a value of 1 (Fig. 10b; Table 9). Jointly these results do not provide a compelling case for a significant difference in catchability between vessels.

3.2.5. Greenland halibut (*Reinhardtius hippoglossoides*)

Standardized catches of Greenland halibut were generally similar between the two vessels (Fig. 11a). There was a tendency for the CCGS Teleost to catch more of this species at lengths around 40 cm. There was similar support for all BI models based on BIC (Table 7), while the only beta-binomial model to converged was BB0. Length-independent models suggest no significant difference between vessels (e.g., BI0, Fig. 11b). While the residuals for BI0 indicate a lack of fit at length ≥ 42 cm (Fig. 11c), there were few individuals caught at these sizes in the experiments (Fig. 11a). Application of a conversion factor is not recommended for this species.

3.2.6. American plaice (*Hippoglossoides platessoides*)

American plaice were captured frequently and broadly in the experiments (Fig. 12a). Standardized catches by the CCGS Capt. Jacques Cartier were consistently larger overall. However, the CCGS Teleost was much more efficient at catching very small plaice (< 5 cm) and the vessels were about equivalent at catching large place > 32 cm. Model BB5 was select and seemed to fit the data well (Figs. 11b,c). The model predicted that the CCGS Teleost was about 10 times more efficient at catching very small plaice, but that relative efficiency dropped rapidly with increasing length to a low at about 10 cm, increasing gradually subsequently to reach a level close to equivalent catchability around 32-35 cm. The relative efficiency above 40 cm was associated with considerable uncertainty and a constant value is recommended for these sizes in future applications.

There was a significant difference in residuals according to the diel period (Table 8), but the distribution of residuals as a function of hour indicates that the effect size is very small and likely inconsequential (Fig. 12c).

3.2.7. Witch flounder (*Glyptocephalus cynoglossus*)

Standardized catches of witch flounder, and the associated length frequencies were similar between vessels (Fig. 13a.). The length-aggregated analysis of catch numbers and catch weights concluded that the CCGS Capt. Jacques Cartier was more efficient (Table 9; see also the blue line and shaded area in the biplot in Fig. 13a). A similar result was obtained in the length-disaggregated analysis (model BB1) although the effect was just marginally different from equal catchability (Fig. 13b).

3.2.8. Yellowtail flounder (*Limanda ferruginea*)

Standardized catches of Yellowtail flounder were generally greater for the CCGS Capt. Jacques Cartier, particularly for sizes < 25 cm (Fig. 14a). Model BB4 was selected and appeared to provide an adequate fit to the data (Figs. 14b,c). The CCGS Capt. Jacques Cartier was relatively most efficient at catching yellowtail flounder < 10 cm, and the relative efficiency of the two vessels became increasingly more similar as length increased to about 20 cm, where the estimated relative efficiency was close to 1 and the confidence intervals overlapped with that value (Fig. 14b). The relative efficiency was highly uncertain for lengths > 28 cm, and a constant relative efficiency with a value of around 0.9 is recommended for adjusting the survey data in future analyses.

3.2.9. Winter flounder (*Pseudopleuronectes americanus*)

Standardized catches of winter flounder by the CCGS Capt. Jacques Cartier were routinely larger, particularly at lengths around 15 cm, which constituted the mode of the length frequency (Fig. 15a). Model BB5 was selected, and estimated that the relative efficiency of the CCGS Teleost declined as length increased to just over 10 cm, and then increased again to values consistent with equivalent efficiency around 28 cm (Fig. 15b). Estimated relative efficiencies below about 5 cm and above 32 cm were quite uncertain and constant values are recommended for these sizes. There were no patterns in the model residuals suggesting an inadequate fit (Fig. 15c).

3.2.10. Atlantic herring (*Clupea harengus*)

Standardized catches of herring by both vessels were generally quite variable and appeared to be of comparable magnitude between vessels except for those of herring 10-16 cm, which constituted one of three length modes in the data, and which were relatively larger for the CCGS Teleost (Fig. 15a). Model BB5 was selected and appeared to provide an adequate fit to the data (Figs. 16b,c). It estimated an irregular relative catch efficiency function characterized by a peak in relative efficiency for the CCGS Teleost at 15 cm. For lengths on either side of this peak, the CCGS Capt. Jacques Cartier was estimated to be more efficient at catching herring, although the confidence intervals overlapped with a value of 1 at all of those sizes.

3.2.11. Atlantic mackerel (*Scomber scombrus*)

Standardized catches of mackerel were generally quite variable. The CCGS Teleost tended to make larger catches, although there was a high incidence of cases in which the CCGS Capt. Jacques Cartier caught a small number of individuals, while the CCGS Telesot caught none (Fig. 20a). Model fits diverged considerably amongst candidate models, particularly those that included site-specific random-effects (Fig. 20b). While model BB4 was favored by AIC and BB5 by BIC, the predictions from these models differ considerably from the empirical estimates. Overall these results suggest that a reliable conversion function cannot be estimated for mackerel with the data available.

3.2.12. Atlantic wolffish (*Anarhichas lupus*)

Atlantic wolffish were captured infrequently and only in small numbers during the comparative fishing (Fig. 46). Estimates of relative catchability for both catch number and weight were not statistically significant (Table 10).

3.2.13. Thorny skate (*Amblyraja radiata*)

Thorny skate were captured principally along the Laurentian Channel and in the Cape Breton trough (Fig. 22a). The CCGS Capt. Jacques Cartier tended to catch more thorny skate at all sizes. Model BB1, which provided a reasonable fit to the data (Figs. 22b,c) estimated that the CCGS Capt. Jacques Cartier was about twice as efficient at capturing thorny skate.

Too few smooth skate (*Malacoraja senta*) and no winter skate (*Leucoraja ocellata*) were captured during the comparative fishing experiments to allow for the estimation of relative catchability between the two vessels.

3.2.14. Snow crab (*Chionoecetes opilio*)

Snow crab were consistently captured in greater standardized numbers by the CCGS Teleost, with an apparent complex size-dependency involving greater catch proportions for this vessel at carapace widths < 40 mm and between about 45 mm and 90 mm (Fig. 41a). Model BB5 provided a strong and apparently adequate fit to the data (Figs. 41b,c). The estimated relative efficiency function is multi-modal, yet associated with fairly elevated precision. It estimates that very small snow crab and individuals between about 50 and 70 mm are 4 to 6 times more catchable by the CCGS Teleost, while the largest individuals are much more catchable by the CCGS Capt. Jacques Cartier.

3.2.15. Lobster (*Homarus americanus*)

Standardized catches of lobster were generally greater for the CCGS Teleost, although not for smaller lobster < 50 mm (Fig. 43a). Model BB5 was selected and appeared to provide an adequate fit (Figs. 43b,c). The CCGS Teleost was estimated to be less efficient at catching lobster smaller than about 60 mm, but more efficient at larger sizes, although the confidence intervals increased considerably in width for lengths > 100 mm.

3.2.16. Other results of note

For smelt, *Osmerus mordax*, models BB1 and BB4, and to a lesser extent BB5 had similar support based on BIC, meanwhile there was only support for BB4 and BB5 based on AIC (Table 7). The relative catch efficiency based on BB4 is shown in Fig. 18b and indicates higher catchability by the Teleost for lengths < 15 cm, and equal catchability otherwise. This model provides an adequate fit to the data (Fig. 18c). The estimates from this model are recommended as conversion factors.

As was the case for mackerel, model predictions for sandlance *Ammodytes dubius* differed considerably amongst models depending on their assumptions (Fig. 33b). There were many set pair in which the species was caught by only one of the vessels, and four instance of fairly large catches that were mainly made by one of the two vessels. Obtaining a reliable conversion factor for this species with the available data does not appear possible.

3.2.17. Recommendations for the application of conversion factors

The preceding subsections provided recommendations for the application of conversion factors for a number of species of interest. Here we provide a brief summary of recommendations for the remaining taxa.

Based on the results of length-disaggregated analyses, there were no statistically significant differences in catchability and therefore no conversion factors for the following taxa:

- Gaspereau, *Alosa pseudo harengus* (Fig. 17b)
- Spiny lumpsucker, *Eumicrotremus spinosus* (Fig. 32b)
- Shortfin squid*, Illex illecebrosus* (Fig. 44b)

In contrast, length-dependent conversion factors are recommended for the following taxa:

- Smelt, *Osmerus mordax* (Fig. 18b)
- Capelin, *Mallotus villosus* (Fig. 19b)
- Fourbeard rockling, *Enchelyopus cimbrius* (Fig. 21b)
- Mailed sculpin, *Triglops murrayi*, although the length-dependent function for the recommended lengths is essentially constant (Fig. 26b)
- Alligatorfish, *Aspidophoroides monopterygius* (Fig. 28b)
- Seasnails, *Liparidae sp.* (Fig. 30b)
- Fouline snakeblenny, *Eumesogrammus praecisus* (Fig. 37b)
- Stout eelblenny, *Anisarchus medius* (Fig. 38b)
- Arctic lyre crab, *Hyas coarctatus* (Fig. 40b)

While length-independent conversions are recommended for:

- Longhorn sculpin, Myoxocephalus octodecemspinosus (Fig. 23b)
- Shorthorn sculpin, Myoxocephalus scorpius (Fig. 24b)
- Arctic staghorn sculpin, Gymnocanthus tricuspis (Fig. 25b)
- Sea raven, Hemitripterus americanus (Fig. 27b)
- Sea poacher, Leptagonus decagonus (Fig. 29b)
- Lumpfish, Cyclopterus lumpus (Fig. 31b)
- Laval`s eelpout, Lycodes lavalaei (Fig. 34b)
- Snakeblenny, Lumpenus lampretaeformis (Fig. 35b)
- Daubed shanny, Leptoclinus maculatus (Fig. 36b)
- Rock crab, Cancer irroratus (Fig. 39b)
- Great spider crab, Hyas araneus (Fig. 42b)

For taxa for which only size-aggregated analyses were undertaken, only those conversion factors that were significantly different from a value of one are recommended (Table 10). Overall, the values in Table 10 and the result shown in Figs. 62 to 112 indicate that the CCGS Teleost was more likely to catch benthic invertebrates, notably those closely associated with the bottom. For taxa such as Ascidia (Fig. 63), *Leptasterias* sp (Figs. 82, 83), *Henricia sanguinolenta* (Fig. 87), Actinaria (Fig. 98) and Hydrozoa (Fig. 106) there were many set pairs in which only the CCGS Teleost captured the taxon. These results suggest that the CCGS Capt. Jacques Cartier fishing the NEST may not provide a reliable survey for these taxa. The results presented in this document in Table 10 and the associated figures should be considered carefully before comparing survey results for years preceding and following the change in vessel and gear.

4. DISCUSSION

Overall, the data obtained in 2021-2022 appear sufficient to reliably test for differences in relative efficiency between vessels and to estimate conversion factors and length-dependent conversion factor functions for the most commonly captured taxa in the survey, which includes most commercially important species. While additional comparative fishing would improve the precision of estimates, particularly for infrequently captured taxa or those with variable catches, the benefits appear small relative to the financial and logistical costs of additional comparative fishing. The peer review meeting of the results of these comparative fishing experiments concluded that no additional comparative fishing was warranted based on these considerations.

Length-dependent conversions were estimated for 17 and length-independent conversions were estimated for 11 of the species that are routinely measured during the survey. As a general result, the CCGS Capt. Jacques Cartier fishing the NEST appeared to be more efficient at catching fishes of intermediate lengths (roughly 20-35 cm), but less efficient at catching very small fish (e.g., ≤ 5cm) and about equally efficient for larger fish of most species.

The experiments in the southern Gulf of St. Lawrence employed a shadow survey design, which helps ensure that the estimated relative catchabilities are relevant for the habitat conditions in the survey area. Furthermore, analyses of survey residuals identified no significant instances where relative catchability was affected by depth and time of day, key factors that can affect overall survey catchability (e.g., Benoît and Swain 2003). These conditions lend support to the reliability of the conversion factor estimates.

The CCGS Capt. Jacques Cartier fishing the NEST was generally much less efficient at catching most benthic invertebrate taxa. For many of these, there were numerous instances where the CCGS Teleost caught the taxon while the CCGS Capt. Jacques Cartier caught none, such as was observed for example for most echinoderms (e.g., Figs. 82, 83, 87, 89), all sponges (Figs. 108-112), hydrozoa (Fig. 106) and actinaria (Fig. 98). Although the estimated conversion factors account for this to some extent, it is likely that catches for many benthic invertebrates will be less frequent with the new vessel and trawl. This will generate a discontinuity in the survey data for the affected taxa whereby it will be difficult to reliably compare catch indices and catch properties (e.g., spatial distribution and habitat associations) between years in which the different vessels were employed for the survey.

5. ACKNOWLEDGEMENTS

Numerous DFO Science and CCG staff participated in the planning and implementation of comparative fishing in the sGSL. We are indebted to Jordan Ouellette-Plante for providing R Markdown code that greatly simplified the process of compiling the numerous figures into the document, and to Paul Regular and Andrea Perreault for identifying and correcting an error in the calculation of AIC and BIC values in earlier analyses. We wish to thank Pablo Vergara for assistance in obtaining the data, and François-Étienne Sylvain, Nicolas Rolland and Daniel Ricard for guidance for the interpretation of the data from the comparative fishing experiments and discussions on the analyses.

6. REFERENCES CITED

Benoît, H.P., Ouellette-Plante, J., Yin, Y, and Brassard, C. 2022. Review of the assessment framework for Atlantic cod in NAFO 3Pn4RS: Fishery independent surveys. DFO Can. Sci. Advis. Sec. Res. Doc. 2022/049. xiii + 130 p.

Benoît, H.P., and Swain, D.P.. 2003. Accounting for length and depth-dependent diel variation in catchability of fish and invertebrates in an annual bottom-trawl survey. ICES J. Mar. Sci. 60: 1297-1316.

Brooks, M.E., Kristensen, K., van Benthem, K.J., Magnusson, A., Berg, C.W., Nielsen, A., Skaug, H.J., Mächler, M., Bolker, B.M. 2017. glmmTMB balances speed and flexibility among packages for zero-inflated generalized linear mixed modeling. R Journal 9(2):378-400.

Cadigan, N.G., Yin, Y., Benoît, H.P., and Walsh, S.J. 2022. A nonparametric-monotone regression model and robust estimation for paired-tow bottom-trawl survey comparative fishing data. Fish. Res. 254: 106422.

Denton, C. M. 2020. Maritimes Region Inshore Lobster Trawl Survey Technical Description. Can. Tech. Rep. Fish. Aquat. Sci. 3376: v + 52 p.

Dunn, P.K. and Smyth, G.K. 1996. Randomized quantile residuals. J. Comput. Graph. Stat 5: 236-244.

Dunn, P.K., and Smyth, G.K.. 2005. Series evaluation of Tweedie exponential dispersion model densities. Statis. Comput. 15:267-280.

Green, P.J., and Silverman, B.W. 1993. Nonparametric regression and generalized linear models. Chapman and Hall/CRC, 184 p.

Hartig, F. 2021. DHARMs: Residual diagnostics for hierarchical (multi-level.mixed) regression models. R package version 0.4.1

Hastie, T., Tibshirani, R. and Friedman, J., 2009. The elements of statistical learning: data mining, inference, and prediction. Springer Science and Business Media.

Hurlbut, T., and Clay, D. 1990. Protocols for research vessel cruises within the Gulf Region (demersal fish) (1970–1987). Can. Manuscr. Rep. Fish. Aquat. Sci. 2082.

Kristensen, K., Nielsen, A., Berg, C.W., Skaug, H., and Bell, B.M. 2016. TMB: Automatic differentiation and Laplace approximation. J. Stat. Softw. 70: 1-21.

Miller, T.J. 2013. A comparison of hierarchical models for relative catch efficiency based on paired-gear data for US Northwest Atlantic fish stocks. Can. J. Fish. Aquat. Sci. 70: 1306-1316.

Miller, T.J., Das, C., Politis, P.J., Miller, A.S., Lucey, S.M., Legault, C.M., Brown, R.W., and Rago, P.J. 2010. Estimation of Albatross IV to Henry B. Bigelow calibration factors. Fish. Sci. Cent. Ref. Doc. 10-05; 233 p.

R Core Team. 2021. R: A language and environment for statistical computing. R Foundation for Statistical Computing, Vienna, Austria.

Ricard, D., Fishman, D., Rolland, N., Sylvain, F.-E., Turcotte, F. and Vergara, P. 2023. Validation of the paired sets from the comparative fishing experiments conducted between CCGS Teleost and CCGS Capt. Jacques Cartier in the southern Gulf of St. Lawrence, September 2021 and 2022. Can. Tech. Rep. Fish. Aquat. Sci. 3547: v + 274 p.

Thiess, M.E., Benoit, H., Clark, D.S. Fong, K. Mello, L.G.S. Mowbray, F. Pepin, P. Cadigan, N.G. Miller, T. Thirkell, D., and Wheeland, L. 2018. Proceedings of the National Comparative Trawl Workshop, November 28-30, 2017, Nanaimo, BC. Can. Tech. Rep. Fish. Aquat. Sci. 3254: x + 40 p.

Thorson, J.T. and Minto, C. 2015. Mixed effects: a unifying framework for statistical modelling in fisheries biology. ICES J. Mar. Sci. 72:1245-1256.

Verbyla, A.P., Cullis, B.R., Kenward, M.G, and Welham, S.J. 1999. The analysis of designed experiments and longitudinal data by using smoothing splines. J. Roy. Stat. Soc. Ser. C 48: 269-311.

Wood, S.N. 2000. Modelling and smoothing parameter estimation with multiple quadratic penalties. J. Royal. Statist. Soc. Ser. B Stat. Methodol. 62: 413–428.

Wood, S.N. 2011. Fast stable restricted maximum likelihood and marginal likelihood estimation of semiparametric generalized linear models. J. R. Stat. Soc. Ser. B Stat. Methodol. 73: 3–36.

Wood, S.N. 2017. Generalized additive models: An introduction with R, 2nd ed. Chapman and Hall/CRC Press, 496 p.

Yin, Y. and Benoît, H.P. 2022a. Re-analysis of comparative fishing experiments in the Gulf of St. Lawrence and other analyses to derive stock-wide bottom-trawl survey indices beginning in 1971 for 4RST Greenland halibut, *Reinhardtius hippoglossoides*v. DFO Can. Sci. Advis. Sec. Res. Doc. 2022/002. vii + 45 p.

Yin, Y. and Benoît, H.P. 2022b. A Comprehensive Simulation Study of A Class of Analysis Methods for Paired-Tow Comparative Fishing Experiments. Can. Tech. Rep. Fish. Aquat. Sci. 3466: vi + 99 p.

7. TABLES

Table 1. Details for the relevant set pairs in the 2021 and 2022 comparative fishing of the sGSL, where columns indicated by TEL represent values for the CCGS Teleost and those indicated by CA represent values for the CCGS Capt. Jacques Cartier. Tow start times (Time) are expressed in decimal hours, latitudes and longitudes are expressed in decimal degrees, and the Distance values represent the trawled distance for each vessel in nm. The date is that of the beginning of the tow by the CCGS Teleost, and the entries for CA Time denoted by [1] indicate that the tow by the CCGS Capt. Jacques Cartier was started the day previous before midnight. The catch for stations 53 and 54, fished on September 18 and 19, 2022 respectively, were inadvertently physically combined aboard the CCGS J. Cartier prior to catch sorting. Data for these stations from the CCGS Teleost were combined for the analysis and the tow distances for each vessel were summed for the two stations.

Date	Station no.	TEL Depth (m)	CA Depth (m)	TEL Time	CA Time	TEL Distance (nm)	CA Distance (nm)	TEL Latitude	TEL Longitude
2021-08-31	91	329	345	14.23	14.28	1.64	1.15	48.397	-62.217
2021-09-01	322	118	127	4.93	23.97[1]	1.20	1.06	48.159	-61.613
2021-09-01	104	73	83	14.65	14.92	1.75	1.05	48.002	-61.298
2021-09-01	326	60	61	23.45	23.68	1.18	1.00	48.039	-61.619
2021-09-02	59	54	54	13.12	13.45	1.74	1.17	47.883	-62.085
2021-09-02	100	78	77	16.02	16.20	1.42	1.01	48.047	-62.146
2021-09-05	24	141	145	12.03	12.38	1.70	1.01	48.570	-63.665
2021-09-05	23	176	173	14.60	14.65	1.74	1.00	48.525	-63.797
2021-09-05	26	130	130	17.52	17.72	1.47	0.98	48.551	-63.477
2021-09-06	39	27	26	12.97	12.57	1.44	1.07	48.013	-64.291
2021-09-06	197	32	40	16.07	16.22	1.77	1.12	48.034	-64.598
2021-09-07	295	36	42	0.05	22.68[1]	1.21	1.03	47.771	-65.392
2021-09-08	38	32	36	17.73	17.83	1.75	0.95	47.948	-65.86
2021-09-08	296	35	37	19.50	19.60	1.65	1.00	48.077	-65.759
2021-09-09	30	54	60	9.45	9.48	1.69	1.00	48.212	-64.118
2021-09-09	191	91	97	15.07	15.20	1.74	0.98	48.311	-64.036
2021-09-09	79	86	89	19.67	19.77	1.73	1.10	48.312	-63.345
2021-09-09	80	63	60	22.97	23.00	1.74	1.01	48.386	-63.096
2021-09-10	81	81	82	1.52	1.68	1.80	1.10	48.314	-62.908
2021-09-10	95	95	97	4.53	4.67	1.79	1.07	48.305	-62.747
2021-09-10	96	99	99	10.82	10.90	1.74	1.03	48.093	-62.690
2021-09-10	69	71	74	16.03	16.18	1.80	1.01	47.961	-62.902
2021-09-10	83	74	74	19.07	19.15	1.75	1.05	48.078	-62.816
2021-09-10	82	71	75	20.88	20.97	1.75	1.10	48.204	-62.946
2021-09-11	85	79	81	3.83	3.95	1.80	1.10	47.862	-63.316
2021-09-11	86	83	80	6.48	6.57	1.65	1.03	47.971	-63.677
2021-09-11	87	80	82	9.22	9.38	1.70	1.03	47.841	-63.721
2021-09-11	50	84	89	12.88	12.05	1.75	1.00	47.920	-63.847
2021-09-11	51	73	72	20.83	20.92	1.80	1.05	47.869	-63.917
2021-09-12	53	68	67	1.47	1.57	1.80	1.05	47.734	-64.195
2021-09-12	40	37	36	3.93	4.03	1.83	1.05	47.794	-64.344
2021-09-12	41	33	32	9.65	9.62	1.70	1.00	47.744	-64.422

Date	Station no.	TEL Depth (m)	CA Depth (m)	TEL Time	CA Time	TEL Distance (nm)	CA Distance (nm)	TEL Latitude	TEL Longitude
2021-09-12	42	27	27	13.05	13.27	1.80	0.88	47.498	-64.615
2021-09-12	43	36	40	15.95	16.00	1.80	0.98	47.332	-64.575
2021-09-12	44	38	39	18.12	18.22	1.80	1.06	47.223	-64.515
2021-09-12	300	30	31	20.77	20.77	1.60	1.07	47.090	-64.560
2021-09-13	58	43	44	0.80	0.92	1.80	1.04	47.242	-64.457
2021-09-13	57	43	43	3.38	3.45	1.80	1.08	47.132	-64.266
2021-09-13	46	40	40	8.03	8.05	1.65	1.02	47.054	-64.214
2021-09-13	207	36	35	14.93	15.03	1.80	0.83	46.967	-64.463
2021-09-13	56	55	56	19.52	19.52	1.60	1.02	47.372	-64.357
2021-09-13	54	65	68	22.13	22.23	1.60	1.08	47.529	-64.184
2021-09-14	55	34	37	4.97	5.22	1.30	1.03	47.225	-63.959
2021-09-14	78	64	64	9.13	7.82	1.70	1.03	47.469	-63.821
2021-09-14	76	71	75	13.33	12.05	1.60	0.92	47.609	-63.574
2021-09-14	70	57	58	23.15	23.20	1.80	1.06	47.634	-62.981
2021-09-15	107	35	34	7.90	8.10	1.70	0.92	47.589	-61.952
2021-09-15	108	36	36	10.75	10.88	1.80	1.02	47.458	-62.078
2021-09-15	63	64	64	14.45	14.57	1.80	1.01	47.314	-62.442
2021-09-15	67	61	62	17.60	17.65	1.70	1.07	47.198	-62.789
2021-09-16	74	71	70	2.53	2.63	1.80	1.07	47.372	-63.200
2021-09-16	75	62	65	5.25	5.38	1.80	1.08	47.279	-63.370
2021-09-16	117	59	57	9.83	9.95	1.70	1.00	47.133	-63.686
2021-09-16	1	26	25	15.40	15.52	1.80	1.00	46.823	-63.906
2021-09-16	118	38	40	17.85	17.93	1.70	1.01	46.860	-63.733
2021-09-16	114	56	58	21.25	21.35	1.70	1.04	46.957	-63.298
2021-09-17	113	64	63	1.08	1.33	1.80	1.05	47.100	-63.149
2021-09-17	111	61	62	5.67	7.08	1.80	1.04	46.853	-62.977
2021-09-17	112	61	63	9.38	9.52	1.70	1.02	46.915	-63.155
2021-09-17	115	46	47	13.07	13.13	1.70	1.00	46.765	-63.357
2021-09-17	2	34	35	17.00	17.08	1.70	1.01	46.532	-63.238
2021-09-17	128	52	53	21.17	21.25	1.70	1.05	46.678	-62.792
2021-09-18	126	64	66	1.00	1.10	1.80	1.04	46.768	-62.533
2021-09-18	121	70	72	9.65	9.77	1.70	0.81	46.748	-62.068
2021-09-18	124	57	58	12.92	12.98	1.65	0.80	46.928	-62.144
2021-09-18	241	51	51	15.82	15.98	1.80	1.00	47.038	-62.012
2021-09-18	352	34	34	21.43	21.13	1.60	1.08	47.118	-61.762
2021-09-19	152	39	36	0.22	0.32	1.30	1.03	47.137	-61.465
2021-09-19	153	36	34	2.98	3.07	1.80	1.05	47.072	-61.474
2021-09-19	143	49	50	5.03	5.15	1.80	1.06	46.930	-61.546
2021-09-19	119	66	73	9.27	9.3	1.70	1.03	46.761	-61.958
2021-09-19	120	65	59	11.87	12.00	1.80	1.00	46.686	-61.882
2021-09-19	146	63	63	14.15	14.30	1.80	1.00	46.589	-61.666
2021-09-19	145	67	70	20.10	20.03	1.60	1.02	46.705	-61.418

Date	Station no.	TEL Depth (m)	CA Depth (m)	TEL Time	CA Time	TEL Distance (nm)	CA Distance (nm)	TEL Latitude	TEL Longitude
2021-09-19	142	59	61	23.77	23.98	1.70	1.07	46.933	-61.275
2021-09-20	141	54	54	2.85	2.95	1.80	1.08	47.158	-61.204
2021-09-20	160	41	41	5.02	5.18	1.30	1.06	47.323	-61.264
2021-09-20	151	31	32	8.12	8.38	1.70	1.08	47.515	-61.197
2021-09-20	150	32	32	10.83	10.85	1.75	1.06	47.645	-61.170
2021-09-20	156	51	54	14.42	14.57	1.80	1.08	47.546	-60.856
2021-09-20	259	55	55	17.67	17.73	1.70	1.06	47.774	-60.964
2021-09-20	361	101	97	22.10	22.22	1.70	1.07	47.934	-60.941
2021-09-21	172	315	347	0.72	0.95	1.80	1.11	47.980	-60.876
2021-09-21	169	146	159	4.18	4.53	1.80	1.06	47.837	-60.755
2021-09-21	173	325	352	7.33	7.42	1.70	1.00	47.850	-60.620
2021-09-21	155	72	72	10.62	10.73	1.70	1.04	47.708	-60.707
2021-09-21	170	108	103	12.88	13.03	1.90	1.03	47.613	-60.545
2021-09-21	161	61	64	15.22	15.33	1.80	1.07	47.491	-60.661
2021-09-21	174	238	232	18.78	19.33	1.70	1.08	47.490	-60.434
2021-09-21	171	98	111	21.67	21.77	1.70	1.08	47.387	-60.326
2021-09-22	176	299	329	0.83	1.07	1.80	1.08	47.320	-60.181
2021-09-22	175	200	209	4.25	4.43	1.80	1.05	47.230	-60.286
2021-09-22	162	180	184	7.70	7.92	1.70	1.07	47.160	-60.348
2021-09-22	165	175	177	10.45	10.48	1.80	1.05	47.116	-60.556
2021-09-22	164	110	120	13.60	13.88	1.80	1.06	47.259	-60.572
2021-09-22	157	65	67	16.23	16.37	1.80	1.05	47.316	-60.736
2021-09-22	158	80	84	18.57	18.68	1.70	1.06	47.300	-60.831
2021-09-22	261	57	59	20.97	21.08	1.70	1.06	47.308	-61.005
2021-09-22	360	119	126	23.87	0.00	1.80	1.06	47.065	-60.865
2021-09-23	166	102	103	1.95	2.10	1.80	1.06	47.042	-60.963
2021-09-23	253	65	68	4.63	4.75	1.80	1.06	46.874	-61.167
2021-09-23	167	125	126	7.97	8.32	1.70	1.02	46.723	-61.043
2021-09-23	148	70	70	12.02	12.13	1.80	1.05	46.553	-61.228
2021-09-23	149	62	66	14.35	14.50	1.70	1.02	46.465	-61.480
2021-09-23	147	60	62	16.08	16.18	1.80	1.03	46.503	-61.525
2021-09-24	273	31	32	0.22	0.43	1.58	0.83	46.519	-62.574
2021-09-24	244	49	51	3.37	3.60	1.80	1.05	46.578	-62.567
2021-09-24	135	45	46	8.02	8.13	1.70	1.04	46.368	-61.782
2021-09-24	134	54	55	10.23	10.30	1.70	1.05	46.217	-61.758
2021-09-24	133	52	50	12.57	12.68	1.80	1.03	46.079	-61.660
2021-09-24	11	37	38	15.32	15.45	1.80	1.05	45.829	-61.654
2021-09-24	10	31	31	19.52	19.58	1.70	1.01	45.740	-61.598
2021-09-25	8	37	35	1.68	23.33[1]	1.80	1.02	45.852	-61.805
2021-09-25	132	46	48	6.67	6.72	1.70	1.08	45.999	-61.757
2021-09-25	136	37	41	9.72	9.87	1.70	1.03	46.096	-62.005
2021-09-25	138	25	26	12.63	12.77	1.79	0.98	46.187	-62.283

Date	Station no.	TEL Depth (m)	CA Depth (m)	TEL Time	CA Time	TEL Distance (nm)	CA Distance (nm)	TEL Latitude	TEL Longitude
2021-09-25	137	43	44	15.18	15.28	1.83	1.05	45.941	-62.104
2021-09-25	139	38	39	17.80	17.93	1.70	1.05	45.883	-62.098
2021-09-25	140	32	32	20.12	20.17	1.70	1.04	45.818	-62.295
2021-09-25	131	28	26	22.62	22.68	1.70	1.05	45.820	-62.371
2021-09-26	130	50	57	1.98	2.27	1.63	1.04	45.928	-62.593
2021-09-26	246	32	30	6.28	6.37	1.70	1.08	45.827	-62.892
2021-09-26	7	22	23	10.00	10.08	1.70	1.06	45.944	-63.352
2021-09-26	4	17	18	14.07	14.10	1.64	1.06	46.115	-63.447
2021-09-26	6	19	18	17.82	17.87	1.70	1.09	46.053	-63.197
2021-09-26	181	23	21	19.85	19.92	1.70	1.09	45.979	-63.170
2021-09-26	340	26	27	22.38	22.47	1.70	1.04	45.939	-63.020
2022-09-17	219	32	33	18.50	18.48	1.77	1.01	48.021	-65.852
2022-09-17	39	52	54	21.53	21.57	1.81	0.99	47.819	-65.449
2022-09-18	37	65	61	0.03	0.08	1.89	1.01	47.883	-65.123
2022-09-18	35	87	87	4.12	4.20	1.76	0.99	48.124	-64.782
2022-09-18	34	92	92	6.55	6.62	1.90	1.01	48.180	-64.592
2022-09-18	31	49	52	9.55	9.58	1.77	1.00	48.184	-64.260
2022-09-18	46	26	26	11.45	11.45	1.63	0.99	48.076	-64.240
2022-09-18	41	29	30	14.58	14.60	1.80	1.00	47.828	-64.429
2022-09-18	316	31	32	17.50	17.55	1.80	1.01	47.582	-64.495
2022-9-18/19	53 + 54	-	-	-	-	3.50	1.90	-	-
2022-09-19	52	52	48	5.12	5.17	1.29	1.00	47.992	-64.043
2022-09-19	308	107	106	8.97	9.03	1.76	1.00	48.286	-64.186
2022-09-19	33	92	91	12.65	12.83	1.84	0.99	48.359	-63.946
2022-09-19	25	119	121	15.70	15.75	1.76	0.99	48.537	-64.018
2022-09-19	29	145	140	19.18	19.20	1.76	1.01	48.620	-63.735
2022-09-19	14	213	205	22.72	22.77	1.62	0.98	48.861	-63.955
2022-09-20	12	325	302	2.12	2.12	1.74	1.00	49.033	-63.984
2022-09-20	13	359	356	6.95	7.08	1.76	0.96	49.112	-63.954
2022-09-21	101	351	355	13.30	13.35	1.80	0.96	48.524	-62.857
2022-09-21	338	103	98	16.58	16.58	1.40	0.97	48.368	-62.783
2022-09-21	102	340	342	19.33	19.37	1.79	0.93	48.419	-62.495
2022-09-21	114	75	73	22.77	22.77	1.26	0.97	48.266	-62.353
2022-09-22	109	115	120	2.62	1.65	1.77	1.00	48.236	-62.026
2022-09-22	121	37	39	8.47	8.53	1.77	1.01	47.572	-62.067
2022-09-22	122	37	36	10.12	10.08	1.75	1.03	47.511	-62.092
2022-09-22	120	34	33	16.12	16.15	1.83	0.99	47.683	-61.743
2022-09-22	117	51	51	17.90	17.95	1.39	0.99	47.834	-61.651
2022-09-22	106	229	240	20.78	20.87	1.80	0.98	48.156	-61.427
2022-09-22	110	102	107	23.58	23.58	1.64	0.99	48.135	-61.657
2022-09-23	116	69	65	1.98	2.17	1.74	1.00	48.043	-61.836
2022-09-23	103	361	366	9.60	9.65	1.75	0.97	48.417	-62.264

Date	Station no.	TEL Depth (m)	CA Depth (m)	TEL Time	CA Time	TEL Distance (nm)	CA Distance (nm)	TEL Latitude	TEL Longitude
2022-09-25	310	65	58	16.52	16.7	1.78	1.00	47.898	-65.041
2022-09-25	215	79	82	20.72	19.63	1.81	0.99	48.107	-64.598
2022-09-26	306	87	89	1.67	1.60	1.45	0.98	48.222	-63.850
2022-09-27	169	34	37	7.37	7.43	1.72	1.02	47.130	-61.788
2022-09-27	167	36	39	10.38	10.48	1.77	1.00	47.260	-61.463
2022-09-27	166	35	39	15.23	13.43	1.78	0.92	47.477	-61.185
2022-09-27	185	106	102	21.37	21.35	1.77	0.99	47.959	-60.970
2022-09-27	190	269	274	23.60	23.70	1.79	0.97	47.846	-60.675
2022-09-28	186	115	111	3.63	3.80	1.78	1.00	47.543	-60.516
2022-09-28	187	85	90	7.88	7.92	1.76	0.99	47.402	-60.374
2022-09-28	192	230	222	10.20	10.33	1.77	1.02	47.286	-60.248
2022-09-28	288	194	193	12.95	12.93	1.77	0.99	47.233	-60.327
2022-09-28	179	125	116	15.37	15.37	1.61	0.97	47.269	-60.515
2022-09-28	180	168	172	19.68	19.65	1.74	0.99	47.123	-60.614
2022-09-28	181	115	115	22.78	22.78	1.77	0.98	47.077	-60.883
2022-09-30	5	19	24	1.93	2.23	1.71	0.99	45.937	-63.398
2022-09-30	292	19	24	4.48	4.43	1.78	1.04	46.091	-63.394
2022-09-30	143	24	27	8.05	8.02	1.78	1.01	45.957	-63.262
2022-09-30	6	22	28	11.78	11.80	1.37	0.97	45.892	-63.162
2022-09-30	358	27	36	15.07	15.10	1.78	0.99	45.899	-62.783
2022-09-30	155	28	32	18.38	18.43	1.83	1.00	45.871	-62.358

Table 2. A set of binomial models with various assumptions for the length effect and station effect in the relative catch efficiency. A smoothing length effect can be considered and the station effect can be added to the intercept, without interaction with the length effect, or added to both the intercept and smoother to allow for interaction between the two effects.

Model	$log(\rho)$	Length Effect	Station Effect
$BI0$	β_0	constant	not considered
$BI1$	$\beta_0 + \delta_{0,i}$	constant	intercept
$BI2$	$\mathbf{X}_f^T \boldsymbol{\beta}_f + \mathbf{X}_r^T \mathbf{b}$	smoothing	not considered
$BI3$	$\mathbf{X}_f^T \boldsymbol{\beta}_f + \mathbf{X}_r^T \mathbf{b} + \delta_{0,i}$	smoothing	intercept
$BI4$	$\mathbf{X}_f^T (\boldsymbol{\beta}_f + \boldsymbol{\delta}_i) + \mathbf{X}_r^T (\mathbf{b} + \boldsymbol{\epsilon}_i)$	smoothing	intercept, smoother

Table 3. A set of beta-binomial models with various assumptions for the length effect and station effect in the relative catch efficiency, and the length effect on the variance parameter. A smoothing length effect can be considered in both the conversion factor and the variance parameter. A possible station effect can be added to the intercept, without interaction with the length effect, or added to both the intercept and the smoother to allow for interaction between the two effects.

Model	$log(\rho)$	$log(\phi)$	Length Effects	Station Effect
$BB0$	β_0	γ_0	constant/constant	not considered
$BB1$	$\beta_0 + \delta_{0,i}$	γ_0	constant/constant	intercept
$BB2$	$\mathbf{X}_f^T \boldsymbol{\beta}_f + \mathbf{X}_r^T \mathbf{b}$	γ_0	smoothing/constant	not considered
$BB3$	$\mathbf{X}_f^T \boldsymbol{\beta}_f + \mathbf{X}_r^T \mathbf{b}$	$\mathbf{X}_f^T \boldsymbol{\gamma} + \mathbf{X}_r^T \mathbf{g}$	smoothing/smoothing	not considered
$BB4$	$\mathbf{X}_f^T \boldsymbol{\beta}_f + \mathbf{X}_r^T \mathbf{b} + \delta_{0,i}$	γ_0	smoothing/constant	intercept
$BB5$	$\mathbf{X}_f^T \boldsymbol{\beta}_f + \mathbf{X}_r^T \mathbf{b} + \delta_{0,i}$	$\mathbf{X}_f^T \boldsymbol{\gamma} + \mathbf{X}_r^T \mathbf{g}$	smoothing/smoothing	intercept
$BB6$	$\mathbf{X}_f^T (\boldsymbol{\beta}_f + \boldsymbol{\delta}_i) + \mathbf{X}_r^T (\mathbf{b} + \boldsymbol{\epsilon}_i)$	γ_0	smoothing/constant	intercept, smoother
$BB7$	$\mathbf{X}_f^T (\boldsymbol{\beta}_f + \boldsymbol{\delta}_i) + \mathbf{X}_r^T (\mathbf{b} + \boldsymbol{\epsilon}_i)$	$\mathbf{X}_f^T \boldsymbol{\gamma} + \mathbf{X}_r^T \mathbf{g}$	smoothing/smoothing	intercept, smoother

Table 4. Taxonomic groupings employed for the analyses of the sGSL comparative fishing data. The codes are those used routinely in DFO's Gulf region, commonly called RVAN codes.

Taxon	**Taxon code**	**Codes in group**
Gadus morhua	10	10, 251
Artediellus sp.	323	323, 306, 880
Liparidae	500	500, 505, 512, 520, 868
Shrimp (Decapoda)	2100	2100 - 2421
Pagurus sp.	2560	2560, 2561, 2562
Polycheatae	3000	3000 - 3104
Aphrodita hastata	3200	3200, 3210
Buccinum sp.	4210	4209, 4210, 4211, 4212
Nudibranchia	4400	4400. 4410
Pycnogonida sp.	5100	5100, 5101, 5102
Ophiuroidea	6200	6200, 6211, 6213
Euryalida	6300	6300, 6310
Strongylocentrotus sp.	6400	6400, 6411
Holothuroidea	6600	6600, 6601, 6611
Scyphozoa	8500	8500, 8511
Porifera	8600	8600-8612, 8614, 8617-8623, 8628-8632, 8637-8699

Table 5. Summary of the catches at length excluded from the length-disaggregated analyses.

Taxon	**Lengths excluded**
Clupea harengus	< 5 cm, > 35 cm
Scomber scombrus	< 6 cm
Osmerus mordax	> 25 cm
Cyclopterus lumpus	< 5 cm
Eumesogrammus praecisus	> 30 cm
Illex illecebrosus	< 10 cm

Table 6. Total number of relevant set pairs (those with at least one capture), and pairs in which the taxon was captured only by the CCGS Capt. Jacques Cartier or only by the CCGS Teleost, along with a reference to the number of the figure in which results are plotted. The lists are sorted by the type of analysis (length-disaggregated vs size-aggregated) and roughly taxonomically.

Taxon	**Code**	**Pairs**	**Cartier only**	**Teleost only**	**Figure number**
Fishes (length-specific)					
Gadus morhua	10	161	19	5	7
Urophycis tenuis	12	56	13	0	8
Sebastes sp.	23	60	23	3	9
Hippoglossus hippoglossus	30	51	15	24	10
Reinhardtius hippoglossoides	31	43	6	8	11
Hippoglossoides platessoides	40	167	14	1	12
Glyptocephalus cynoglossus	41	40	12	2	13
Limanda ferruginea	42	96	17	6	14
Pseudopleuronectes americanus	43	70	9	2	15
Clupea harengus	60	86	23	18	16
Alosa pseudoharengus	62	58	12	5	17
Osmerus mordax	63	42	8	4	18
Mallotus villosus	64	102	16	9	19
Scomber scombrus	70	83	34	3	20
Enchelyopus cimbrius	114	44	17	11	21
Amblyraja radiata	201	57	15	6	22
Myoxocephalus octodecemspinosus	300	72	31	5	23
Myoxocephalus scorpius	301	85	46	9	24
Gymnocanthus tricuspis	302	95	57	2	25
Triglops murrayi	304	67	36	6	26
Hemitripterus americanus	320	39	14	7	27
Aspidophoroides monopterygius	323	33	11	13	28

Taxon	Code	Pairs	Cartier only	Teleost only	Figure number
Leptagonus decagonus	340	109	37	16	29
Liparidae	350	38	12	5	30
Cyclopterus lumpus	500	42	19	12	31
Eumicrotremus spinosus	501	32	22	6	32
Ammodytes dubius	502	27	11	7	33
Lycodes lavalaei	610	50	22	8	34
Lumpenus lampretaeformis	620	50	22	9	35
Leptoclinus maculatus	622	26	2	14	36
Eumesogrammus praecisus	623	48	4	21	37
Anisarchus medius	626	47	21	7	38
Crustaceans (length-specific)					
Cancer irroratus	2513	43	1	20	39
Hyas coarctatus	2521	121	10	54	40
Chionoecetes opilio	2526	139	7	17	41
Hyas araneus	2527	72	23	29	42
Homarus americanus	2550	63	8	7	43
Squid (length-specific)					
Illex illecebrosus	4511	71	23	16	44
Size-aggregated analyses					
Fishes					
Merluccius bilinearis	14	23	6	5	45
Anarhichas lupus	50	17	5	8	46
Alosa sapidissima	61	20	4	9	47
Gadus macrocephalus	118	20	12	4	48
Tautogolabrus adspersus	122	19	6	4	49
Scophthalmus aquosus	143	19	3	1	50
Malacoraja senta	202	22	5	4	51
Myxine limosa	241	15	0	4	52
Icelus spatula	314	15	9	5	53
Artediellus sp.	323	33	11	13	54
Gasterosteus aculeatus	361	19	7	6	55
Nezumia bairdii	410	18	5	0	56
Zoarces americanus	640	20	14	1	57
Arctozenus risso	712	16	5	2	58
Eggs					
Rajidae eggs	1224	20	1	11	59
Buccinidae eggs	1510	57	13	28	60
Gastropoda eggs	1511	20	6	10	61
Tunicates & Bryozoa					
Tunicata (s.p.)	1810	57	10	37	62
Ascidia sp.	1821	40	5	34	63
Boltenia sp.	1823	105	11	43	64
Halocynthia pyriformis	1827	15	2	10	65

Taxon	Code	Pairs	Cartier only	Teleost only	Figure number
Bryozoa (p.)	1900	60	6	45	66
Crustaceans					
Decapod shrimp	2100	171	7	17	67
Anonyx sp.	2833	19	1	15	68
Annelids and polychaetes					
Annelida (p.)	3000	94	9	58	69
Aphrodita hastata	3200	20	3	11	70
Molluscs					
Buccinum sp.	4210	55	6	37	71
Neptunea decemcostata	4227	32	4	25	72
Chlamys islandica	4322	24	4	17	73
Ciliatocardium ciliatum	4342	19	6	9	74
Mollusca sp. empty	4348	157	3	56	75
Nudibranchia (o.)	4400	49	10	25	76
Semirossia tenera	4522	18	12	5	77
Bathypolypus arcticus	4524	19	3	7	78
Sea spider					
Pycnogonida sp.	5100	27	5	13	79
Echinoderms					
Asterias sp.	6110	38	15	18	80
Asterias rubens	6111	15	9	6	81
Leptasterias (Hexasterias) polaris	6113	58	4	44	82
Leptasterias sp.	6114	15	4	11	83
Ctenodiscus crispatus	6115	31	4	11	84
Hippasteria phrygiana	6117	27	6	11	85
Henricia sp.	6118	24	17	7	86
Henricia sanguinolenta	6119	88	5	58	87
Solaster endeca	6121	41	6	23	88
Crossaster papposus	6123	109	5	26	89
Pteraster militaris	6125	20	4	13	90
Ophiuroidea (c.)	6200	109	12	58	91
Euryalida (f.)	6300	98	10	40	92
Strongylocentrotus sp.	6400	120	3	39	93
Clypeasteroida (o.)	6500	68	8	27	94
Holothuroidea (c.)	6600	64	9	30	95
Psolus fabricii	6713	21	1	16	96
Psolus phantapus	6715	25	5	17	97
Actinaria					
Actiniaria (o.)	8208	41	7	32	98
Anthozoa (c.)	8300	78	33	31	99
Stomphia coccinea	8313	22	8	14	100
Pennatulacea sp.	8318	20	5	12	101
Gersemia rubiformis	8324	83	7	44	102

Taxon	Code	Pairs	Cartier only	Teleost only	Figure number
Soft coral unidentified	8327	25	10	11	103
Pseudarchaster parelii	8346	18	0	9	104
Ptilella grandis	8360	20	5	8	105
Hydrozoa (c.)	8400	67	6	58	106
Scyphozoa (c.)	8500	133	38	11	107
Porifera					
Porifera (other)	8600	75	11	37	108
Suberites ficus	8613	19	3	13	109
Mycale (Mycale) lingua	8616	50	5	32	110
Cladocroce spatula	8627	33	3	25	111
Semisuberites cribrosa	8633	32	5	24	112

Table 7a. Relative evidence for length-disaggregated binomial and beta-binomial models based on delta values of the Aikaike Information Criterion (AIC). Entries with '–' indicate models that did not converge. Model BB7 did not converge for any taxon and are not included in the table.

Taxon	**ΔAIC**											
	BI0	**BI1**	**BI2**	**BI3**	**BI4**	**BB0**	**BB1**	**BB2**	**BB3**	**BB4**	**BB5**	**BB6**
Gadus morhua	3657	515	2399	161	-	1240	341	837	832	64	0	821
Urophycis tenuis	272	35	272	16	-	87	7	79	69	1	0	-
Sebastes sp.	1024	156	791	43	-	208	66	134	137	0	-	-
Hippoglossus hippoglossus	31	0	35	4	-	21	1	25	-	5	-	-
Reinhardtius hippoglossoides	18	11	6	0	-	20	-	-	-	-	-	-
Hippoglossoides platessoides	5376	2665	2588	409	-	-	1357	1049	969	157	0	-
Glyptocephalus cynoglossus	69	15	73	18	-	33	0	37	41	4	4	-
Limanda ferruginea	2071	340	1490	75	-	602	186	463	451	6	0	-
P. americanus	2450	852	1624	324	-	394	196	266	227	20	0	-
Clupea harengus	7911	2265	7071	1841	-	669	48	656	620	20	0	-
Alosa pseudoharengus	1138	191	882	94	-	158	10	154	154	0	3	-
Osmerus mordax	1612	337	1451	224	61	153	18	144	147	6	0	-
Mallotus villosus	4800	1589	4498	1308	26	281	94	262	222	77	0	-
Scomber scombrus	4419	680	4202	392	-	425	23	393	390	2	0	-
Enchelyopus cimbrius	15	13	3	0	-	17	15	-	-	-	-	-
Amblyraja radiata	235	34	210	8	127	124	14	114	118	0	1	-
Myoxocephalus octodecemspinosus	185	8	160	0	-	68	7	62	66	0	-	-
Myoxocephalus scorpius	7	2	2	0	-	7	4	4	8	-	-	12
Gymnocanthus tricuspis	28	0	26	4	-	22	2	21	24	5	-	-
Triglops murrayi	36	14	26	0	-	16	11	10	10	0	3	-
Hemitripterus americanus	3	0	6	4	-	2	0	5	-	4	8	-
Aspidophoroides monopterygius	259	58	191	0	-	128	55	87	89	2	-	-
Leptagonus decagonus	6	0	9	4	-	4	1	7	10	5	-	-
Liparidae sp.	24	22	3	4	-	13	12	0	4	2	5	-
Cyclopterus lumpus	0	2	4	5	-	-	-	-	-	-	-	-
Eumicrotremus spinosus	2	0	5	4	-	2	2	6	10	-	-	-
Ammodytes dubius	1931	425	1242	88	-	175	48	166	169	1	0	-

Taxon	ΔAIC											
	BI0	BI1	BI2	BI3	BI4	BB0	BB1	BB2	BB3	BB4	BB5	BB6
Lycodes lavalaei	89	5	54	4	-	64	1	42	46	0	4	-
Lumpenus lampretaeformis	7	8	3	0	-	8	9	3	-	-	-	-
Leptoclinus maculatus	189	123	144	54	-	6	0	4	4	3	-	-
Eumesogrammus praecisus	304	16	277	0	-	116	13	111	113	1	-	119
Anisarchus medius	347	19	342	0	-	72	11	75	76	0	-	-
Cancer irroratus	195	1	198	0	-	166	3	169	168	2	-	-
Hyas coarctatus	580	43	524	16	-	265	23	216	215	1	0	-
Chionoecetes opilio	1913	1062	896	232	-	1006	618	409	333	41	0	-
Hyas araneus	170	21	159	22	-	51	0	53	55	3	6	-
Homarus americanus	2542	567	2316	315	-	1011	253	890	874	71	0	-
Illex illecebrosus	80	0	81	4	-	23	1	26	29	5	9	-

Table 7b. Relative evidence for length-disaggregated binomial and beta-binomial models based on delta values of the Bayesian Information Criterion (BIC) values. Entries with '–' indicate models that did not converge. Model BB7 did not converge for any taxon and are not included in the table.

Taxon	ΔBIC											
	BI0	BI1	BI2	BI3	BI4	BB0	BB1	BB2	BB3	BB4	BB5	BB6
Gadus morhua	3612	478	2370	138	-	1203	312	815	825	49	0	828
Urophycis tenuis	250	20	265	17	-	73	0	79	84	9	23	-
Sebastes sp.	997	136	778	36	-	187	52	127	144	0	-	-
Hippoglossus hippoglossus	23	0	44	20	-	21	9	42	-	30	-	-
Reinhardtius hippoglossoides	0	1	3	4	-	9	-	-	-	-	-	-
Hippoglossoides platessoides	5332	2628	2559	388	-	-	1328	1027	962	143	0	-
Glyptocephalus cynoglossus	56	8	73	25	-	26	0	44	61	18	31	-
Limanda ferruginea	2038	314	1471	62	-	576	167	450	452	0	8	-
P. americanus	2408	817	1596	304	-	360	168	245	220	6	0	-
Clupea harengus	7867	2229	7043	1819	-	633	19	634	613	6	0	-
Alosa pseudoharengus	1116	174	872	90	-	141	0	151	163	3	19	-
Osmerus mordax	1581	313	1433	213	68	129	0	132	148	1	7	-
Mallotus villosus	4765	1560	4474	1290	26	251	70	244	216	65	0	-

Taxon	ΔBIC											
	BI0	BI1	BI2	BI3	BI4	BB0	BB1	BB2	BB3	BB4	BB5	BB6
Scomber scombrus	4392	659	4187	383	-	404	8	385	394	0	10	-
Enchelyopus cimbrius	0	4	0	4	-	8	12	-	-	-	-	-
Amblyraja radiata	206	13	196	1	142	102	0	107	125	0	16	-
Myoxocephalus octodecemspinosus	169	0	159	5	-	60	5	67	84	12	-	-
Myoxocephalus scorpius	0	2	9	14	-	7	11	17	35	-	-	53
Gymnocanthus tricuspis	21	0	33	17	-	22	8	34	50	25	-	-
Triglops murrayi	19	2	20	0	-	4	6	10	21	6	21	-
Hemitripterus americanus	0	4	18	22	-	6	12	23	-	29	47	-
Aspidophoroides monopterygius	241	46	186	0	-	116	49	87	101	7	-	-
Leptagonus decagonus	0	1	16	17	-	4	8	21	35	24	-	-
Liparidae sp.	7	12	0	7	-	3	9	3	20	12	29	-
Cyclopterus lumpus	0	7	15	22	-	-	-	-	-	-	-	-
Eumicrotremus spinosus	0	4	14	18	-	6	11	21	36	-	-	-
Ammodytes dubius	1905	405	1229	81	-	156	35	159	174	0	11	-
Lycodes lavalaei	76	0	56	13	-	59	3	51	70	17	35	-
Lumpenus lampretaeformis	0	7	8	12	-	7	15	15	-	-	-	-
Leptoclinus maculatus	177	116	144	59	-	0	3	14	25	16	23	-
Eumesogrammus praecisus	286	4	271	0	-	104	7	111	125	7	-	144
Anisarchus medius	329	7	336	0	-	60	5	75	88	6	-	-
Cancer irroratus	187	0	205	15	-	165	10	184	199	25	-	-
Hyas coarctatus	549	20	508	7	-	241	6	207	222	0	14	-
Chionoecetes opilio	1864	1021	863	208	-	965	585	385	325	25	0	-
Hyas araneus	155	13	159	29	-	43	0	61	78	18	36	-
Homarus americanus	2492	526	2283	290	-	969	220	865	865	54	0	-
Illex illecebrosus	74	0	87	16	-	23	7	38	53	23	38	-

Table 8. P-values associated with tests for a smooth effect of depth, a smooth effect of time and a fixed effect of day on the normalized quantile residuals from the length-disaggregated selected best model. Values < 0.01 are indicated in bold.

Taxon	s(depth)	s(time)	day
Gadus morhua	0.468	0.612	0.627
Urophycis tenuis	0.886	0.698	0.758
Sebastes sp.	0.829	0.800	0.368
Hippoglossus hippoglossus	0.488	0.156	0.029
Reinhardtius hippoglossoides	0.305	0.962	0.719
Hippoglossoides platessoides	0.657	0.050	**0.007**
Glyptocephalus cynoglossus	0.136	0.503	0.134
Limanda ferruginea	0.793	0.782	0.779
Pseudopleuronectes americanus	0.339	0.550	0.531
Clupea harengus	0.739	0.628	0.593
Alosa pseudoharengus	0.663	0.715	0.312
Osmerus mordax	0.348	0.864	0.540
Mallotus villosus	0.572	0.769	0.960
Scomber scombrus	0.346	0.160	0.128
Enchelyopus cimbrius	0.021	0.139	0.340
Amblyraja radiata	0.330	0.383	0.107
Myoxocephalus octodecemspinosus	0.312	0.980	0.225
Myoxocephalus scorpius	0.405	0.782	0.377
Gymnocanthus tricuspis	0.064	0.410	0.566
Triglops murrayi	0.926	0.188	0.039
Hemitripterus americanus	0.545	0.326	0.748
Aspidophoroides monopterygius	0.326	0.655	0.505
Leptagonus decagonus	0.406	0.413	0.560
Liparidae	0.117	0.653	0.768
Cyclopterus lumpus	0.910	0.185	0.945
Eumicrotremus spinosus	0.906	0.205	0.650
Ammodytes dubius	0.408	0.615	0.574
Lycodes lavalaei	0.088	0.169	0.572
Lumpenus lampretaeformis	0.493	0.559	0.279
Leptoclinus maculatus	0.416	0.609	0.639
Eumesogrammus praecisus	0.724	0.475	0.735
Anisarchus medius	0.346	0.423	0.821
Cancer irroratus	0.017	0.102	0.486
Hyas coarctatus	0.830	0.860	0.905
Chionoecetes opilio	0.830	0.890	0.440
Hyas araneus	0.931	0.798	0.738
Homarus americanus	0.406	0.827	0.312
Illex illecebrosus	0.468	0.612	0.627

Table 9. Relative evidence for size-aggregated binomial and beta-binomial models for catch counts based on Aikaike Information Criterion (AIC) and the Bayesian Information Criterion (BIC) values, and estimates of the conversion factor Rho, and approximate 95% confidence intervals, for catches in numbers and in weights for taxa for which length-disaggregated analyses were also undertaken. Recall that a single model was used for catch weights and thus AIC and BIC values are not shown.

Taxon	AIC			BIC			Rho (numbers)	Rho (weights)
	BI1	BB0	BB1	BI1	BB0	BB1		
Gadus morhua	1158	1157	1159	1164	1163	1168	0.26 (0.22-0.31)	0.29 (0.25-0.34)
Urophycis tenuis	280	278	280	284	282	286	0.28 (0.22-0.35)	0.31 (0.27-0.36)
Sebastes sp.	426	422	424	430	426	430	0.27 (0.20-0.36)	0.46 (0.39-0.55)
Hippoglossus hippoglossus	115	114	116	119	118	122	0.93 (0.58-1.48)	0.97 (0.51-1.87)
Reinhardtius hippoglossoides	149	148	150	152	152	156	0.66 (0.51-0.85)	0.78 (0.58-1.06)
Hippoglossoides platessoides	1523	1512	1506	1529	1518	1515	0.20 (0.17-0.24)	0.28 (0.26-0.31)
Glyptocephalus cynoglossus	164	163	165	168	167	170	0.39 (0.28-0.56)	0.58 (0.46-0.73)
Limanda ferruginea	707	701	702	712	706	709	0.42 (0.34-0.52)	0.44 (0.38-0.50)
Pseudopleuronectes americanus	611	612	614	616	616	620	0.3 0(0.24-0.38)	0.40 (0.36-0.44)
Clupea harengus	566	559	560	571	563	568	0.51 (0.38-0.70)	0.57 (0.39-0.83)
Alosa pseudoharengus	409	404	406	413	408	412	0.74 (0.54-1.02)	0.77 (0.61-0.97)
Osmerus mordax	401	397	398	404	401	404	0.65 (0.44-0.95)	0.79 (0.62-1.00)
Mallotus villosus	864	852	852	870	857	860	0.50 (0.39-0.63)	0.43 (0.36-0.52)
Scomber scombrus	542	540	542	547	545	550	0.40 (0.29-0.56)	1.41 (1.01-1.96)
Enchelyopus cimbrius	126	124	126	129	128	132	0.36 (0.23-0.56)	0.21 (0.15-0.29)
Amblyraja radiata	263	261	263	267	265	269	0.35 (0.25-0.49)	0.29 (0.22-0.39)
Myoxocephalus octodecemspinosus	266	267	269	271	271	275	0.14 (0.09-0.21)	0.19 (0.15-0.25)
Myoxocephalus scorpius	175	175	177	180	180	184	0.20 (0.15-0.28)	0.25 (0.19-0.33)
Gymnocanthus tricuspis	220	220	222	225	225	230	0.06 (0.04-0.10)	0.10 (0.08-0.12)
Triglops murrayi	176	178	180	181	183	187	0.08 (0.04-0.14)	0.08 (0.06-0.11)
Hemitripterus americanus	102	102	104	105	105	109	0.31 (0.21-0.46)	0.27 (0.18-0.38)
Aspidophoroides monopterygius	411	413	415	416	419	423	0.13 (0.09-0.20)	0.12 (0.10-0.15)
Leptagonus decagonus	115	115	117	118	118	122	0.31 (0.21-0.44)	0.31 (0.23-0.41)
Liparidae	102	101	103	105	104	108	0.40 (0.25-0.66)	0.13 (0.06-0.32)
Cyclopterus lumpus	50	49	51	52	52	56	0.18 (0.09-0.37)	0.15 (0.08-0.29)
Eumicrotremus spinosus	65	65	67	68	67	71	0.49 (0.28-0.86)	0.55 (0.33-0.92)
Ammodytes dubius	207	202	204	210	206	210	0.39 (0.25-0.62)	1.24 (0.59-2.63)
Lycodes lavalaei	167	165	167	171	169	173	0.34 (0.22-0.53)	0.30 (0.21-0.42)
Lumpenus lampretaeformis	53	53	55	56	56	59	1.70 (0.86-3.37)	1.17 (0.78-1.74)
Leptoclinus maculatus	164	163	165	168	167	170	3.47 (2.29-5.25)	3.12 (2.38-4.09)
Eumesogrammus praecisus	166	166	168	170	169	173	0.27 (0.17-0.45)	0.20 (0.12-0.31)
Anisarchus medius	151	149	151	153	151	155	1.26 (0.70-2.26)	1.86 (1.21-2.85)
Cancer irroratus	151	150	152	155	154	157	1.83 (1.15-2.92)	1.69 (1.08-2.64)
Hyas coarctatus	435	431	433	441	437	441	2.15 (1.63-2.83)	3.11 (2.3-4.20)
Chionoecetes opilio	925	914	913	930	920	922	1.31 (1.11-1.54)	0.95 (0.83-1.08)
Hyas araneus	199	195	197	204	200	204	0.92 (0.61-1.39)	1.35 (0.87-2.09)

Taxon	AIC			BIC			Rho (numbers)	Rho (weights)
	BI1	BB0	BB1	BI1	BB0	BB1		
Homarus americanus	622	620	622	627	624	628	0.67 (0.53-0.84)	0.76 (0.65-0.89)
Illex illecebrosus	197	195	197	201	199	203	0.51 (0.37-0.70)	0.61 (0.45-0.81)

Table 10. Relative evidence for size-aggregated binomial and beta-binomial models for catch counts based on Aikaike's Information Criterion (AIC) and the Bayesian Information Criterion (BIC) values, and estimates of the conversion factor Rho, and approximate 95% confidence intervals, for catches in numbers and in weights for taxa for which only size-aggregated analyses were also undertaken. Recall that a single model was used for catch weights and thus AIC and BIC values are not shown. Entries with 'NC' indicate models that did not converge.

Taxon	AIC			BIC			Rho (numbers)	Rho (weights)
	BI1	BB0	BB1	BI1	BB0	BB1		
Merluccius bilinearis	61	61	63	63	63	66	0.38 (0.24-0.61)	0.45 (0.28-0.73)
Anarhichas lupus	42	42	44	43	43	46	0.96 (0.43-2.11)	1.05 (0.43-2.55)
Alosa sapidissima	63	62	64	65	64	67	1.31 (0.61-2.84)	4.24 (1.86-9.70)
Gadus macrocephalus	45	46	48	47	48	51	0.04 (0.00-0.64)	0.19 (0.09-0.38)
Tautogolabrus adspersus	80	80	82	82	82	85	0.16 (0.04-0.65)	0.18 (0.09-0.39)
Scophthalmus aquosus	124	124	126	126	126	129	0.24 (0.19-0.03)	0.30 (0.26-0.35)
Malacoraja senta	64	64	66	67	67	70	0.26 (0.18-0.38)	0.24 (0.15-0.38)
Myxine limosa	51	51	NC	52	52	NC	0.58 (0.40-0.85)	0.50 (0.39-0.63)
Artediellus sp.	92	90	92	95	93	96	0.70 (0.38-1.28)	0.51 (0.31-0.82)
Icelus spatula	28	30	32	29	31	34	0 (0.00-0.04)	0.15 (0.05-0.45)
Gasterosteus aculeatus	70	70	72	72	72	75	0.65 (0.35-1.23)	0.26 (0.14-0.47)
Nezumia bairdii	75	75	77	77	77	80	0.07 (0.05-0.10)	0.07 (0.05-0.10)
Zoarces americanus	34	34	36	36	36	39	0.10 (0.04-0.24)	0.06 (0.03-0.13)
Arctozenus risso	53	53	55	55	54	57	0.58 (0.32-1.04)	0.57 (0.38-0.87)
Rajidae eggs	-	-	-	-	-	-	-	1.05 (0.61-1.83)
Buccinidae eggs	-	-	-	-	-	-	-	1.56 (0.90-2.71)
Gastropoda eggs	-	-	-	-	-	-	-	0.70 (0.36-1.34)
Tunicata (s.p.)	-	-	-	-	-	-	-	1.63 (0.86-3.12)
Ascidia	-	-	-	-	-	-	-	10.55 (4.50-24.74)
Boltenia sp.	-	-	-	-	-	-	-	1.69 (1.28-2.21)
Halocynthia pyriformis	-	-	-	-	-	-	-	2.21 (0.72-6.71)
Bryozoa (p.)	-	-	-	-	-	-	-	11.56 (7.54-17.7)
Decapod shrimp	-	-	-	-	-	-	-	0.52 (0.46-0.60)
Anonyx sp.	-	-	-	-	-	-	-	3.36 (1.86-6.08)
Annelida (p.)	-	-	-	-	-	-	-	2.05 (1.48-2.83)
Aphrodita hastata	-	-	-	-	-	-	-	3.76 (2.19-6.48)
Buccinum sp.	-	-	-	-	-	-	-	5.24 (3.56-7.72)
Neptunea decemcostata	-	-	-	-	-	-	-	3.27 (1.66-6.43)
Chlamys islandica	-	-	-	-	-	-	-	3.53 (1.16-10.76)
Ciliatocardium ciliatum	-	-	-	-	-	-	-	0.58 (0.22-1.56)
Mollusca sp. empty	-	-	-	-	-	-	-	2.98 (2.38-3.74)
Nudibranchia (o.)	-	-	-	-	-	-	-	1.12 (0.77-1.64)

Taxon	AIC			BIC			Rho (numbers)	Rho (weights)
	BI1	BB0	BB1	BI1	BB0	BB1		
Semirossia tenera	-	-	-	-	-	-	-	0.19 (0.08-0.46)
Bathypolypus arcticus	-	-	-	-	-	-	-	1.38 (0.78-2.42)
Pycnogonida	-	-	-	-	-	-	-	0.87 (0.53-1.43)
Asterias sp.	-	-	-	-	-	-	-	0.49 (0.17-1.41)
Asterias rubens	-	-	-	-	-	-	-	0.68 (0.09-4.95)
Leptasterias (Hexasterias) polaris	-	-	-	-	-	-	-	5.66 (3.13-10.23)
Leptasterias sp.	-	-	-	-	-	-	-	13.97 (1.93-101.35)
Ctenodiscus crispatus	-	-	-	-	-	-	-	0.97 (0.67-1.41)
Hippasteria phrygiana	-	-	-	-	-	-	-	1.87 (1.02-3.44)
Henricia sp.	-	-	-	-	-	-	-	0.26 (0.10-0.69)
Henricia sanguinolenta	-	-	-	-	-	-	-	2.45 (1.72-3.49)
Solaster endeca	-	-	-	-	-	-	-	1.76 (0.85-3.65)
Crossaster papposus	-	-	-	-	-	-	-	1.82 (1.43-2.31)
Pteraster militaris	-	-	-	-	-	-	-	1.12 (0.46-2.73)
Ophiuroidea (c.)	-	-	-	-	-	-	-	3.38 (2.51-4.55)
Euryalida (f.)	-	-	-	-	-	-	-	1.45 (1.12-1.88)
Strongylocentrotus sp.	-	-	-	-	-	-	-	3.17 (2.49-4.03)
Clypeasteroida (o.)	-	-	-	-	-	-	-	1.41 (0.99-2.01)
Holothuroidea (c.)	-	-	-	-	-	-	-	1.67 (1.15-2.44)
Psolus fabricii	-	-	-	-	-	-	-	8.73 (3.95-19.3)
Psolus phantapus	-	-	-	-	-	-	-	1.66 (0.70-3.95)
Actiniaria (o.)	-	-	-	-	-	-	-	4.04 (1.60-10.23)
Anthozoa (c.)	-	-	-	-	-	-	-	0.71 (0.42-1.20)
Stomphia coccinea	-	-	-	-	-	-	-	0.70 (0.26-1.90)
Pennatulacea	-	-	-	-	-	-	-	5.30 (2.27-12.35)
Gersemia rubiformis	-	-	-	-	-	-	-	2.40 (1.63-3.53)
Soft coral unidentified	-	-	-	-	-	-	-	0.76 (0.27-2.11)
Pseudarchaster parelii	-	-	-	-	-	-	-	3.98 (2.27-7)
Ptilella grandis	-	-	-	-	-	-	-	2.66 (1.47-4.79)
Hydrozoa (c.)	-	-	-	-	-	-	-	16.93 (9.94-28.86)
Scyphozoa (c.)	-	-	-	-	-	-	-	0.25 (0.21-0.31)
Porifera (other)	-	-	-	-	-	-	-	1.98 (1.16-3.37)
Suberites ficus	-	-	-	-	-	-	-	2.30 (0.82-6.44)
Mycale (Mycale) lingua	-	-	-	-	-	-	-	2.32 (1.20-4.48)
Cladocroce spatula	-	-	-	-	-	-	-	3.36 (1.74-6.49)
Semisuberites cribrosa	-	-	-	-	-	-	-	2.40 (0.97-5.97)

8. FIGURES

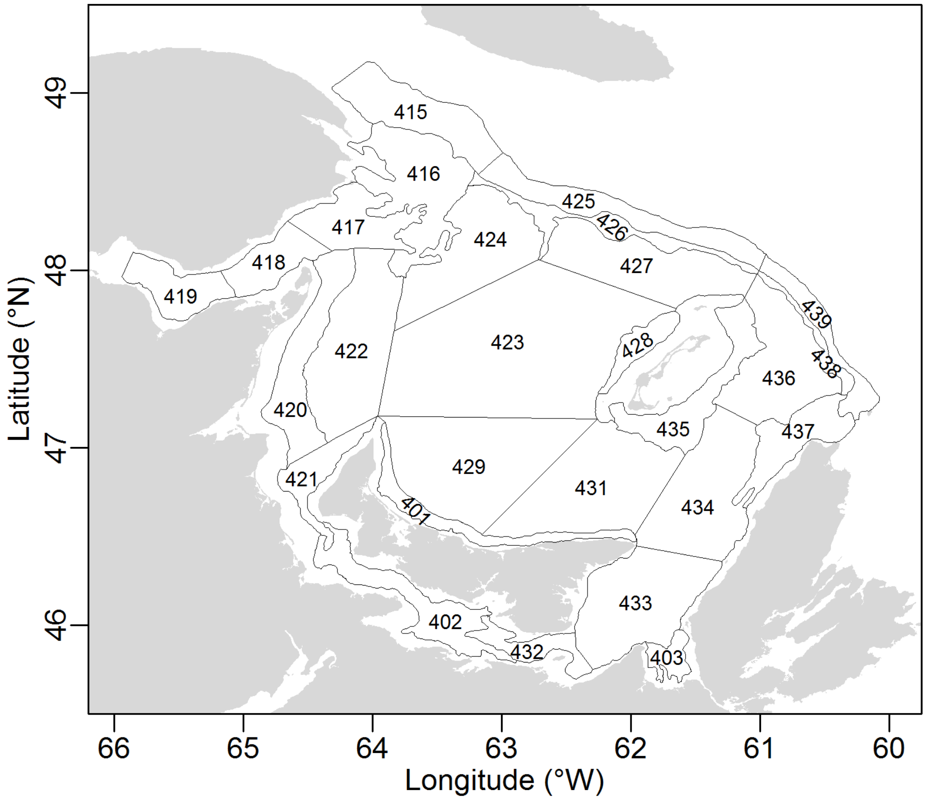

Figure 1. Stratification scheme for the southern Gulf of St. Lawrence multi-species bottom-trawl survey.

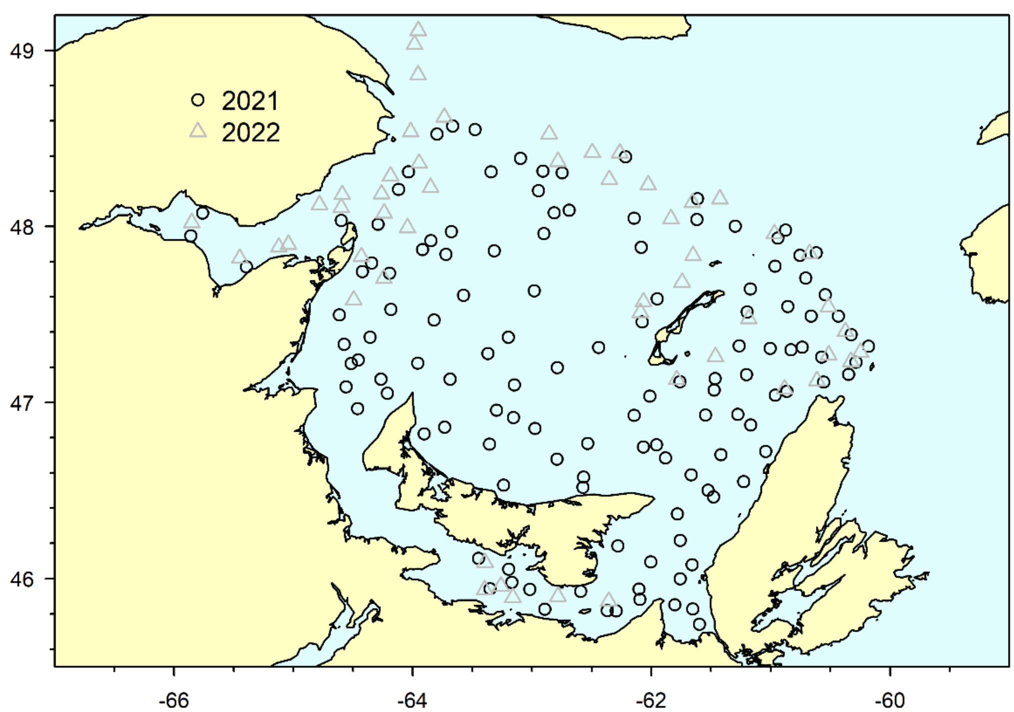

Figure 2. Location of comparative fishing set pairs fished in 2021 and in 2022.

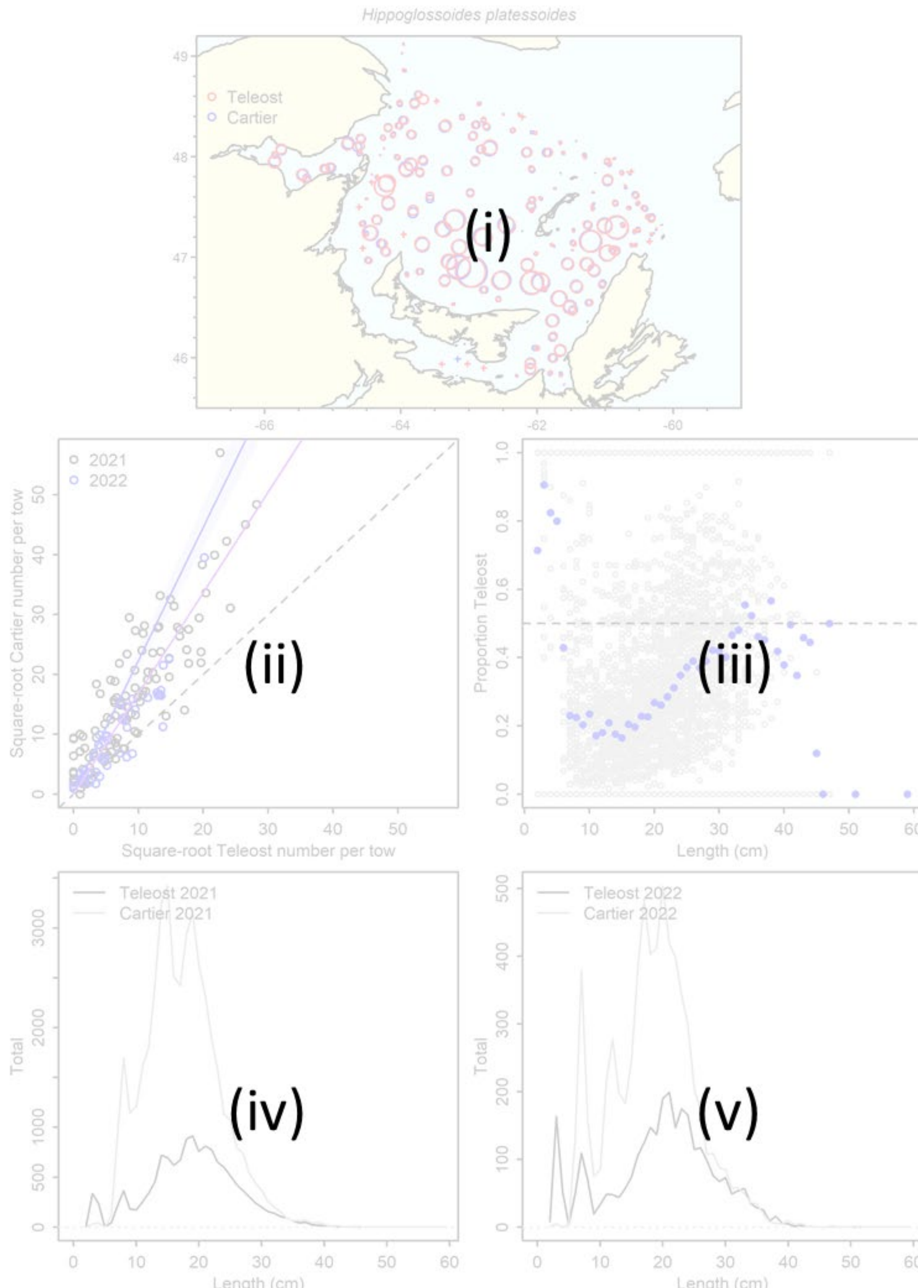

Figure 3. Interpretation for the first of three sets of figures presenting the data and results for taxa for which length-disaggregated analyses were undertaken. (i) Presents a map of catches by the CCGS Teleost (red circles) and by the CCGS Capt. Jacques Cartier (blue circles) in comparative fishing sets, where circle size is proportional to the square root of the number caught and nil catches are indicated by +. (ii) Biplot of the square-root of CCGS Capt. Jacques Cartier catch numbers against the square-root of CCGS Teleost catch numbers, where the blue line and shaded interval show the estimated conversion and approximate 95%CI from the best length-aggregated model, and the purple line shows the estimated length-independent conversion and approximate 95%CI from the best length-based model. (iii) Plot of the empirical proportion of total catch in a pair made by the CCGS Teleost as a function of length for each set pair (grey dots) and averaged across set pairs in each length interval (blue dots). (iv) Total length frequencies for catches made by the CCGS Teleost (black line) and by the CCGS Capt. Jacques Cartier (grey line) in 2021. (v) Same as (iv) except for 2022.

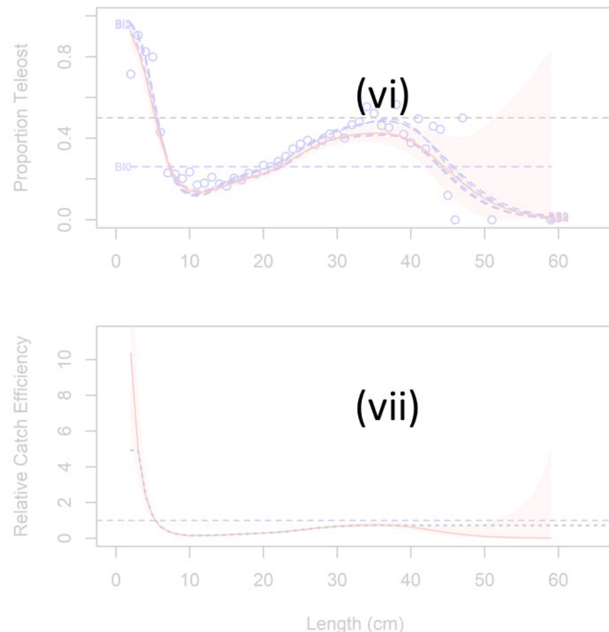

Figure 4. Interpretation for the second of three sets of figures presenting the data and results for taxa for which length-disaggregated analyses were undertaken. (vi) Estimated length-specific catch proportion functions, $logit(p_{Ai}(l))$, for each converged model, with the selected model plotted using a red line along with its approximate 95% CI (shaded area), as well as the length class-specific mean empirical proportion of total catch in a pair made by the CCGS Teleost (blue dots). (vii) Estimated relative catch efficiency (conversion factor) function from the best model (with 95% CI). The horizontal dashed blue line indicates equivalent efficiency between vessels and the dotted black line indicates the relative catch efficiency function that assumes a constant efficiency at small and large sizes.

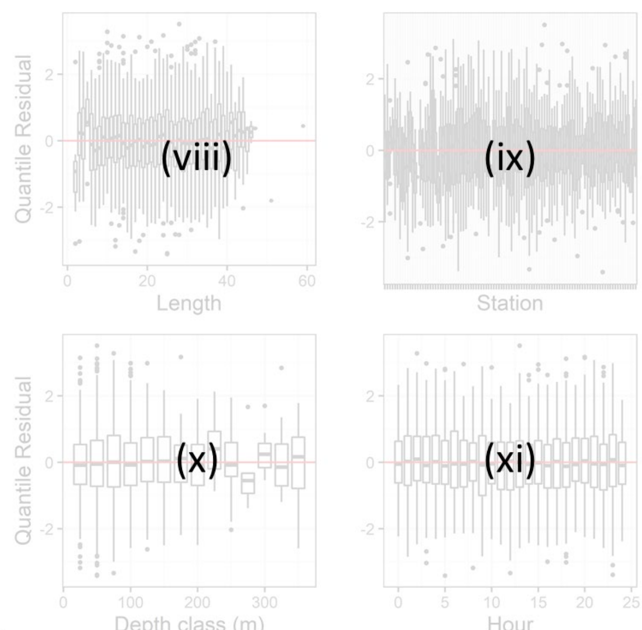

Figure 5. Interpretation for the third of three sets of figures presenting the data and results for taxa for which length-disaggregated analyses were undertaken. Boxplot of normalized quantile residuals as a function of (viii) length, (ix) station, (x) depth class, and (xi) hour.

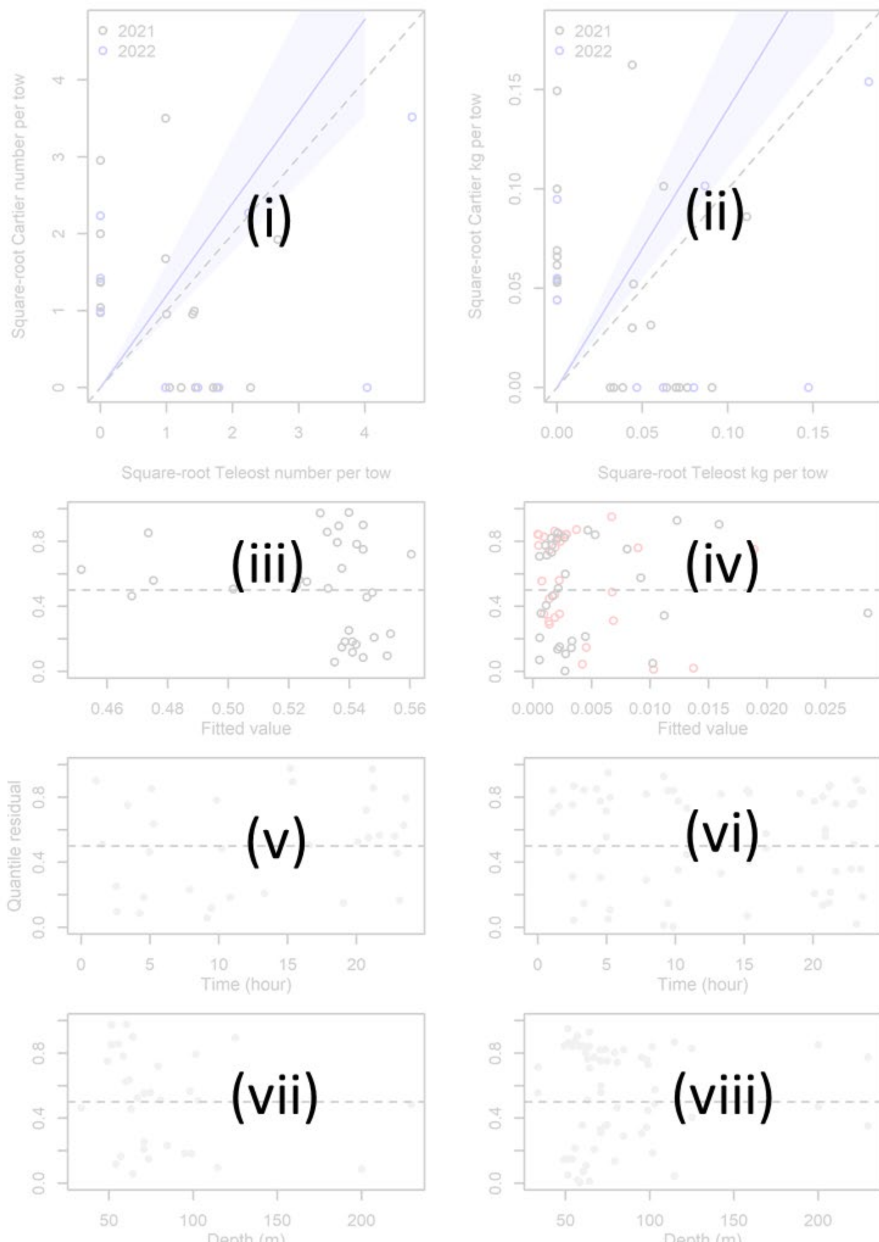

Figure 6. Interpretation for the figures presenting the data and results for taxa for which size-aggregated analyses were undertaken. (i) Biplot of the square-root of CCGS Capt. Jacques Cartier catch numbers against the square-root of CCGS Teleost catch numbers, where the blue line and shaded interval show the estimated conversion and approximate 95% CI from the best size-aggregated model, and where the pairs made in 2021 and 2022 are distinguished by colour. (ii) As in (i), except for catch weights. Quantile residuals from the analysis of catch numbers are plotted as a function of (iii) fitted values, and the (v) time and (vii) depth of the paired set, where values are coloured according to the same scheme as in panel (i). Similarly, quantile residuals from the analysis of catch weights are plotted as a function of (iv) fitted values, with values for the CCGS Teleost plotted with red circles and those for the CCGS Capt. Jacques Cartier in black, and the (vi) time and (viii) depth of the paired set, again where values are coloured according to the same scheme as in panel (i). Note that for taxa that are not measured, only panels (ii), (iv), (vi) and (viii) are shown.

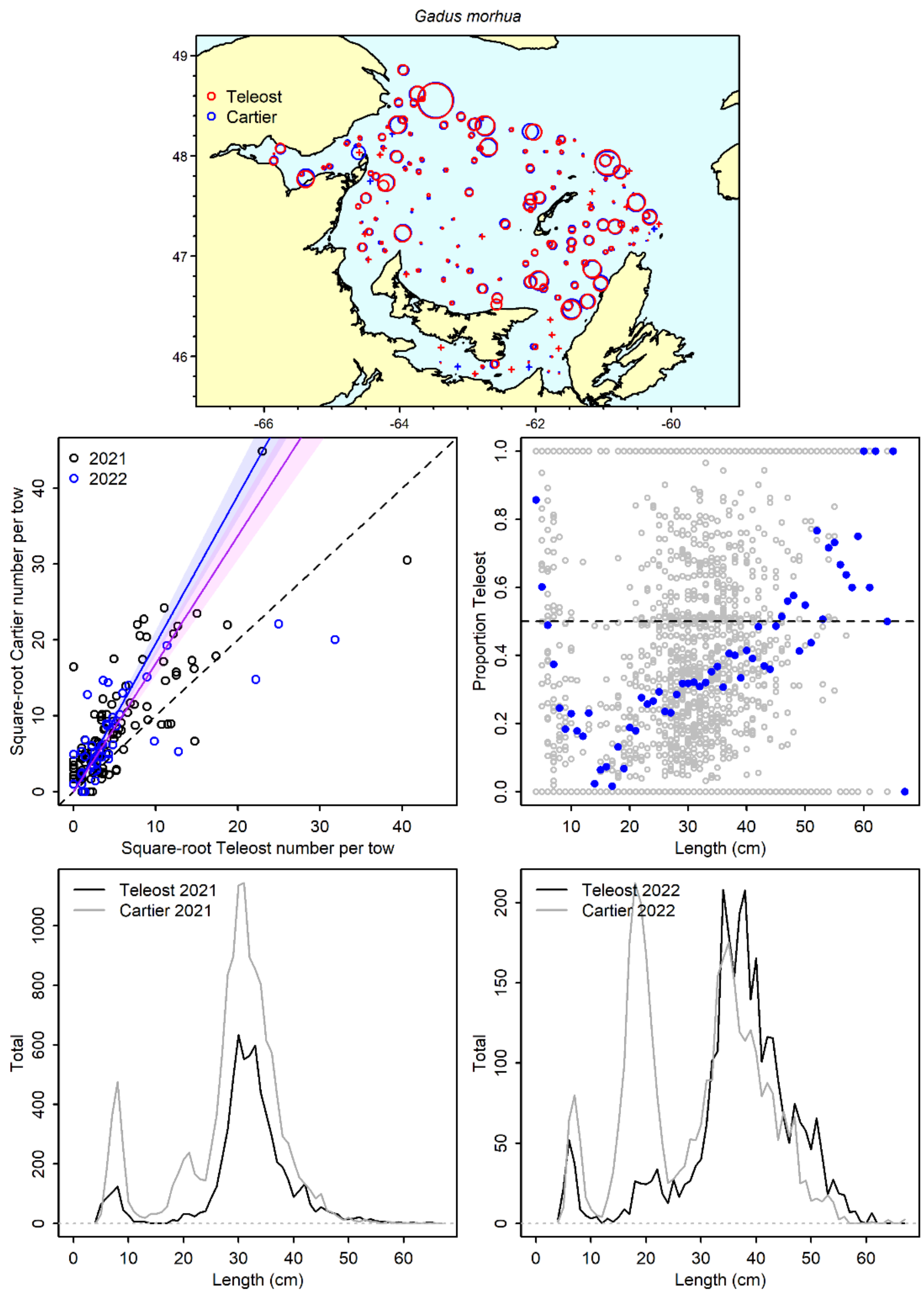

Figure 7a. Visualisation of comparative fishing data and size-aggregated model predictions for Gadus morhua*.*

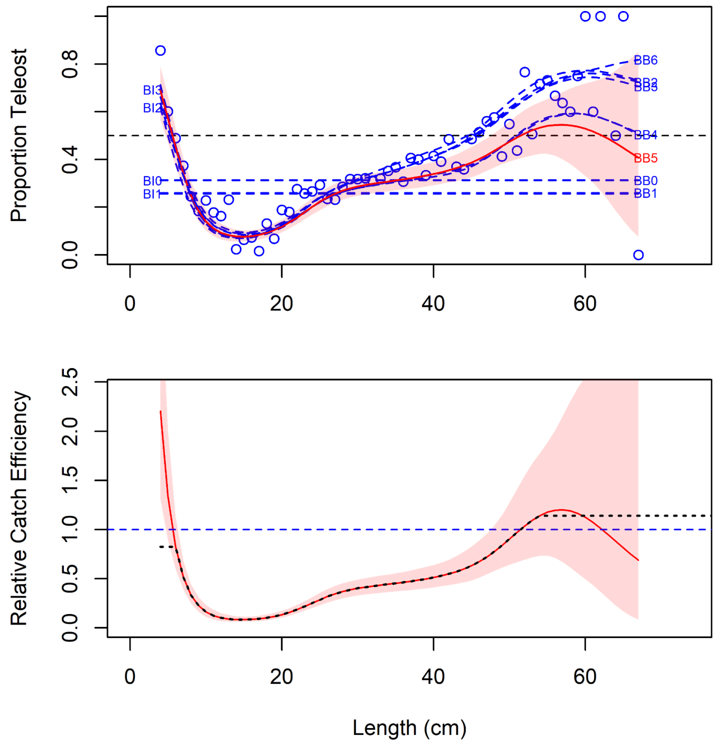

Figure 7b. Model fits and the selected length-based calibration for Gadus morhua*.*

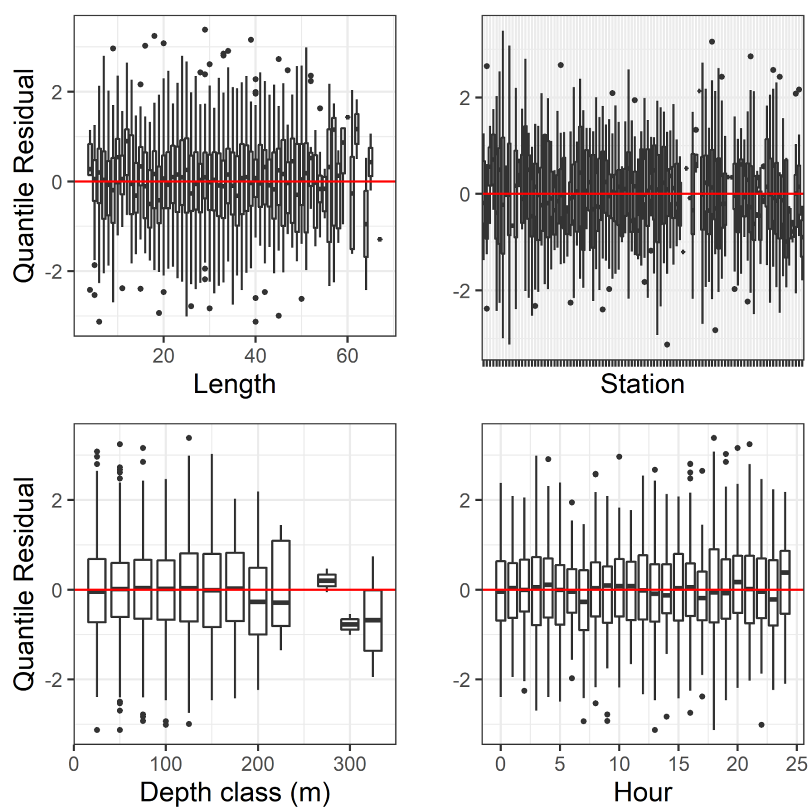

Figure 7c. Normalized quantile residuals for the selected model for Gadus morhua*.*

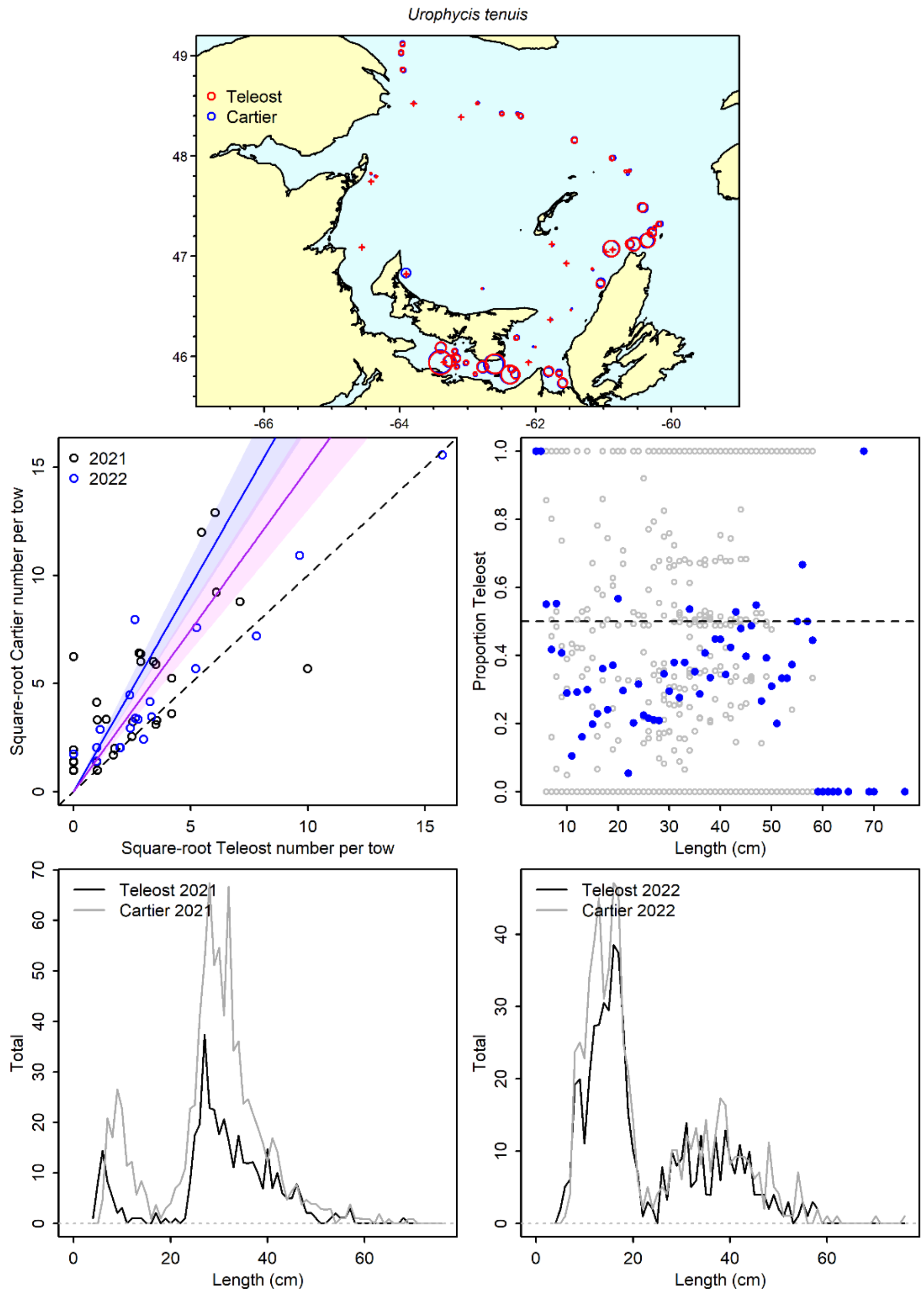

Figure 8a. Visualisation of comparative fishing data and size-aggregated model predictions for Urophycis tenuis*.*

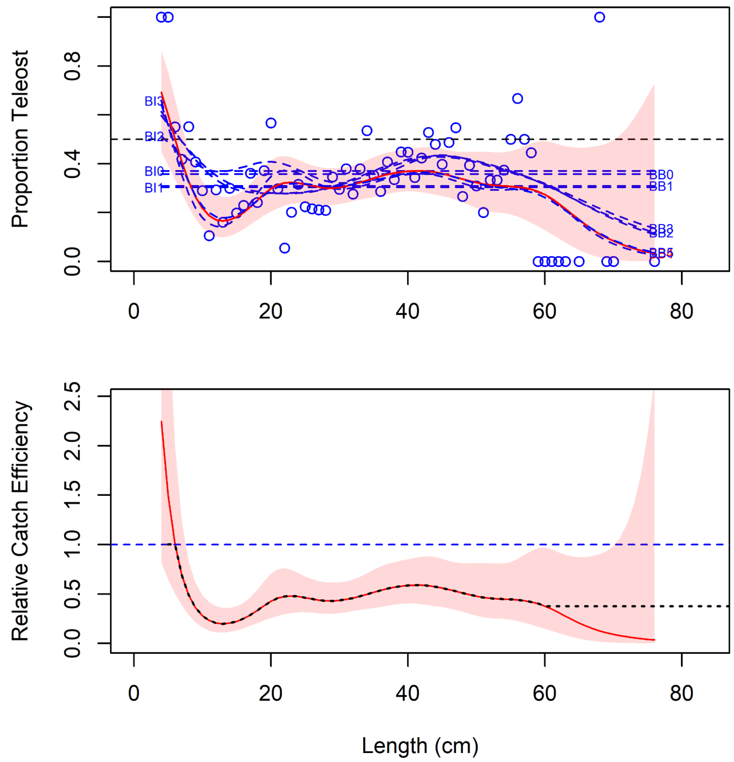

Figure 8b. Model fits and the selected length-based calibration for Urophycis tenuis.

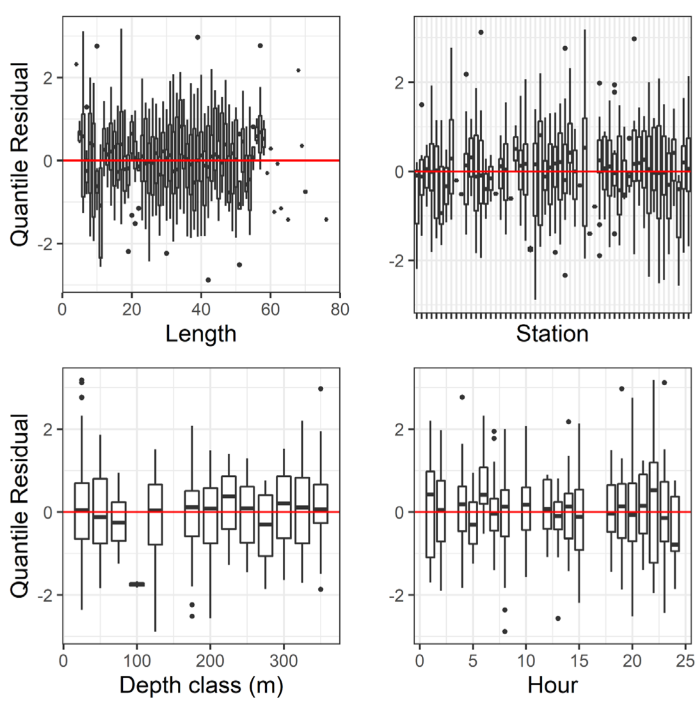

Figure 8c. Normalized quantile residuals for the selected model for Urophycis tenuis.

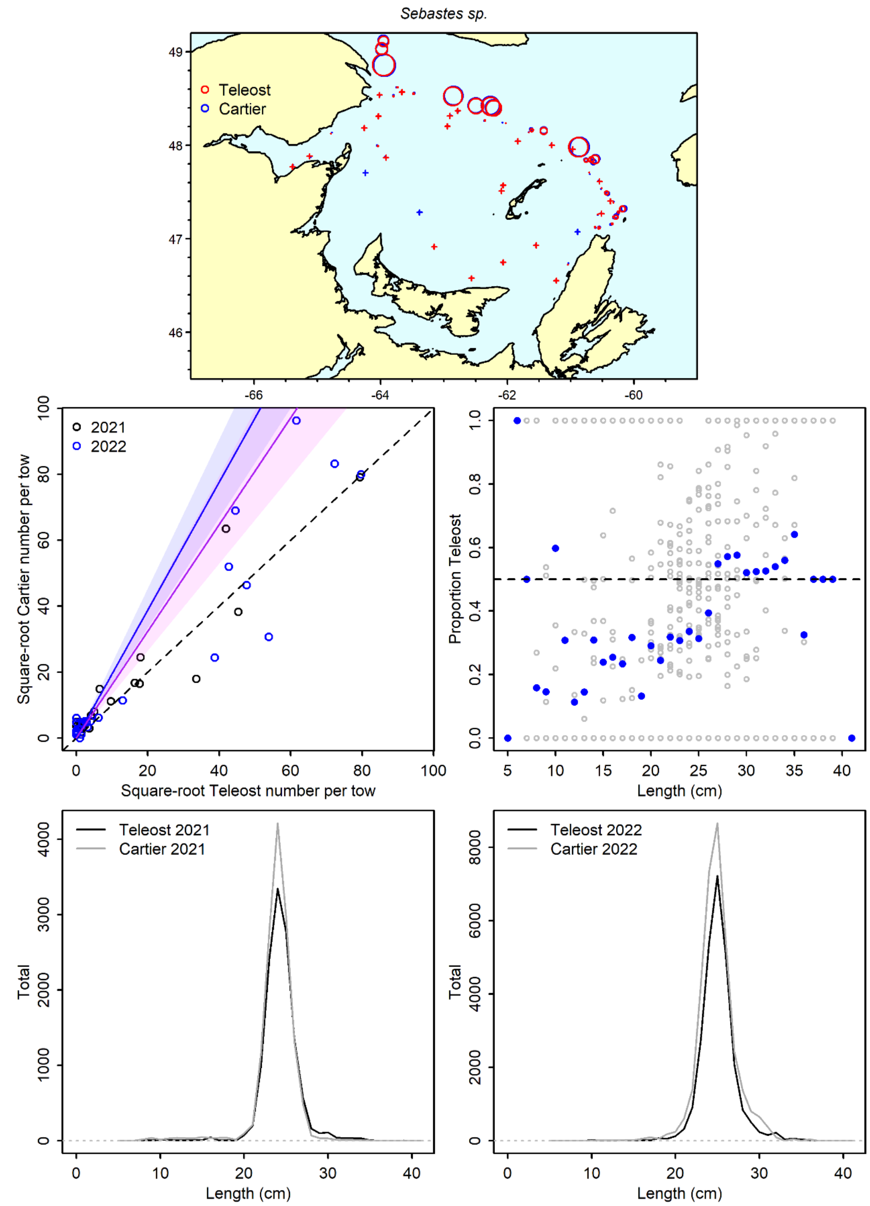

Figure 9a. Visualisation of comparative fishing data and size-aggregated model predictions for Sebastes sp..

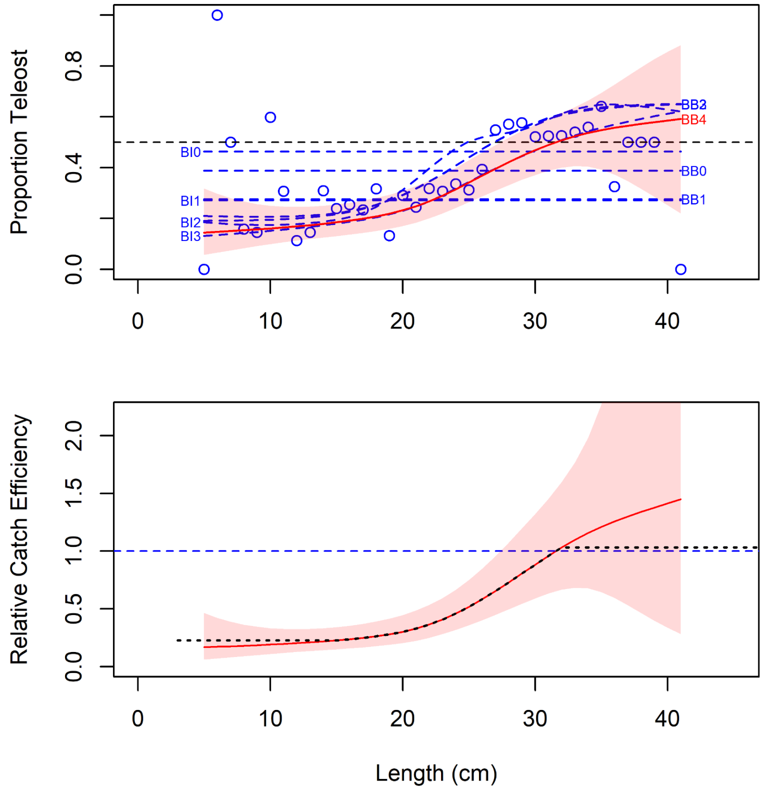

Figure 9b. Model fits and the selected length-based calibration for Sebastes sp..

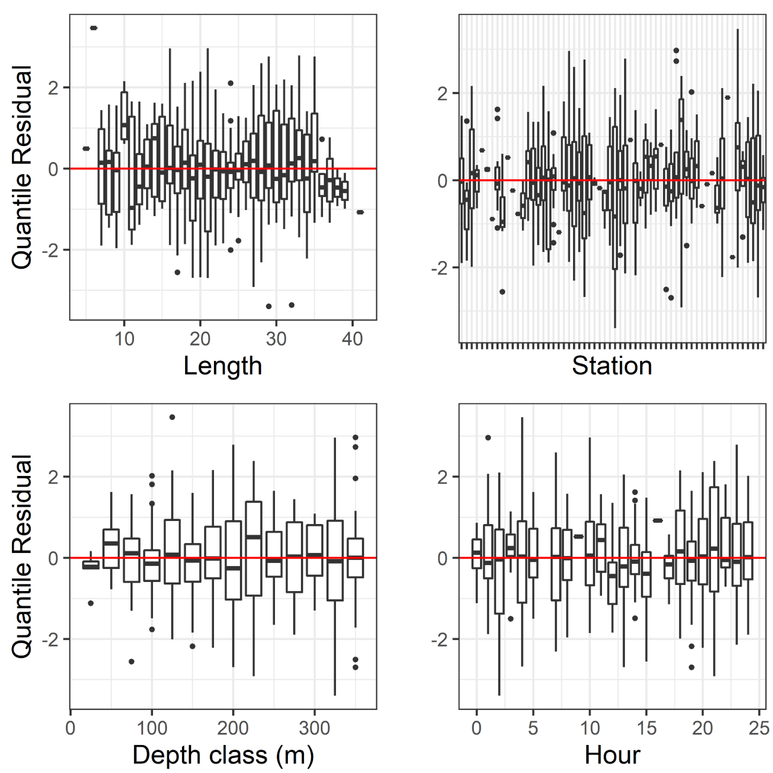

Figure 9c. Normalized quantile residuals for the selected model for Sebastes sp..

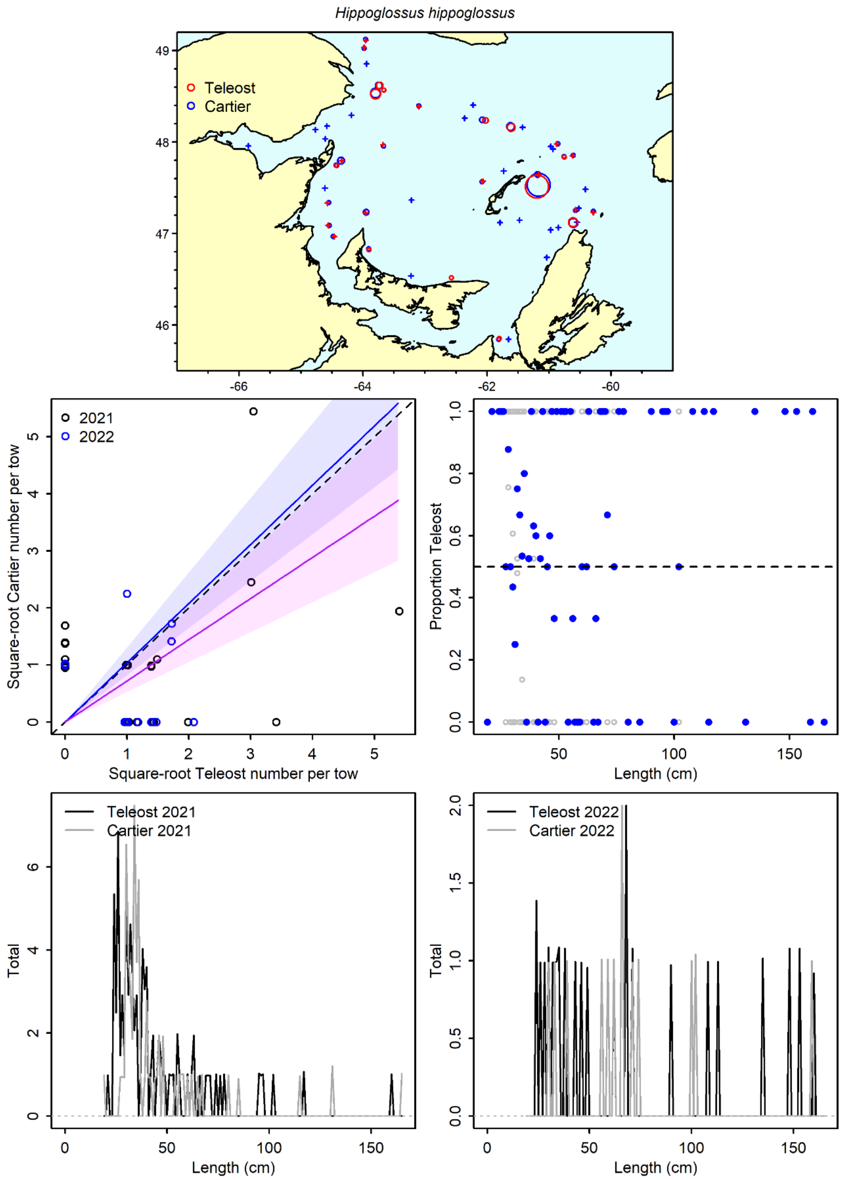

Figure 10a. Visualisation of comparative fishing data and size-aggregated model predictions for Hippoglossus hippoglossus*.*

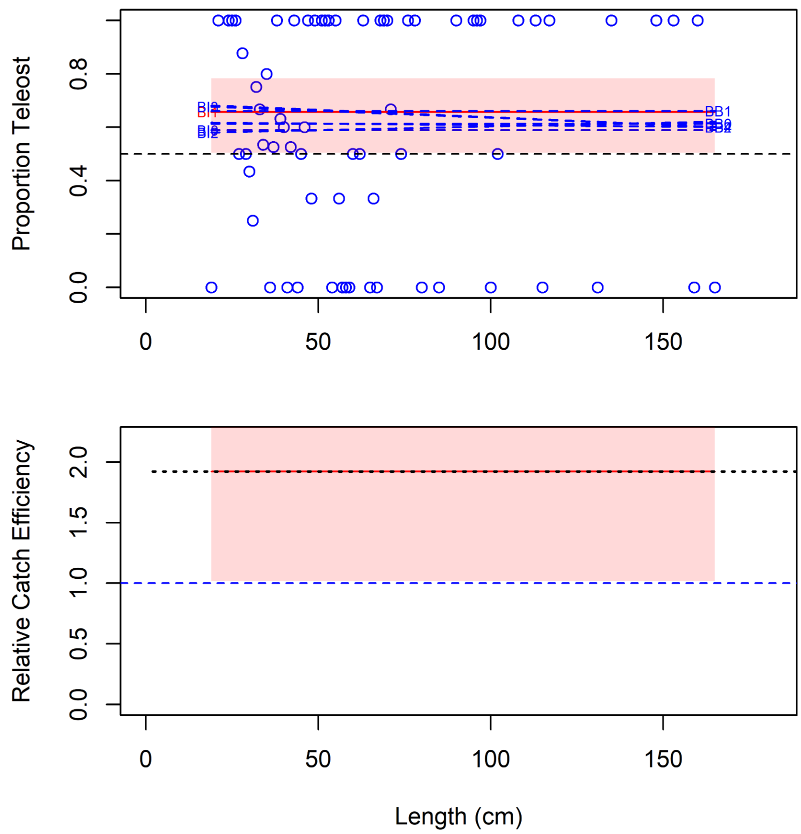

Figure 10b. Model fits and the selected length-based calibration for Hippoglossus hippoglossus.

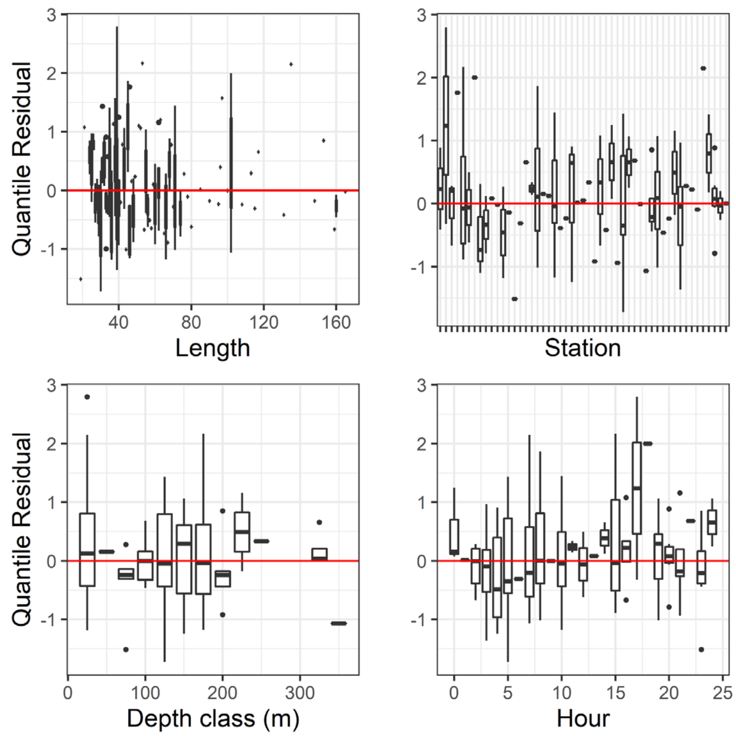

Figure 10c. Normalized quantile residuals for the selected model for Hippoglossus hippoglossus.

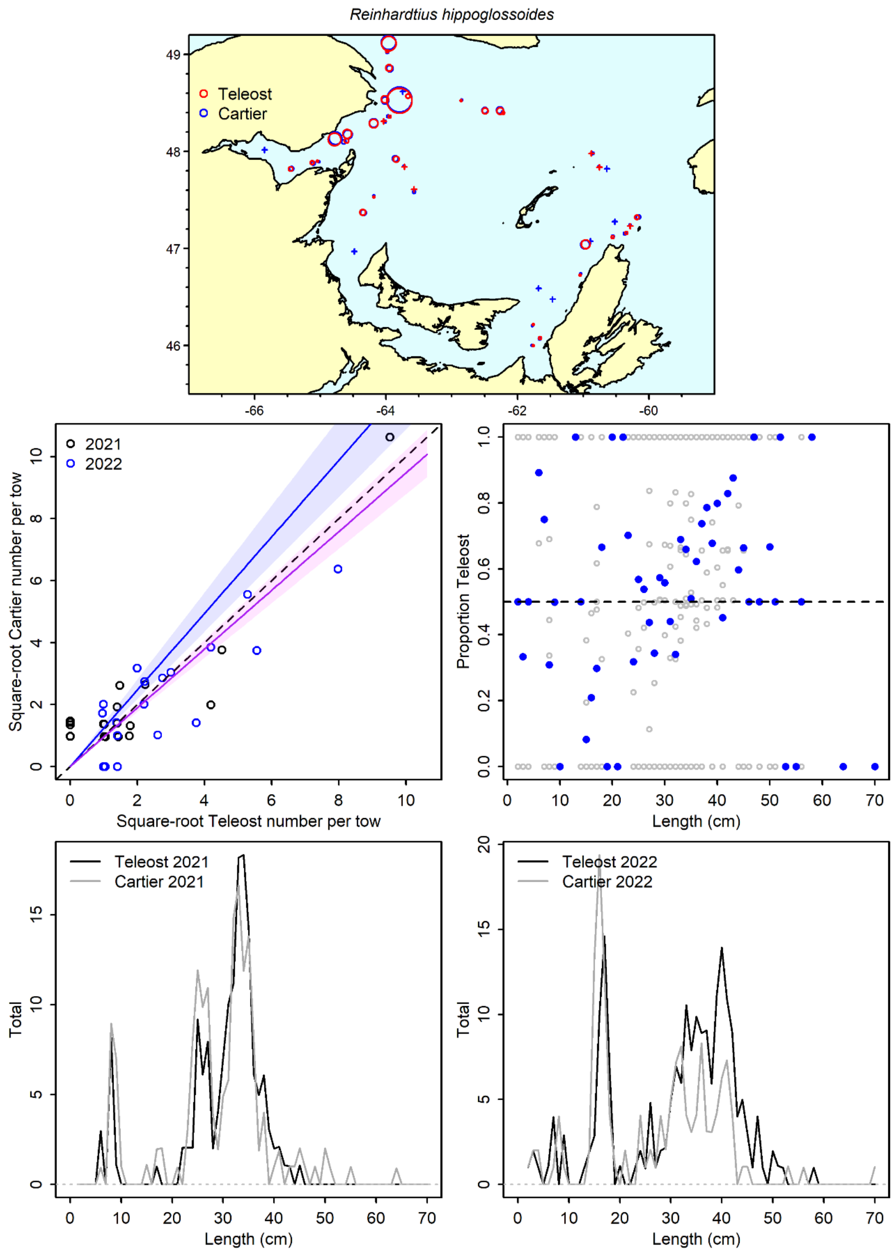

Figure 11a. Visualisation of comparative fishing data and size-aggregated model predictions for Reinhardtius hippoglossoides*.*

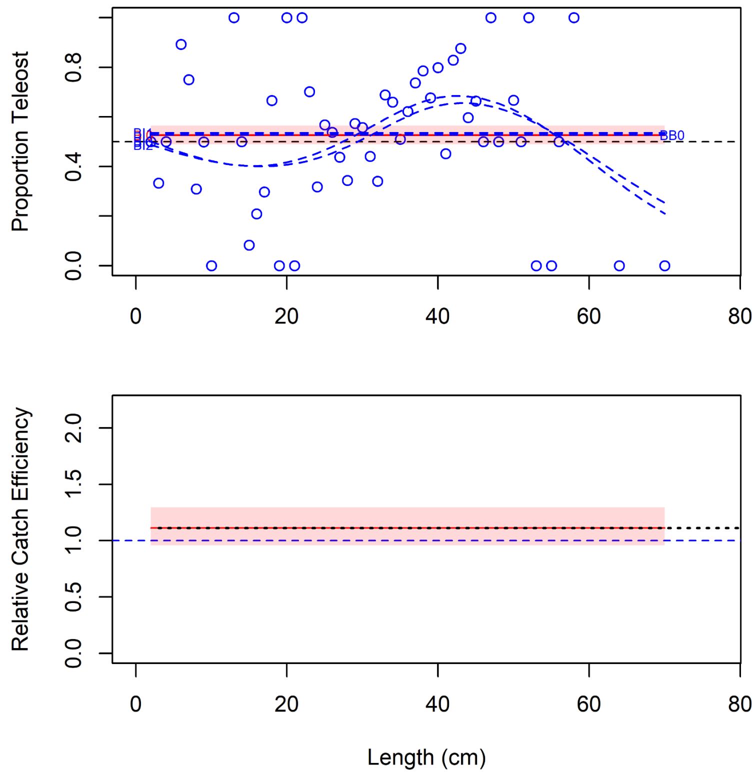

Figure 11b. Model fits and the selected length-based calibration for Reinhardtius hippoglossoides.

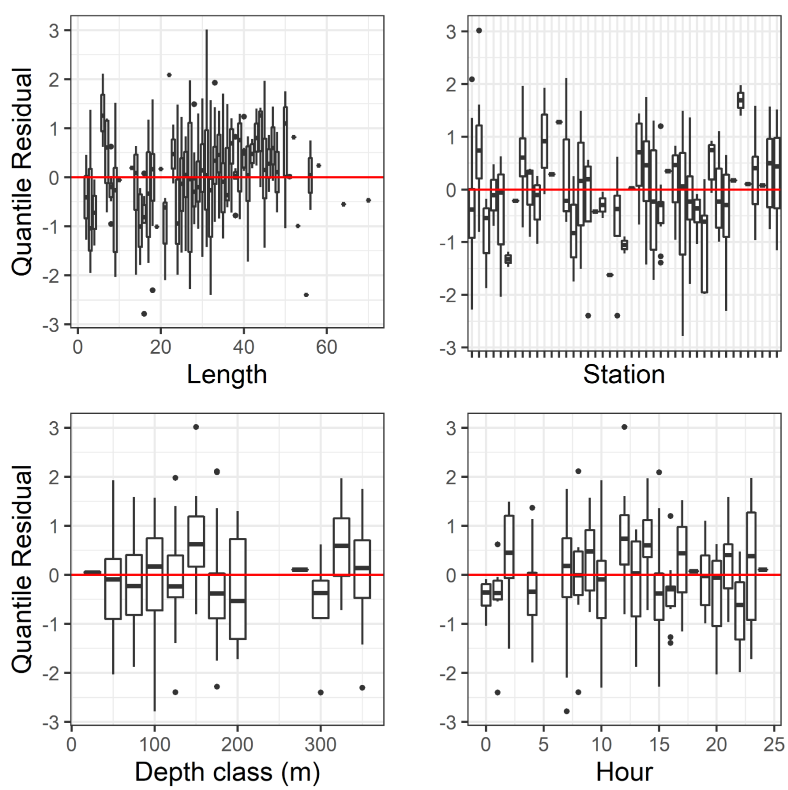

Figure 11c. Normalized quantile residuals for the selected model for Reinhardtius hippoglossoides.

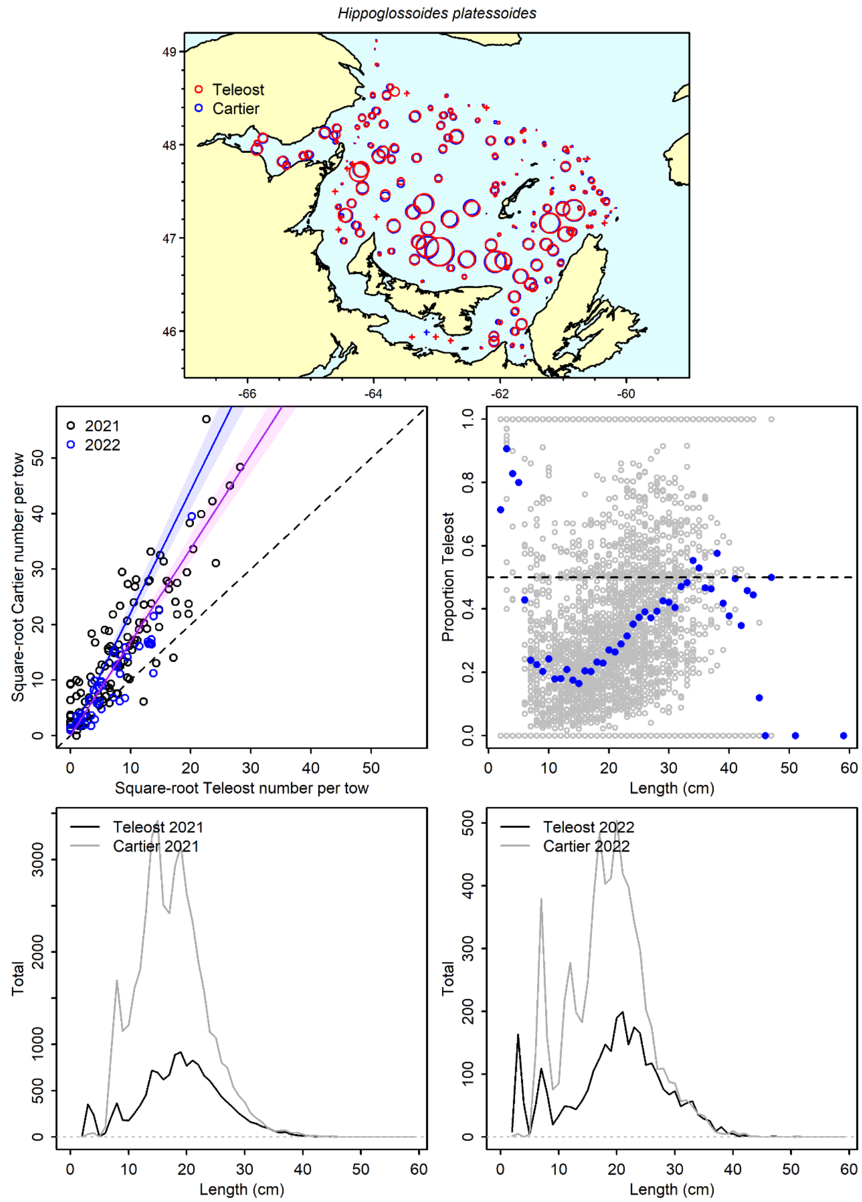

Figure 12a. Visualisation of comparative fishing data and size-aggregated model predictions for Hippoglossoides platessoides.

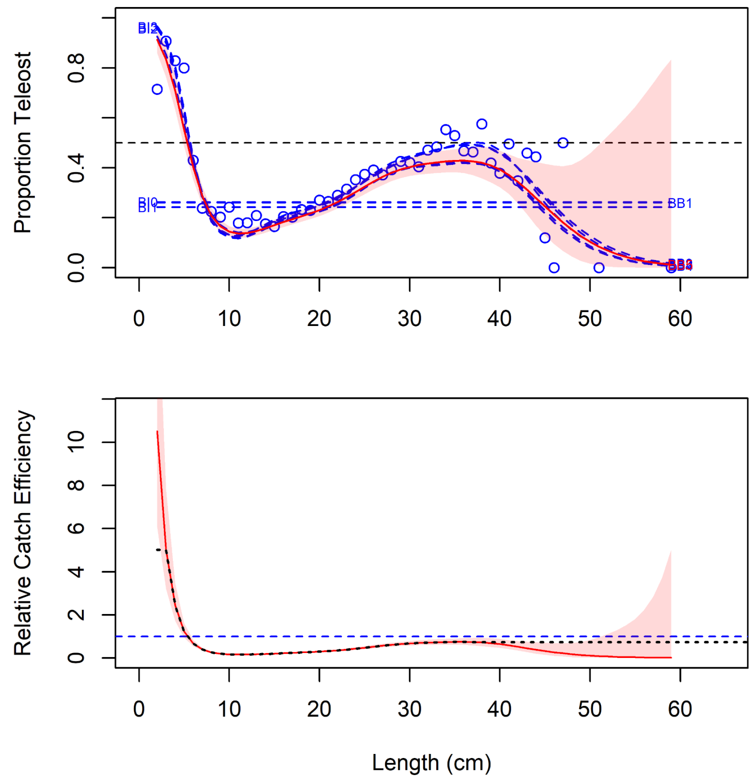

Figure 12b. Model fits and the selected length-based calibration for Hippoglossoides platessoides*.*

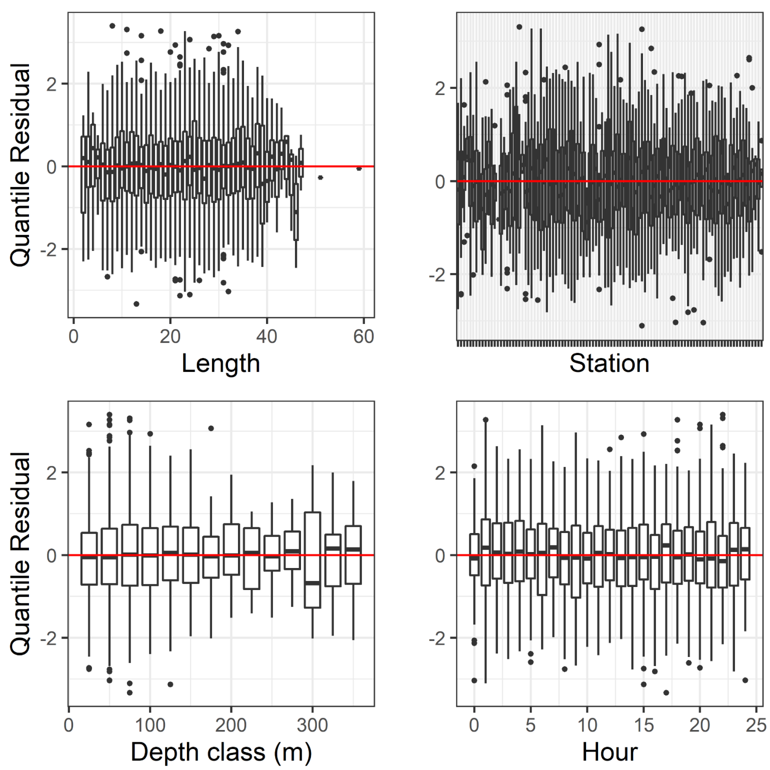

Figure 12c. Normalized quantile residuals for the selected model for Hippoglossoides platessoides*.*

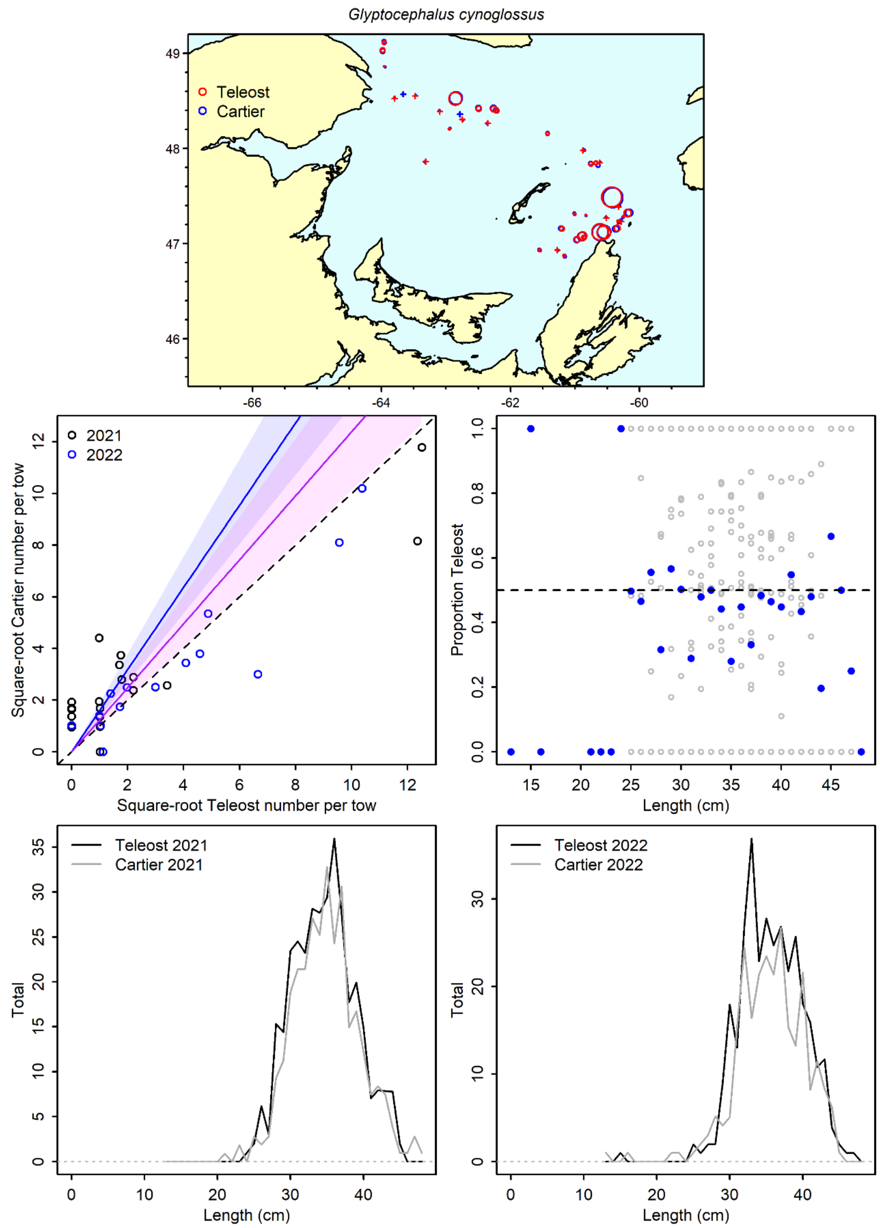

Figure 13a. Visualisation of comparative fishing data and size-aggregated model predictions for Glyptocephalus cynoglossus.

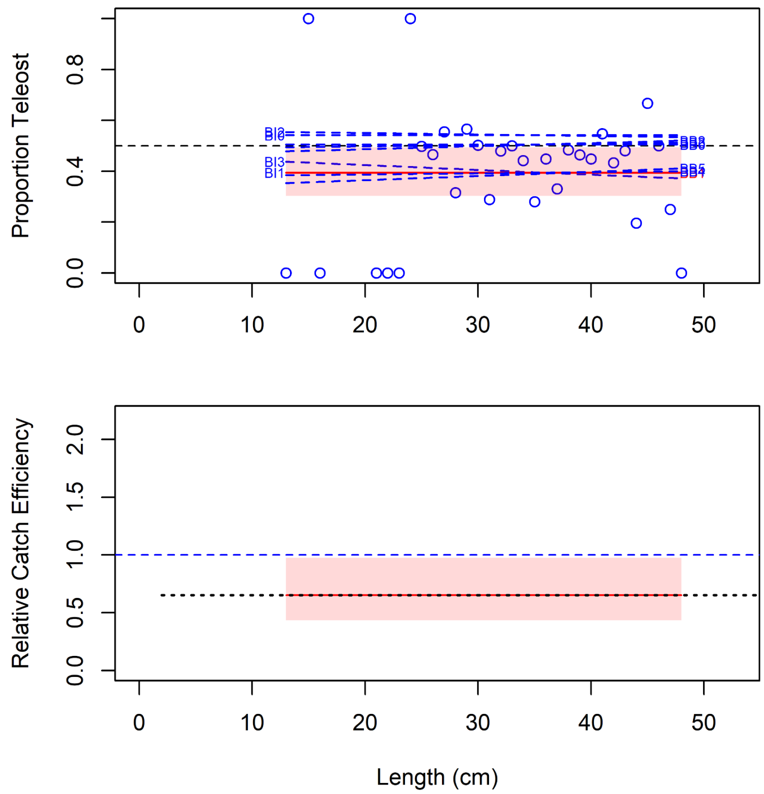

Figure 13b. Model fits and the selected length-based calibration for Glyptocephalus cynoglossus*.*

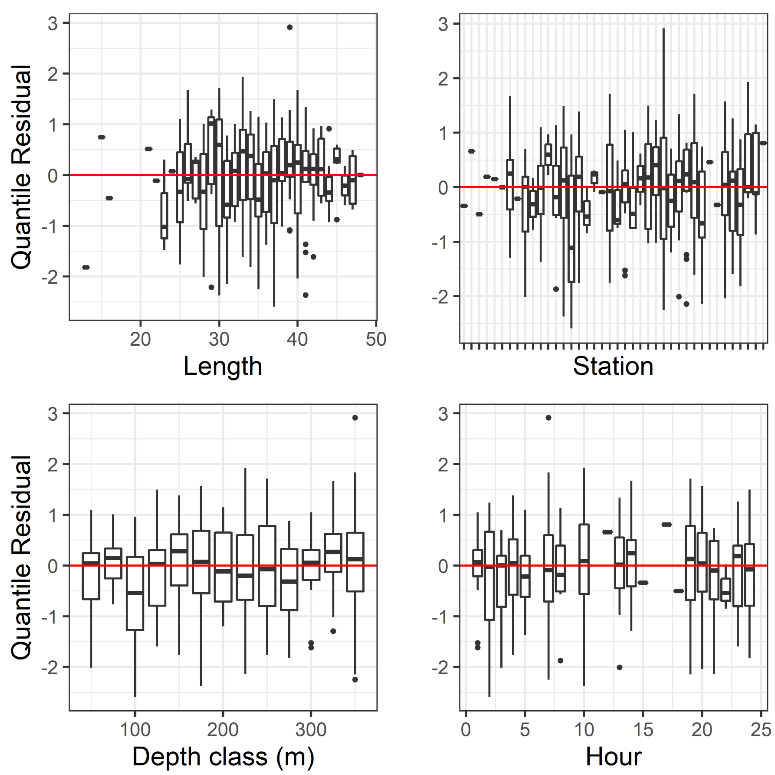

Figure 13c. Normalized quantile residuals for the selected model for Glyptocephalus cynoglossus*.*

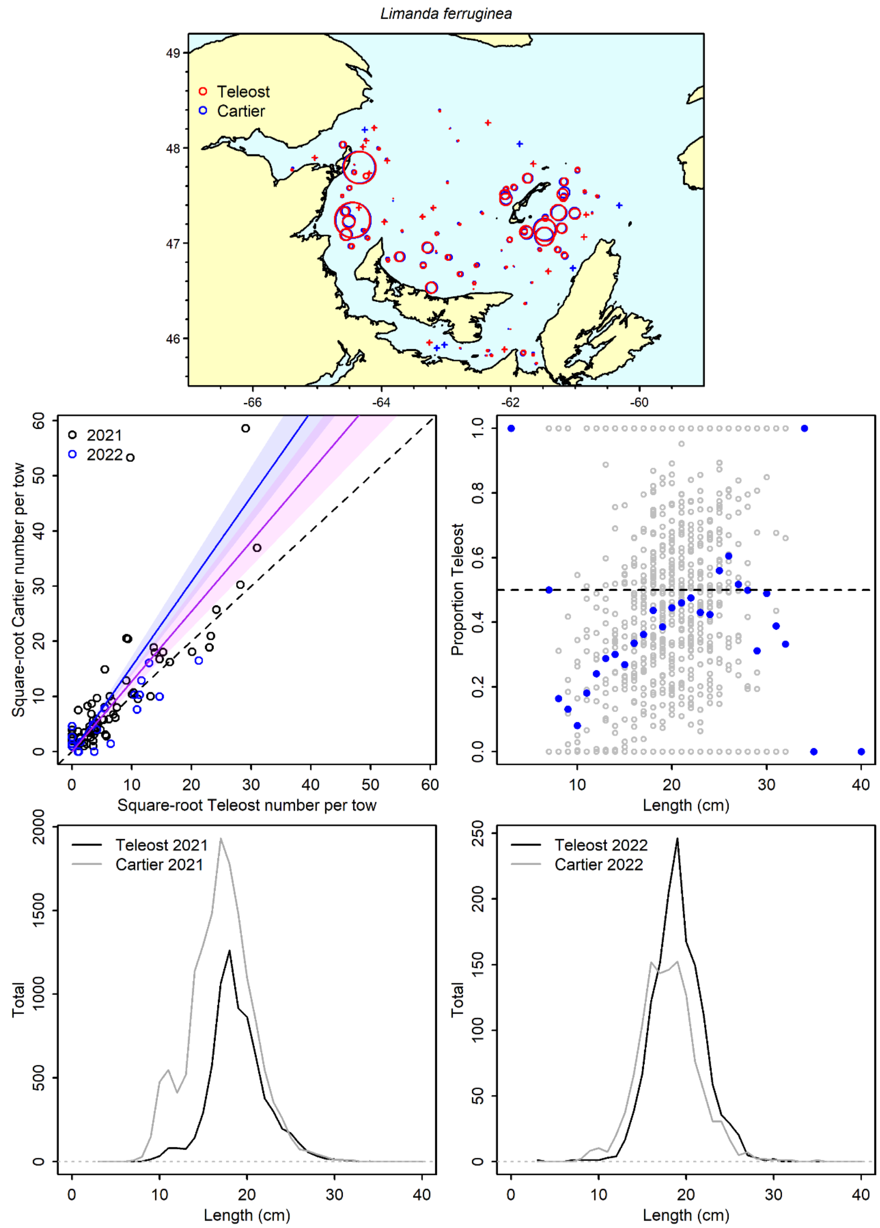

Figure 14a. Visualisation of comparative fishing data and size-aggregated model predictions for Limanda ferruginea*.*

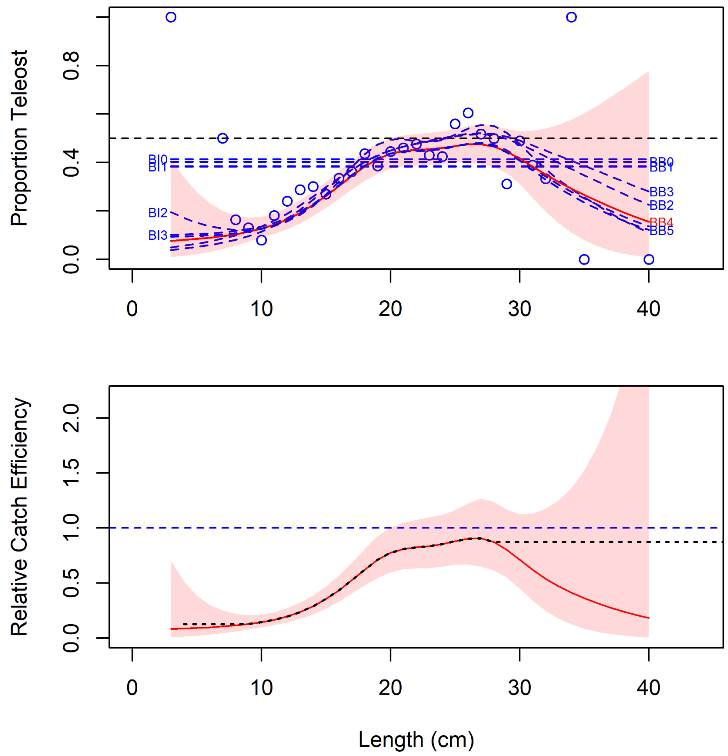

Figure 14b. Model fits and the selected length-based calibration for Limanda ferruginea.

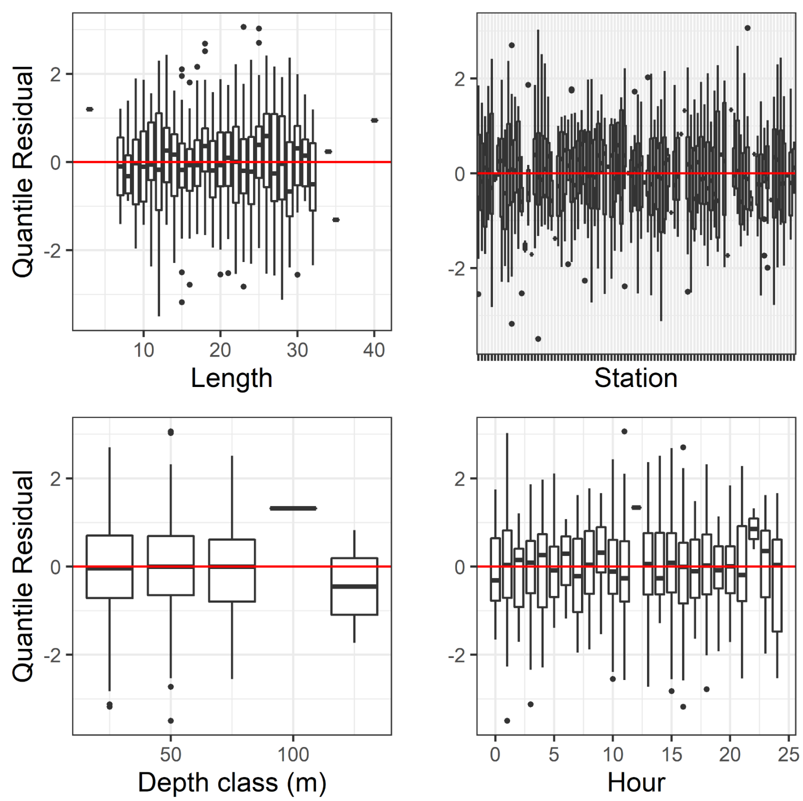

Figure 14c. Normalized quantile residuals for the selected model for Limanda ferruginea.

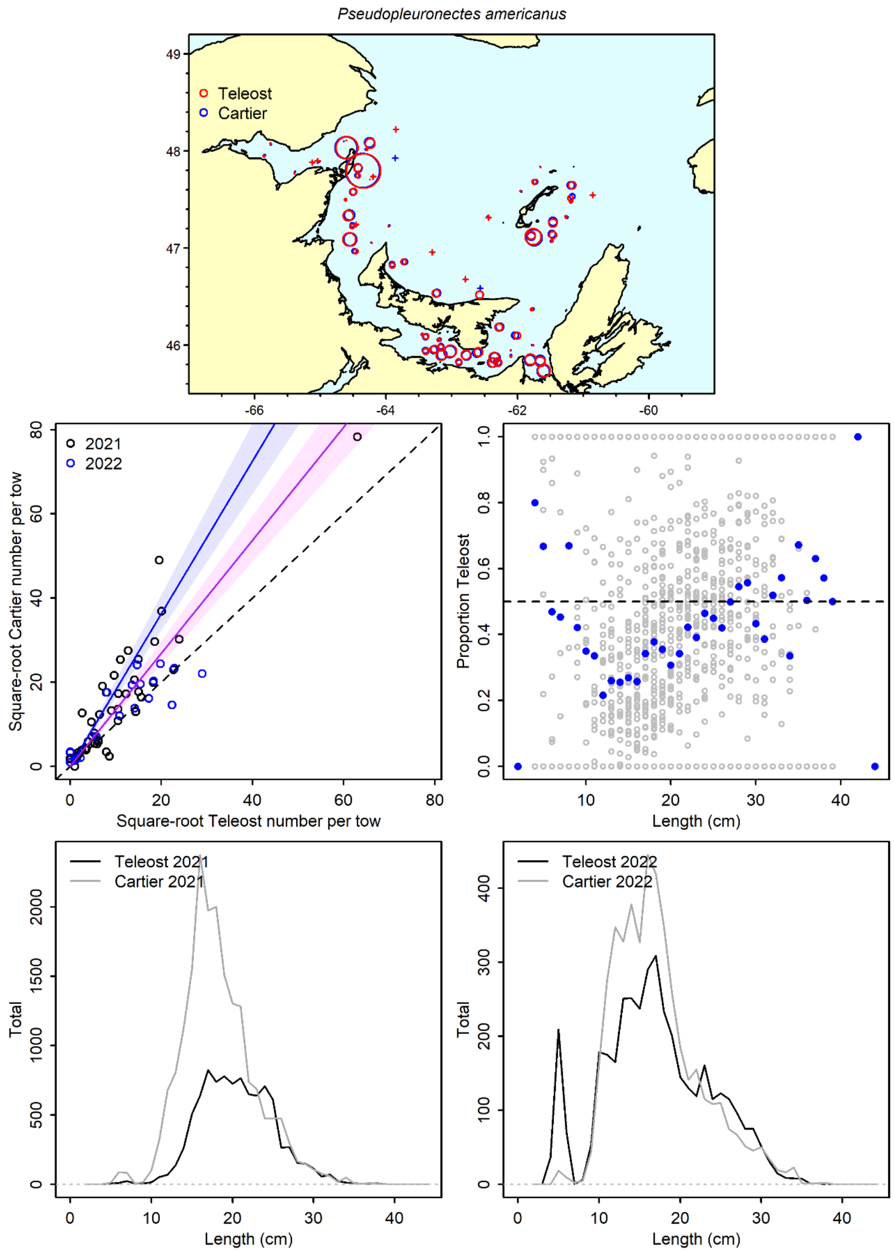

Figure 15a .Visualisation of comparative fishing data and size-aggregated model predictions for Pseudopleuronectes americanus*.*

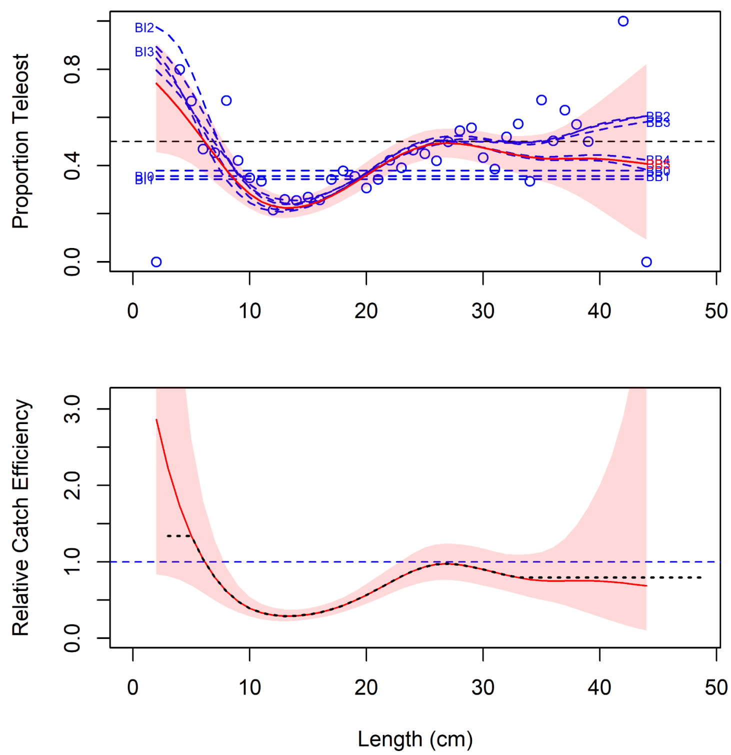

Figure 15b. Model fits and the selected length-based calibration for Pseudopleuronectes americanus.

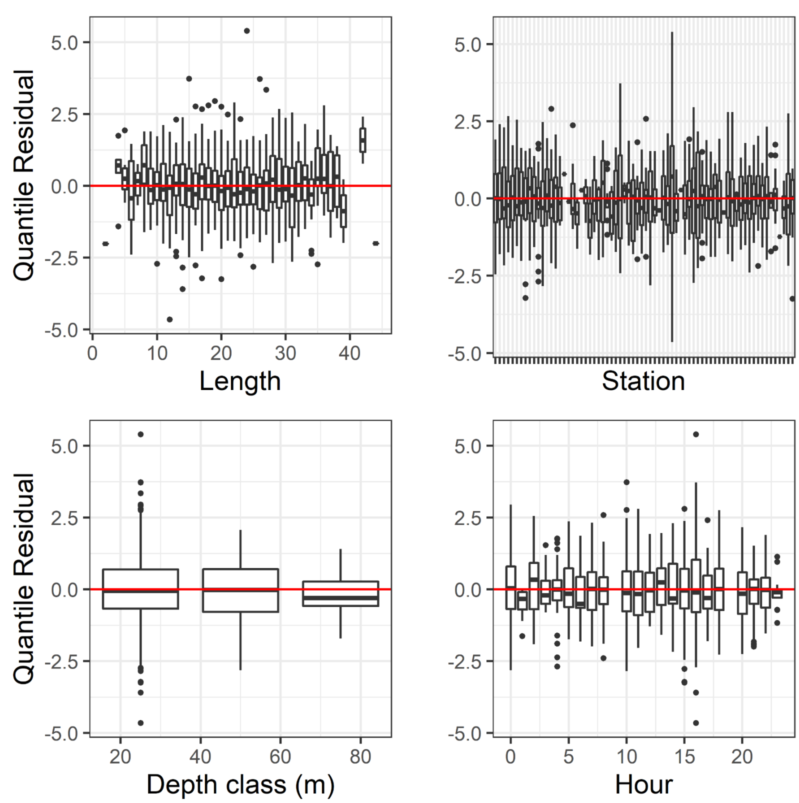

Figure 15c. Normalized quantile residuals for the selected model for Pseudopleuronectes americanus.

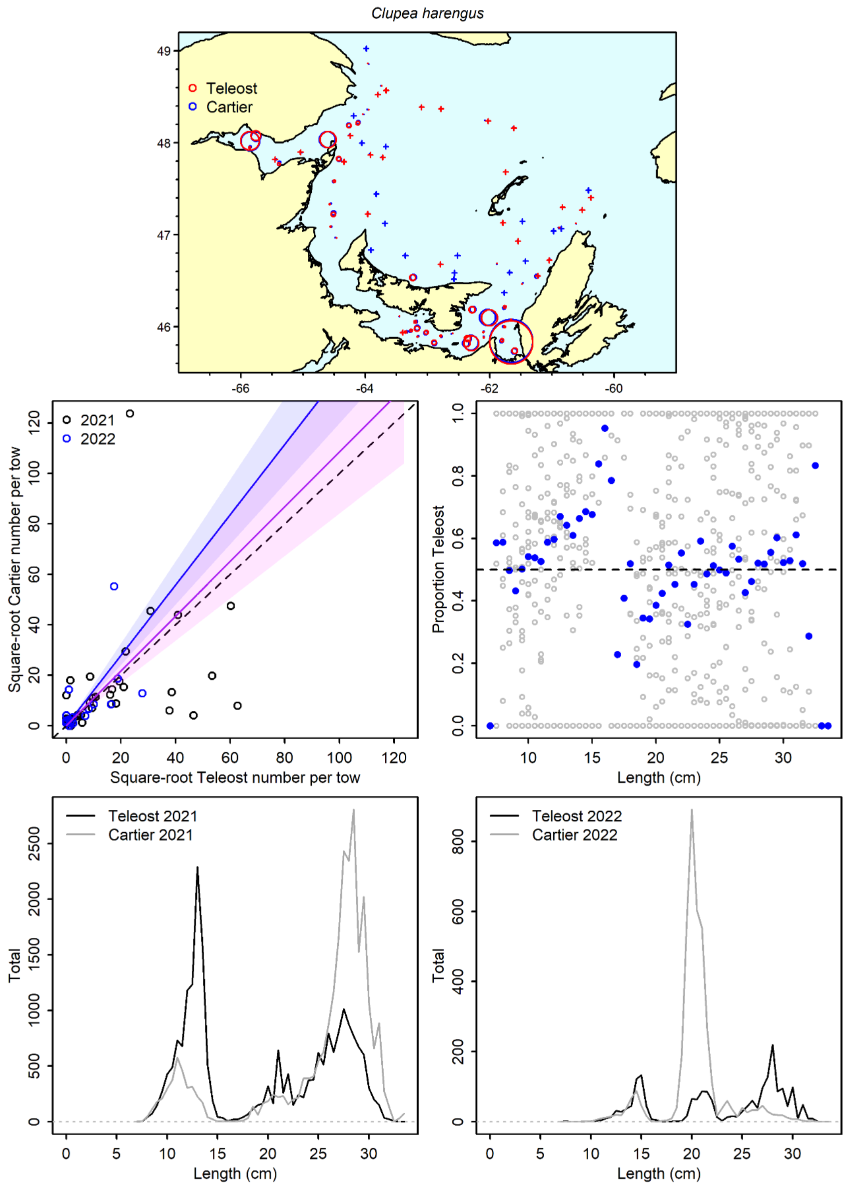

Figure 16a. Visualisation of comparative fishing data and size-aggregated model predictions for Clupea harengus.

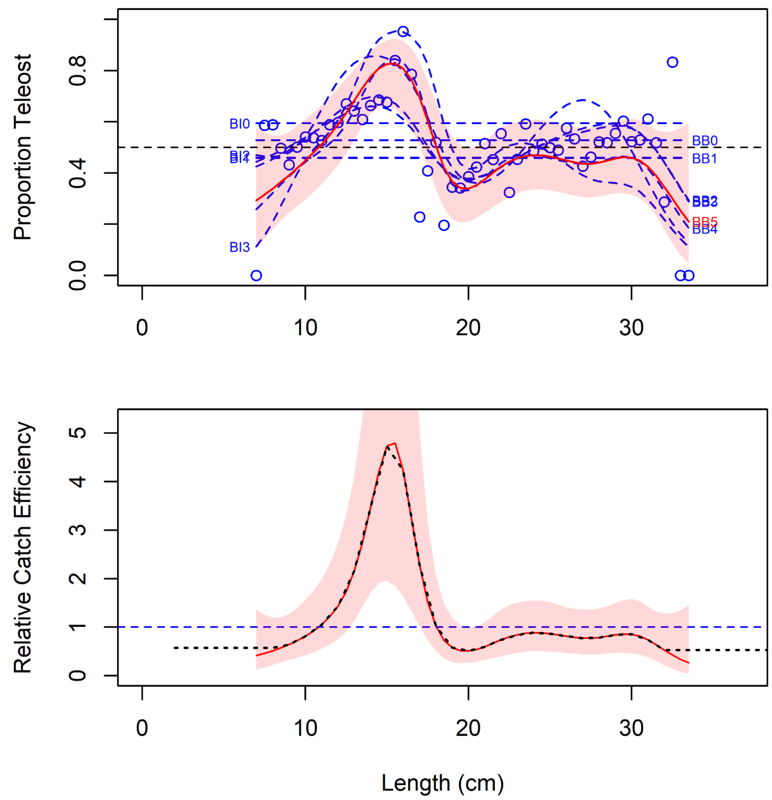

Figure 16b. Model fits and the selected length-based calibration for Clupea harengus.

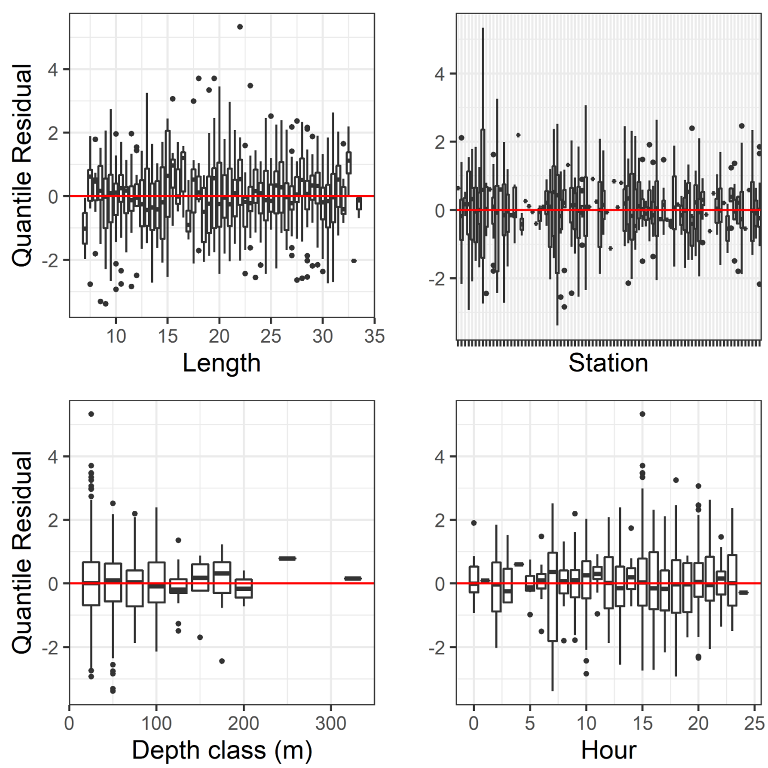

Figure 16c. Normalized quantile residuals for the selected model for Clupea harengus.

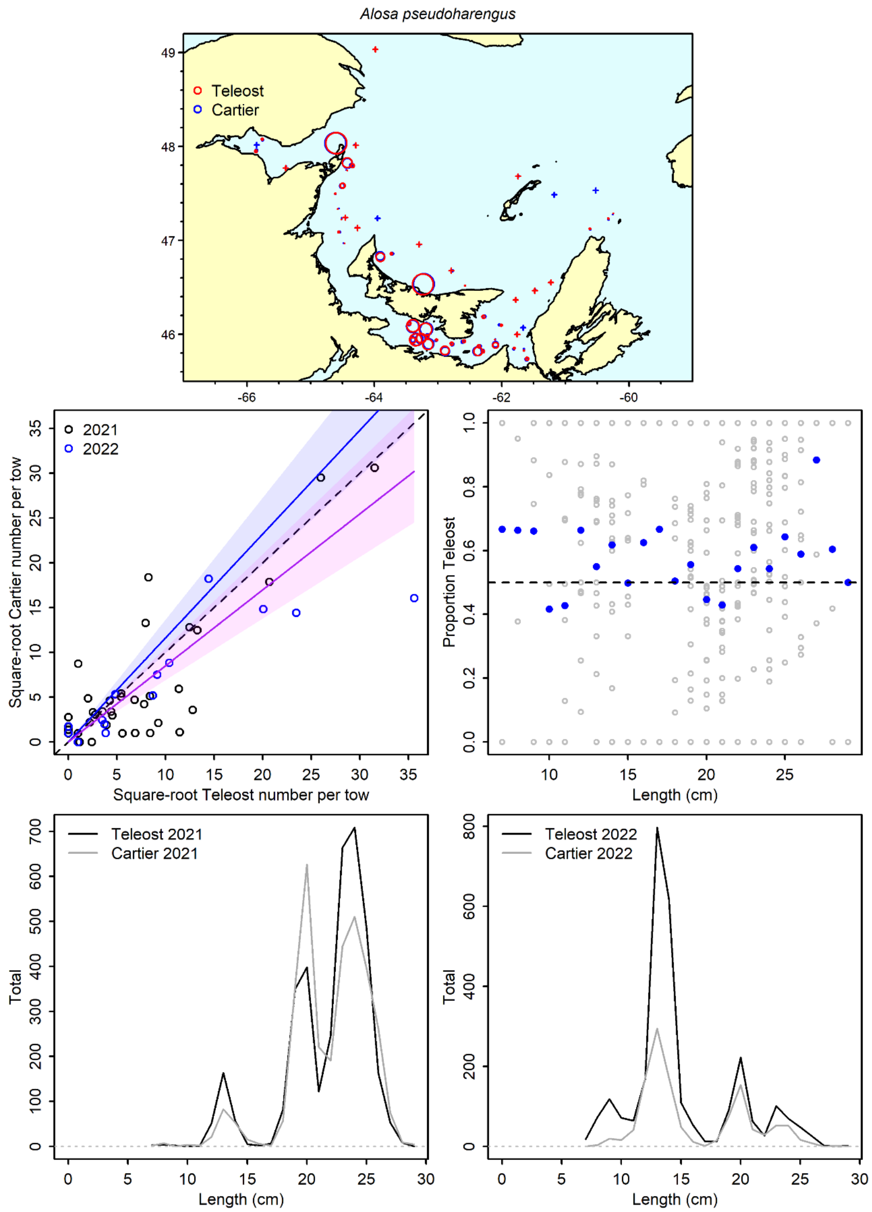

Figure 17a. Visualisation of comparative fishing data and size-aggregated model predictions for Alosa pseudoharengus*.*

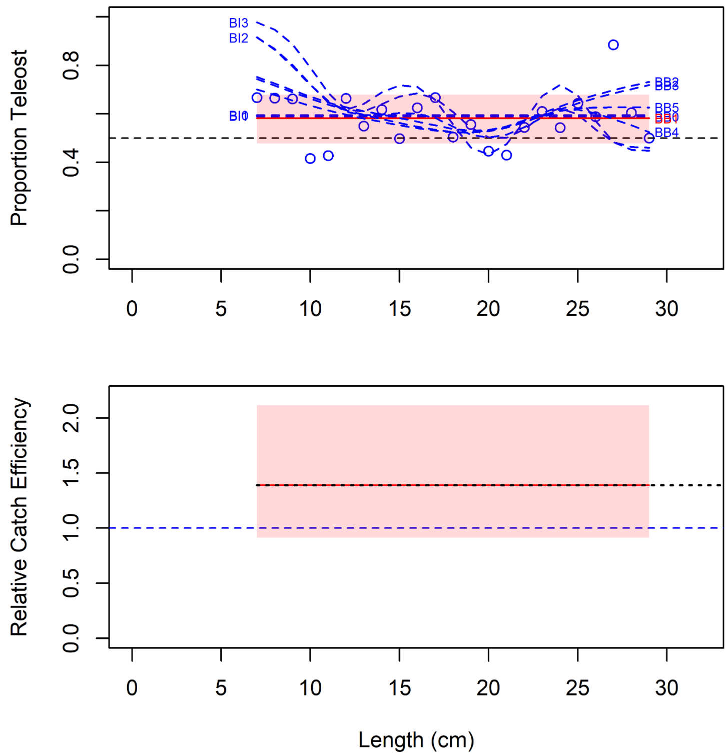

Figure 17b. Model fits and the selected length-based calibration for Alosa pseudoharengus.

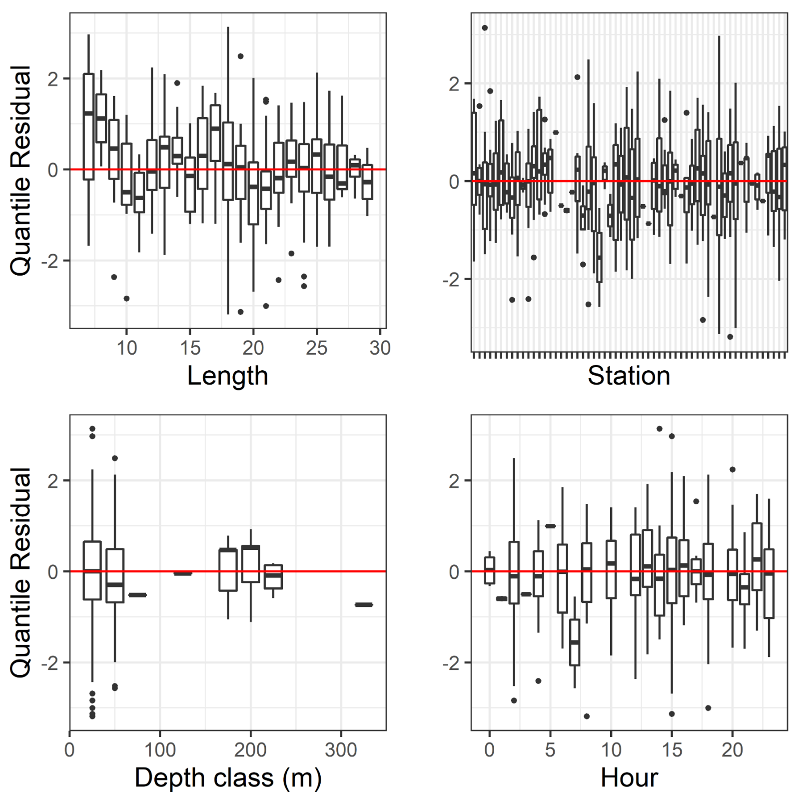

Figure 17c. Normalized quantile residuals for the selected model for Alosa pseudoharengus.

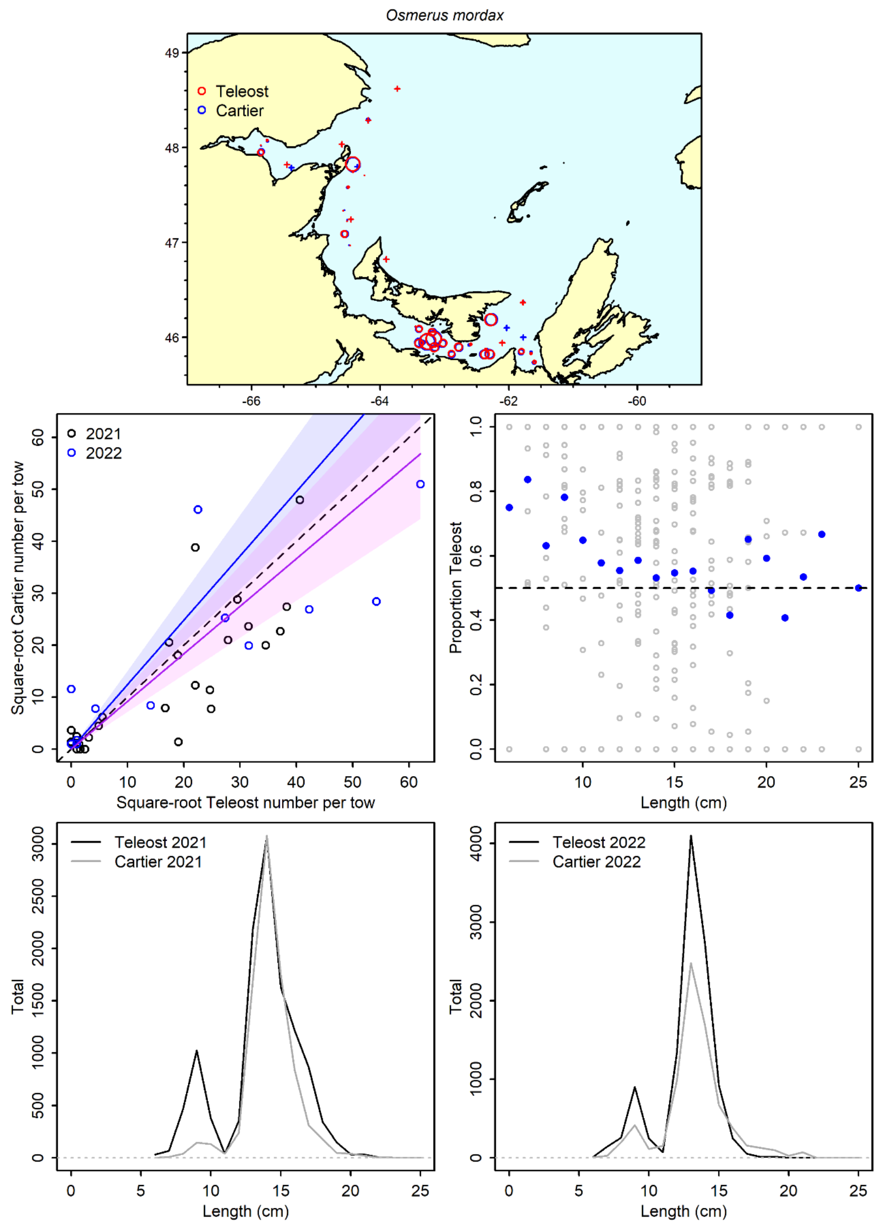

Figure 18a. Visualisation of comparative fishing data and size-aggregated model predictions for Osmerus mordax.

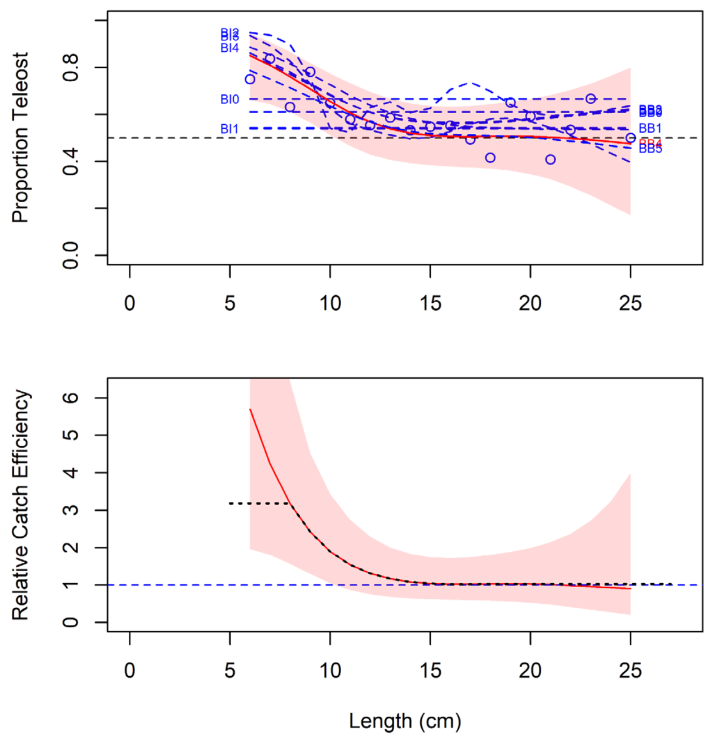

Figure 18b. Model fits and the selected length-based calibration for Osmerus mordax.

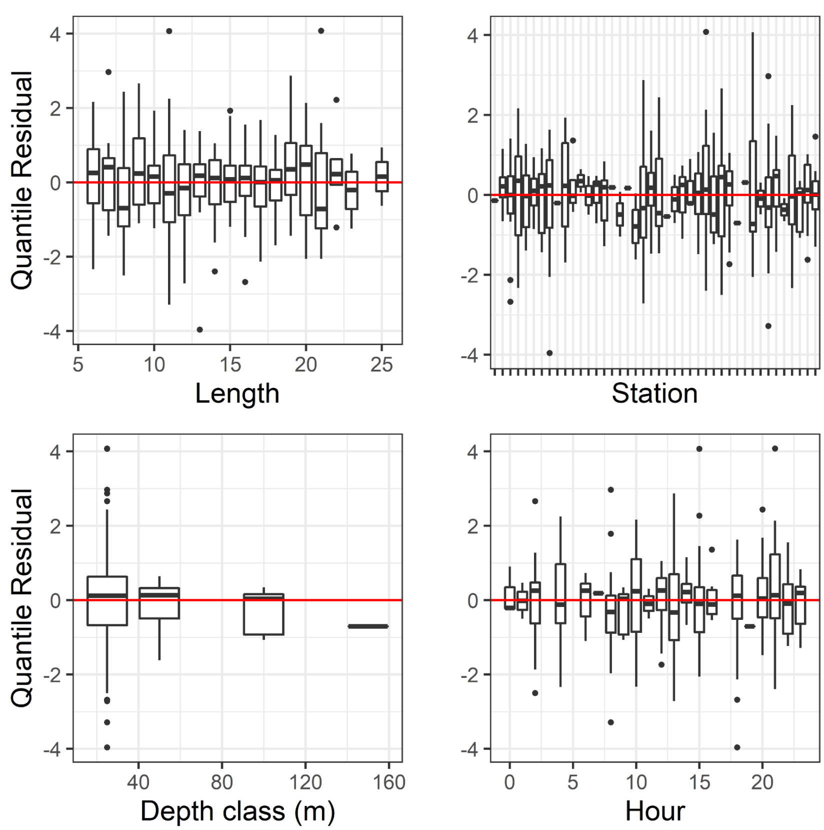

Figure 18c. Normalized quantile residuals for the selected model for Osmerus mordax.

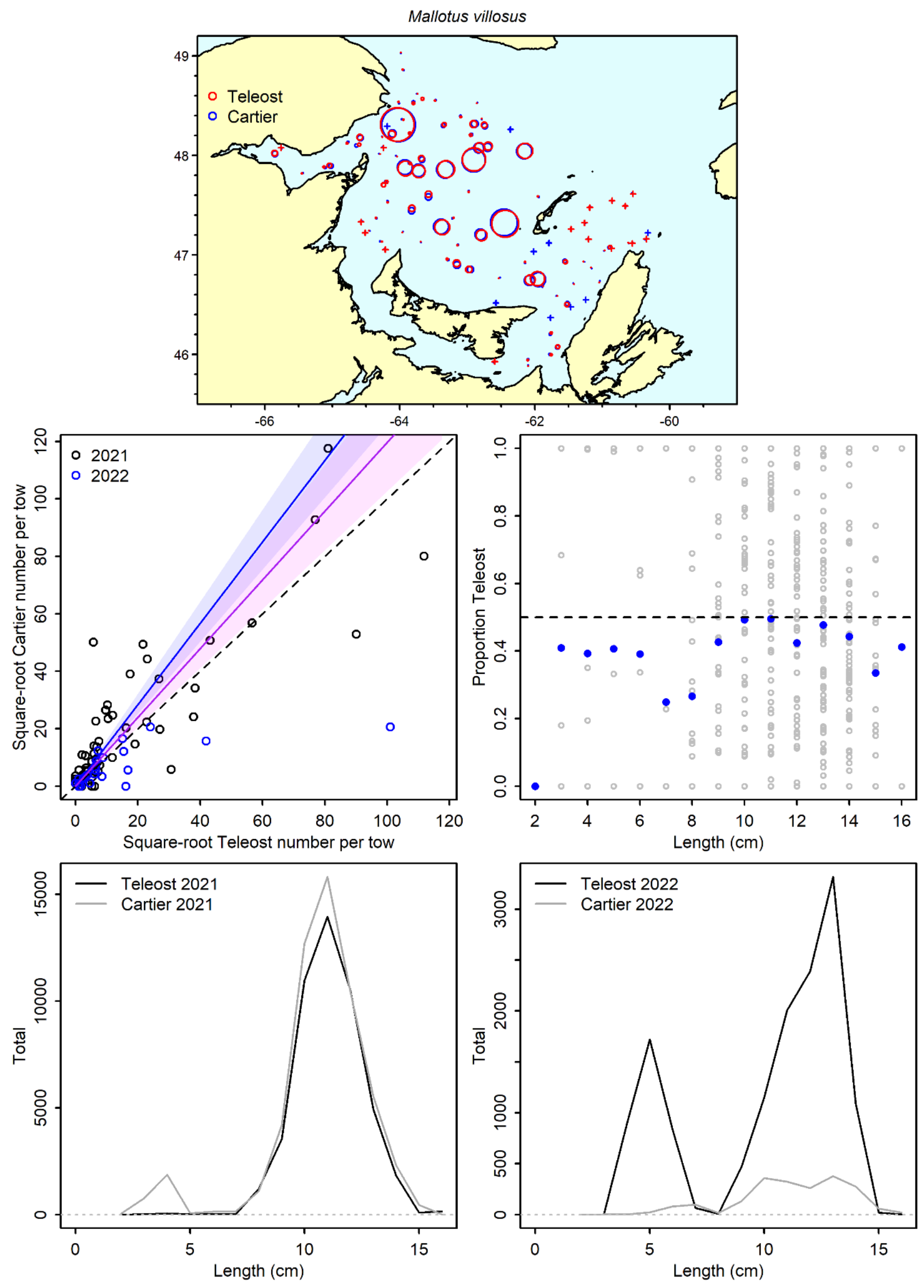

Figure 19a. Visualisation of comparative fishing data and size-aggregated model predictions for Mallotus villosus.

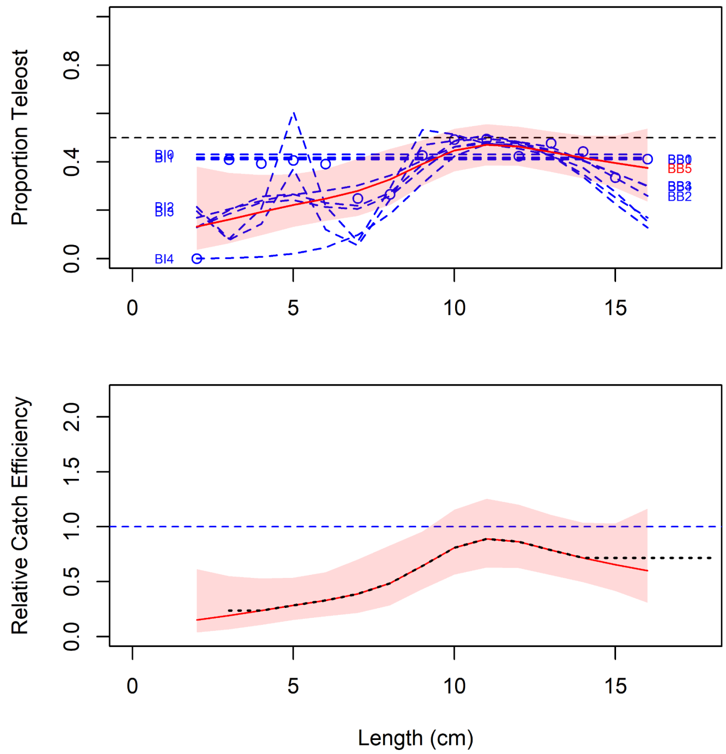

Figure 19b. Model fits and the selected length-based calibration for Mallotus villosus.

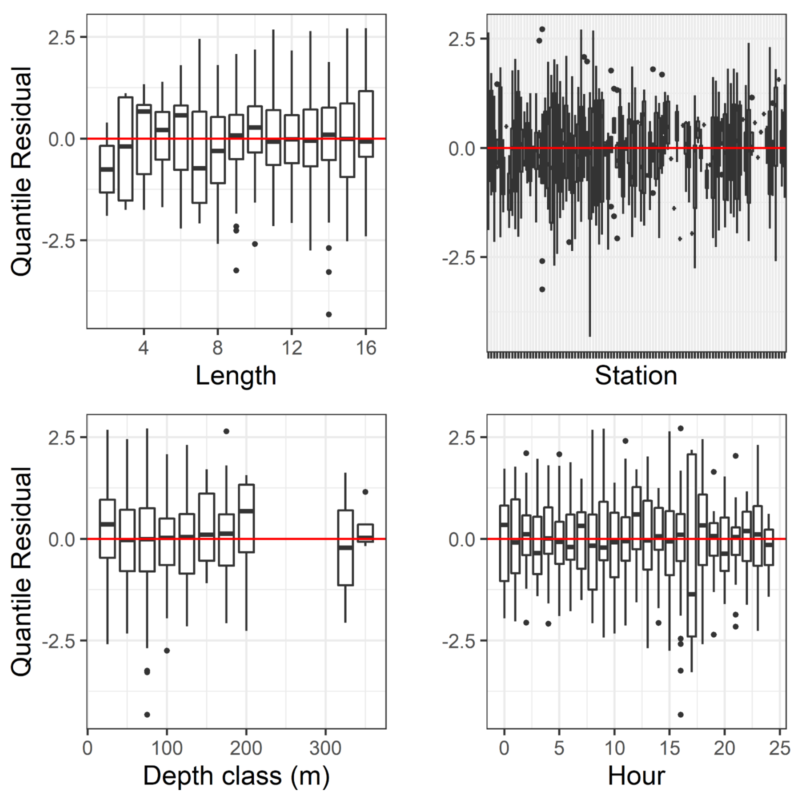

Figure 19c. Normalized quantile residuals for the selected model for Mallotus villosus.

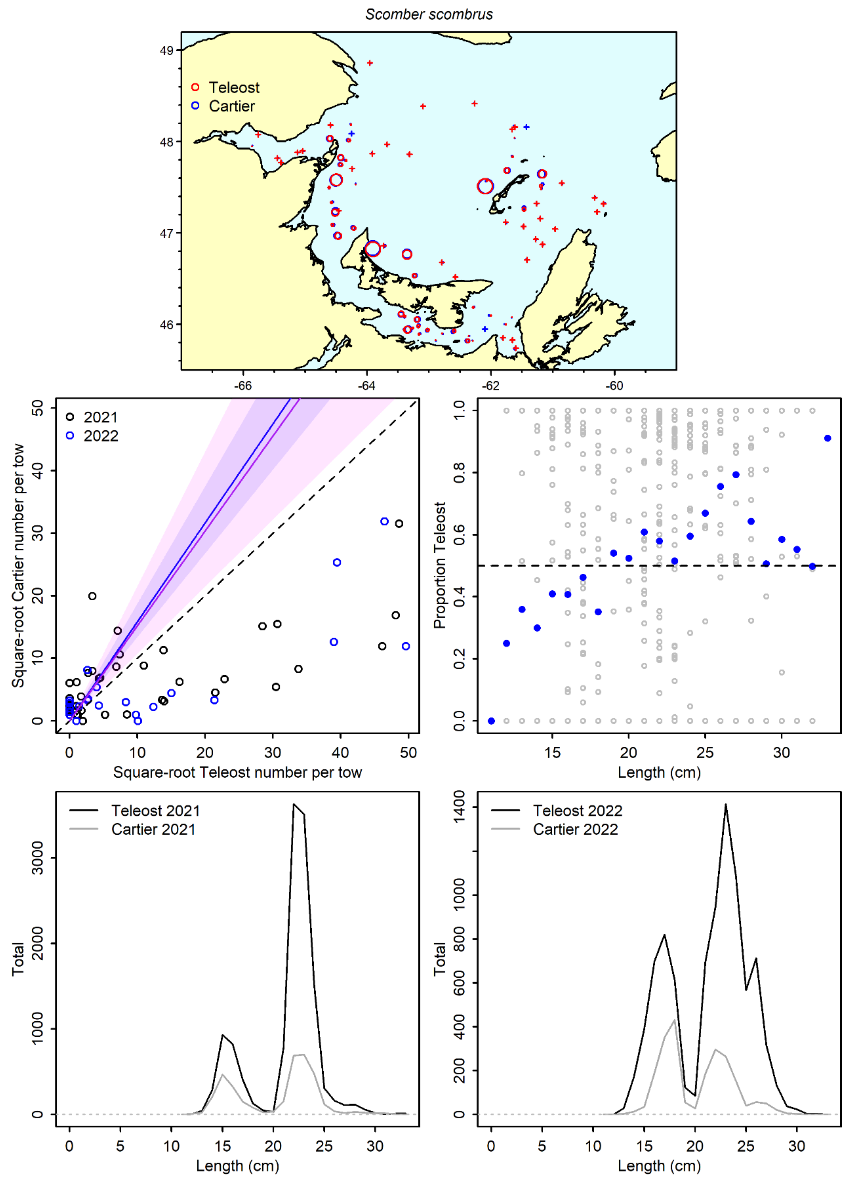

Figure 20a. Visualisation of comparative fishing data and size-aggregated model predictions for Scomber scombrus.

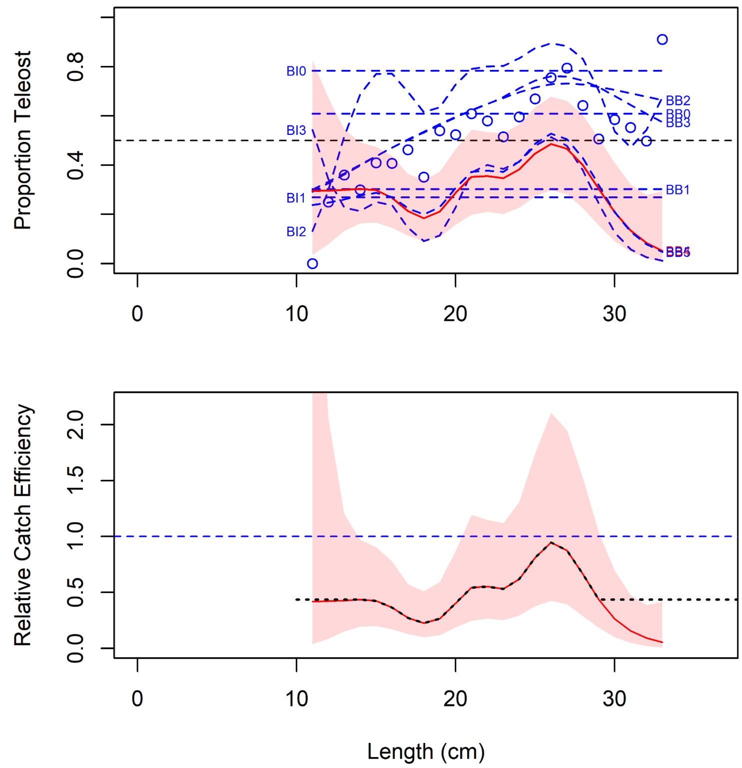

Figure 20b. Model fits and the selected length-based calibration for Scomber scombrus*.*

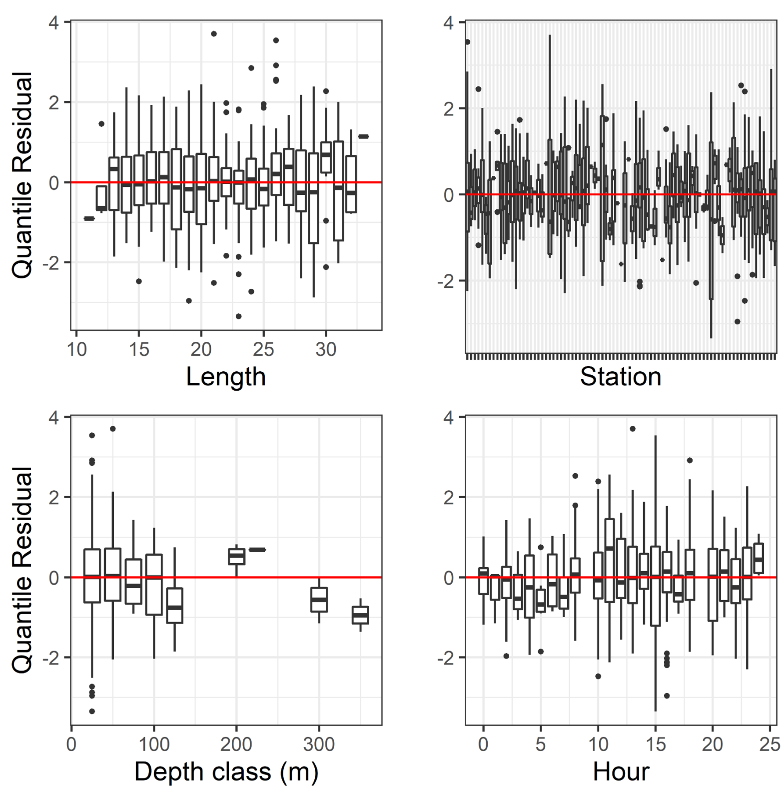

Figure 20c. Normalized quantile residuals for the selected model for Scomber scombrus*.*

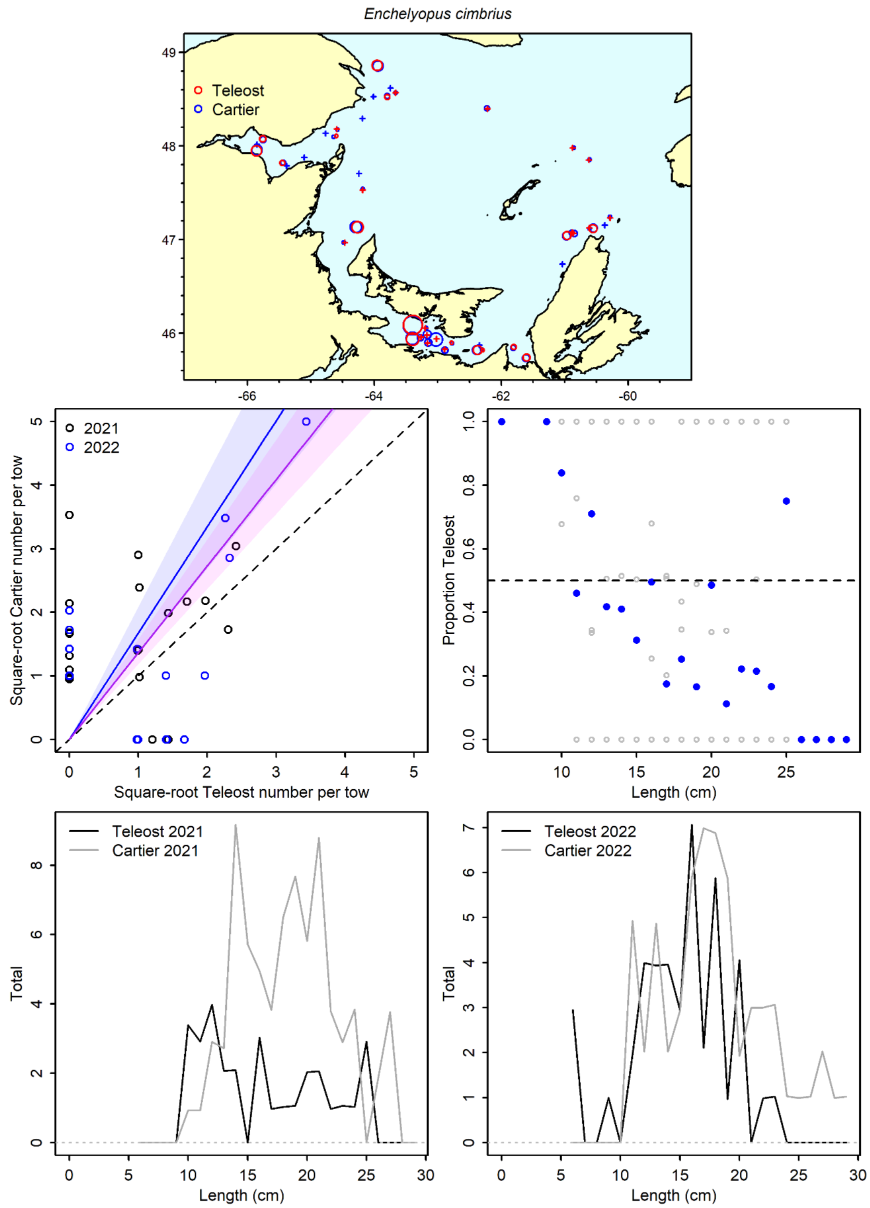

Figure 21a. Visualisation of comparative fishing data and size-aggregated model predictions for Enchelyopus cimbrius*.*

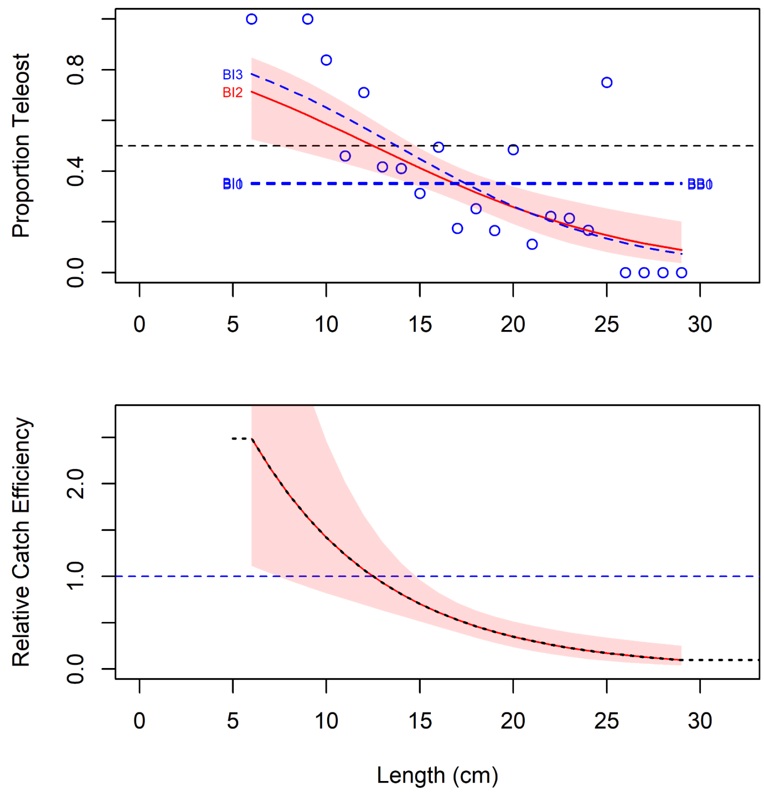

Figure 21b. Model fits and the selected length-based calibration for Enchelyopus cimbrius.

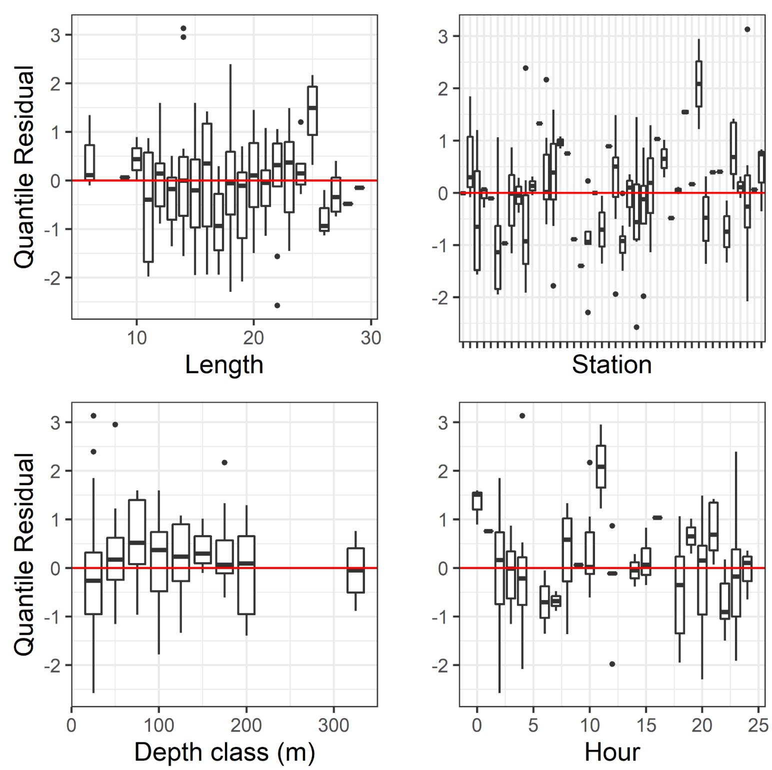

Figure 21c. Normalized quantile residuals for the selected model for Enchelyopus cimbrius.

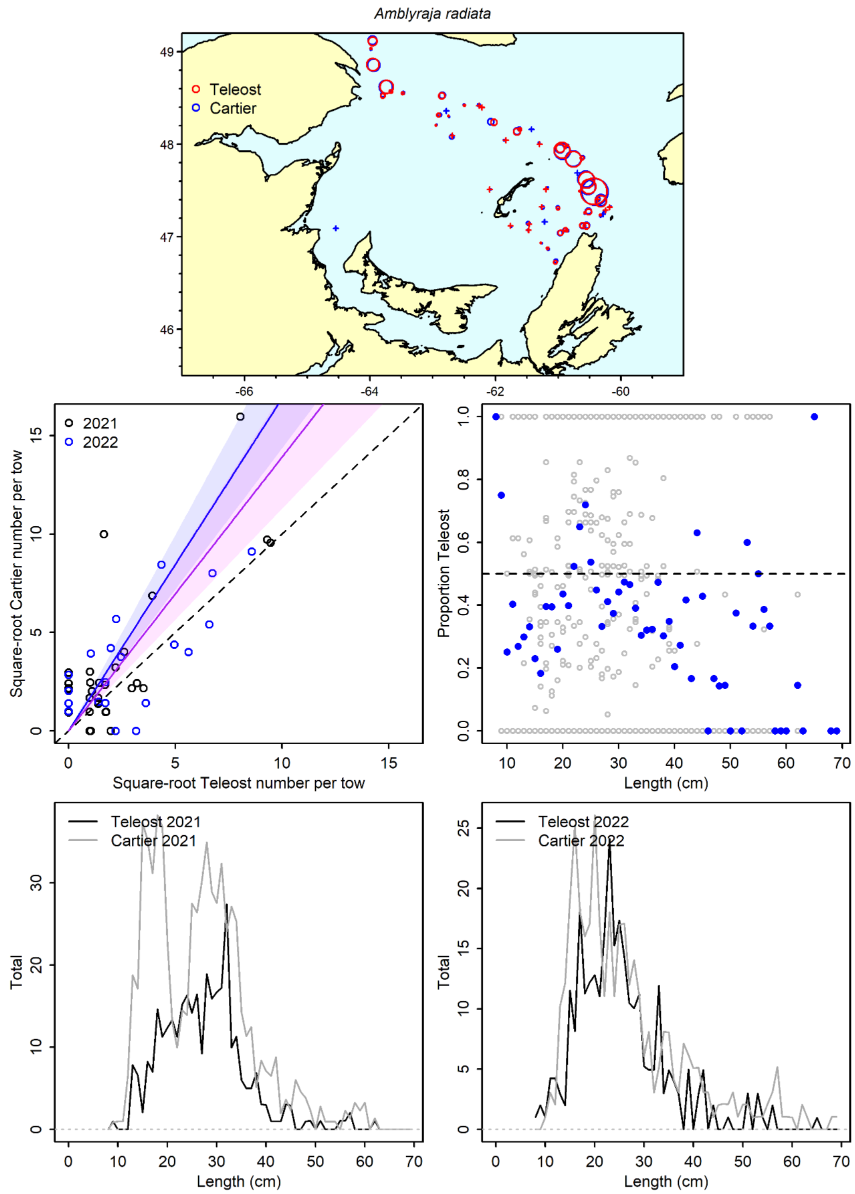

Figure 22a. Visualisation of comparative fishing data and size-aggregated model predictions for Amblyraja radiata.

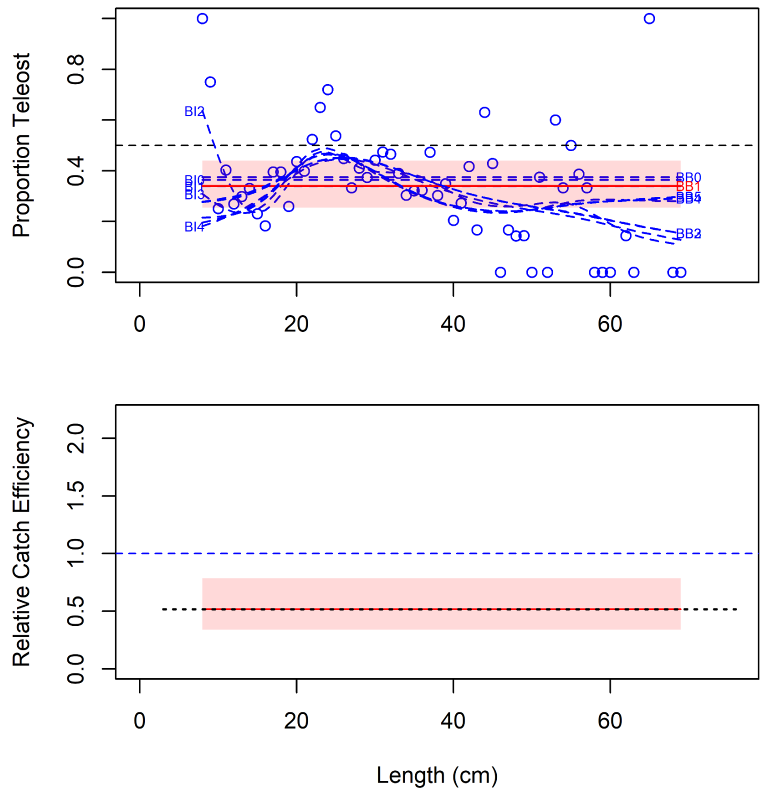

Figure 22b. Model fits and the selected length-based calibration for Amblyraja radiata.

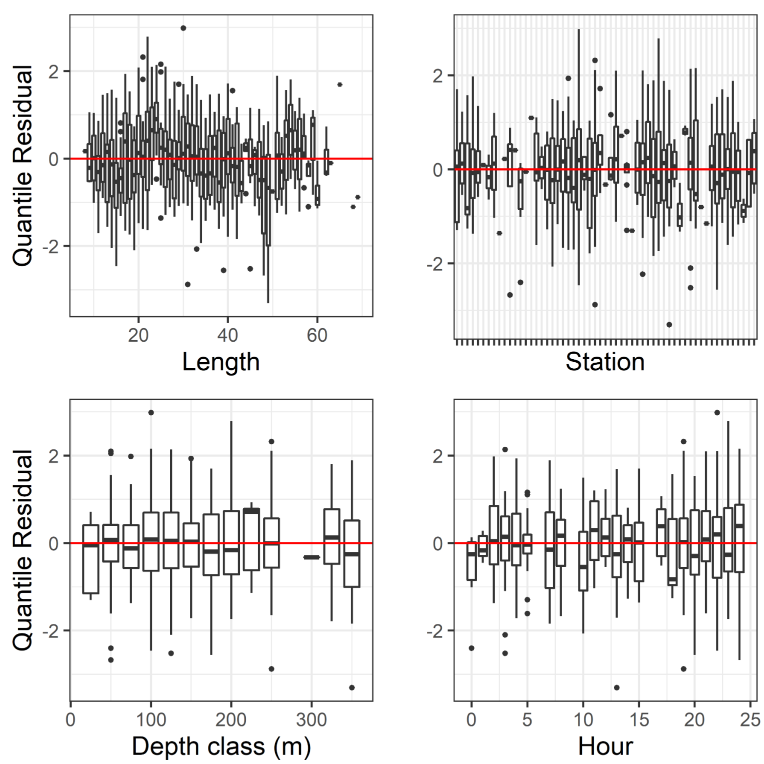

Figure 22c. Normalized quantile residuals for the selected model for Amblyraja radiata.

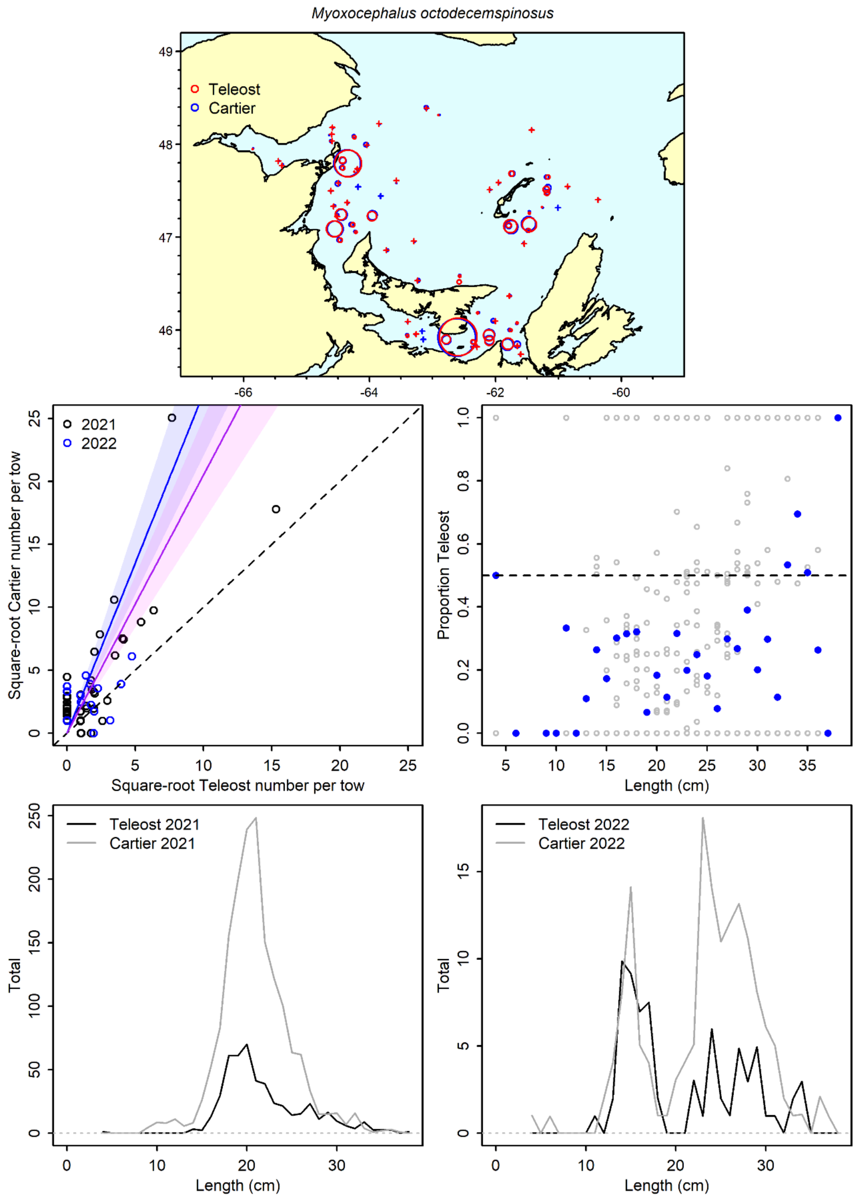

Figure 23a. Visualisation of comparative fishing data and size-aggregated model predictions for Myoxocephalus octodecemspinosus.

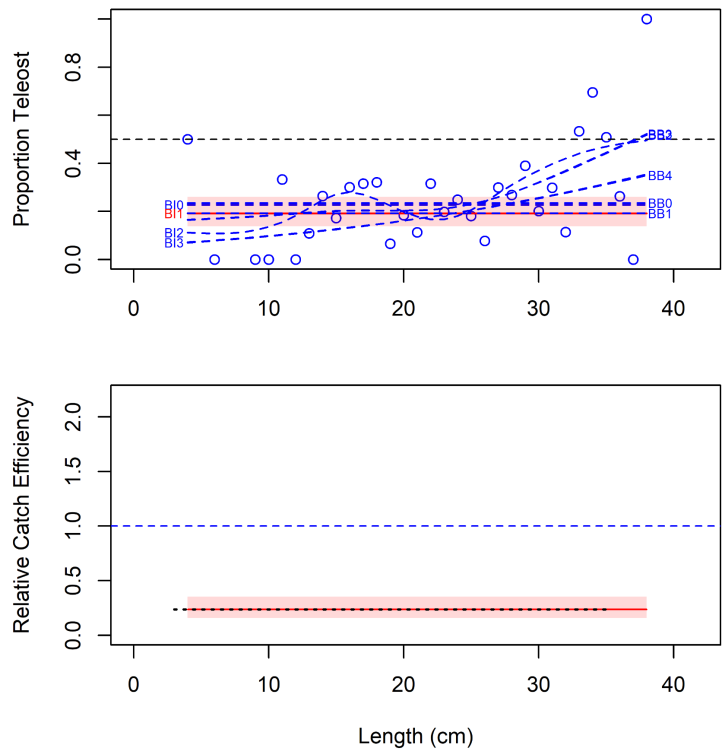

Figure 23b. Model fits and the selected length-based calibration for Myoxocephalus octodecemspinosus.

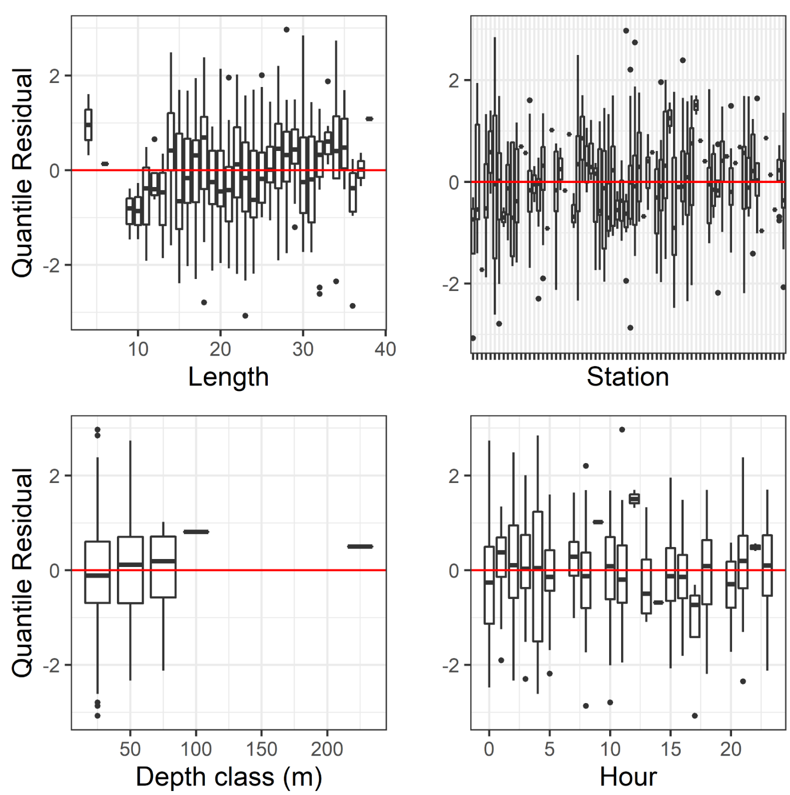

Figure 23c. Normalized quantile residuals for the selected model for Myoxocephalus octodecemspinosus.

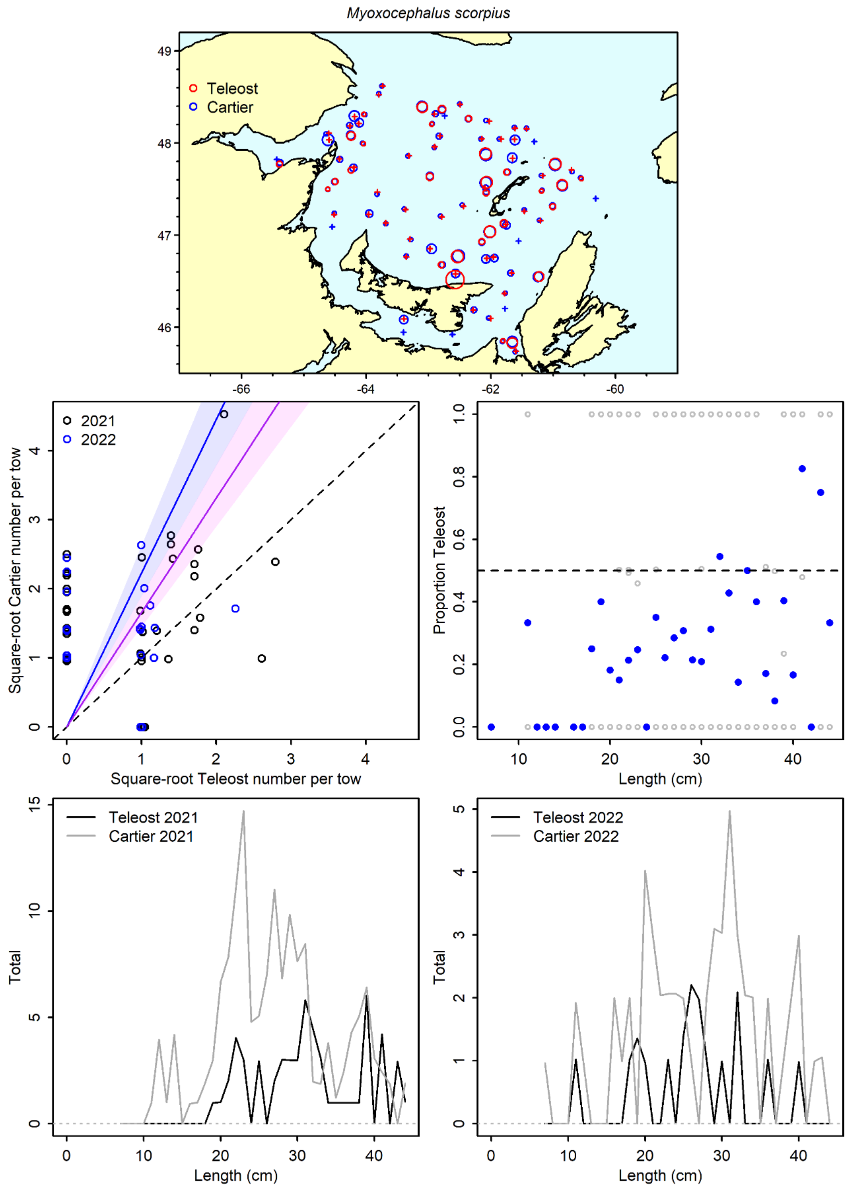

Figure 24a. Visualisation of comparative fishing data and size-aggregated model predictions for Myoxocephalus scorpius.

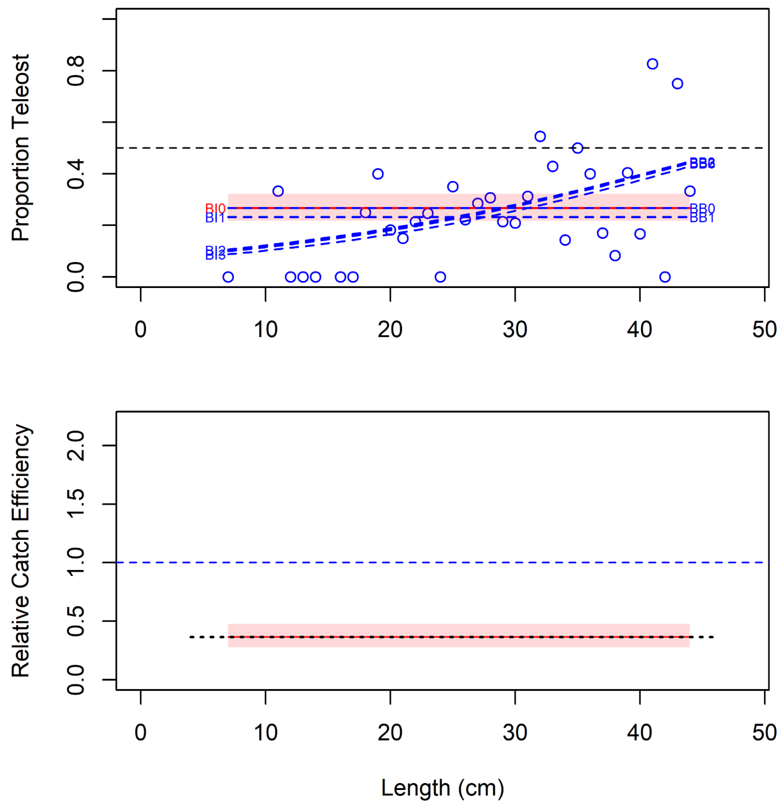

Figure 24b. Model fits and the selected length-based calibration for Myoxocephalus scorpius.

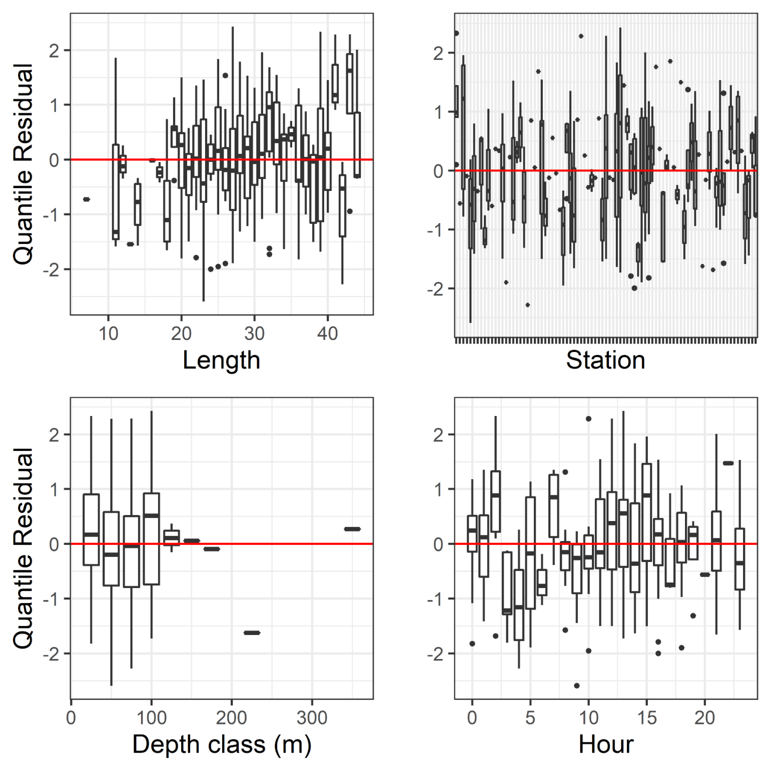

Figure 24c. Normalized quantile residuals for the selected model for Myoxocephalus scorpius.

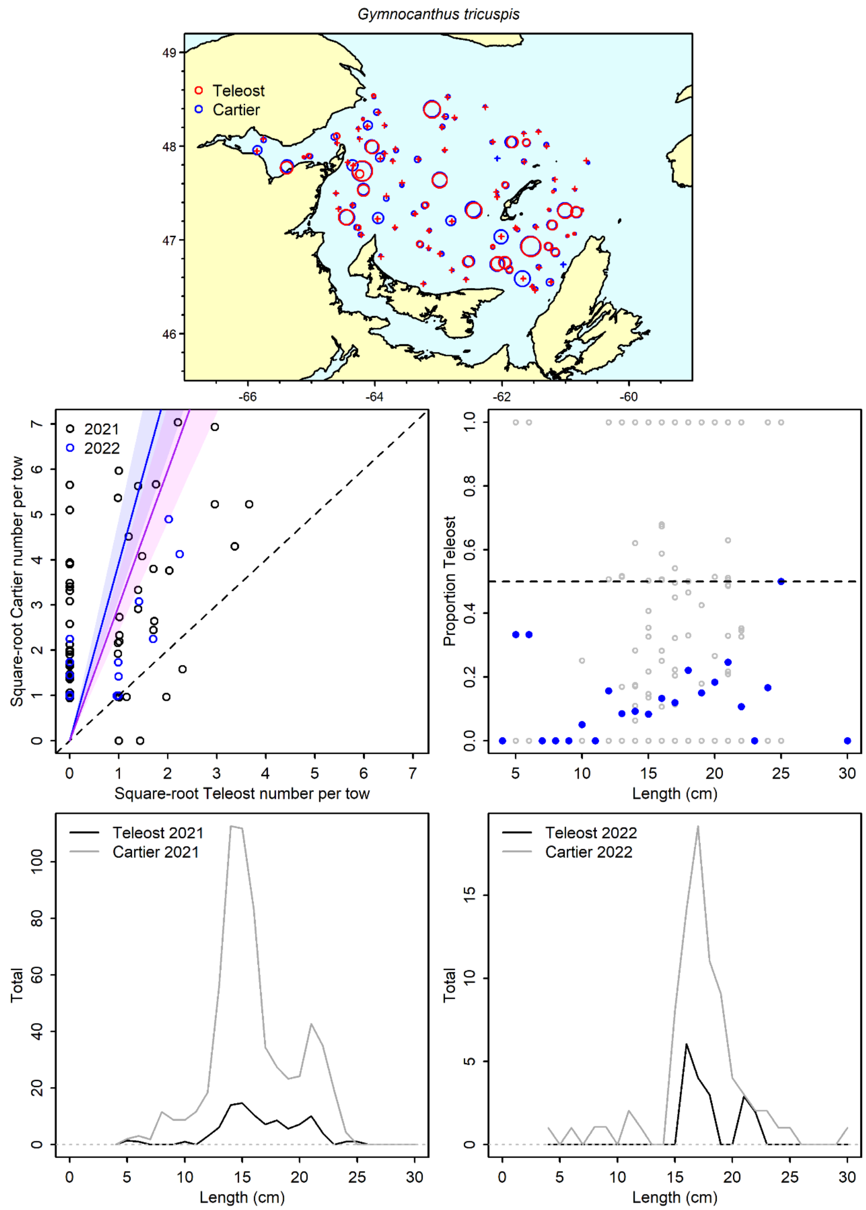

Figure 25a. Visualisation of comparative fishing data and size-aggregated model predictions for Gymnocanthus tricuspis*.*

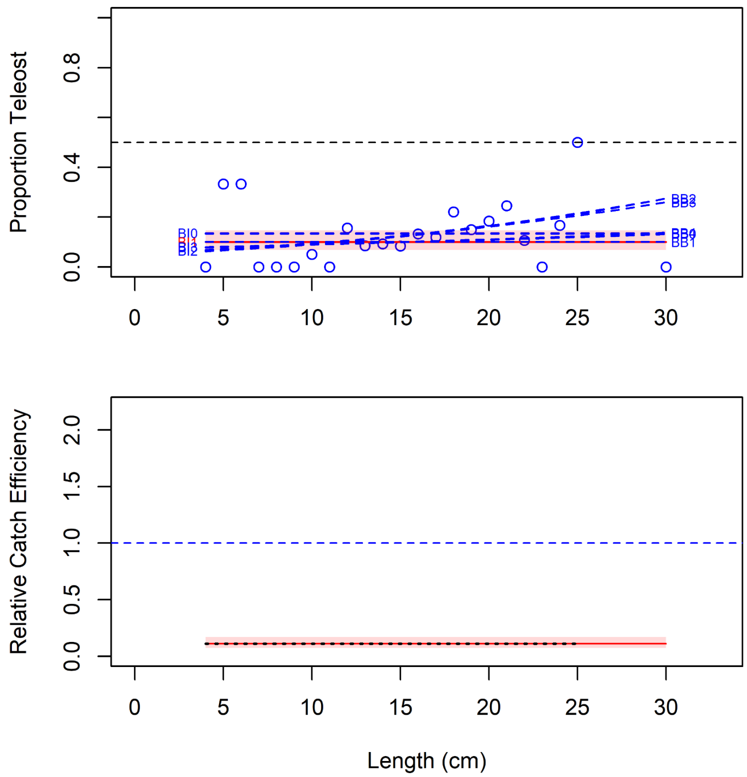

Figure 25b. Model fits and the selected length-based calibration for Gymnocanthus tricuspis.

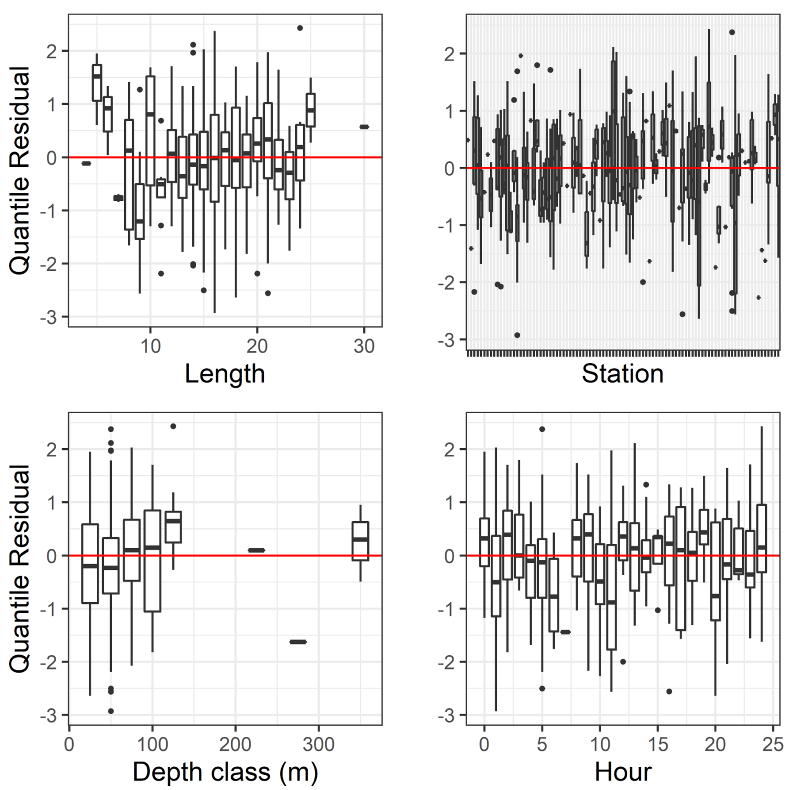

Figure 25c. Normalized quantile residuals for the selected model for Gymnocanthus tricuspis.

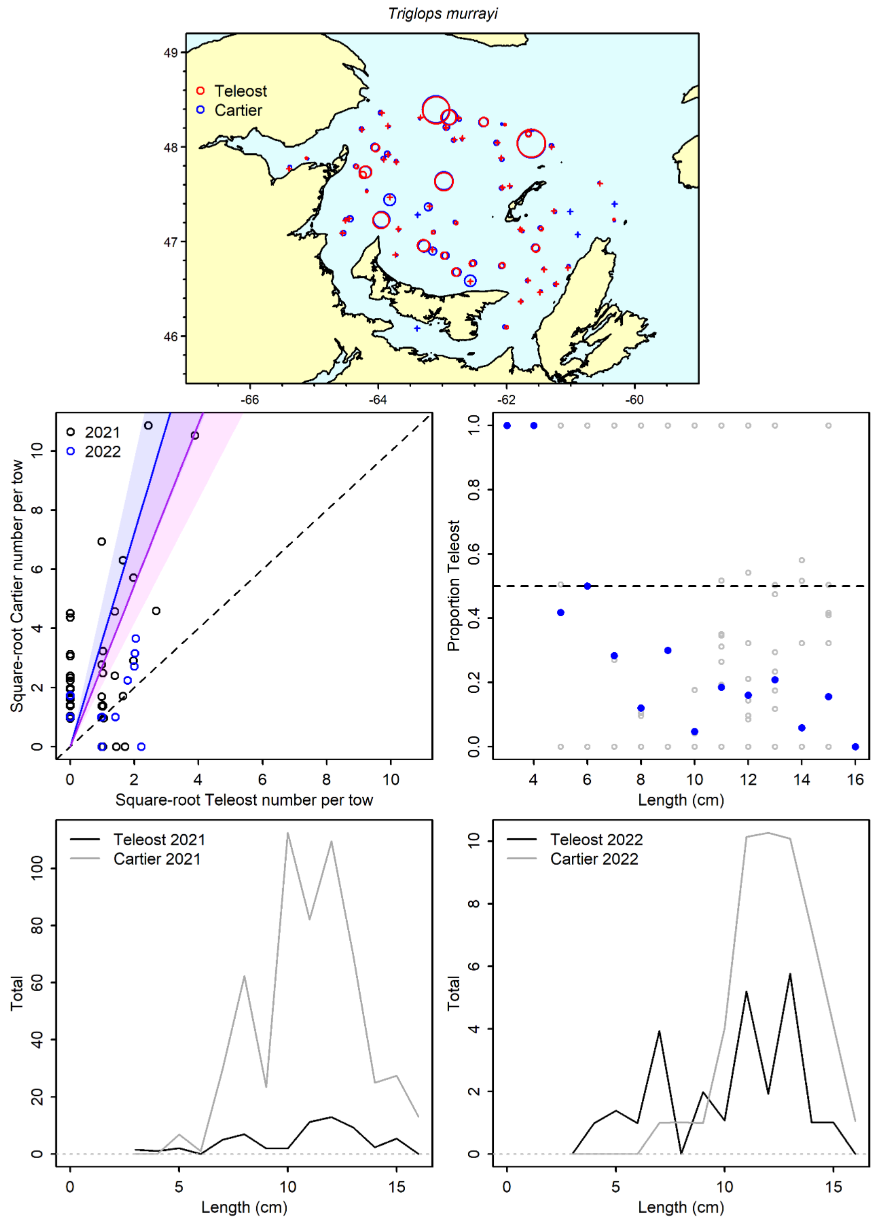

Figure 26a. Visualisation of comparative fishing data and size-aggregated model predictions for Triglops murrayi*.*

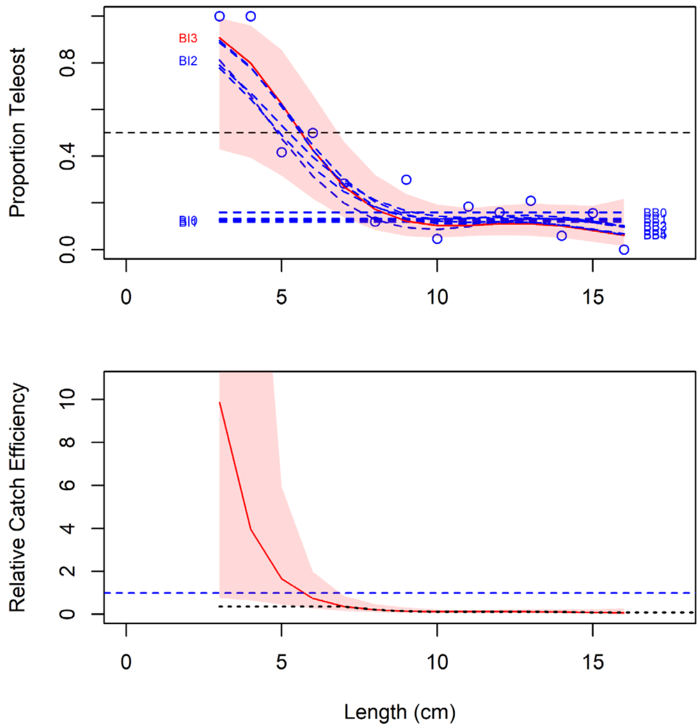

Figure 26b. Model fits and the selected length-based calibration for Triglops murrayi.

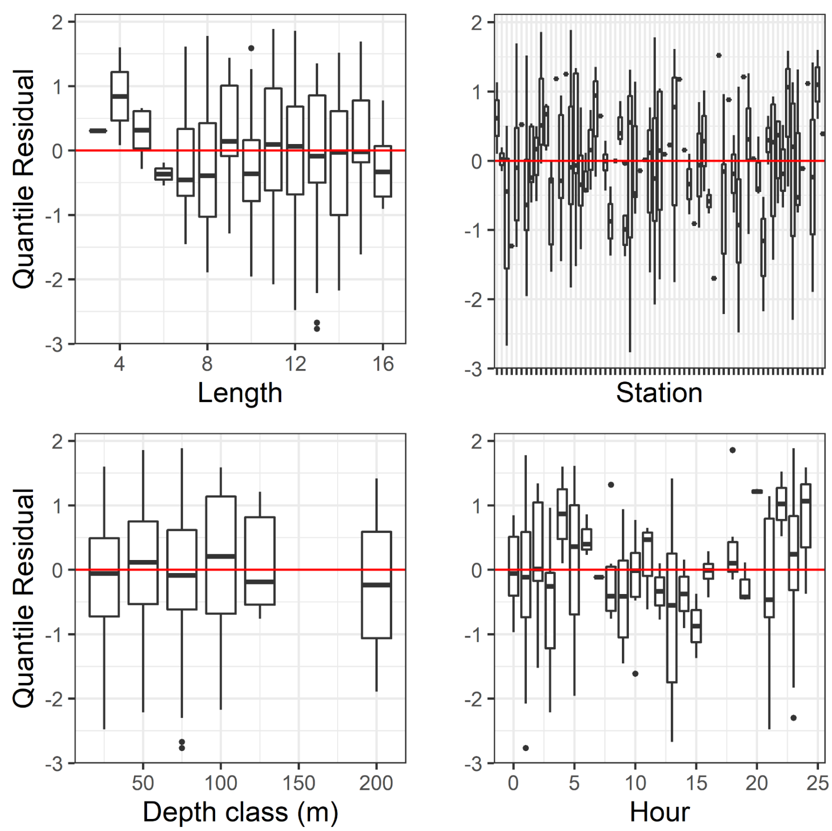

Figure 26c. Normalized quantile residuals for the selected model for Triglops murrayi.

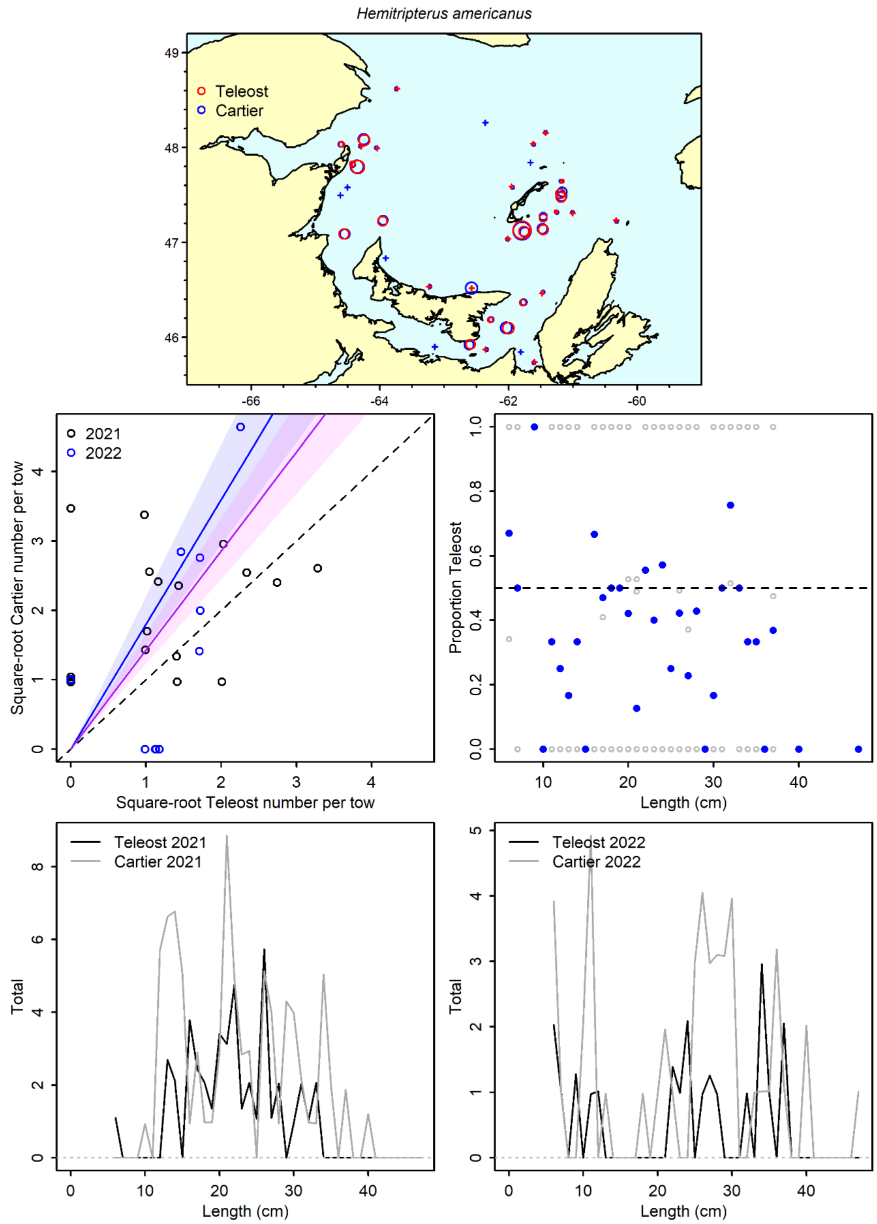

Figure 27a. Visualisation of comparative fishing data and size-aggregated model predictions for Hemitripterus americanus.

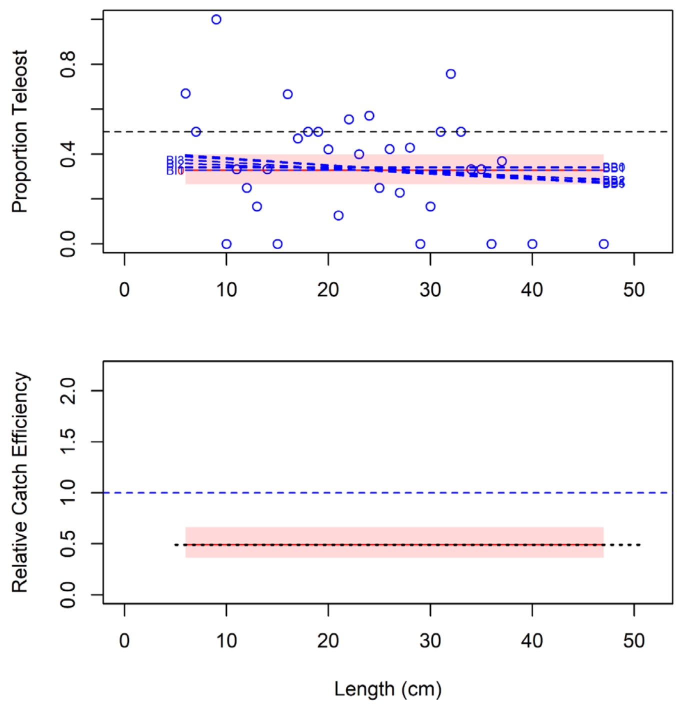

Figure 27b. Model fits and the selected length-based calibration for Hemitripterus americanus.

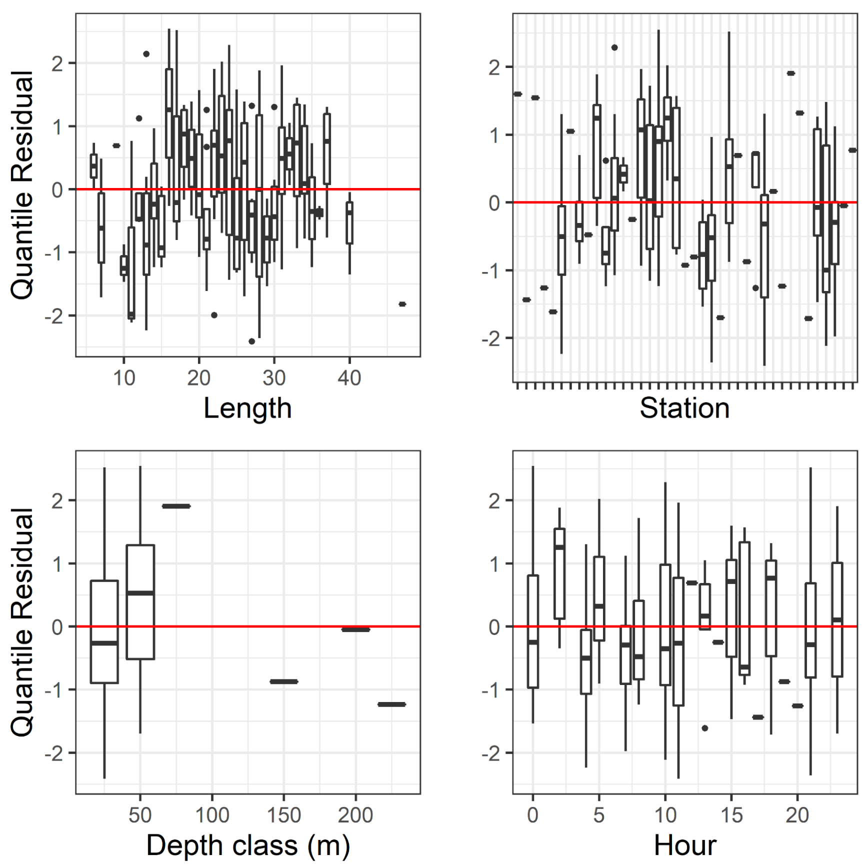

Figure 27c. Normalized quantile residuals for the selected model for Hemitripterus americanus.

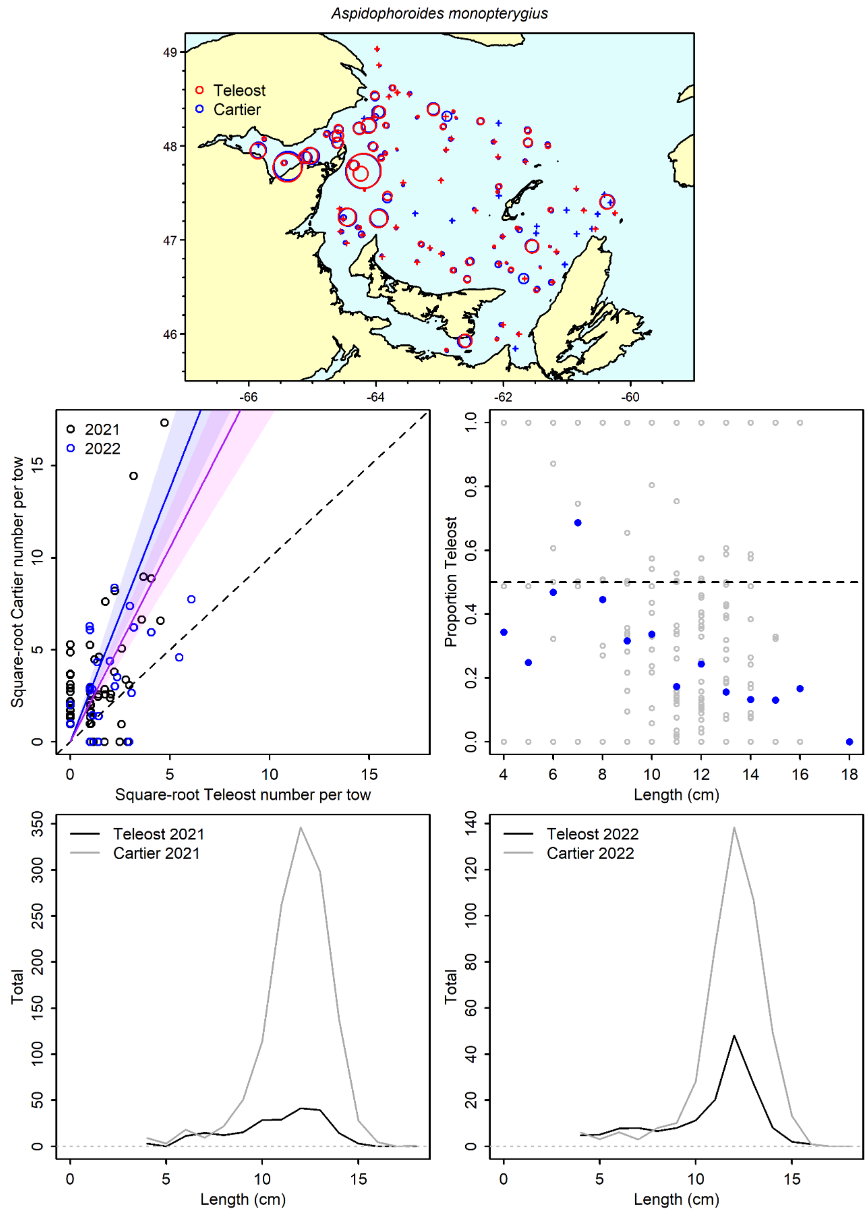

Figure 28a. Visualisation of comparative fishing data and size-aggregated model predictions for Aspidophoroides monopterygius.

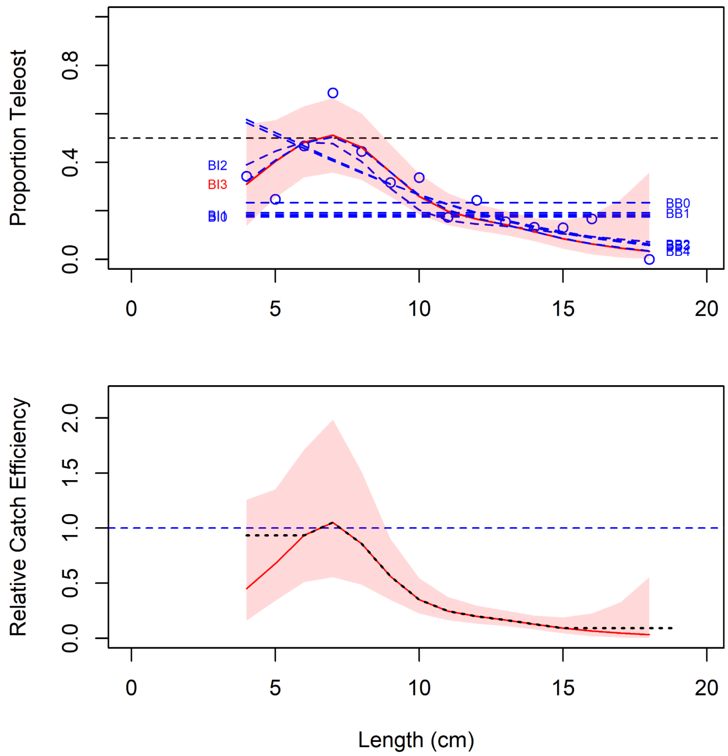

Figure 28b. Model fits and the selected length-based calibration for Aspidophoroides monopterygius.

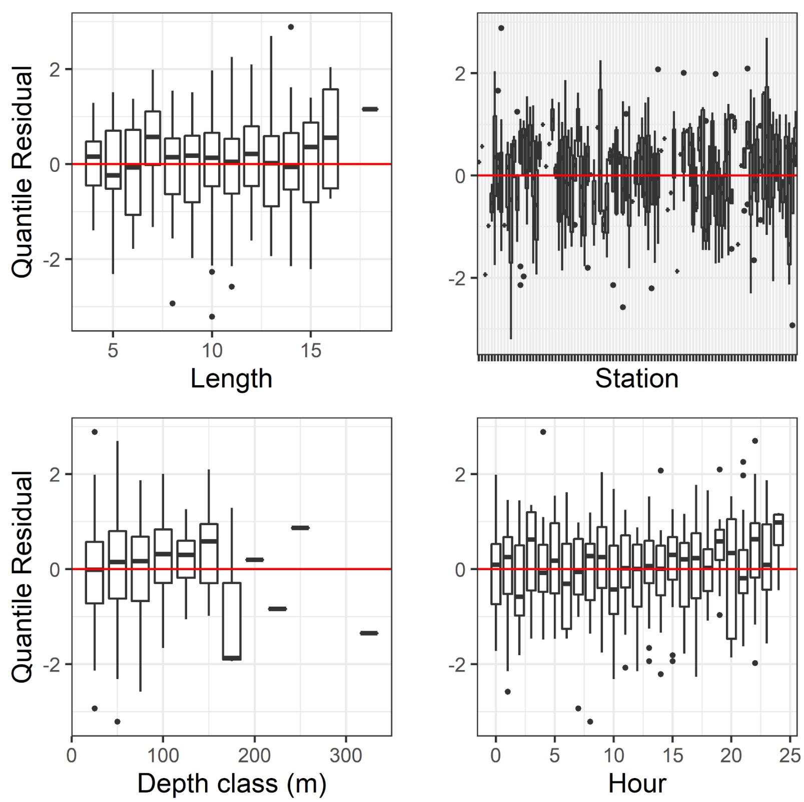

Figure 28c. Normalized quantile residuals for the selected model for Aspidophoroides monopterygius.

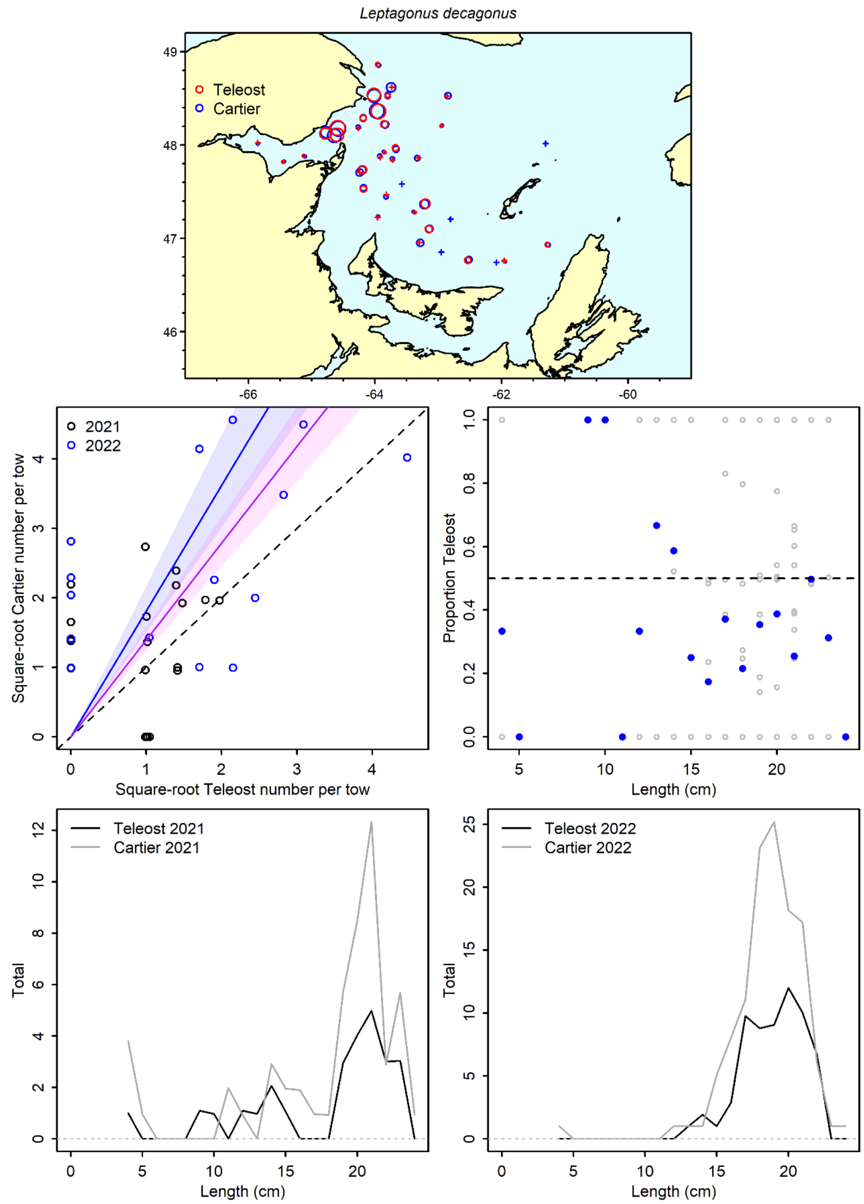

Figure 29a. Visualisation of comparative fishing data and size-aggregated model predictions for Leptagonus decagonus.

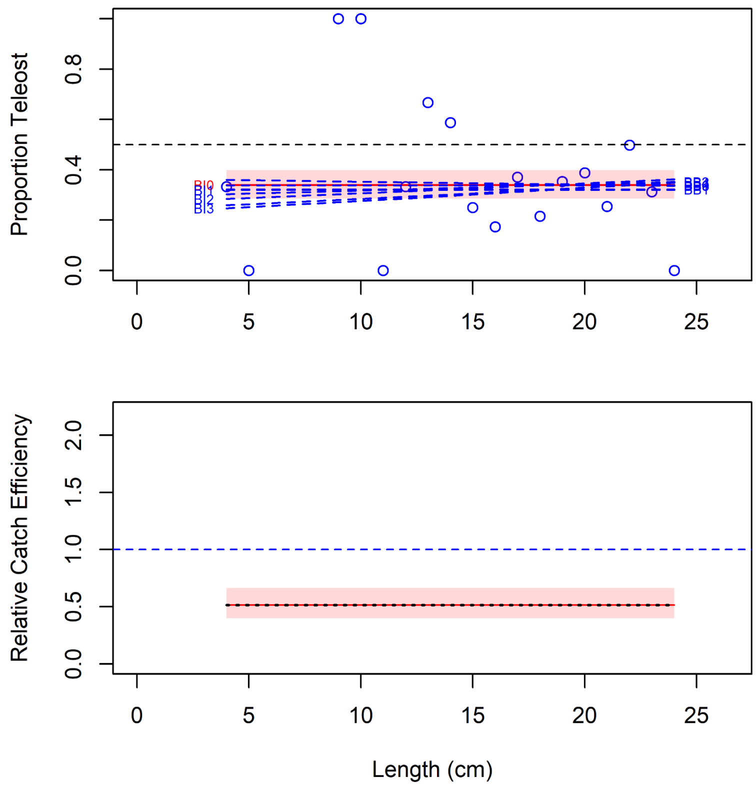

Figure 29b. Model fits and the selected length-based calibration for Leptagonus decagonus.

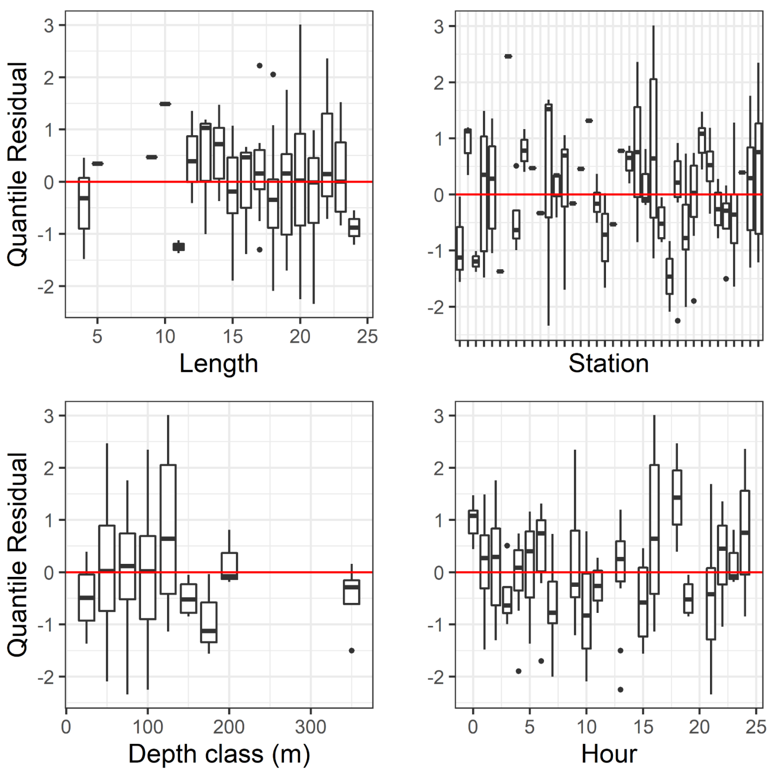

Figure 29c. Normalized quantile residuals for the selected model for Leptagonus decagonus.

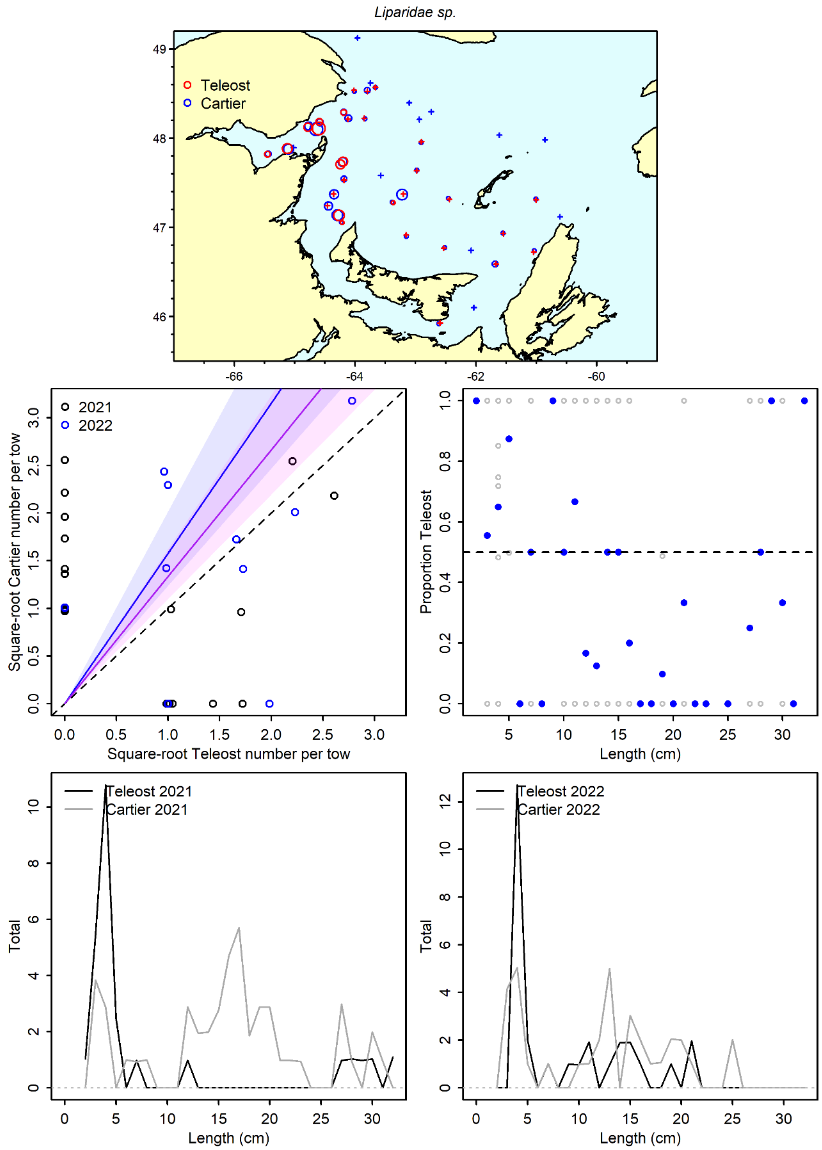

Figure 30a. Visualisation of comparative fishing data and size-aggregated model predictions for Liparidae sp..

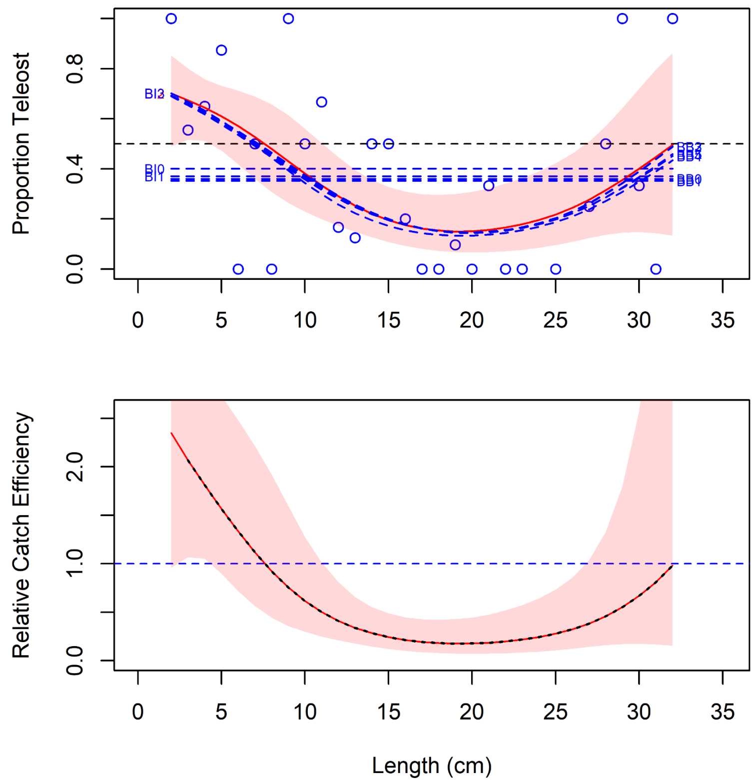

Figure 30b. Model fits and the selected length-based calibration for Liparidae sp..

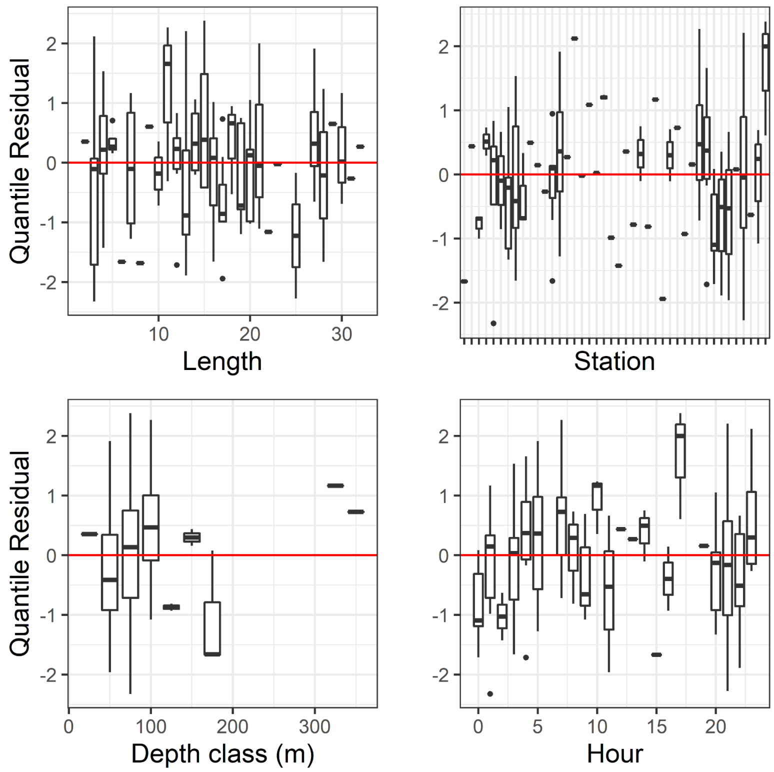

Figure 30c. Normalized quantile residuals for the selected model for Liparidae sp..

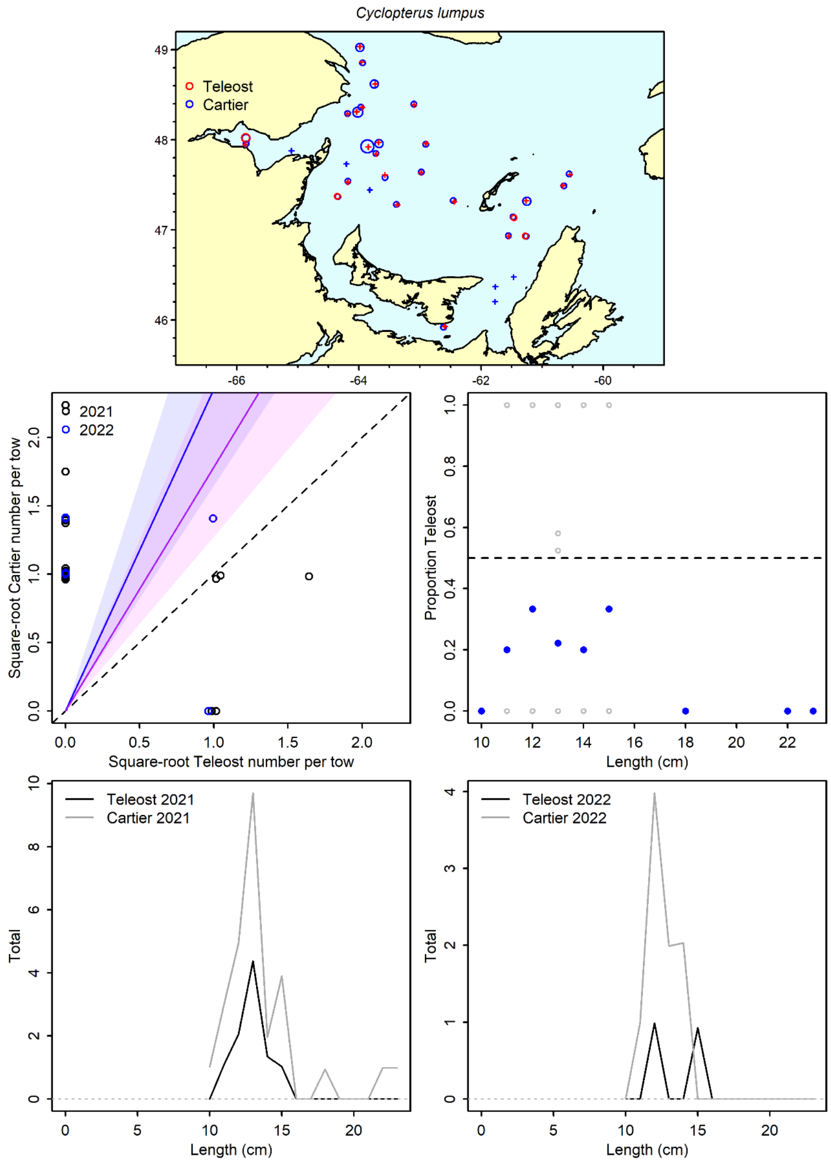

Figure 31a. Visualisation of comparative fishing data and size-aggregated model predictions for Cyclopterus lumpus.

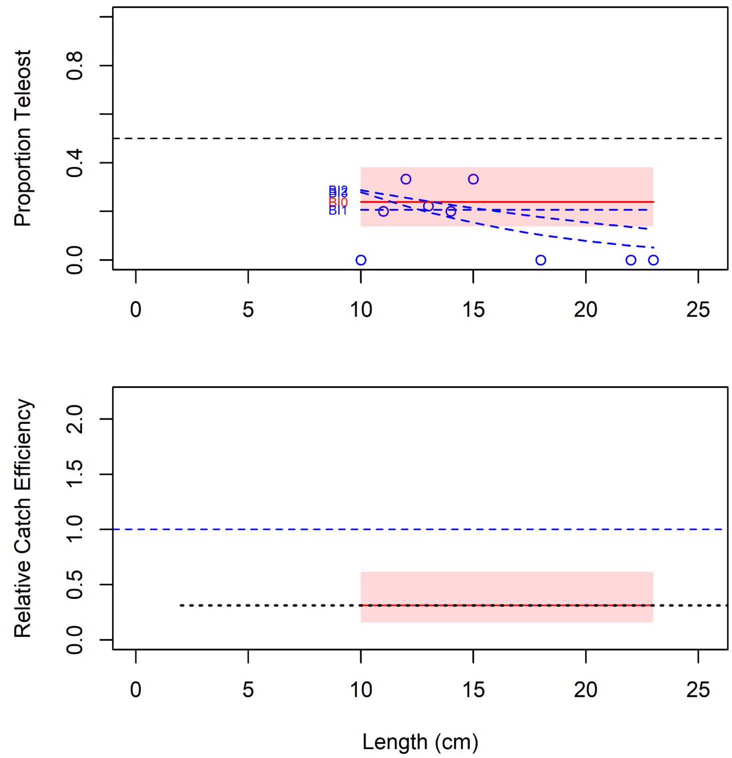

Figure 31b. Model fits and the selected length-based calibration for Cyclopterus lumpus.

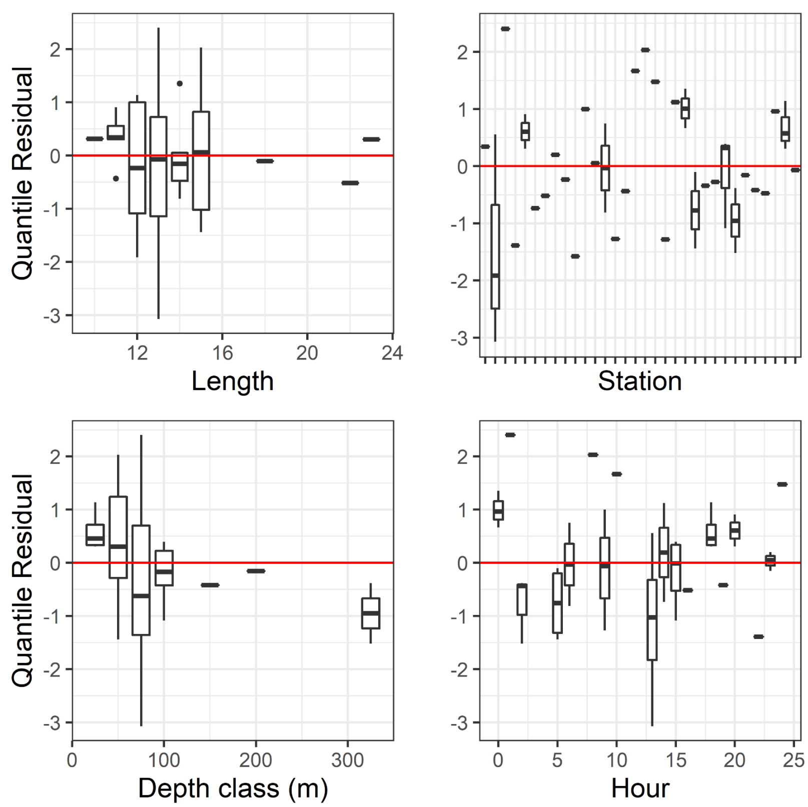

Figure 31c. Normalized quantile residuals for the selected model for Cyclopterus lumpus.

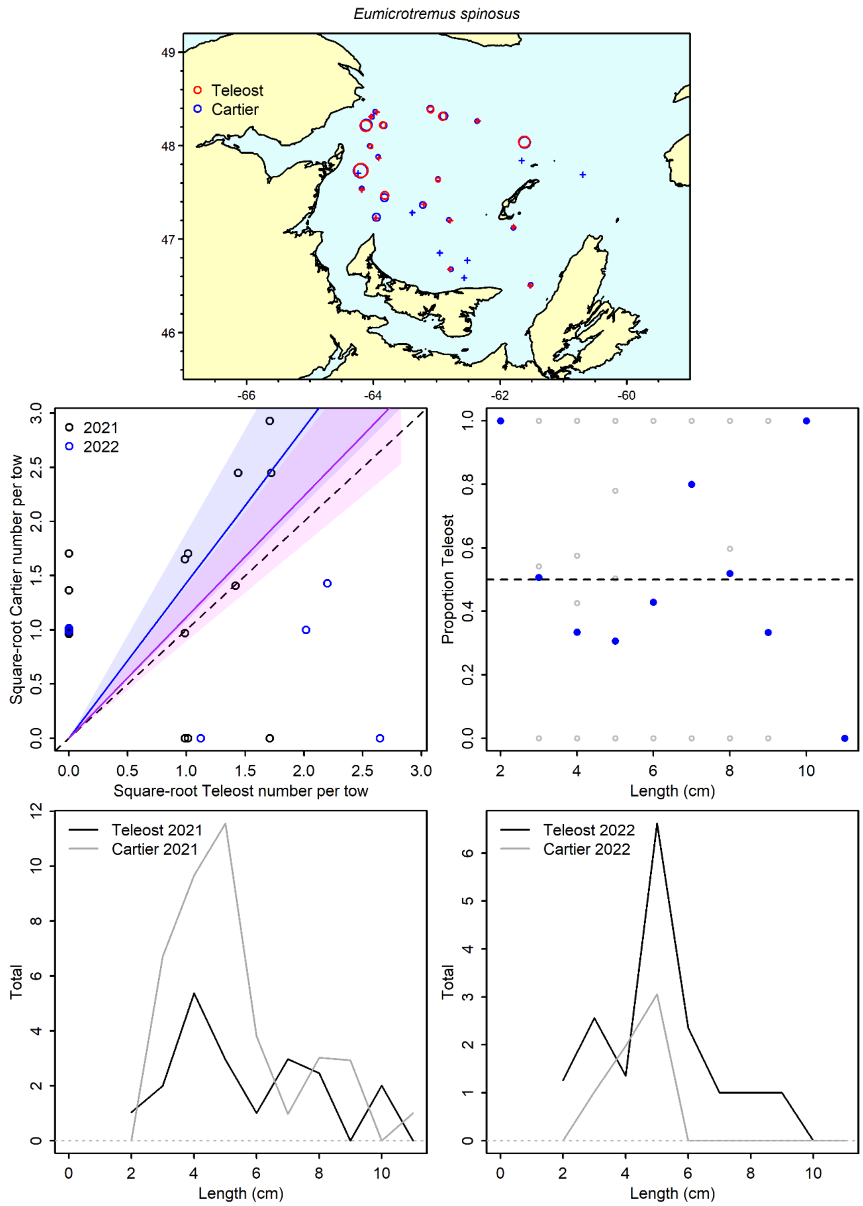

Figure 32a. Visualisation of comparative fishing data and size-aggregated model predictions for Eumicrotremus spinosus*.*

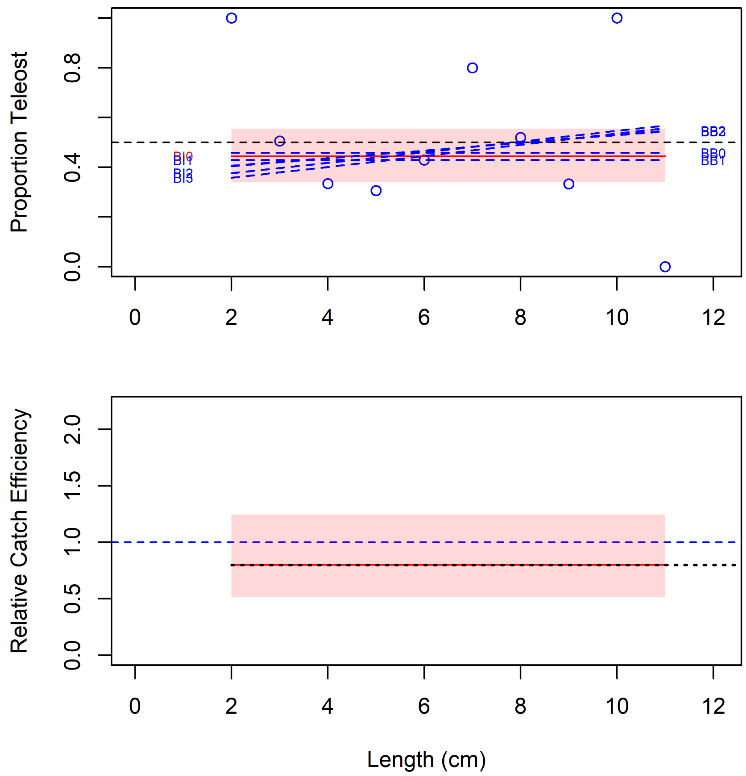

Figure 32b. Model fits and the selected length-based calibration for Eumicrotremus spinosus.

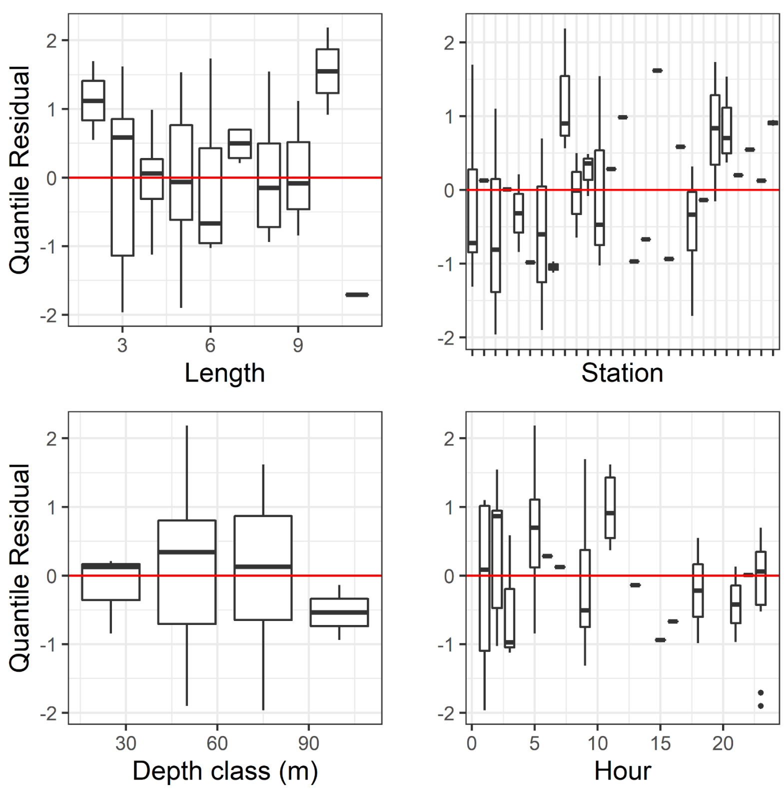

Figure 32c. Normalized quantile residuals for the selected model for Eumicrotremus spinosus.

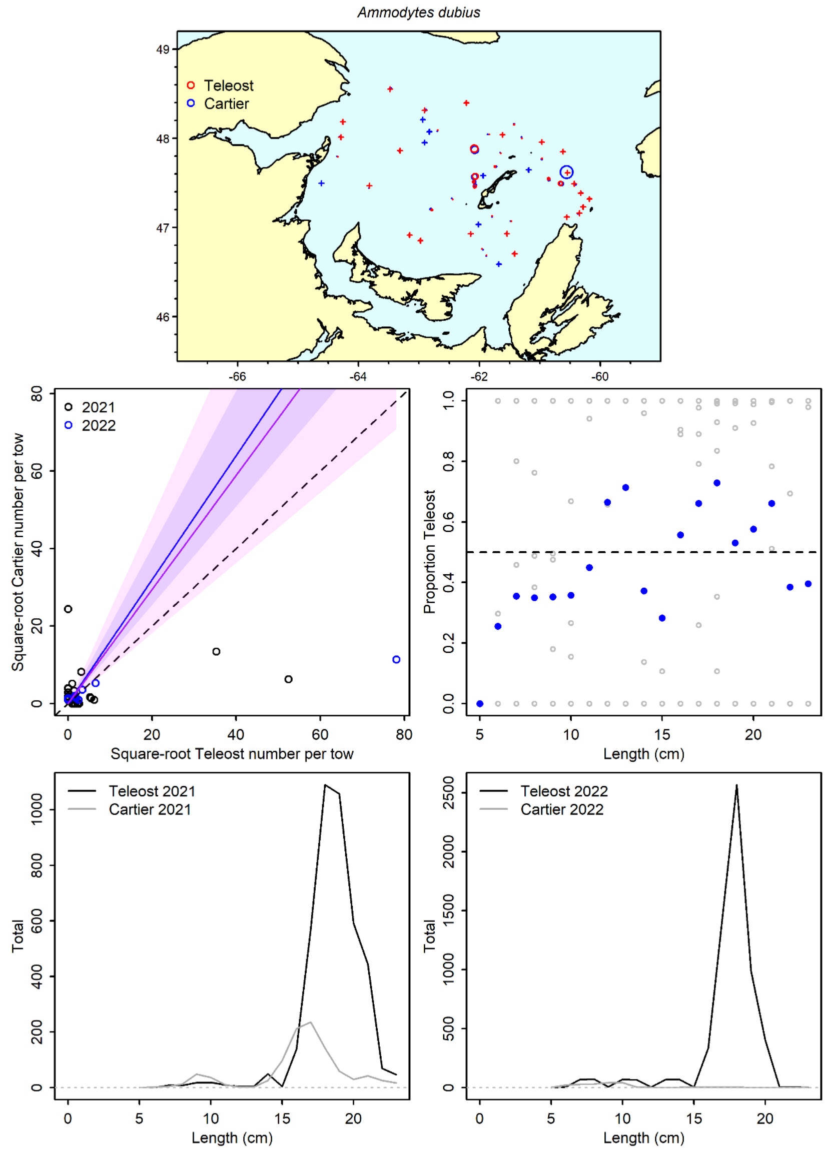

Figure 33a. Visualisation of comparative fishing data and size-aggregated model predictions for Ammodytes dubius*.*

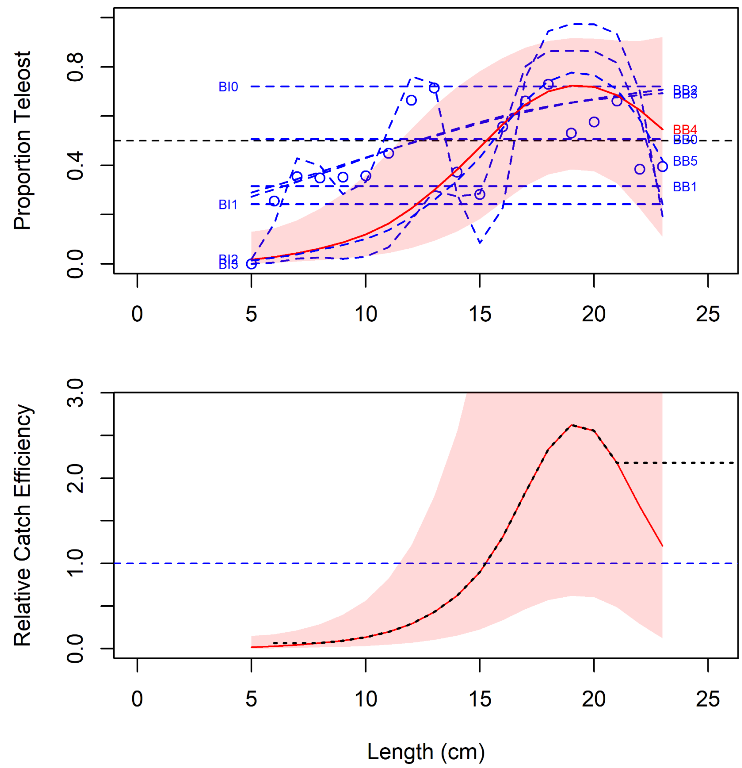

Figure 33b. Model fits and the selected length-based calibration for Ammodytes dubius.

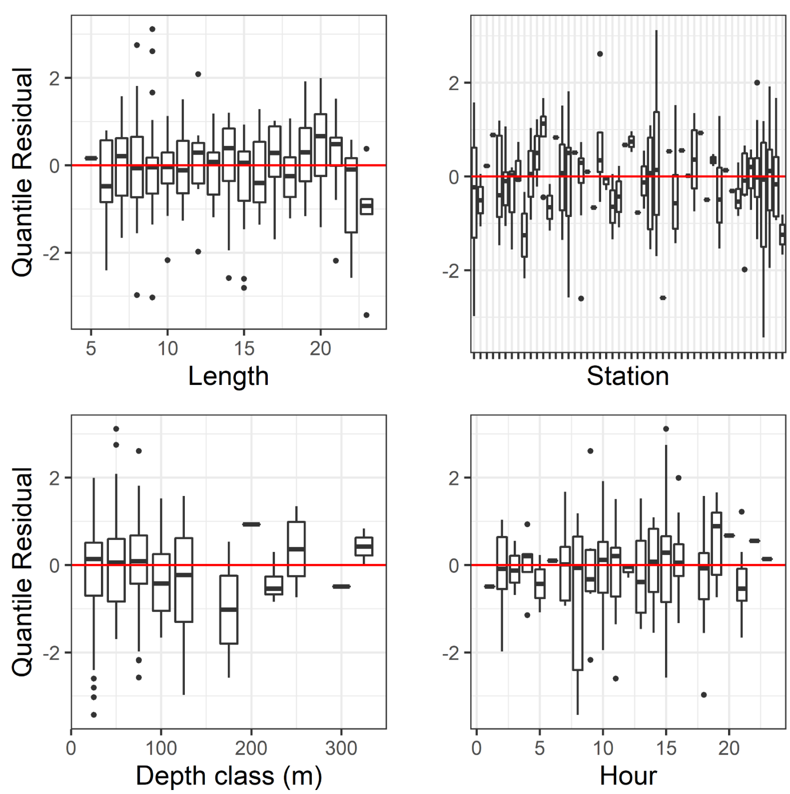

Figure 33c. Normalized quantile residuals for the selected model for Ammodytes dubius.

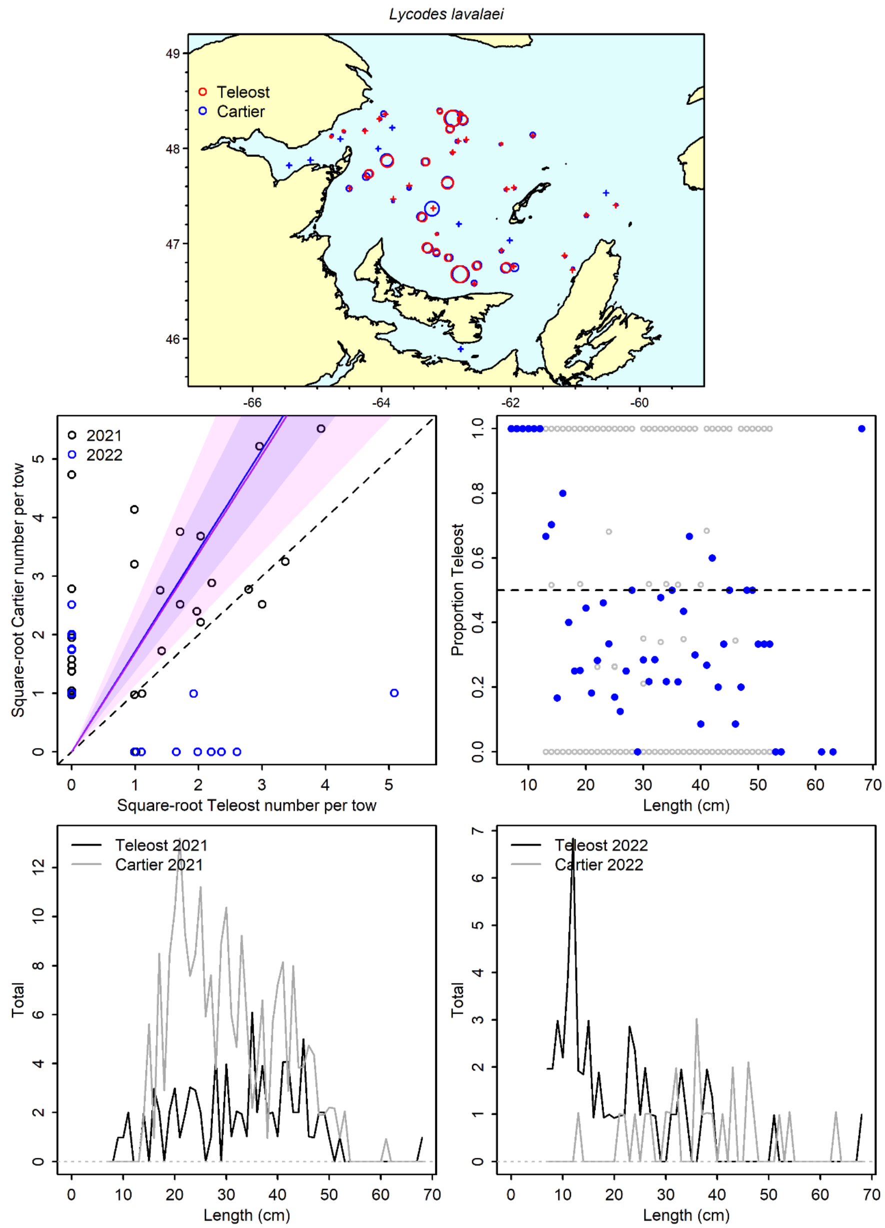

Figure 34a. Visualisation of comparative fishing data and size-aggregated model predictions for Lycodes lavalaei.

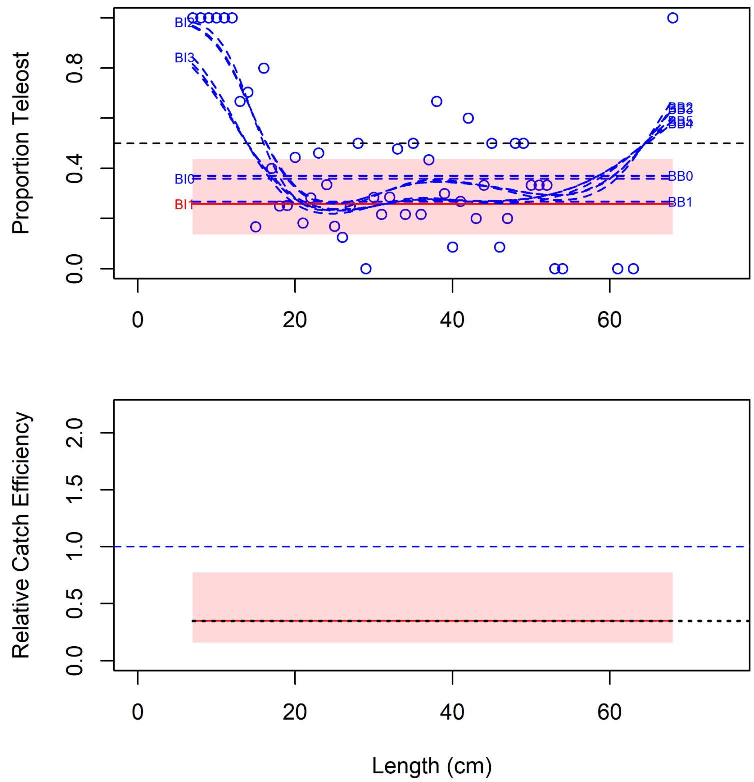

Figure 34b. Model fits and the selected length-based calibration for Lycodes lavalaei*.*

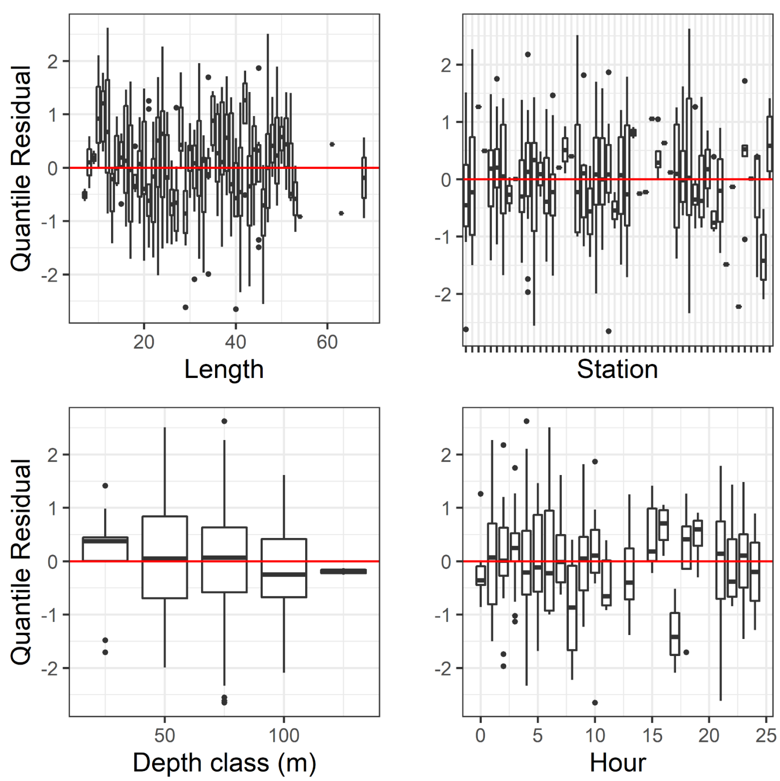

Figure 34c. Normalized quantile residuals for the selected model for Lycodes lavalaei*.*

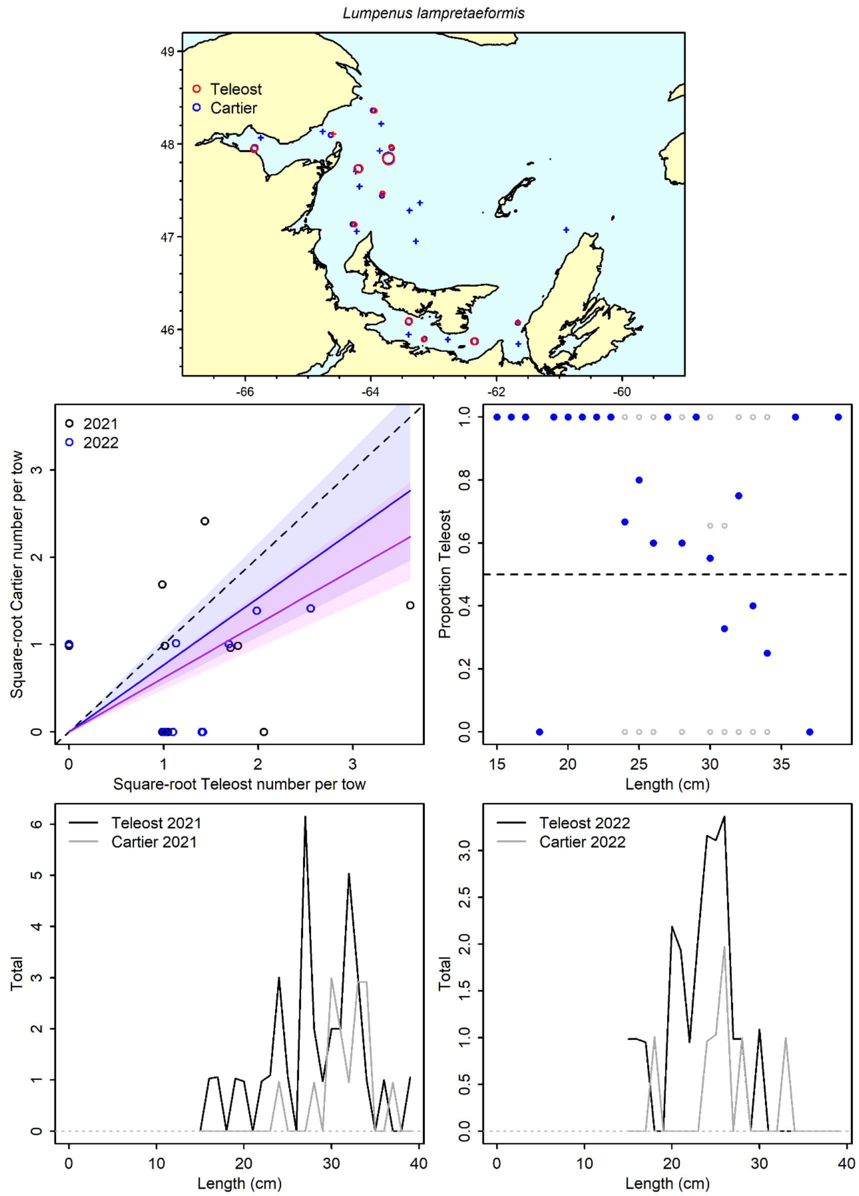

Figure 35a. Visualisation of comparative fishing data and size-aggregated model predictions for Lumpenus lampretaeformis*.*

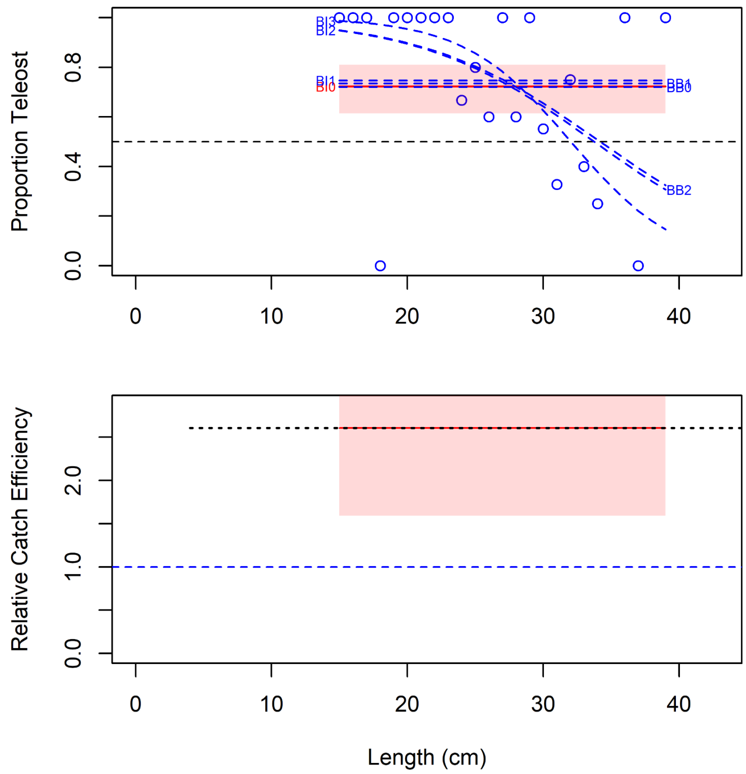

Figure 35b. Model fits and the selected length-based calibration for Lumpenus lampretaeformis.

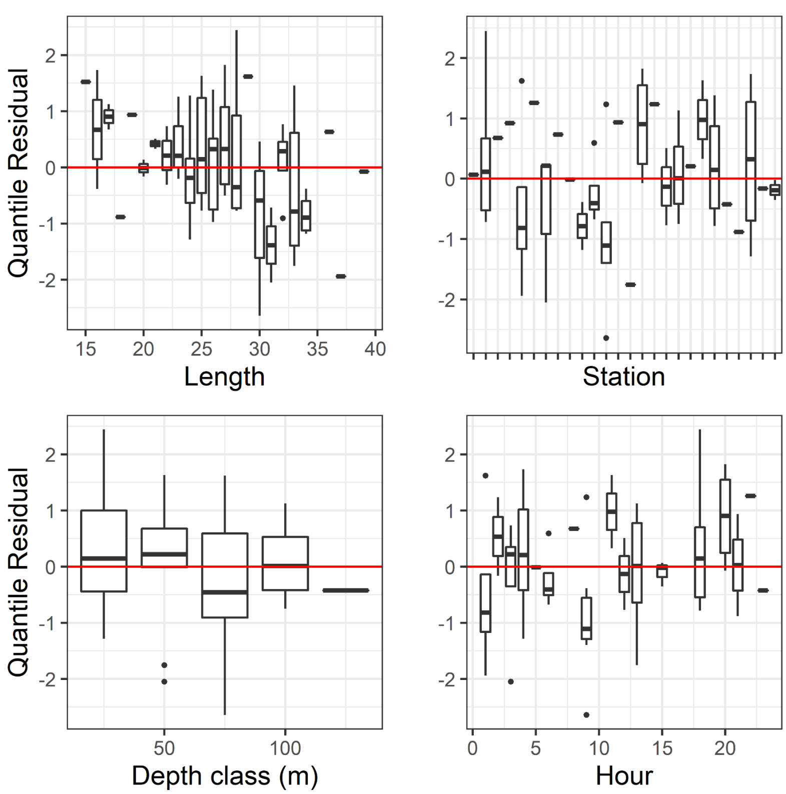

Figure 35c. Normalized quantile residuals for the selected model for Lumpenus lampretaeformis.

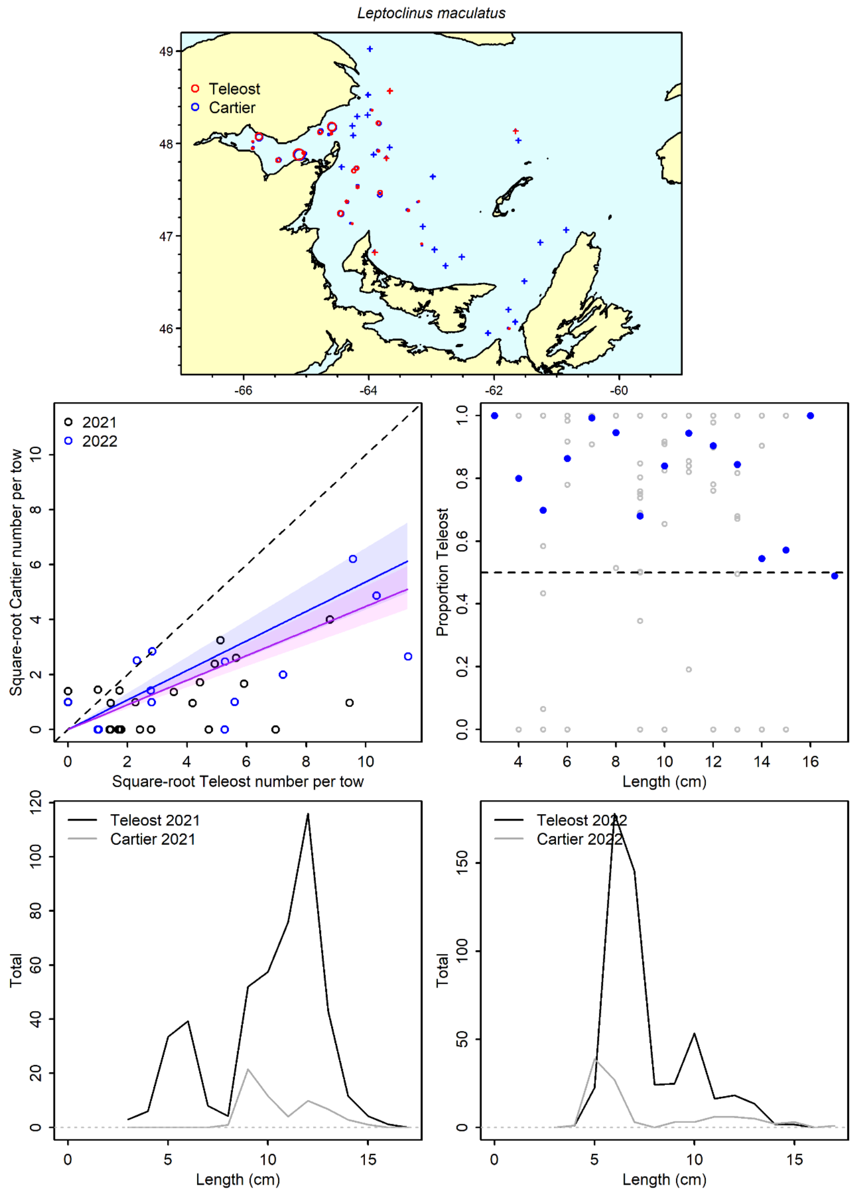

Figure 36a. Visualisation of comparative fishing data and size-aggregated model predictions for Leptoclinus maculatus.

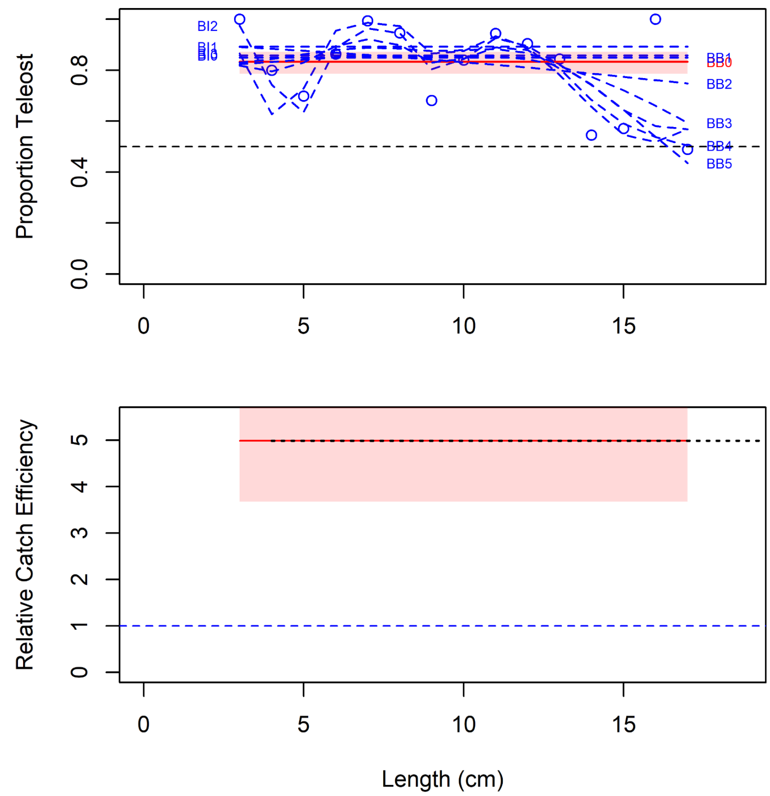

Figure 36b. Model fits and the selected length-based calibration for Leptoclinus maculatus.

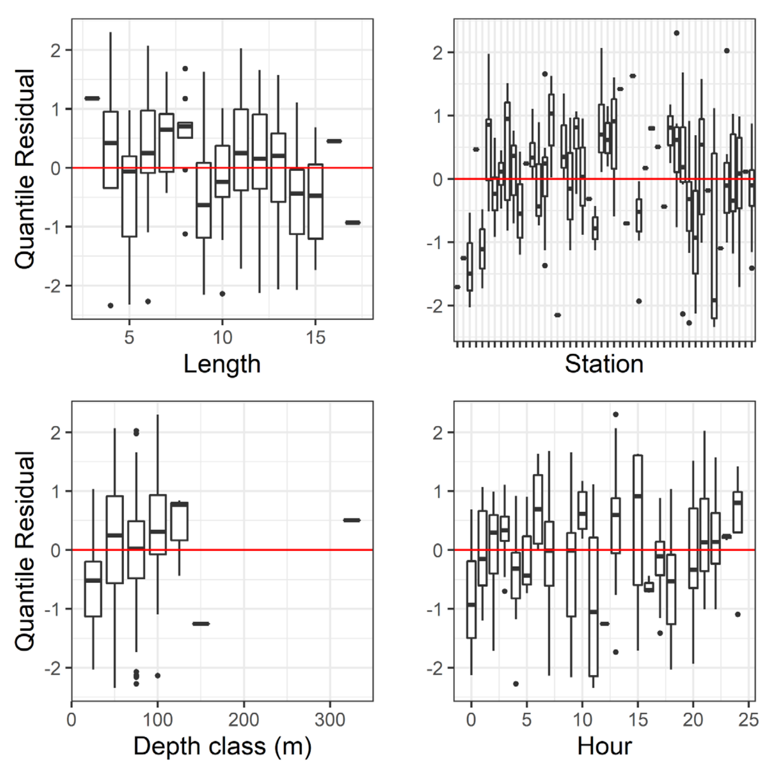

Figure 36c. Normalized quantile residuals for the selected model for Leptoclinus maculatus.

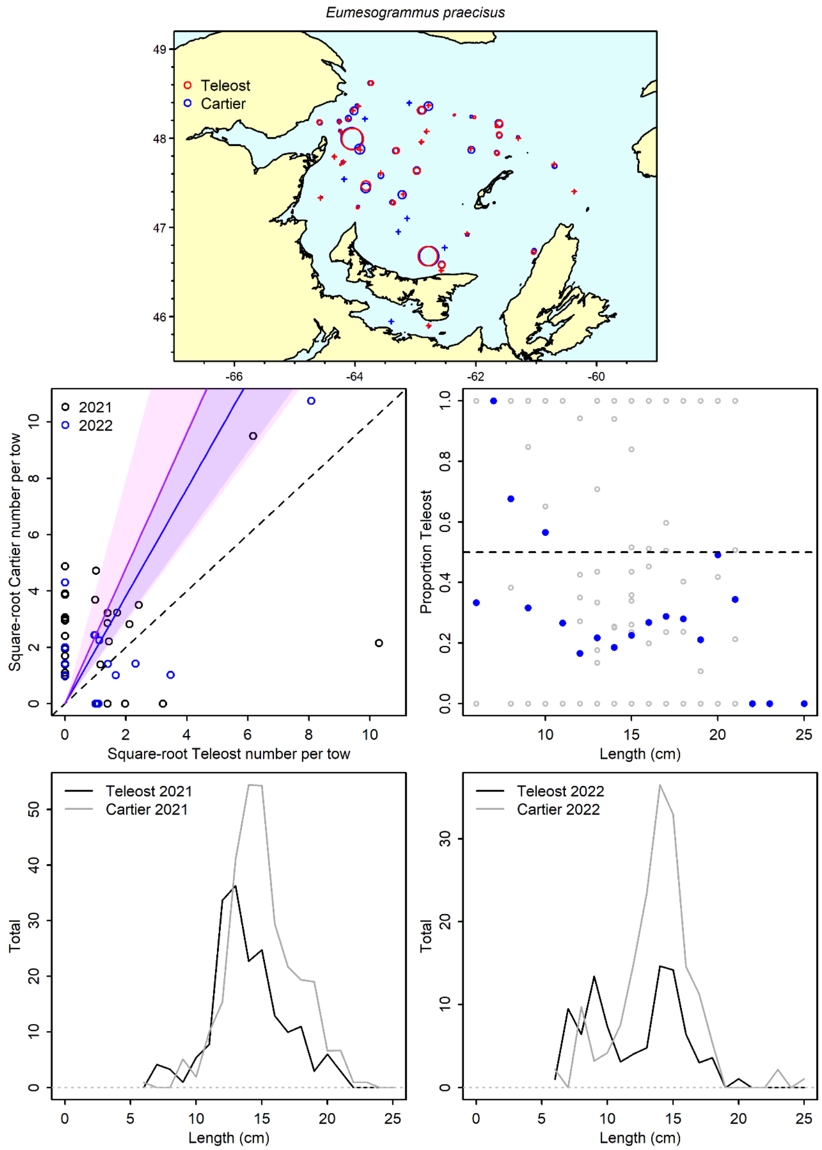

Figure 37a. Visualisation of comparative fishing data and size-aggregated model predictions for Eumesogrammus praecisus.

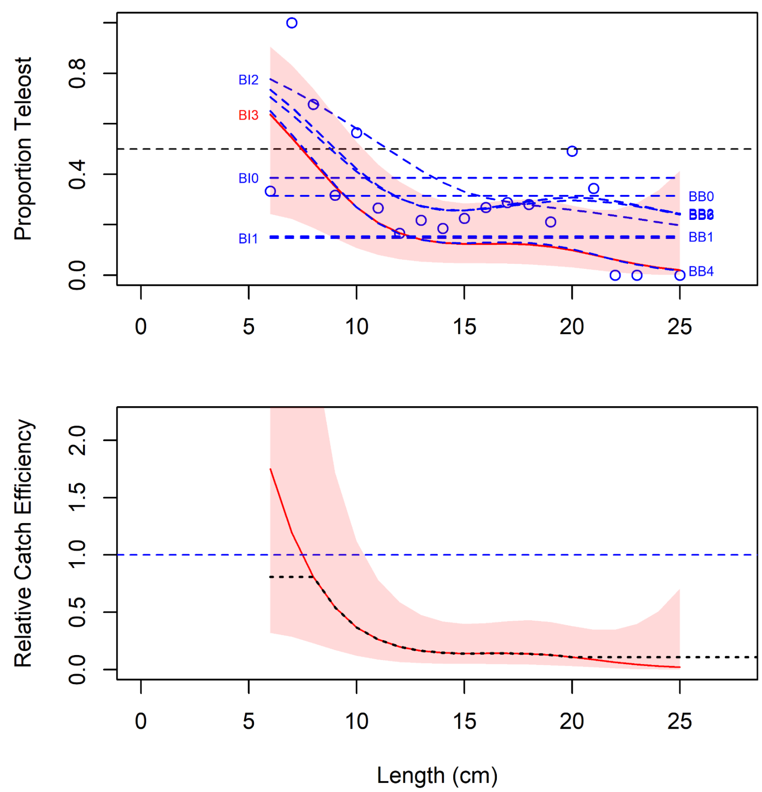

Figure 37b. Model fits and the selected length-based calibration for Eumesogrammus praecisus*.*

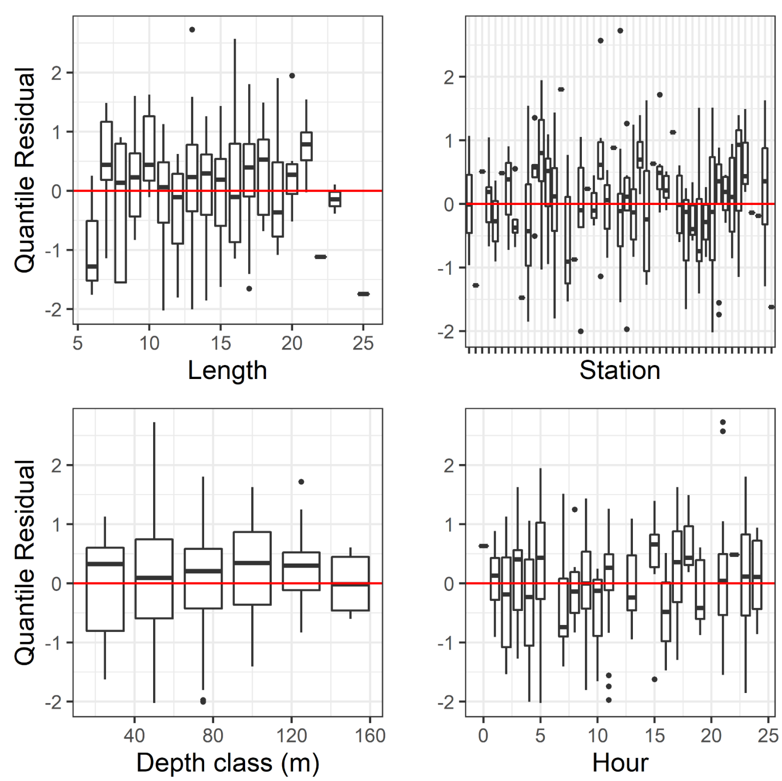

Figure 37c. Normalized quantile residuals for the selected model for Eumesogrammus praecisus*.*

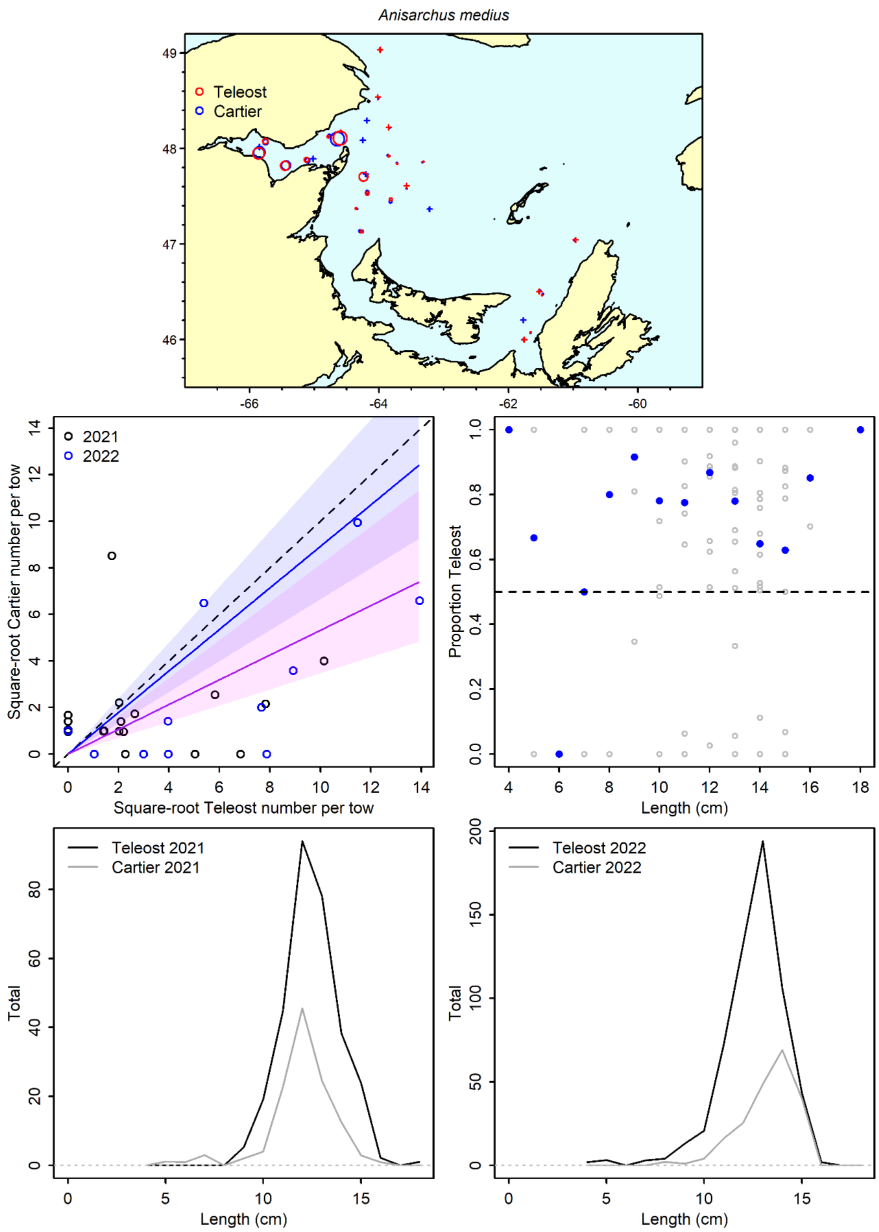

Figure 38a. Visualisation of comparative fishing data and size-aggregated model predictions for Anisarchus medius*.*

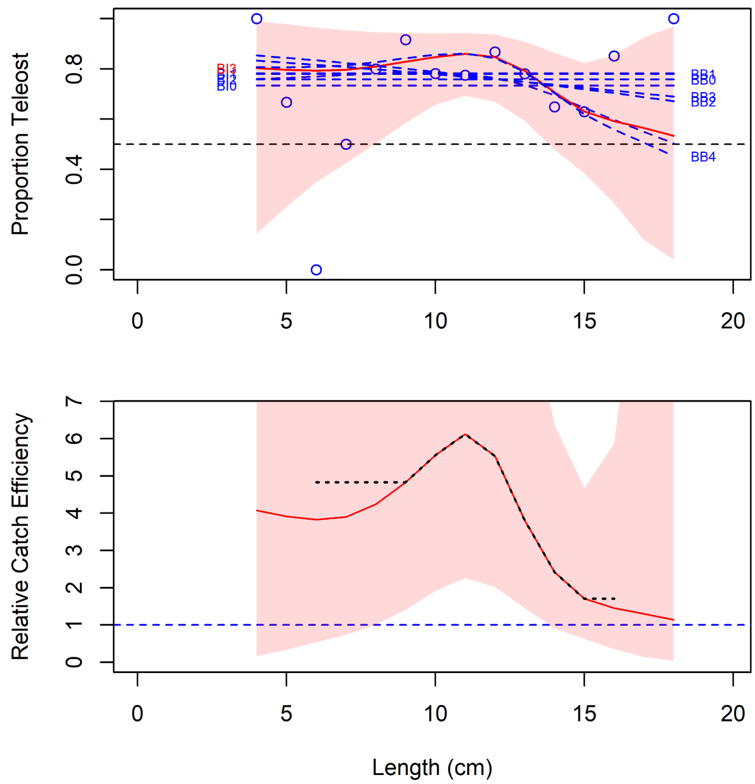

Figure 38b. Model fits and the selected length-based calibration for Anisarchus medius.

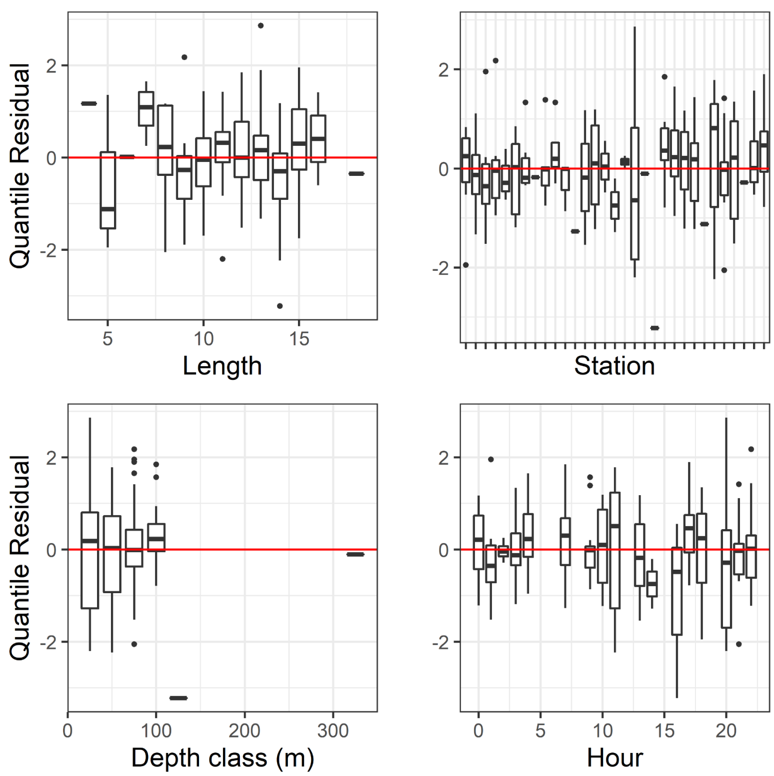

Figure 38c. Normalized quantile residuals for the selected model for Anisarchus medius.

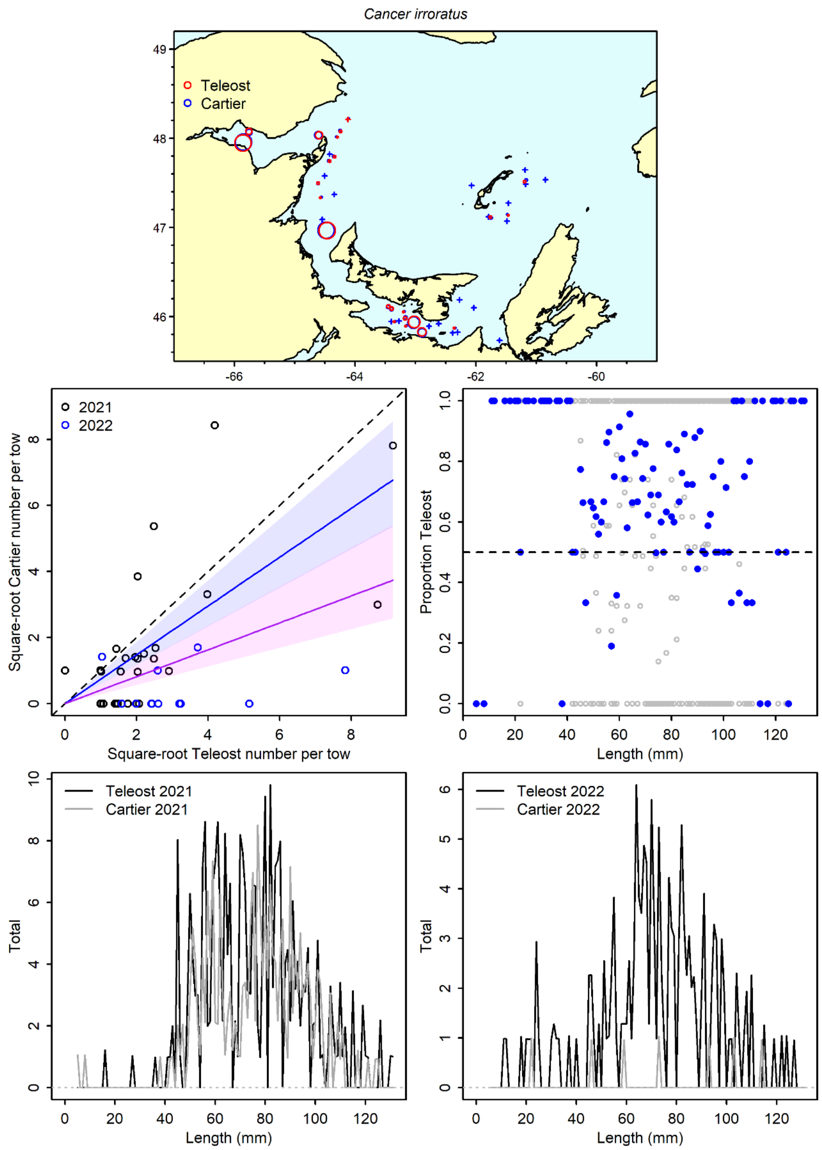

Figure 39a. Visualisation of comparative fishing data and size-aggregated model predictions for Cancer irroratus*.*

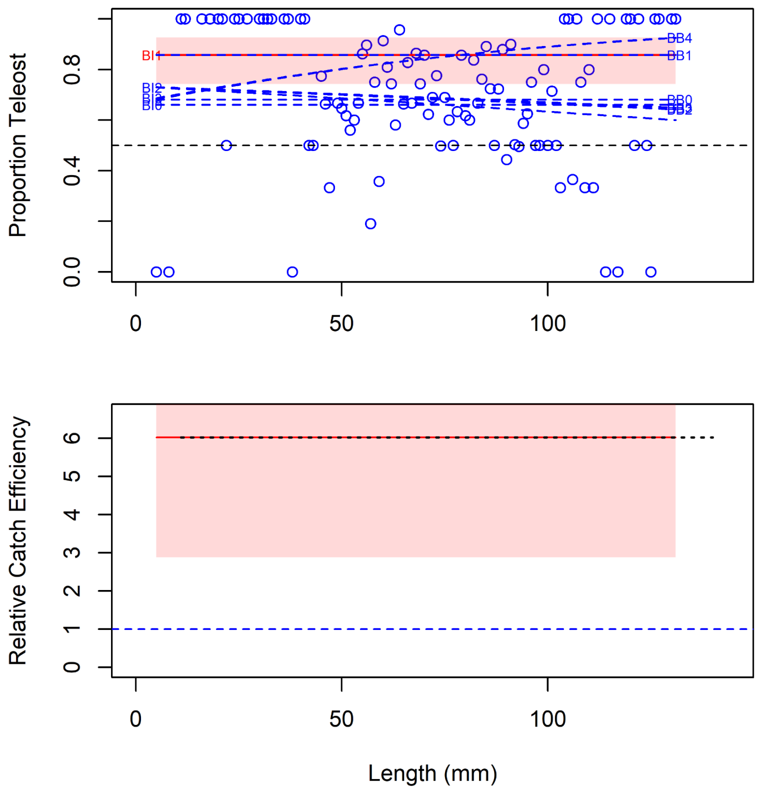

Figure 39b. Model fits and the selected length-based calibration for Cancer irroratus.

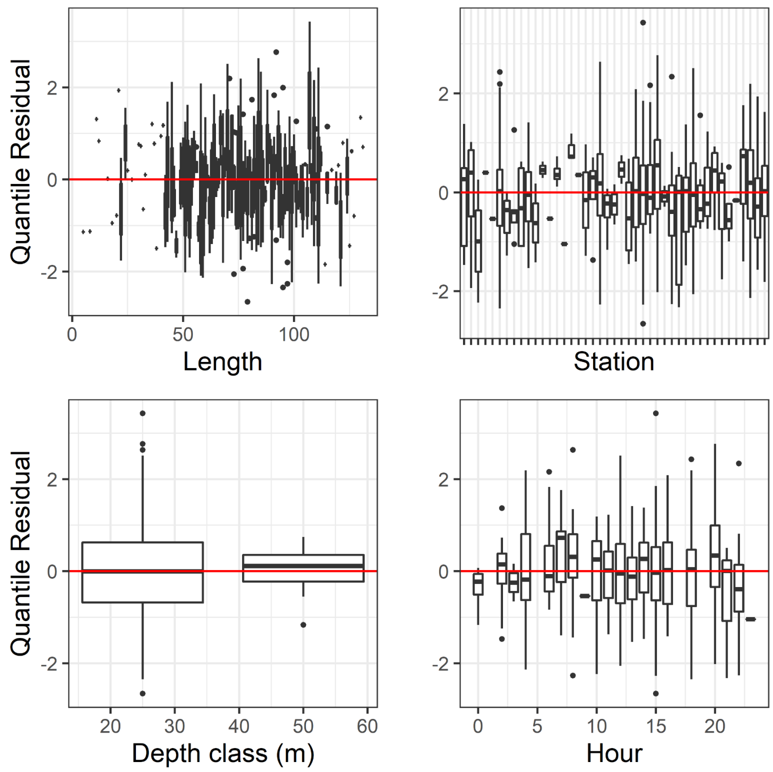

Figure 39c. Normalized quantile residuals for the selected model for Cancer irroratus.

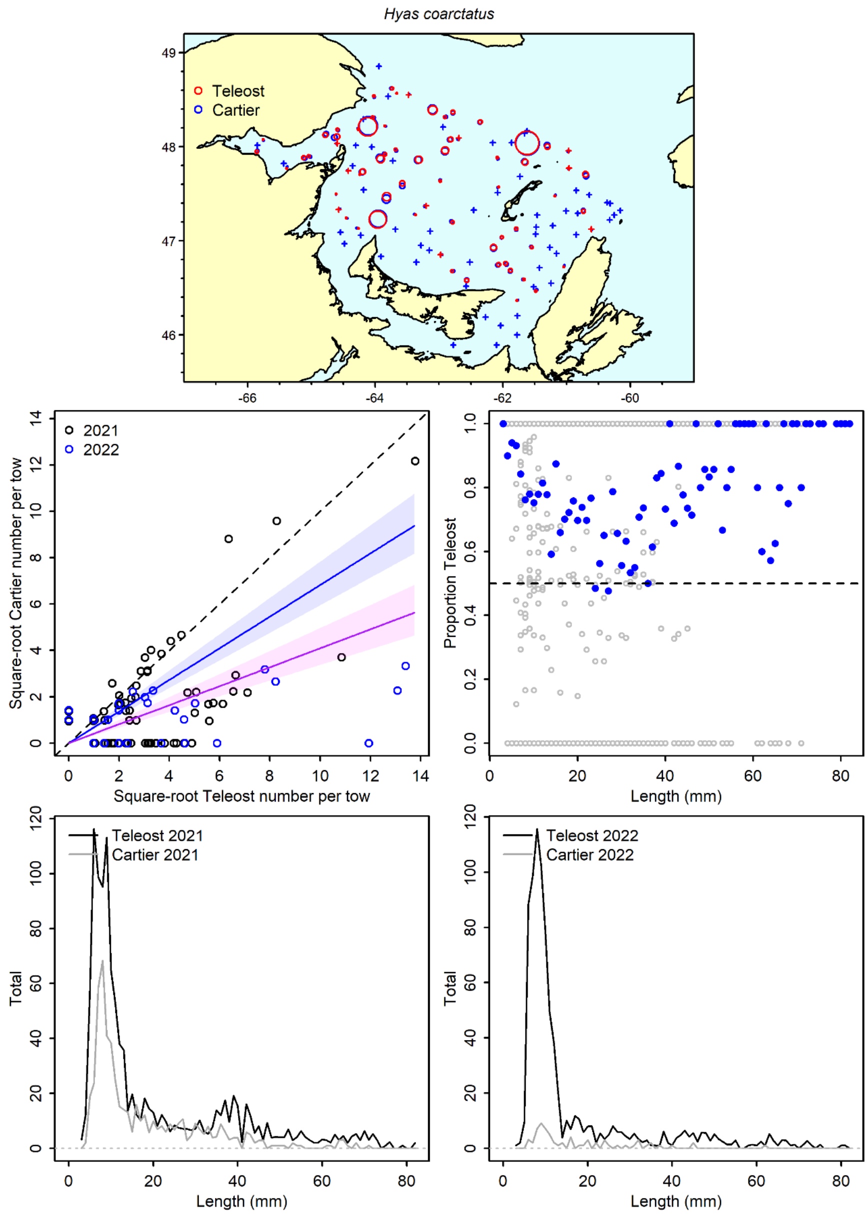

Figure 40a. Visualisation of comparative fishing data and size-aggregated model predictions for Hyas coarctatus.

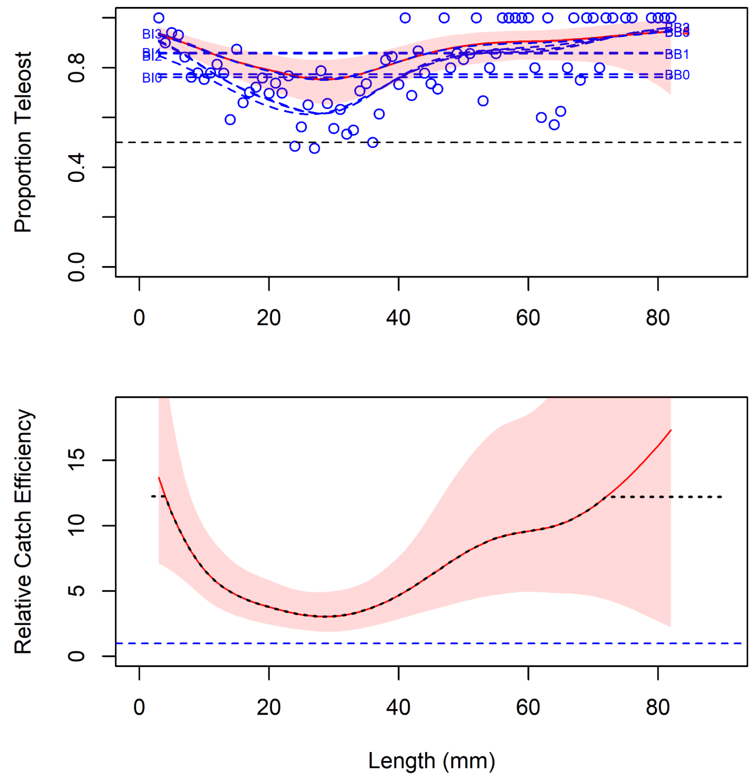

Figure 40b. Model fits and the selected length-based calibration for Hyas coarctatus.

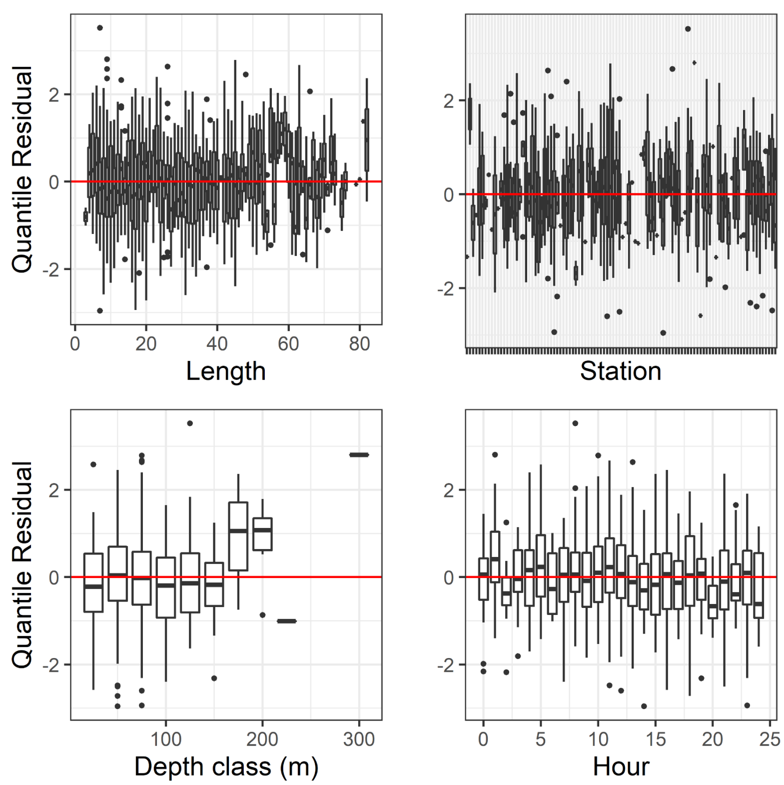

Figure 40c. Normalized quantile residuals for the selected model for Hyas coarctatus.

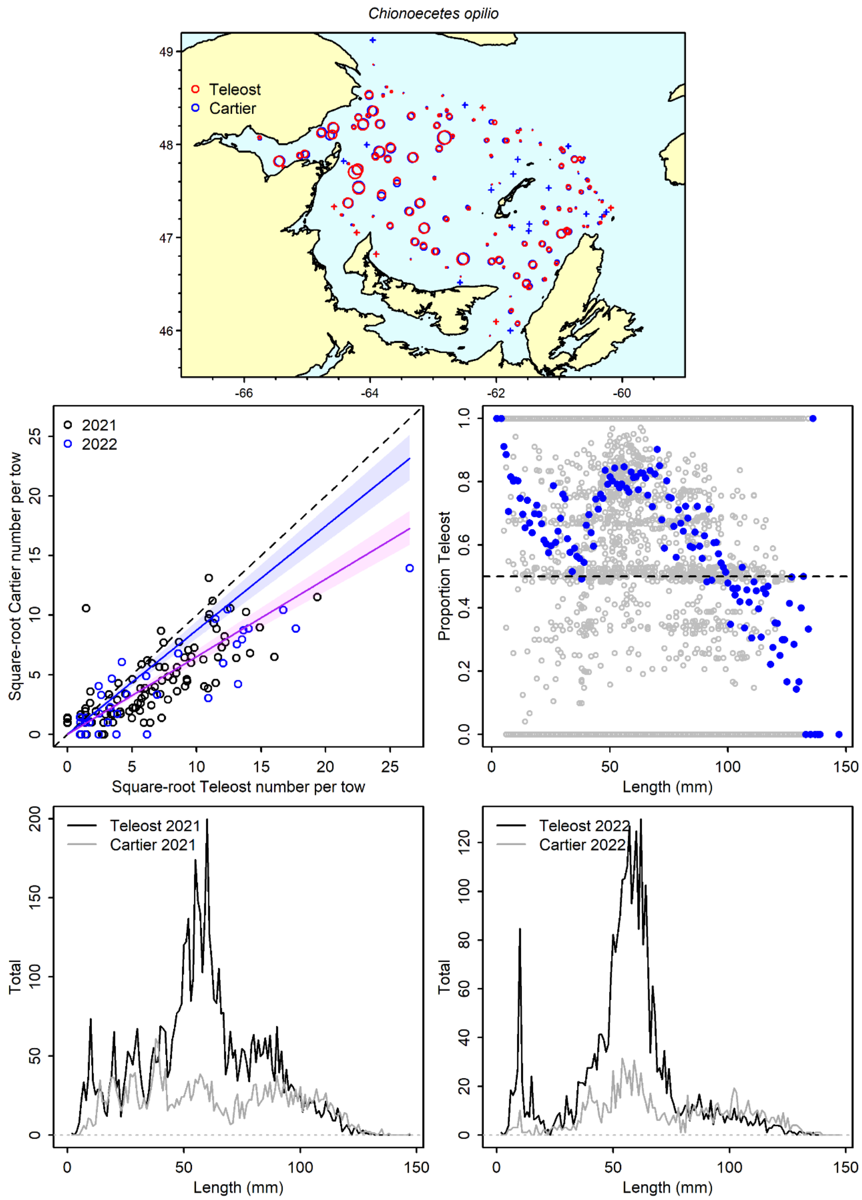

Figure 41a. Visualisation of comparative fishing data and size-aggregated model predictions for Chionoecetes opilio*.*

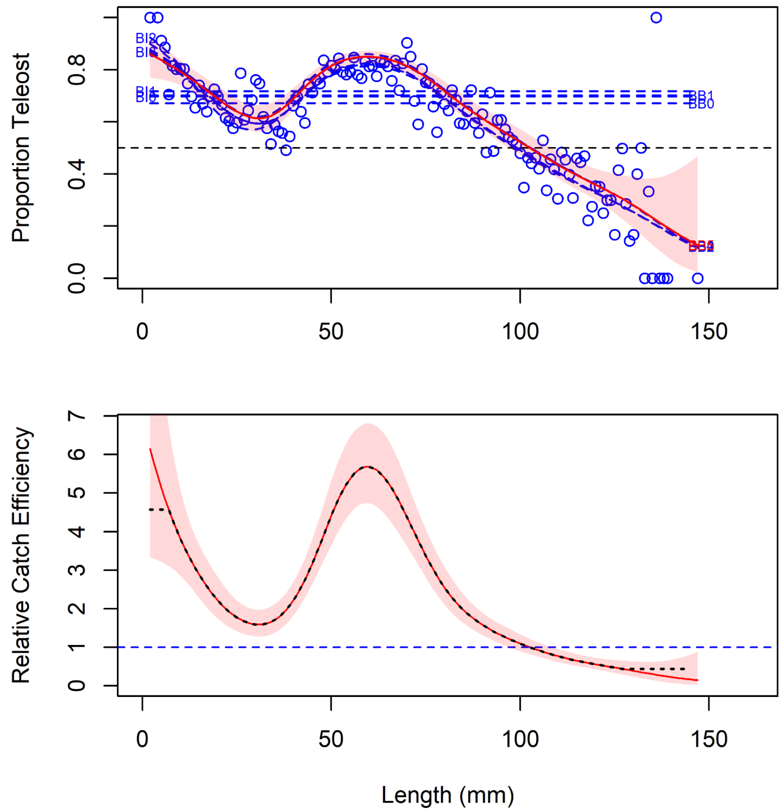

Figure 41b. Model fits and the selected length-based calibration for Chionoecetes opilio.

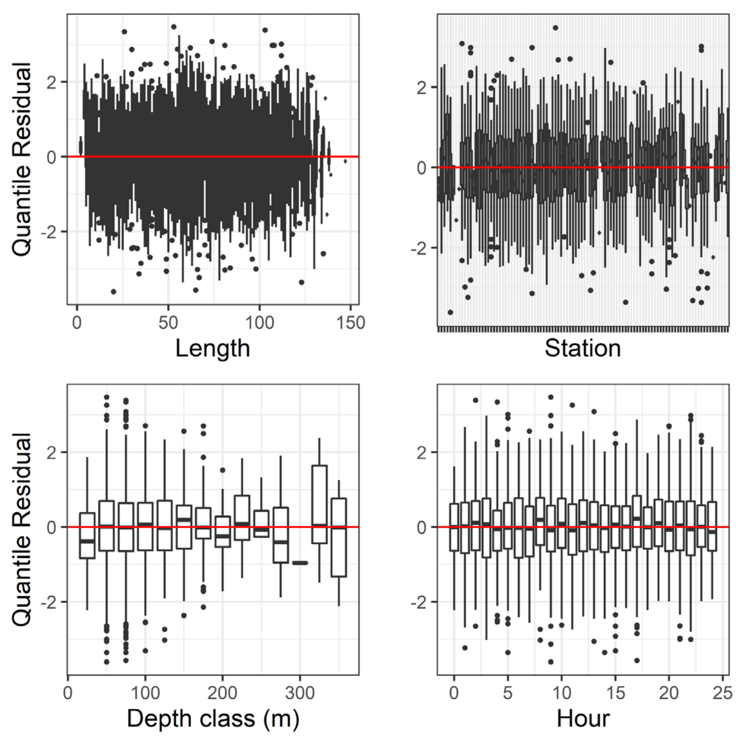

Figure 41c. Normalized quantile residuals for the selected model for Chionoecetes opilio.

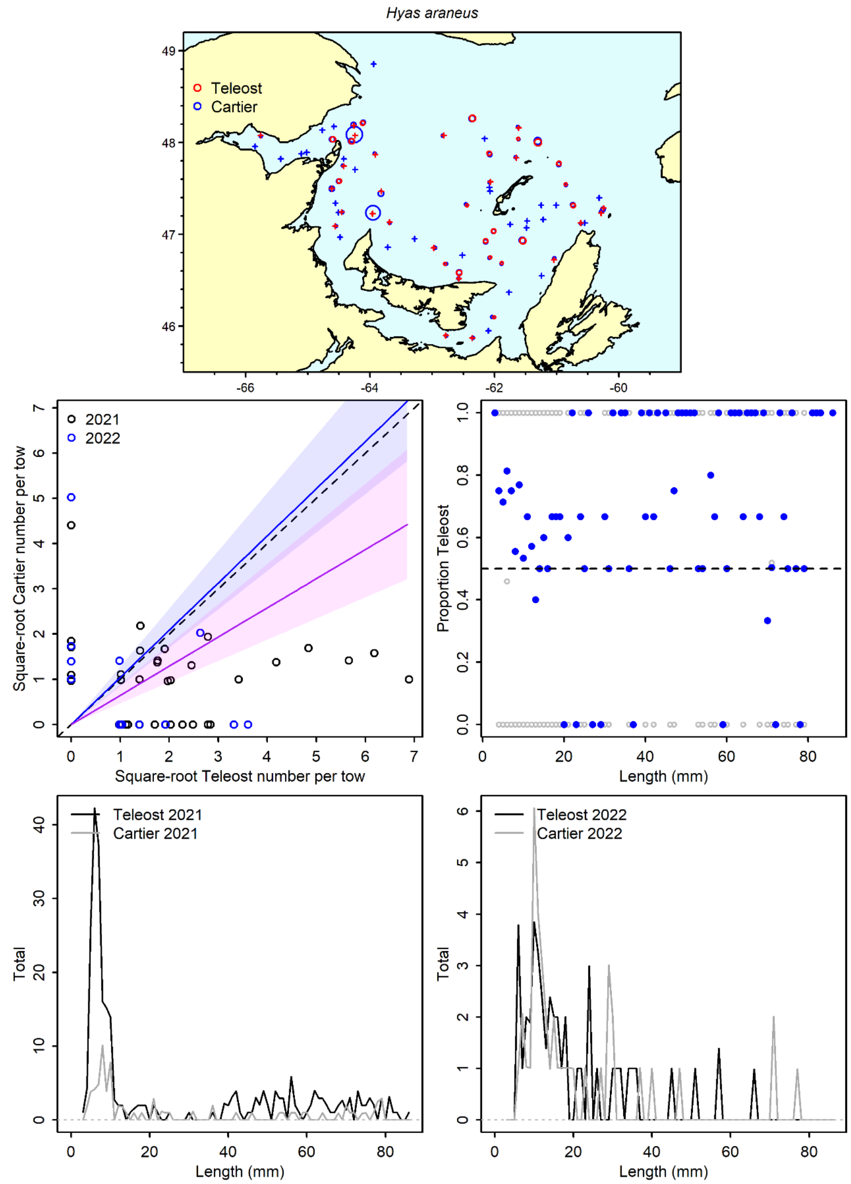

Figure 42a. Visualisation of comparative fishing data and size-aggregated model predictions for Hyas araneus*.*

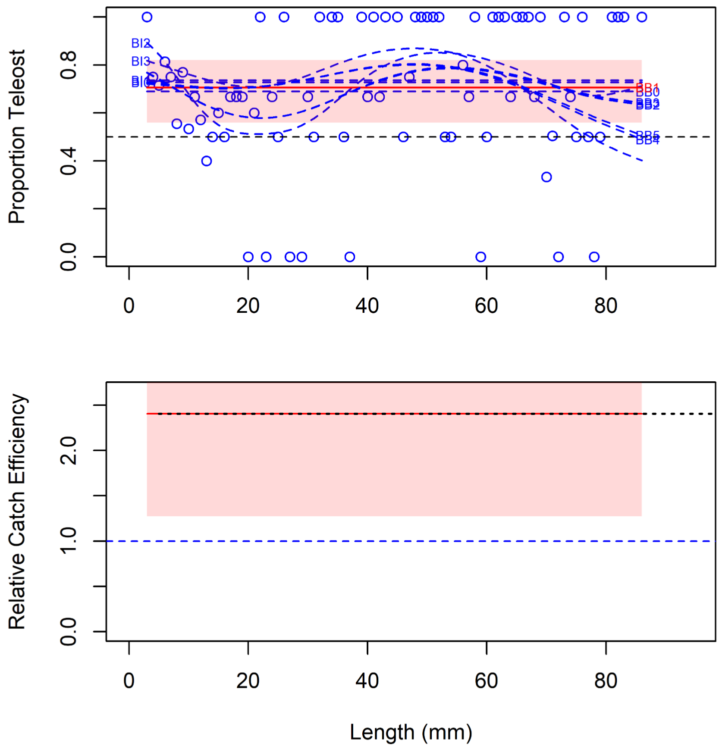

Figure 42b. Model fits and the selected length-based calibration for Hyas araneus.

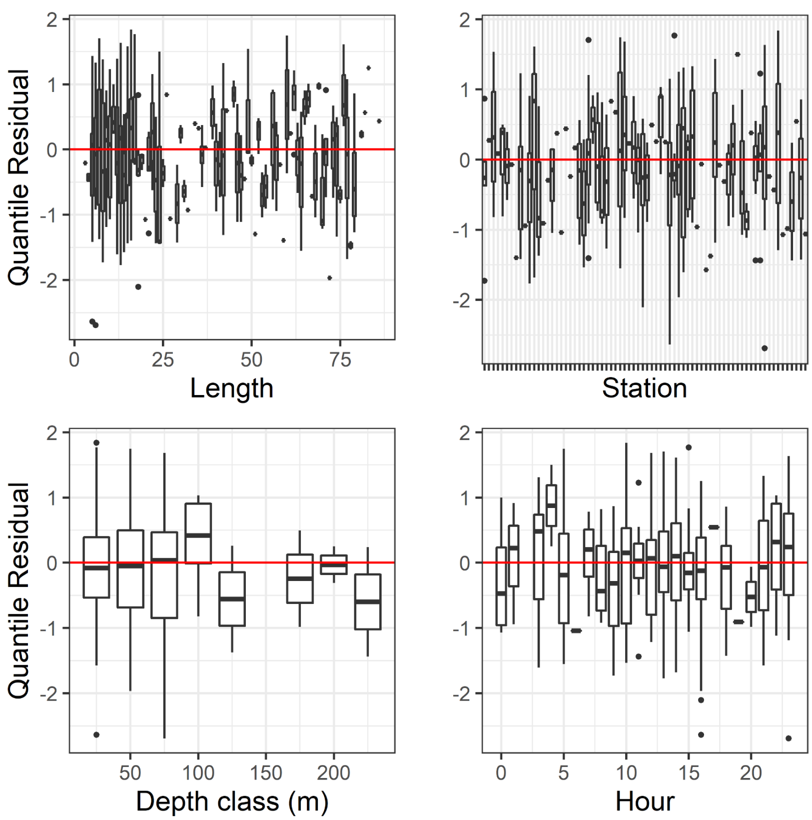

Figure 42c. Normalized quantile residuals for the selected model for Hyas araneus.

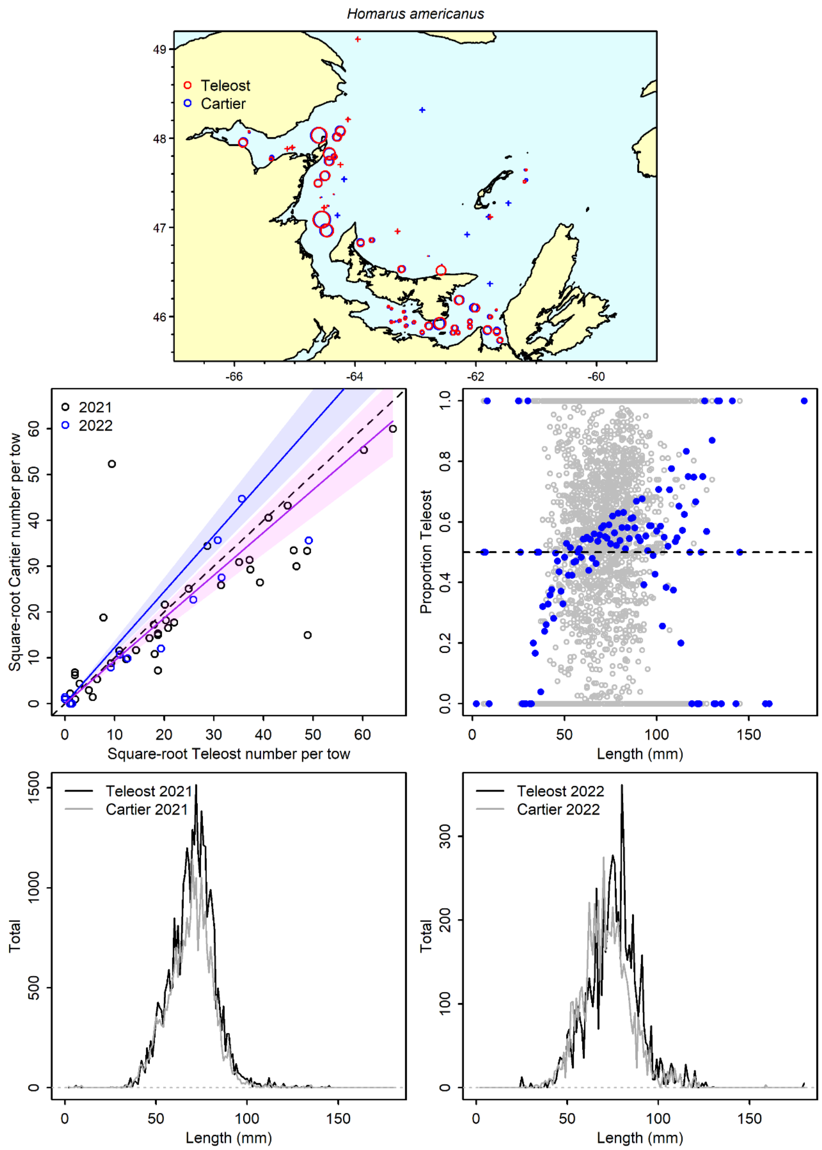

Figure 43a. Visualisation of comparative fishing data and size-aggregated model predictions for Homarus americanus.

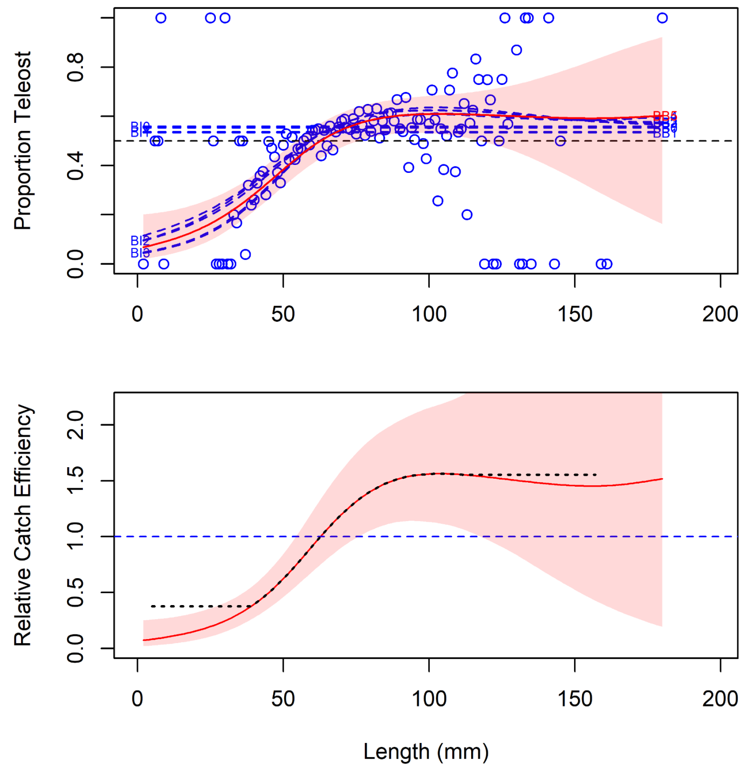

Figure 43b. Model fits and the selected length-based calibration for Homarus americanus*.*

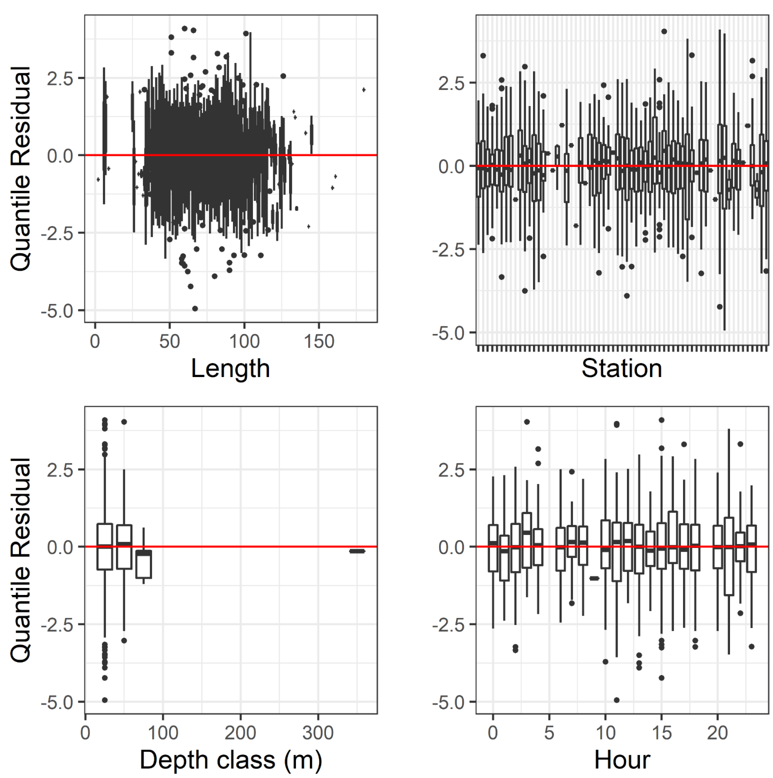

Figure 43c. Normalized quantile residuals for the selected model for Homarus americanus*.*

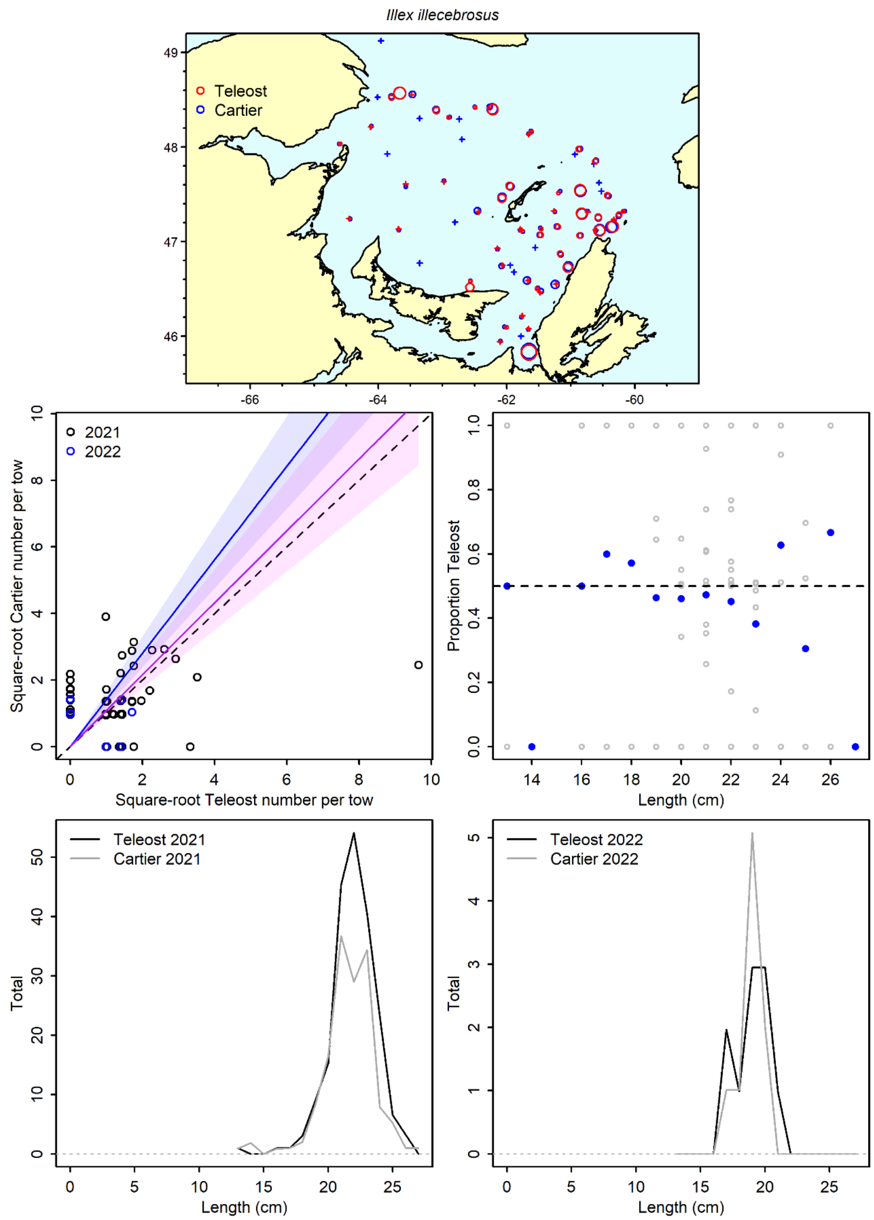

Figure 44a. Visualisation of comparative fishing data and size-aggregated model predictions for Illex illecebrosus.

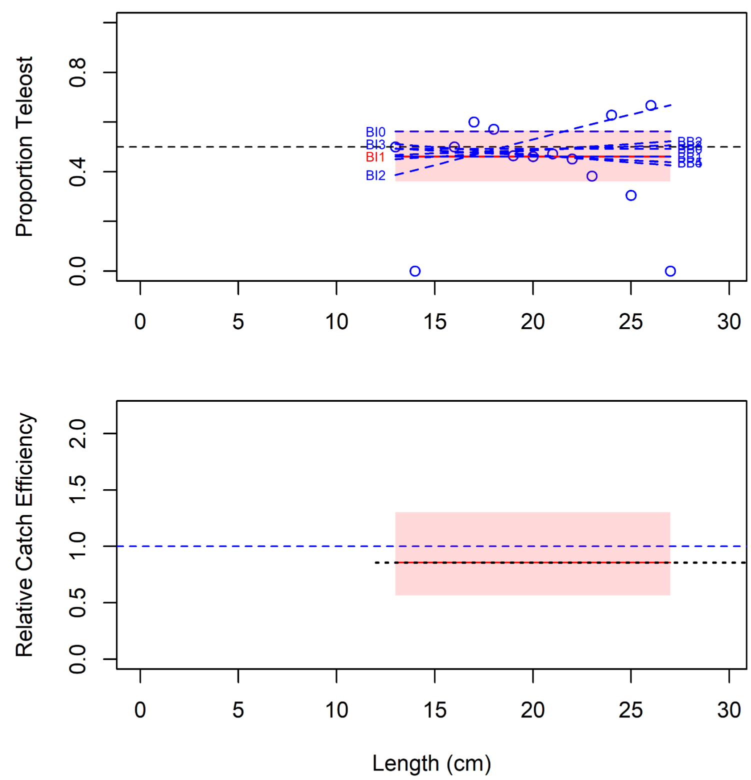

Figure 44b. Model fits and the selected length-based calibration for Illex illecebrosus*.*

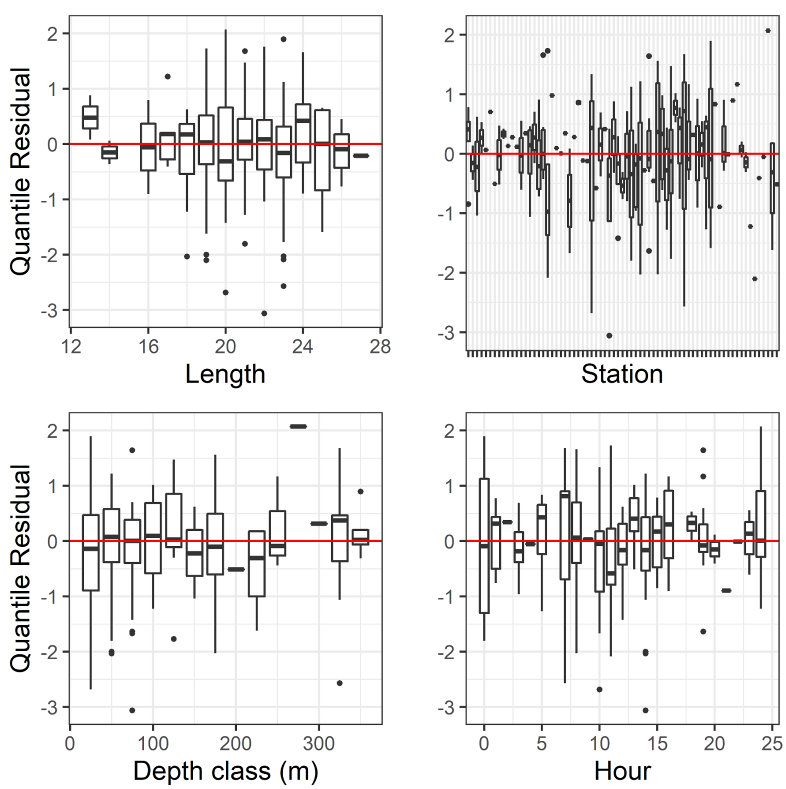

Figure 44c. Normalized quantile residuals for the selected model for Illex illecebrosus*.*

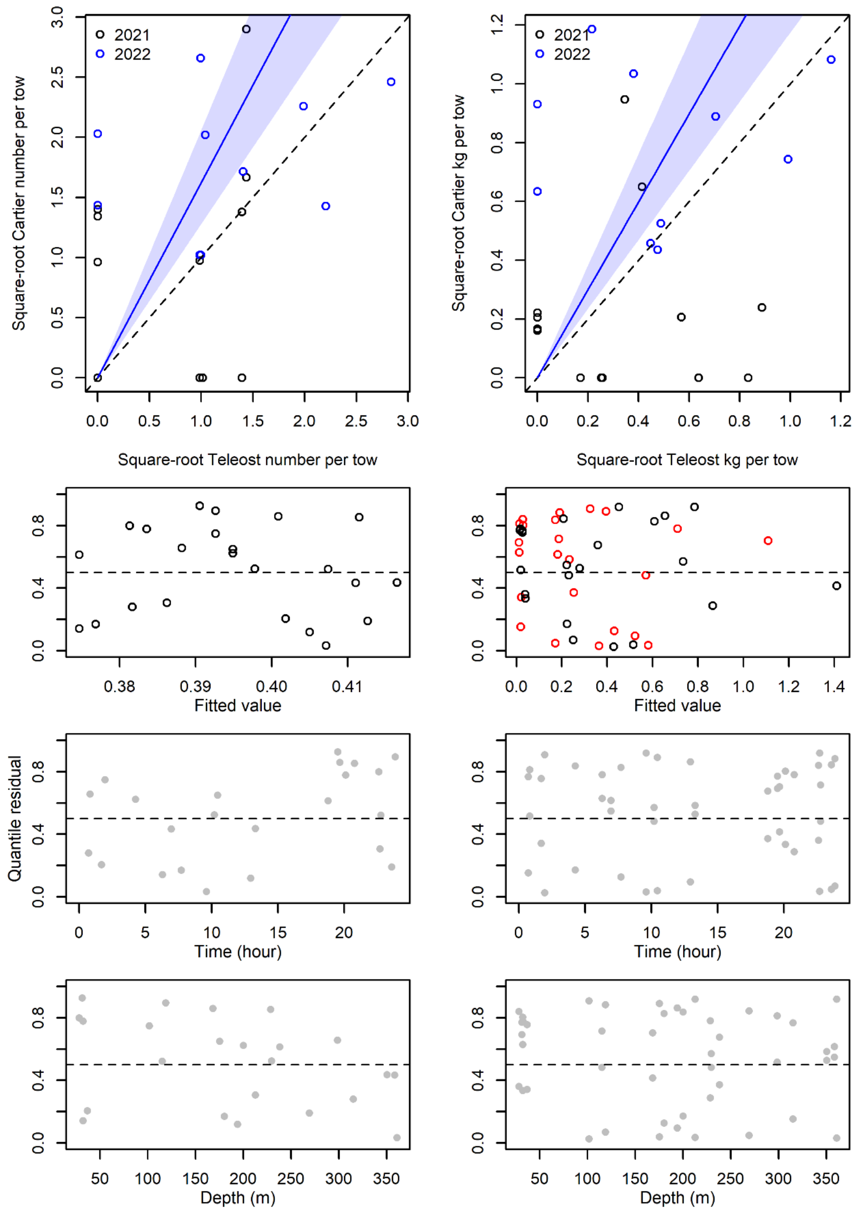

Figure 45. Visualisation of comparative fishing data, size-aggregated model predictions and residual plots for Merluccius bilinearis.

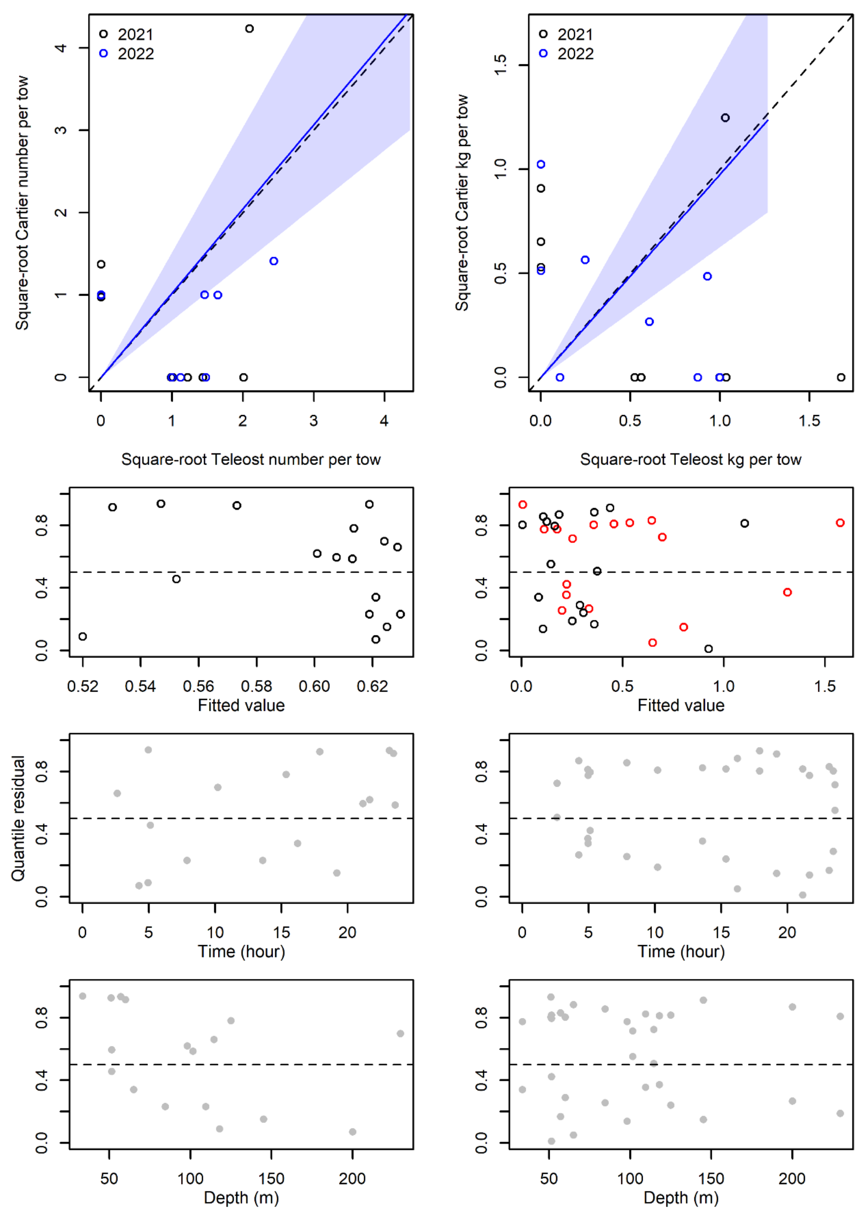

Figure 46. Visualisation of comparative fishing data, size-aggregated model predictions and residual plots for Anarhichas lupus*.*

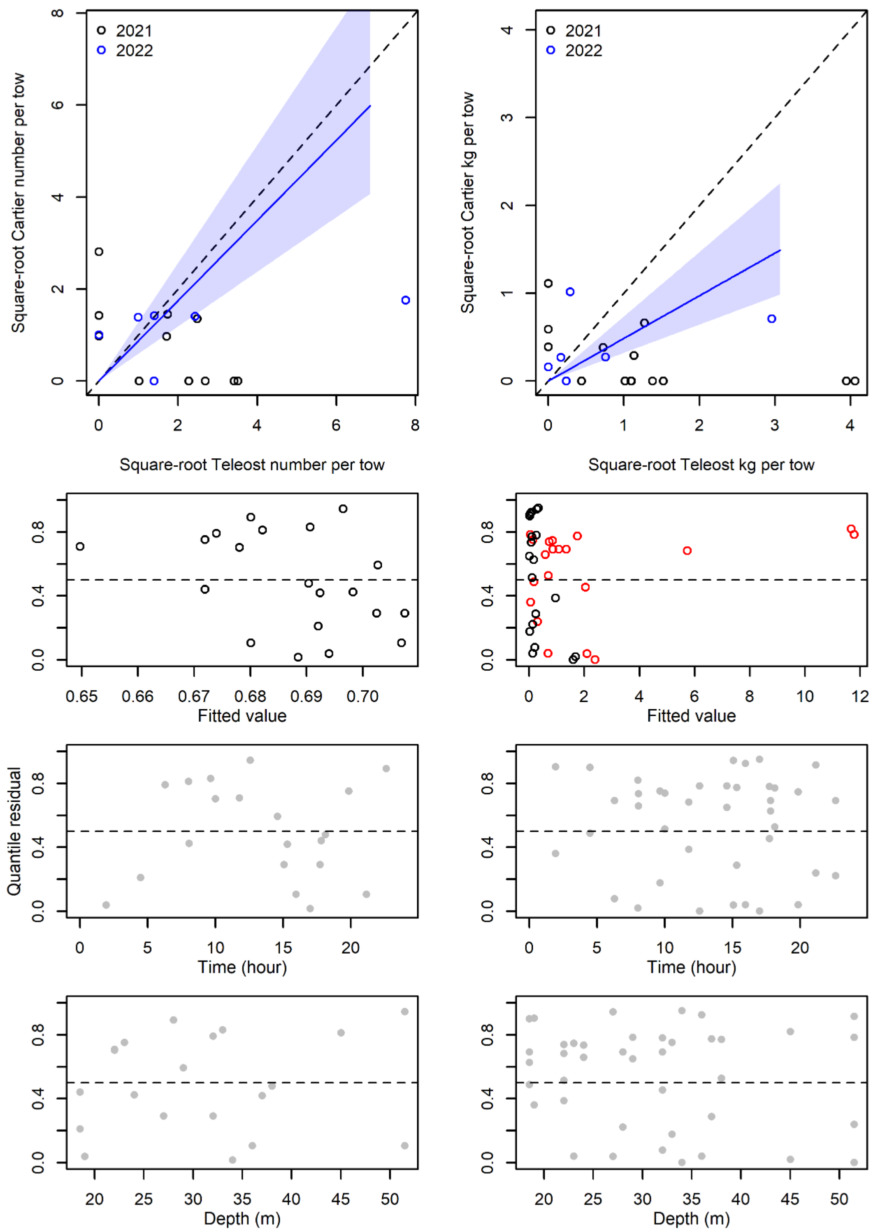

Figure 47. Visualisation of comparative fishing data, size-aggregated model predictions and residual plots for Alosa sapidissima.

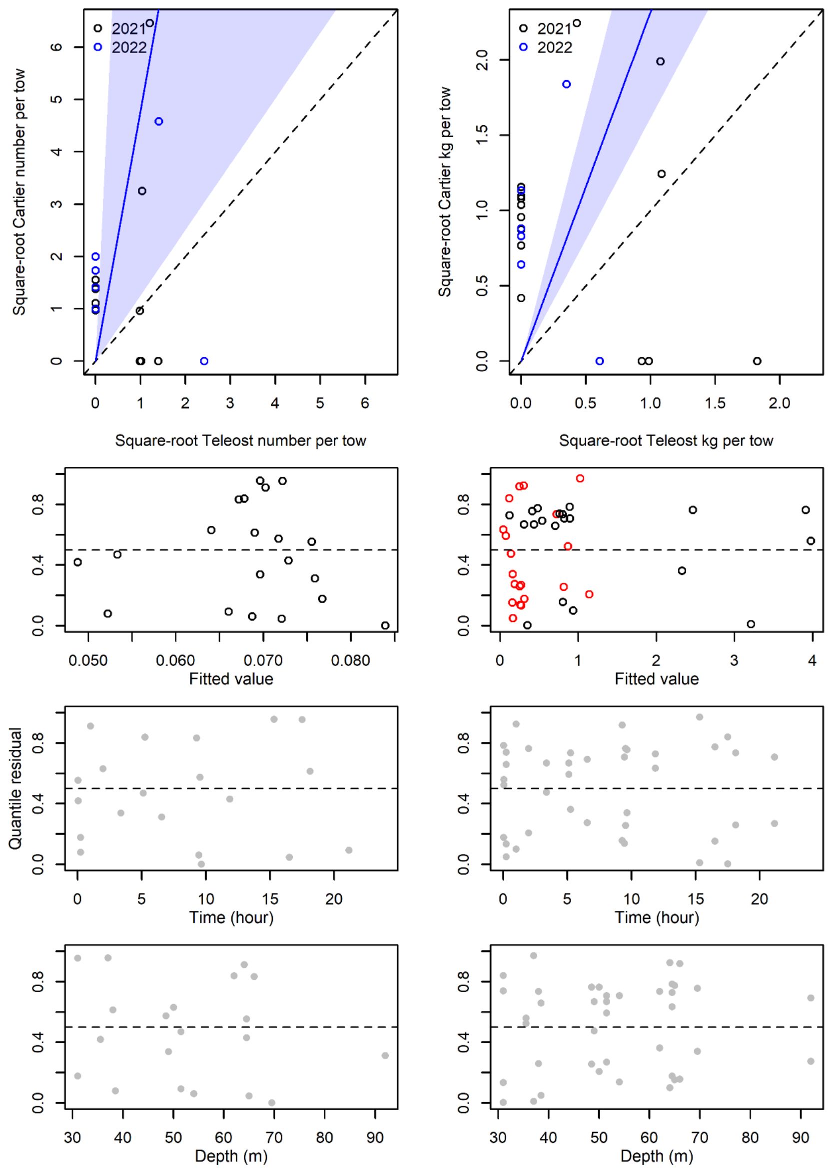

Figure 48. Visualisation of comparative fishing data, size-aggregated model predictions and residual plots for Gadus macrocephalus.

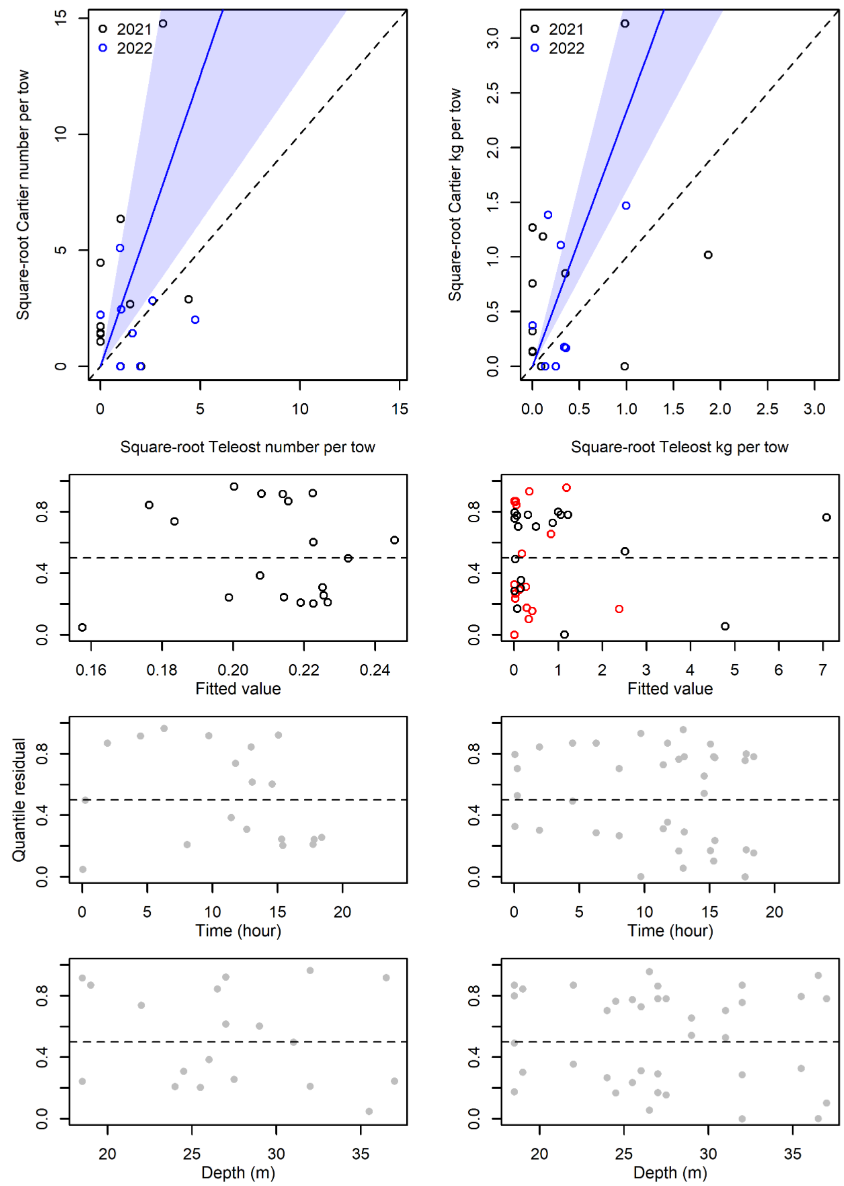

Figure 49. Visualisation of comparative fishing data, size-aggregated model predictions and residual plots for Tautogolabrus adspersus.

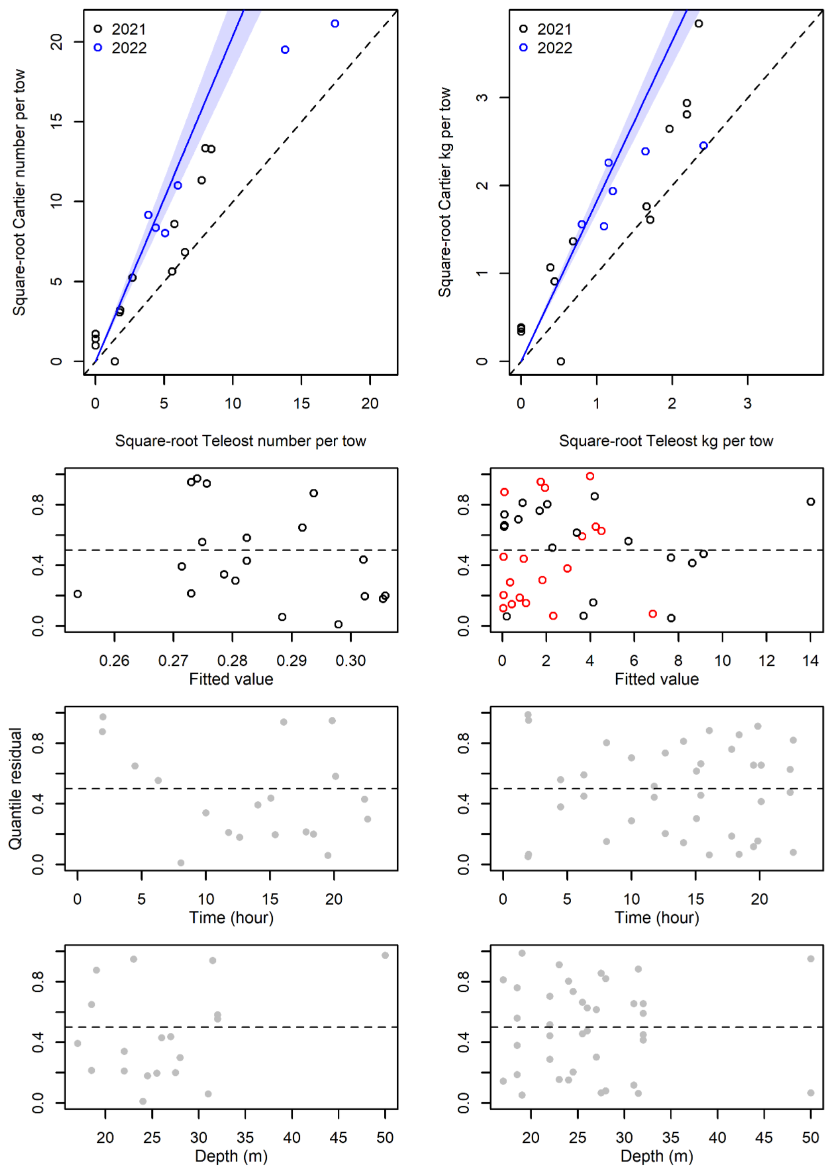

Figure 50. Visualisation of comparative fishing data, size-aggregated model predictions and residual plots for Scophthalmus aquosus*.*

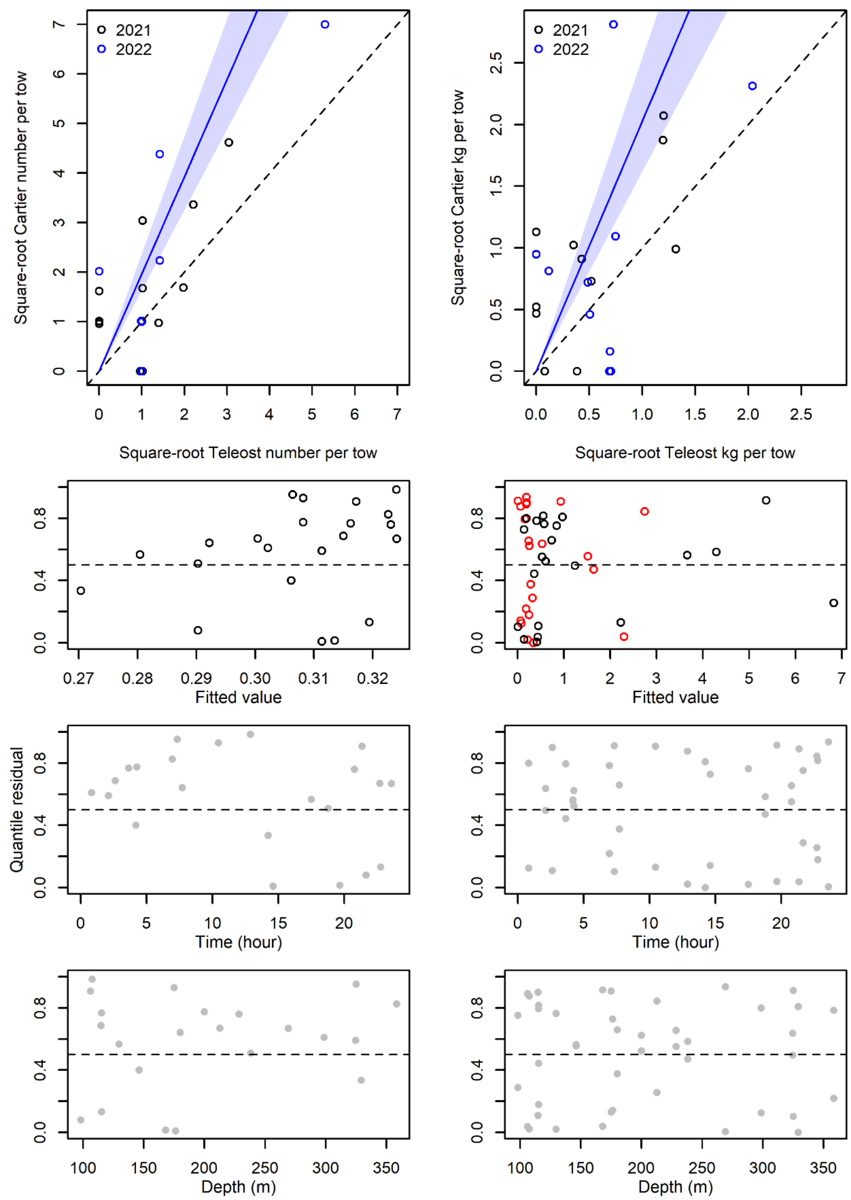

Figure 51. Visualisation of comparative fishing data, size-aggregated model predictions and residual plots for Malacoraja senta*.*

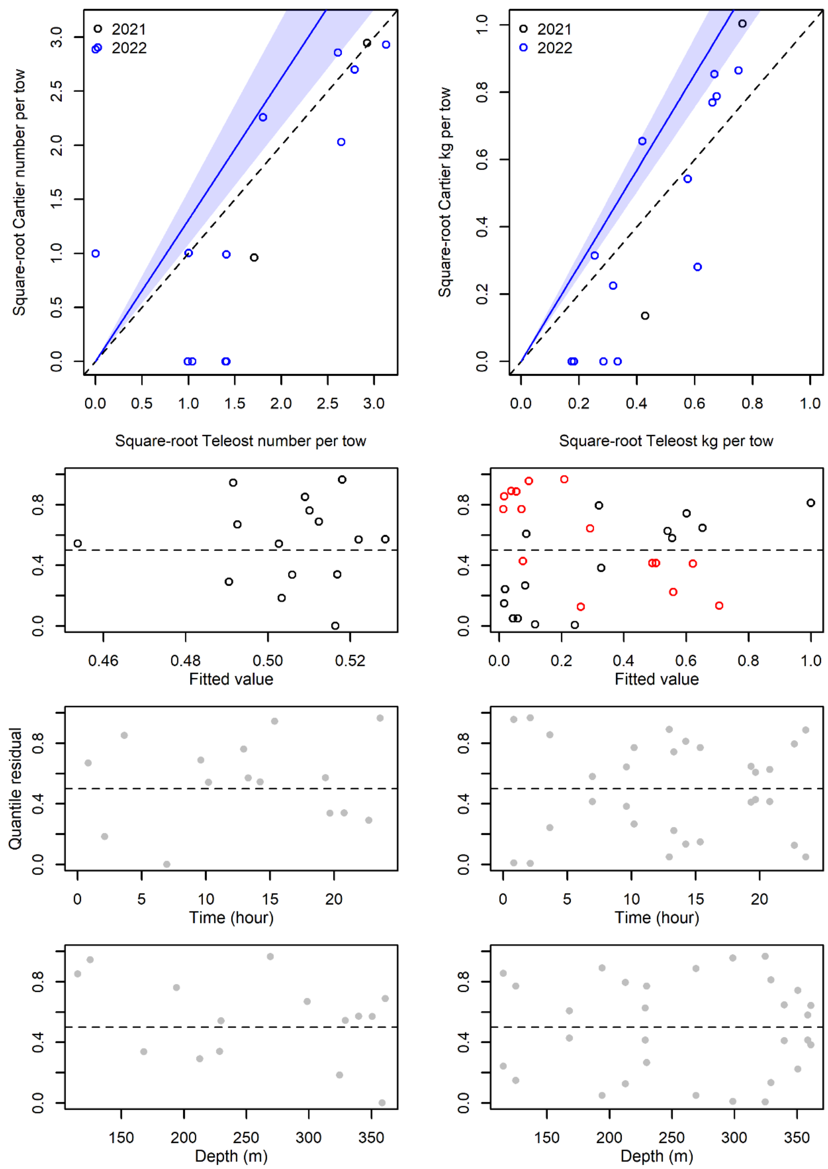

Figure 52. Visualisation of comparative fishing data, size-aggregated model predictions and residual plots for Myxine limosa.

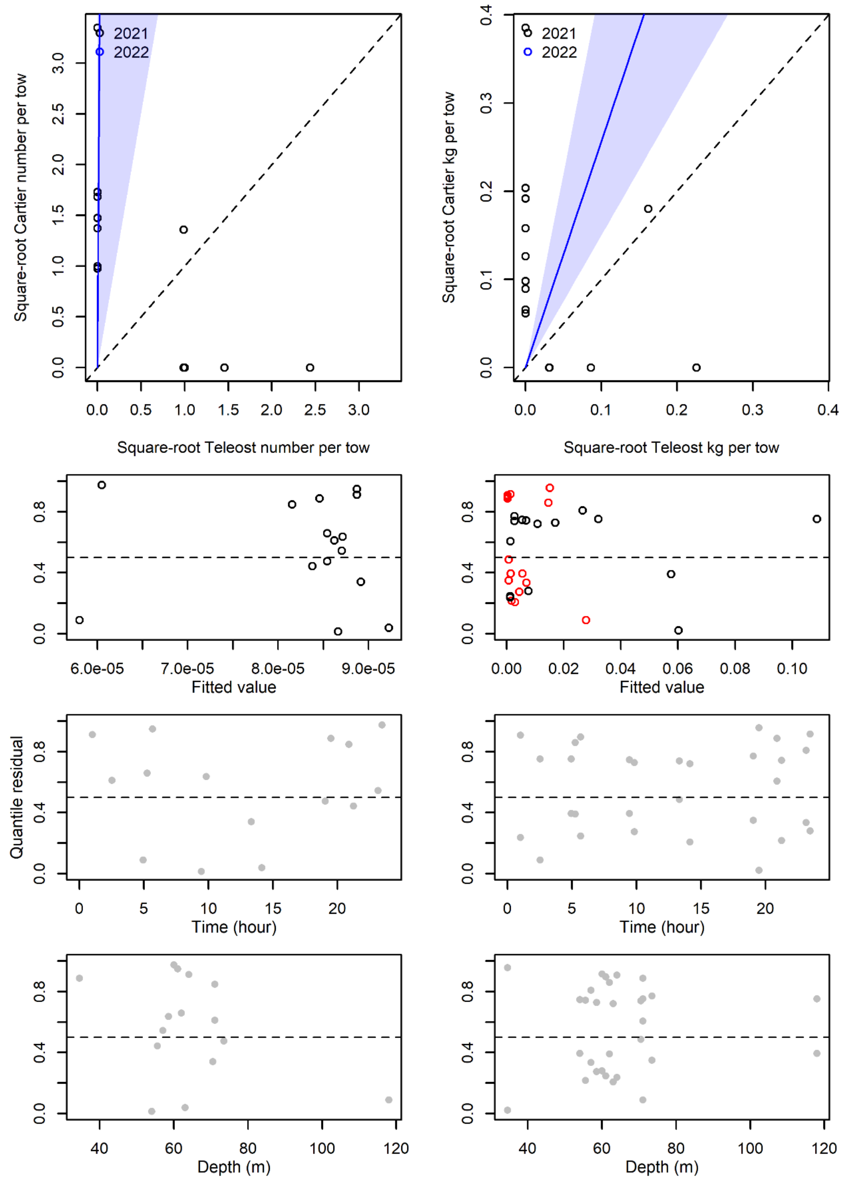

Figure 53. Visualisation of comparative fishing data, size-aggregated model predictions and residual plots for Icelus spatula*.*

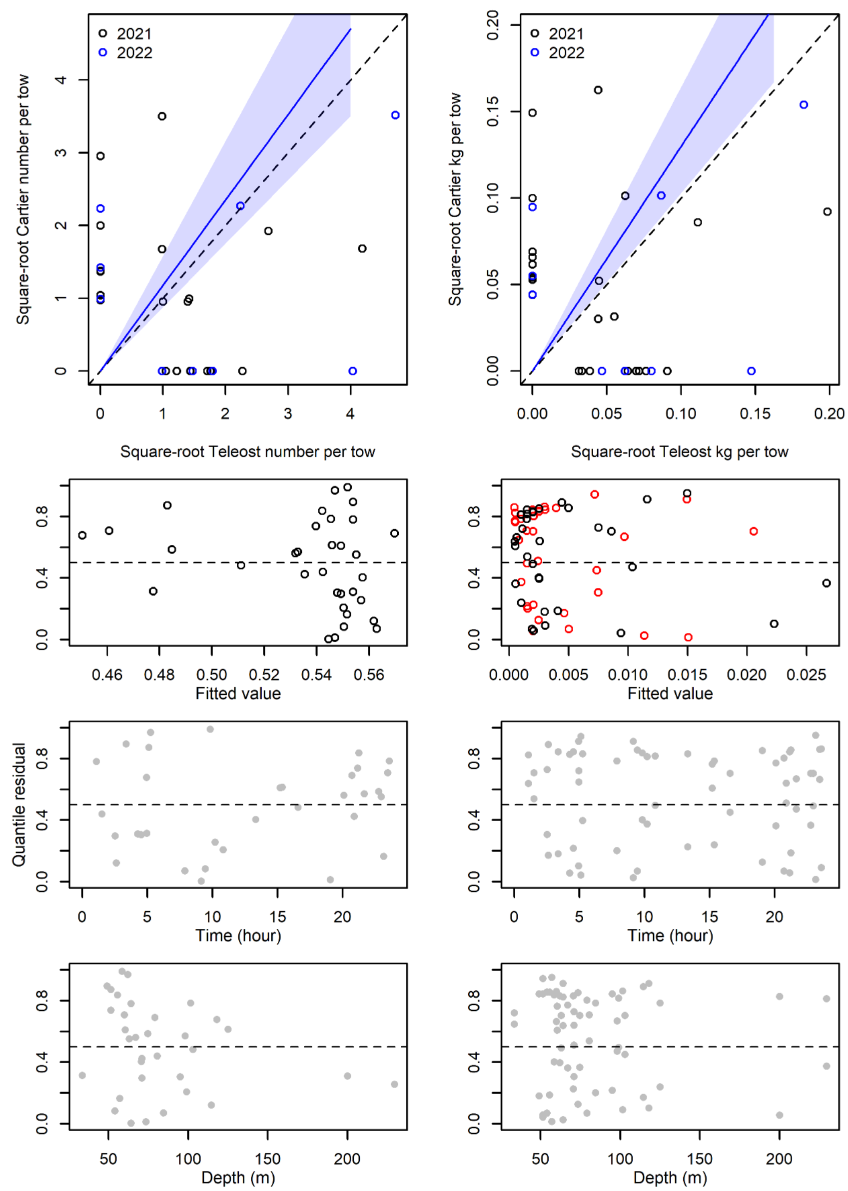

Figure 54. Visualisation of comparative fishing data, size-aggregated model predictions and residual plots for Artediellus sp..

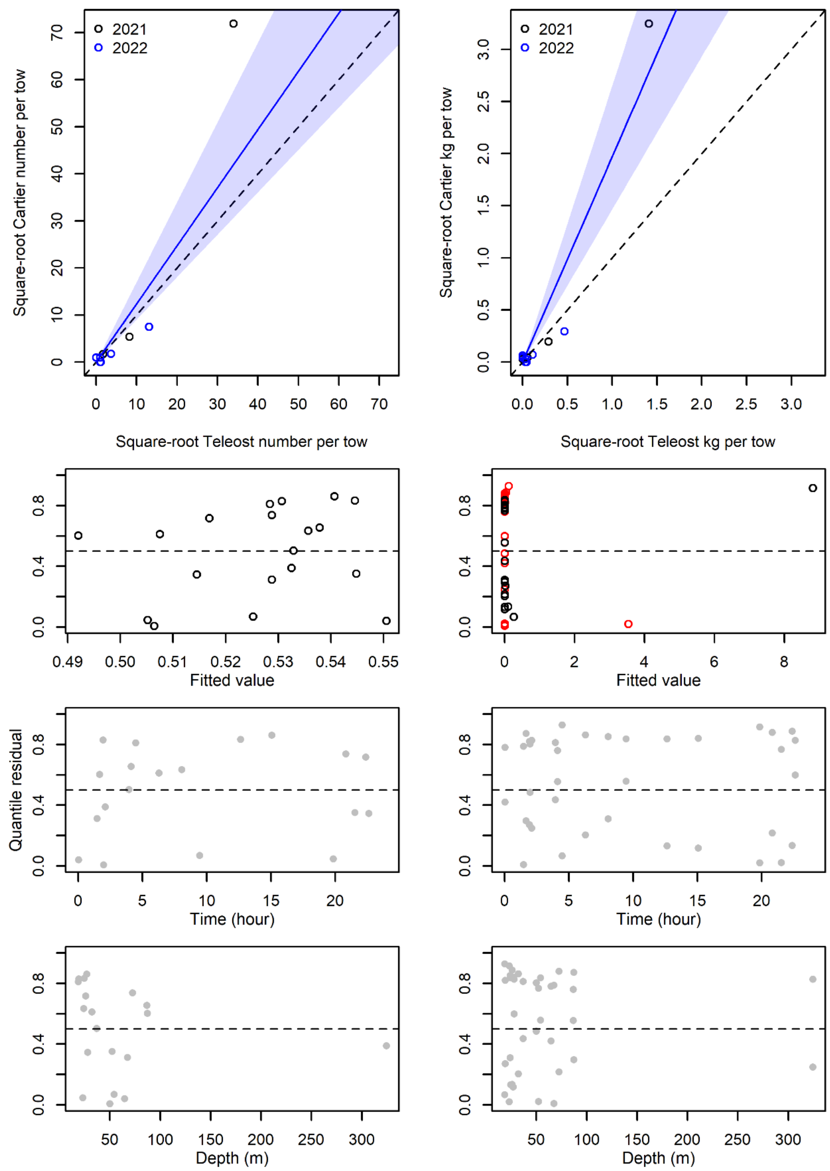

Figure 55. Visualisation of comparative fishing data, size-aggregated model predictions and residual plots for Gasterosteus aculeatus.

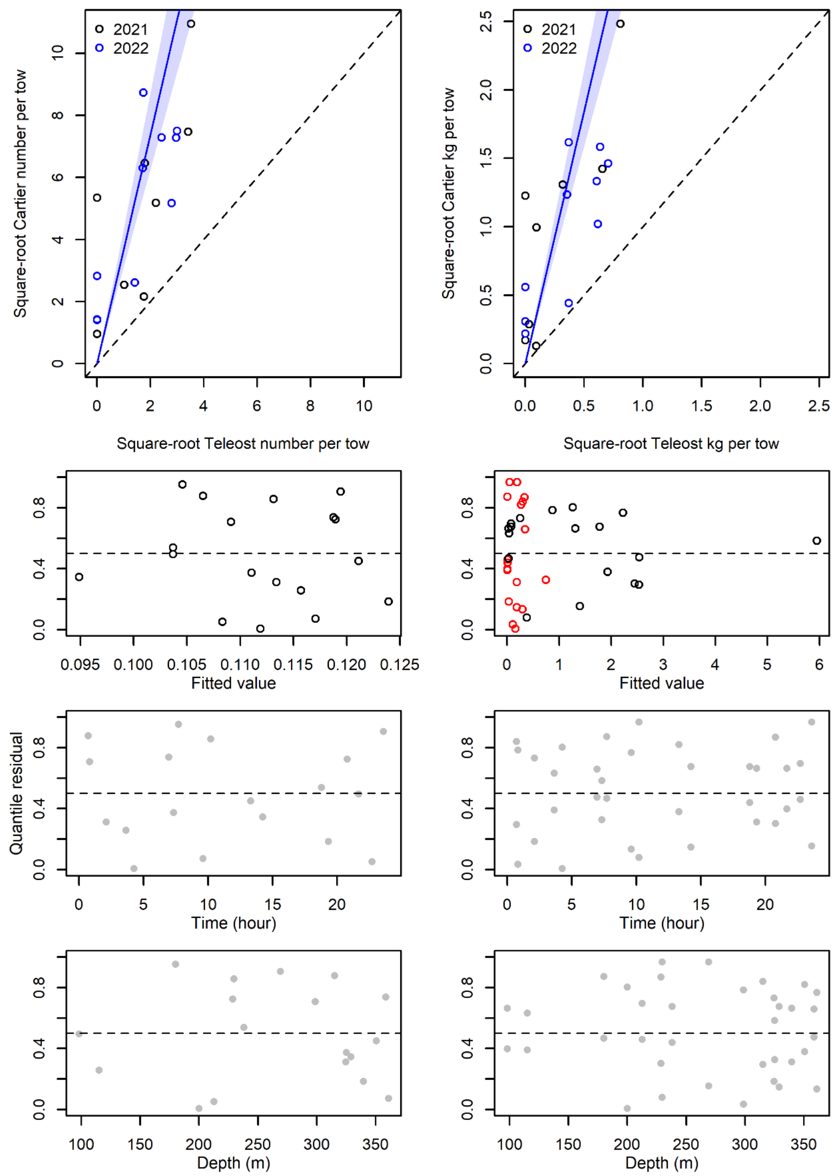

Figure 56. Visualisation of comparative fishing data, size-aggregated model predictions and residual plots for Nezumia bairdii.

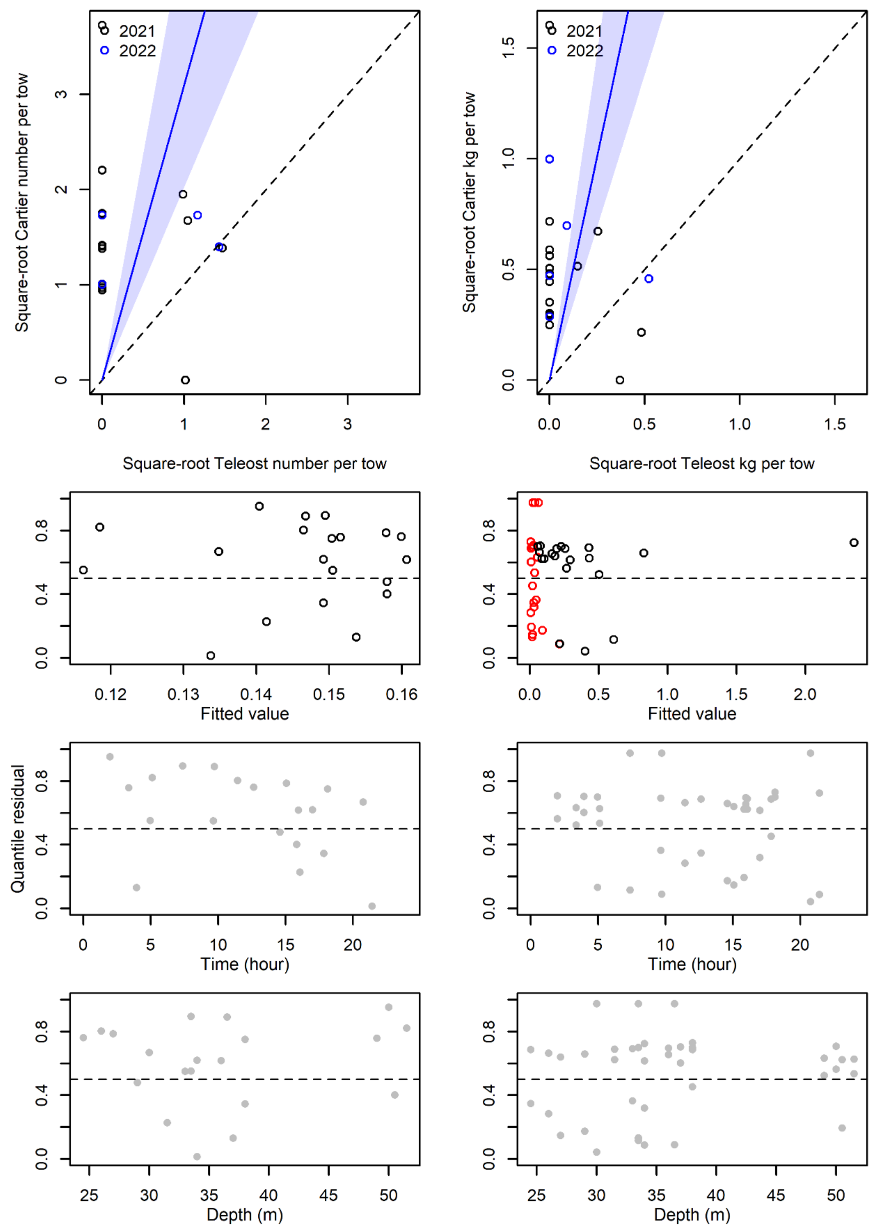

Figure 57. Visualisation of comparative fishing data, size-aggregated model predictions and residual plots for Zoarces americanus*.*

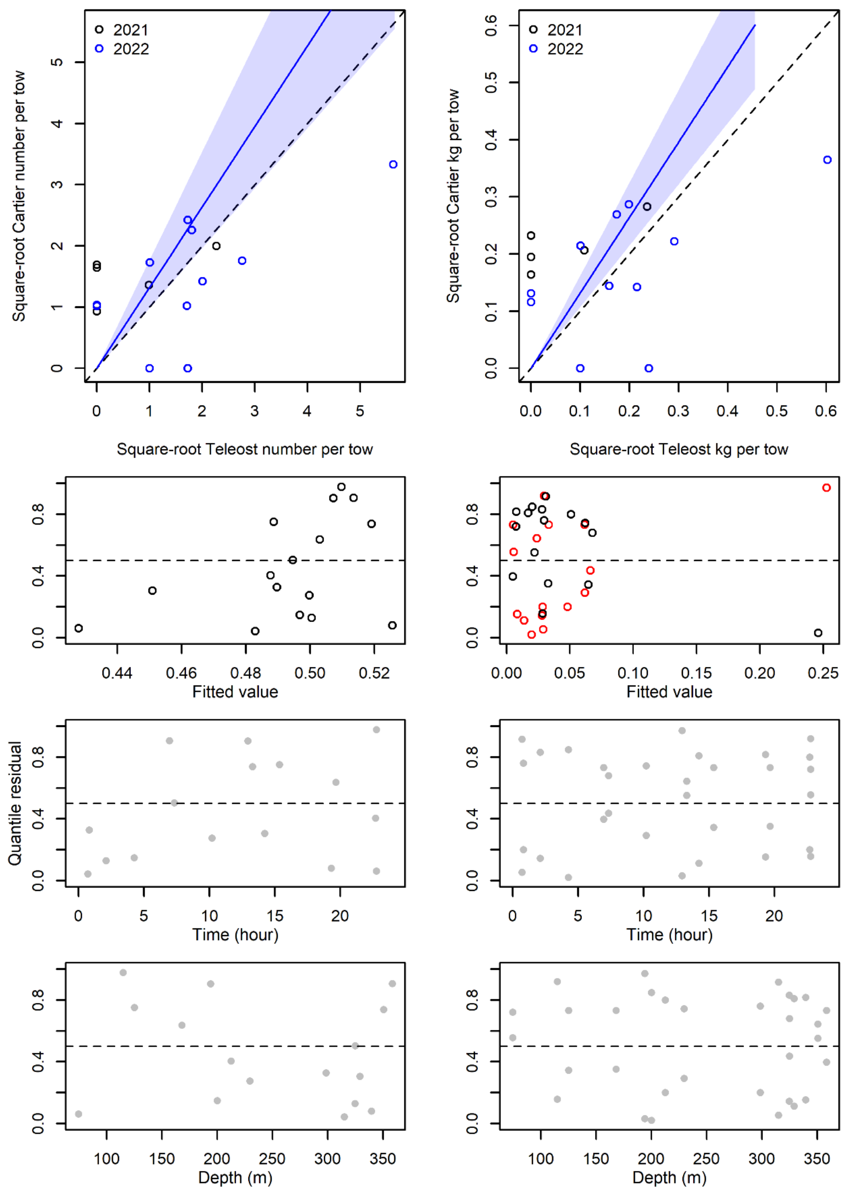

Figure 58. Visualisation of comparative fishing data, size-aggregated model predictions and residual plots for Arctozenus risso*.*

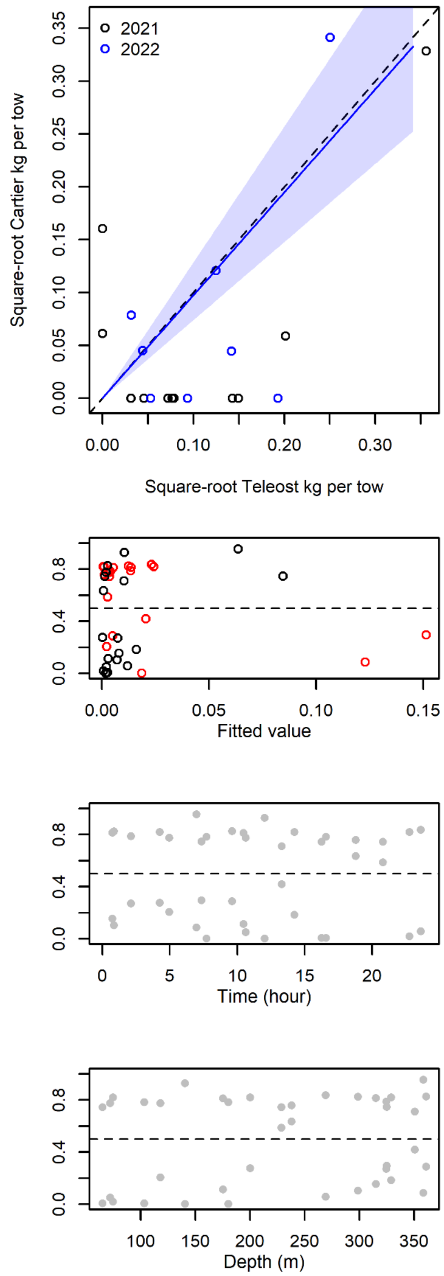

Figure 59. Visualisation of comparative fishing data, size-aggregated model predictions and residual plots for Rajidae sp. *eggs.*

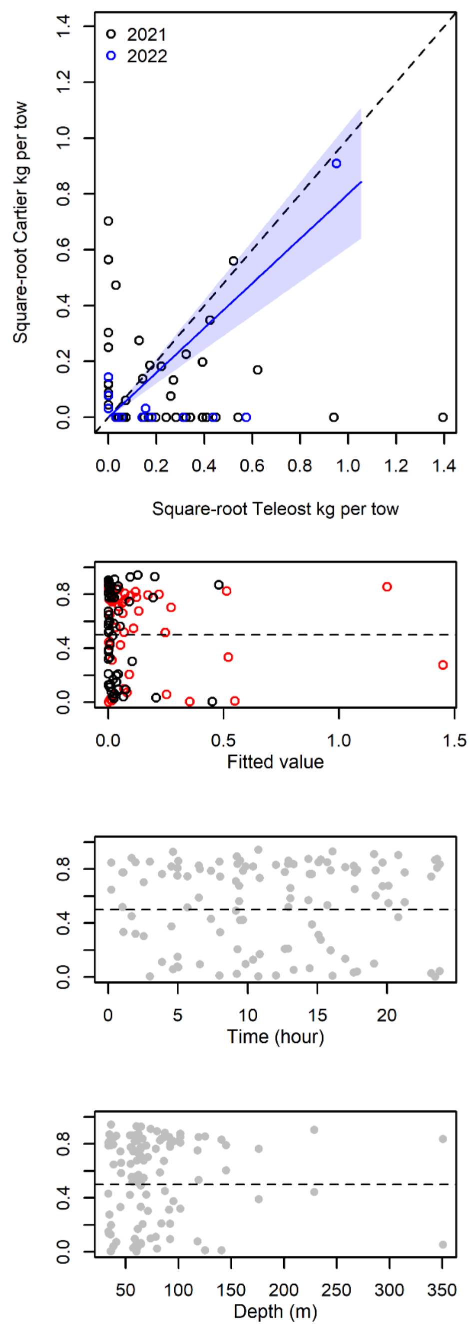

Figure 60. Visualisation of comparative fishing data, size-aggregated model predictions and residual plots for Buccinidae sp*. eggs.*

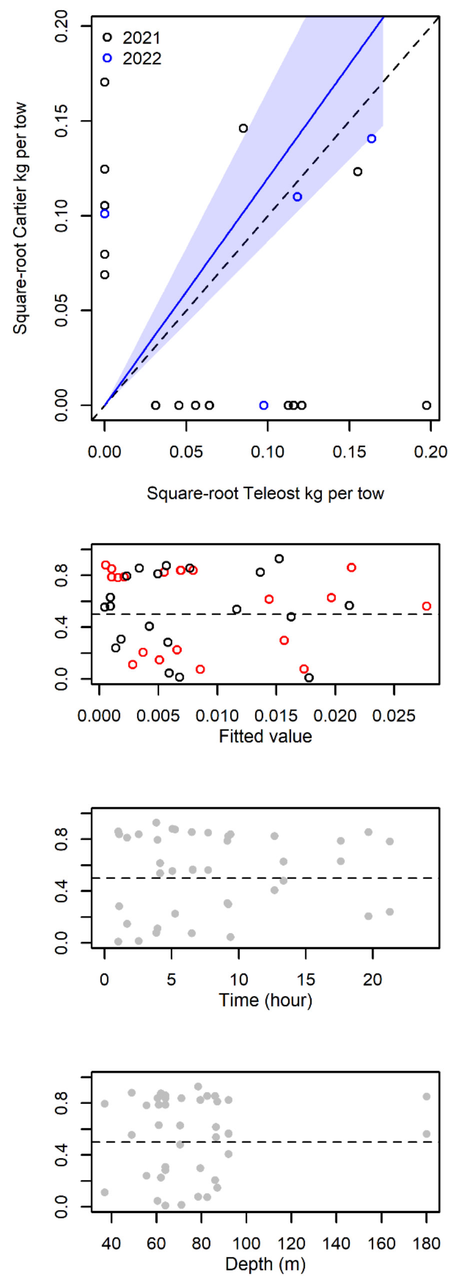

Figure 61. Visualisation of comparative fishing data, size-aggregated model predictions and residual plots for Gastropoda sp*. eggs.*

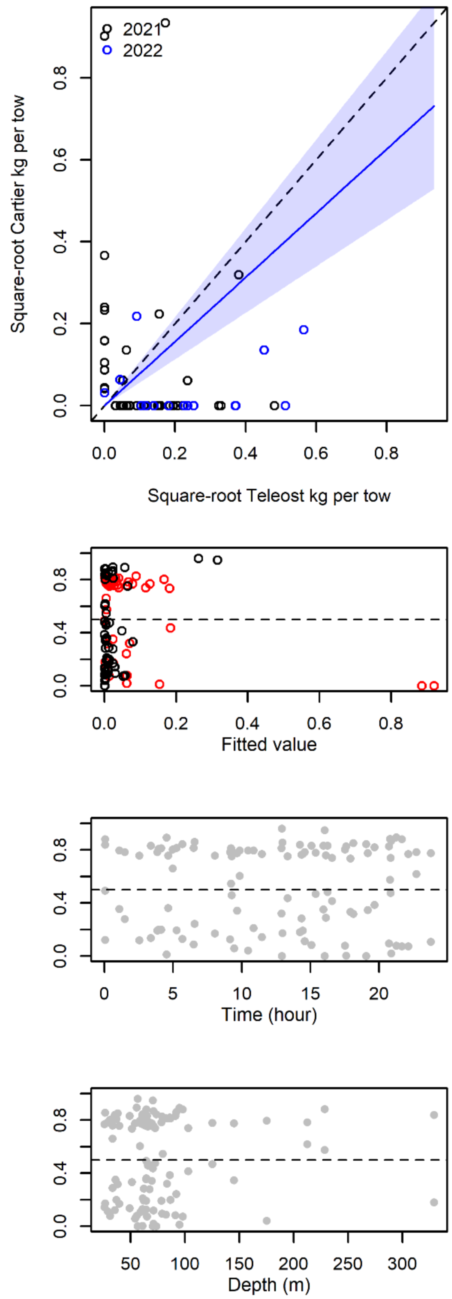

Figure 62. Visualisation of comparative fishing data, size-aggregated model predictions and residual plots for Tunicata (s.p.).

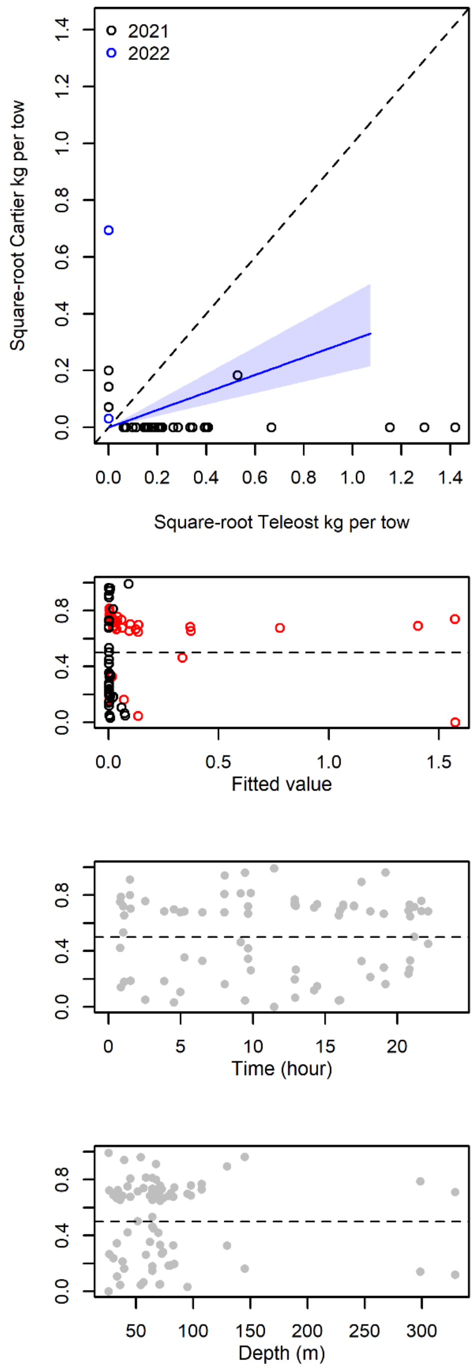

Figure 63. Visualisation of comparative fishing data, size-aggregated model predictions and residual plots for Ascidia sp..

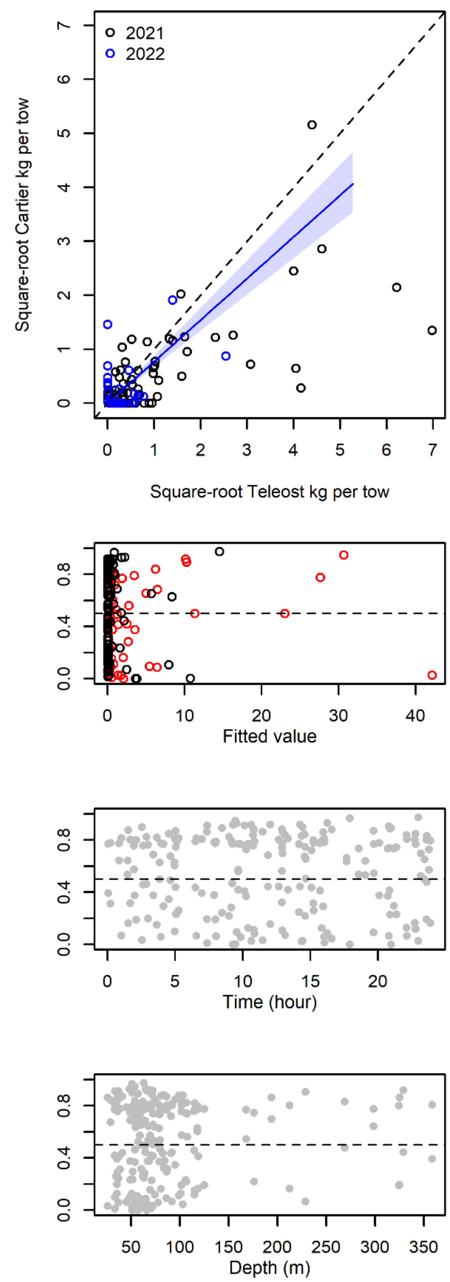

Figure 64. Visualisation of comparative fishing data, size-aggregated model predictions and residual plots for Boltenia sp..

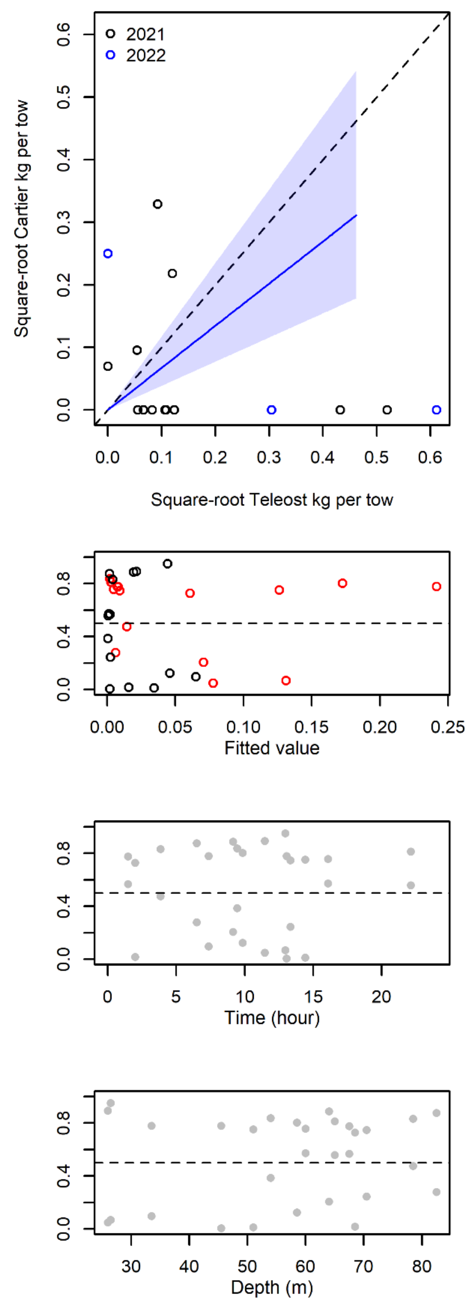

Figure 65. Visualisation of comparative fishing data, size-aggregated model predictions and residual plots for Halocynthia pyriformis.

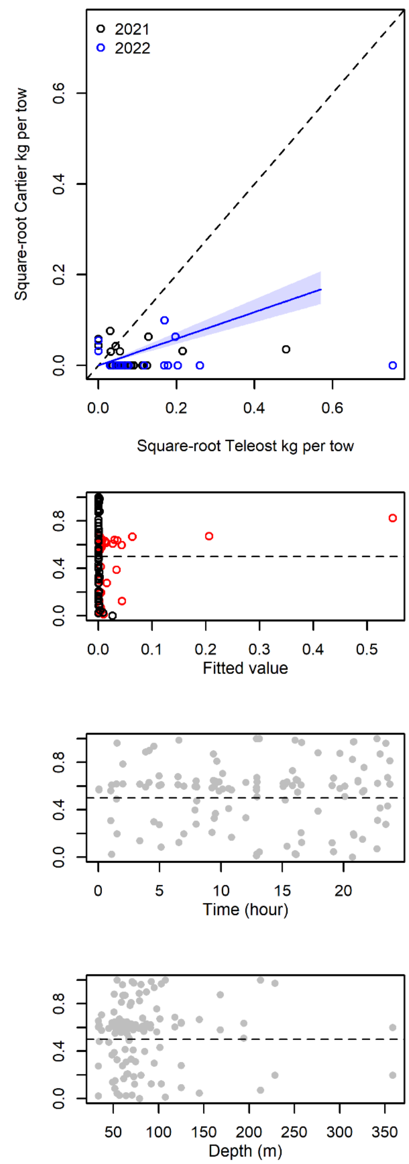

Figure 66. Visualisation of comparative fishing data, size-aggregated model predictions and residual plots for Bryozoa (p.)*.*

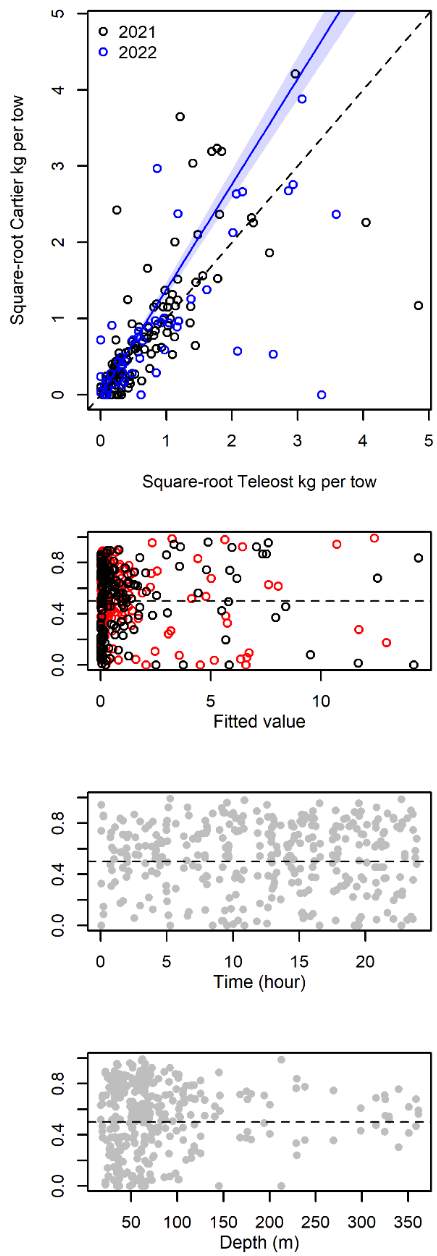

Figure 67. Visualisation of comparative fishing data, size-aggregated model predictions and residual plots for Decapoda (o.).

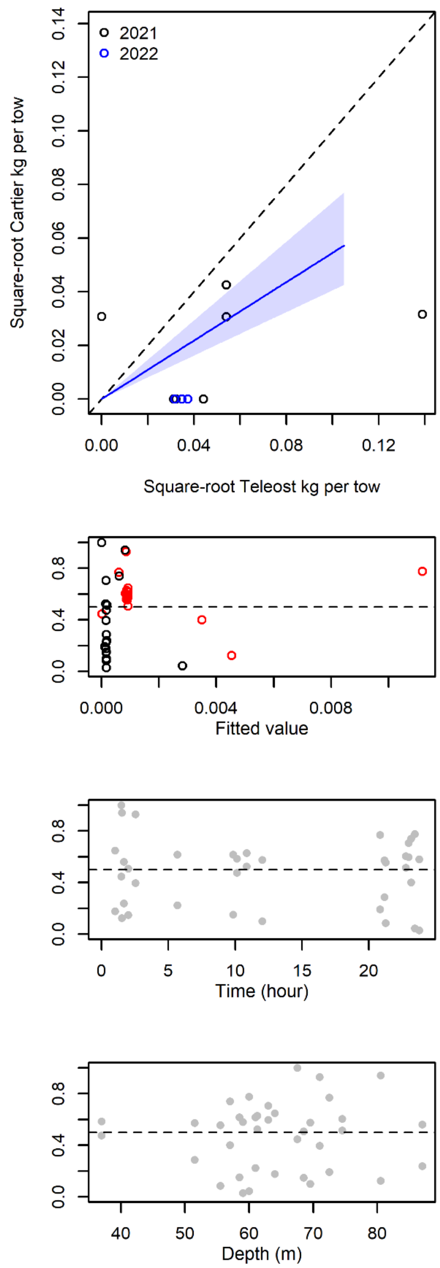

Figure 68. Visualisation of comparative fishing data, size-aggregated model predictions and residual plots for Anonyx sp..

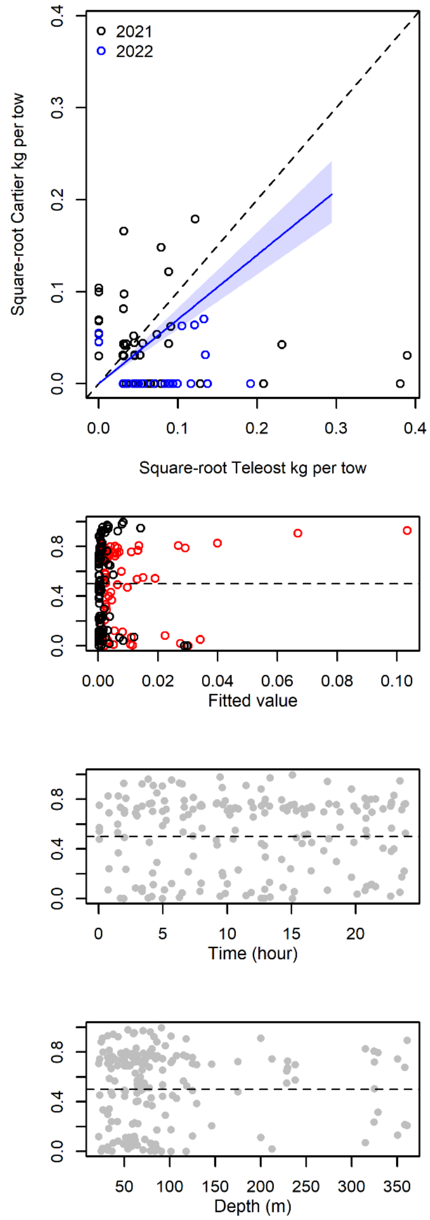

Figure 69. Visualisation of comparative fishing data, size-aggregated model predictions and residual plots for Annelida (p.).

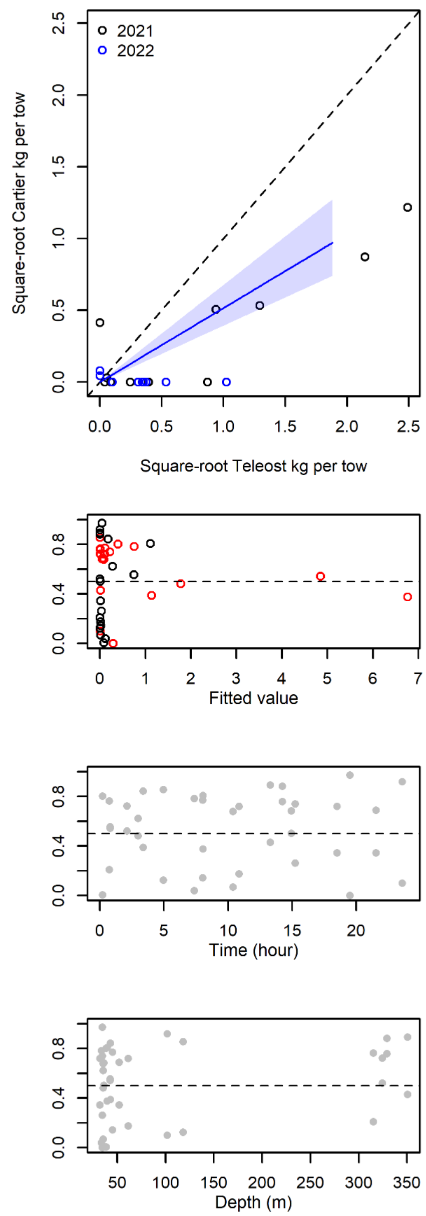

Figure 70. Visualisation of comparative fishing data, size-aggregated model predictions and residual plots for Aphrodita hastata*.*

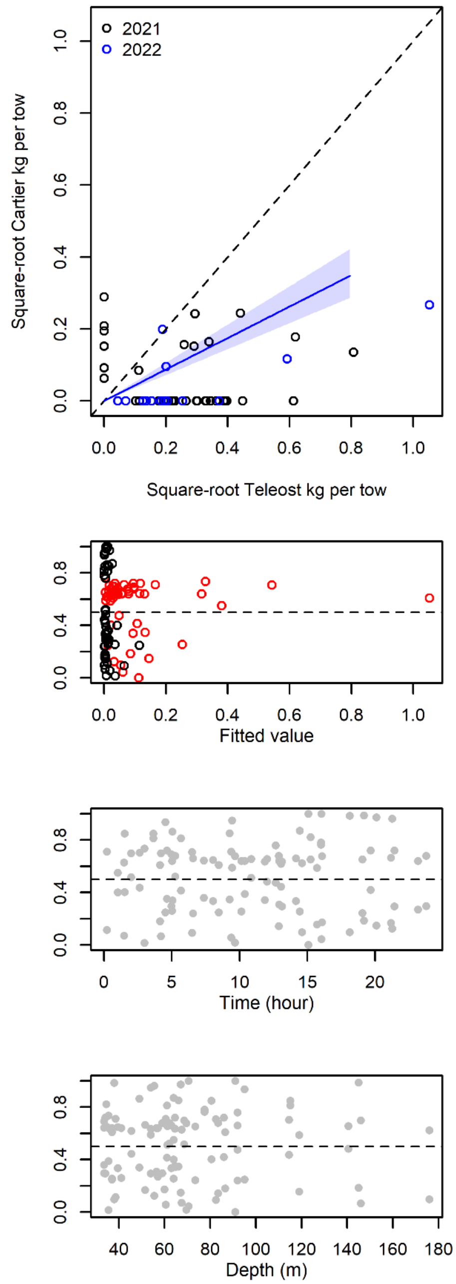

Figure 71. Visualisation of comparative fishing data, size-aggregated model predictions and residual plots for Buccinum sp..

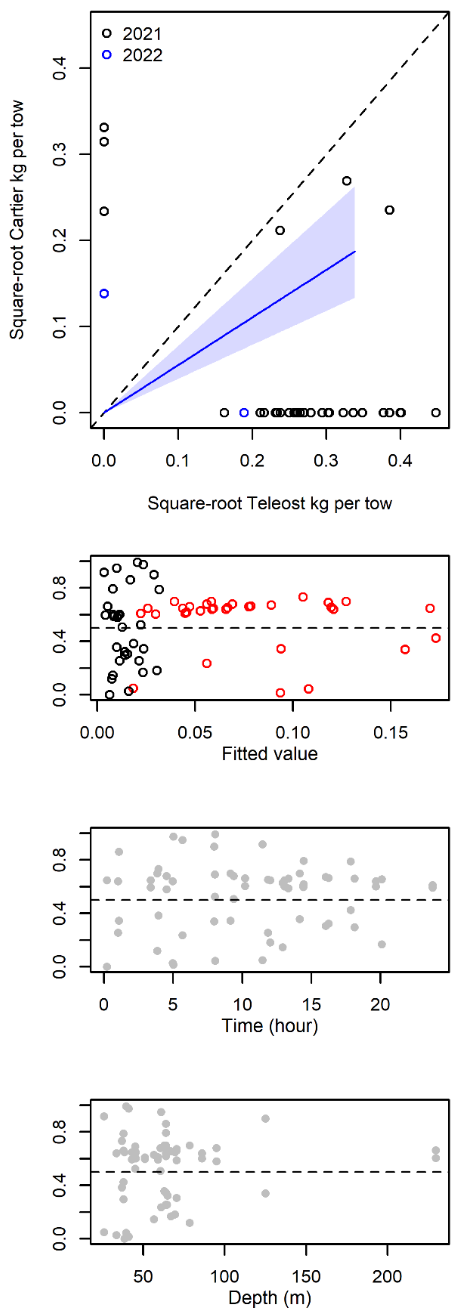

Figure 72. Visualisation of comparative fishing data, size-aggregated model predictions and residual plots for Neptunea decemcostata*.*

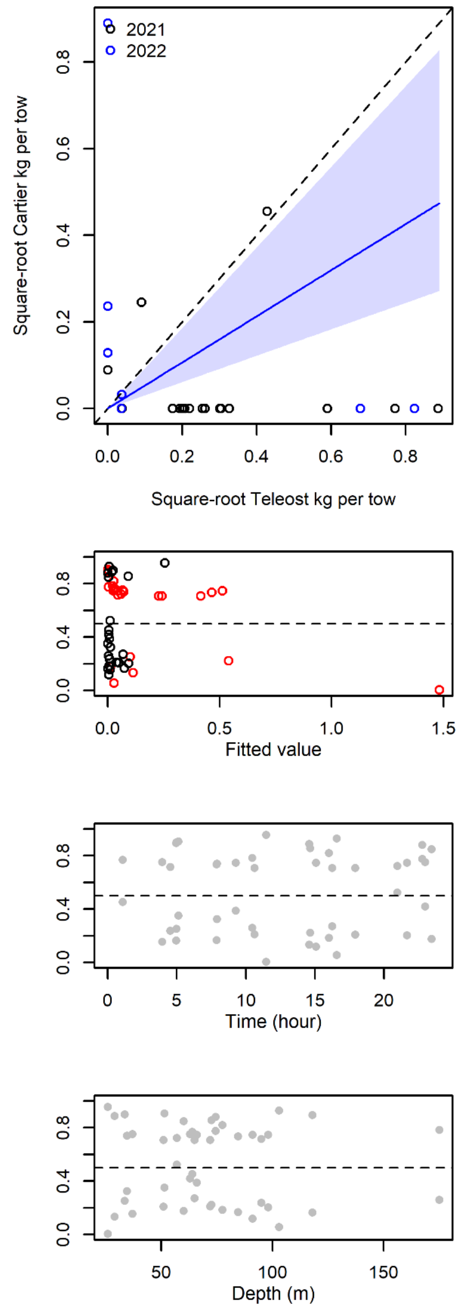

Figure 73. Visualisation of comparative fishing data, size-aggregated model predictions and residual plots for Chlamys islandica*.*

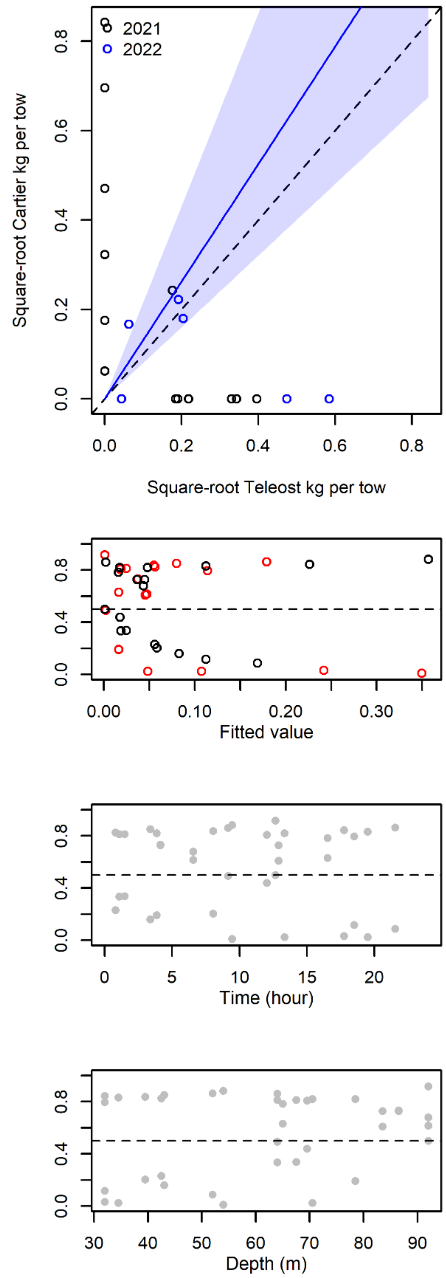

Figure 74. Visualisation of comparative fishing data, size-aggregated model predictions and residual plots for Ciliatocardium ciliatum*.*

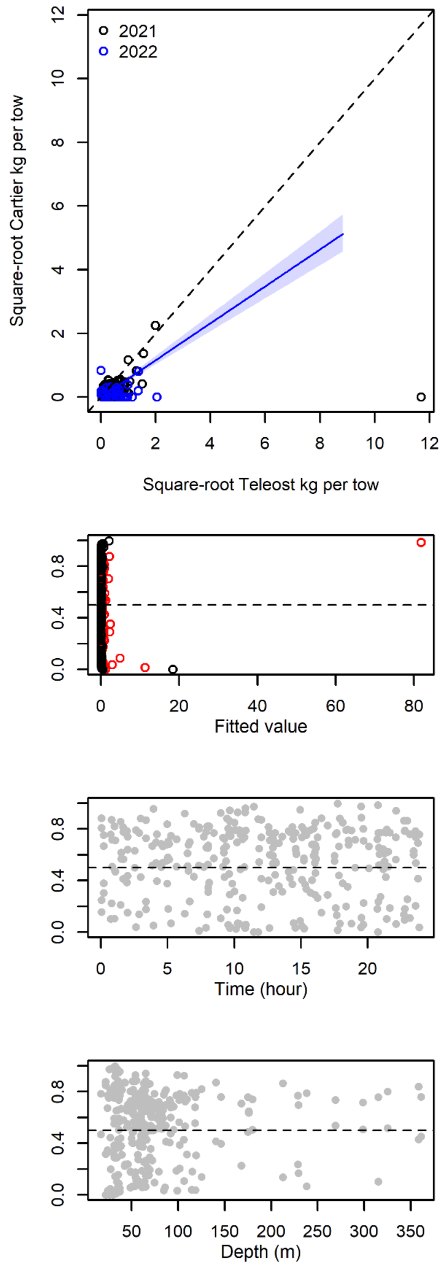

Figure 75. Visualisation of comparative fishing data, size-aggregated model predictions and residual plots for Mollusca sp. *empty.*

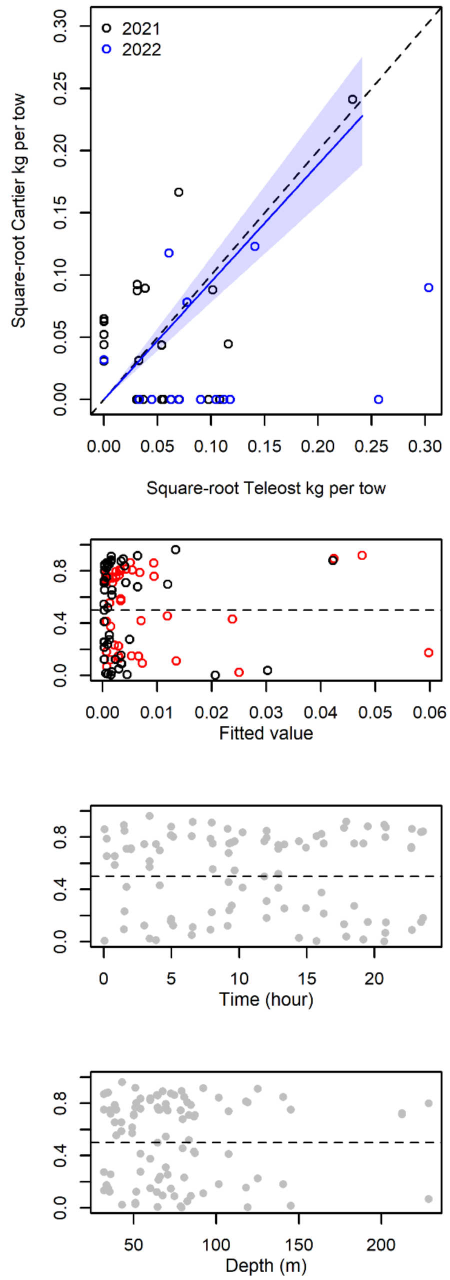

Figure 76. Visualisation of comparative fishing data, size-aggregated model predictions and residual plots for Nudibranchia (o.).

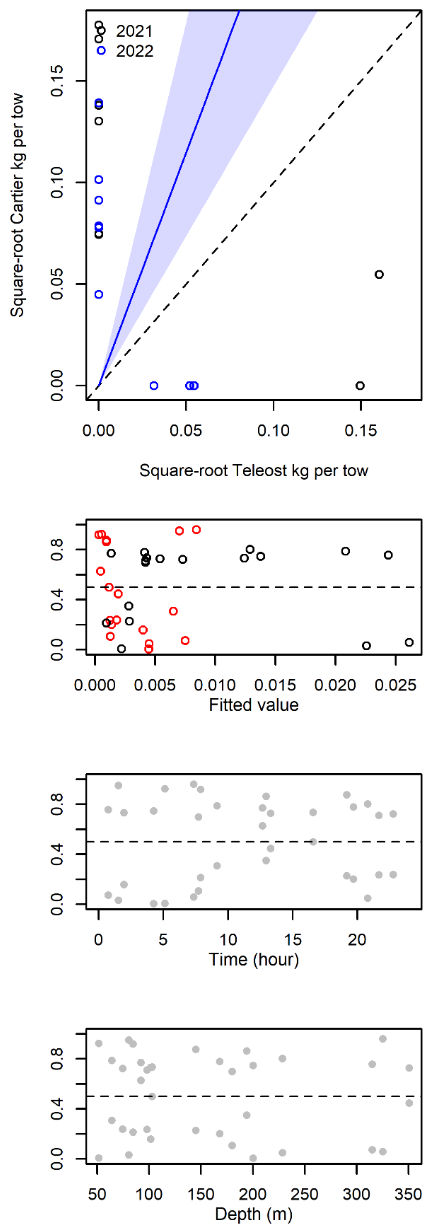

Figure 77. Visualisation of comparative fishing data, size-aggregated model predictions and residual plots for Semirossia tenera*.*

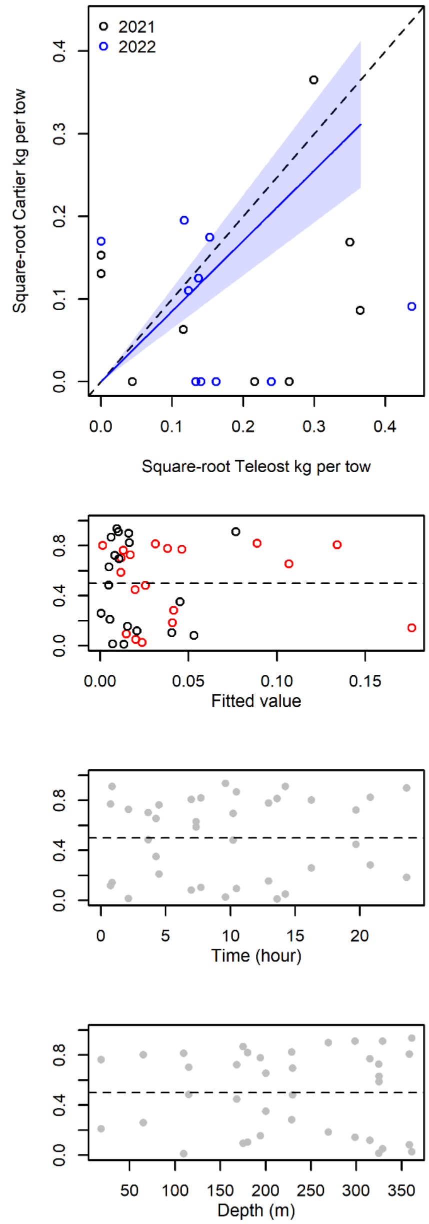

Figure 78. Visualisation of comparative fishing data, size-aggregated model predictions and residual plots for Bathypolypus arcticus.

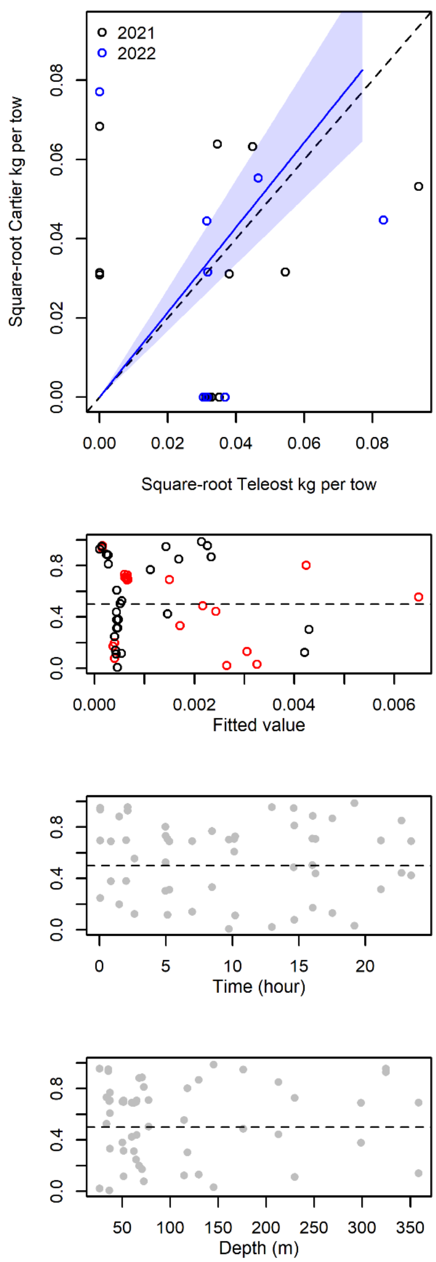

Figure 79. Visualisation of comparative fishing data, size-aggregated model predictions and residual plots for Pycnogonida sp..

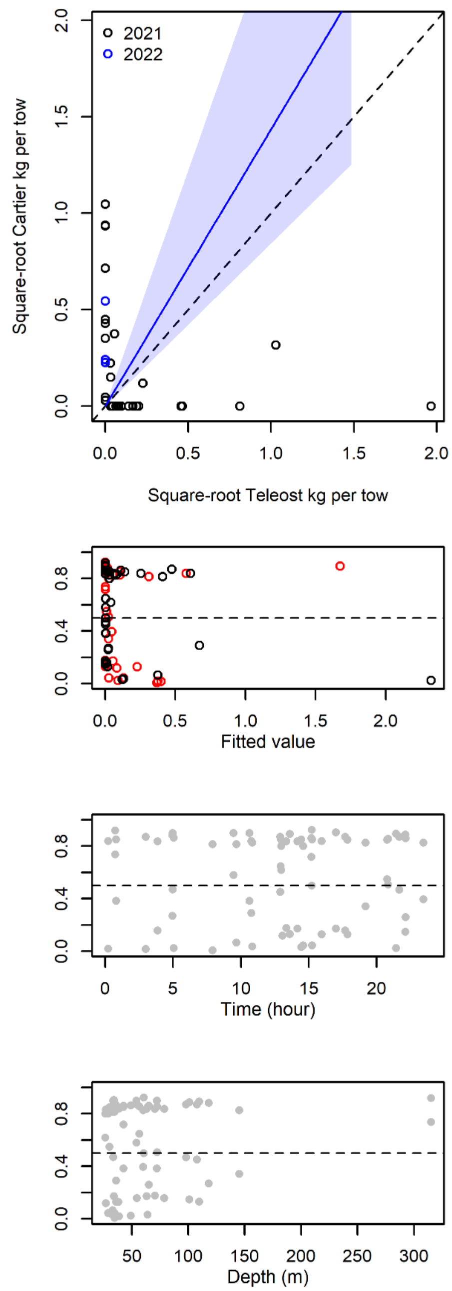

Figure 80. Visualisation of comparative fishing data, size-aggregated model predictions and residual plots for Asterias sp..

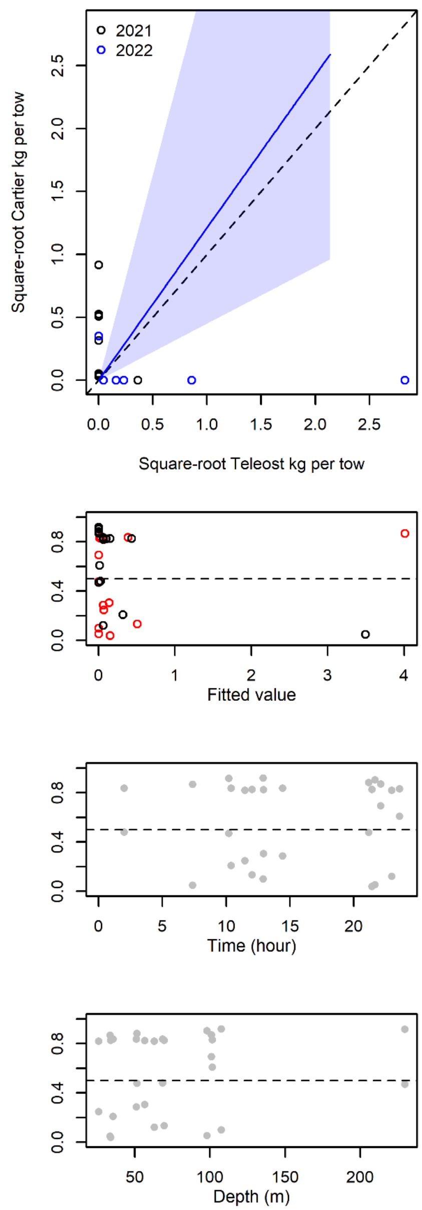

Figure 81. Visualisation of comparative fishing data, size-aggregated model predictions and residual plots for Asterias rubens*.*

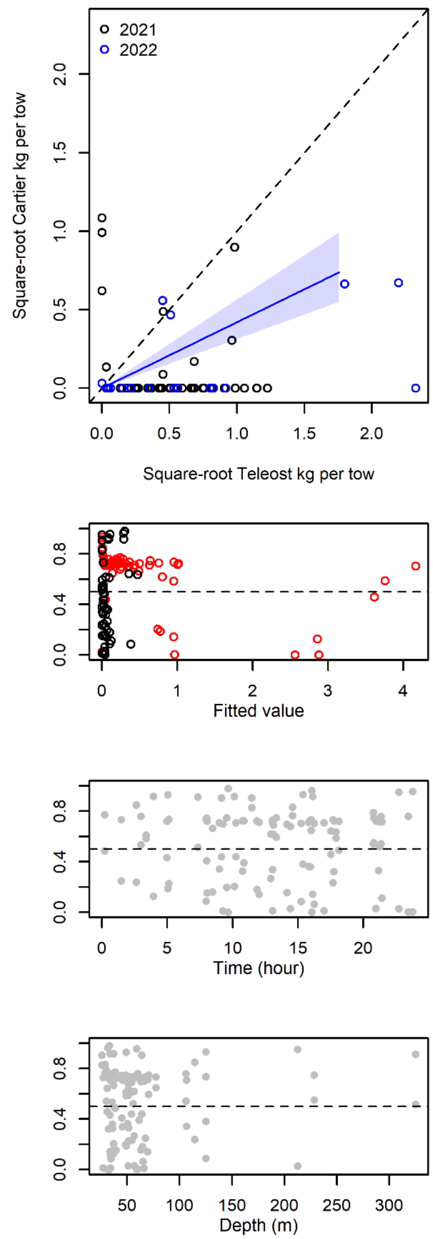

Figure 82. Visualisation of comparative fishing data, size-aggregated model predictions and residual plots for Leptasterias (Hexasterias) polaris*.*

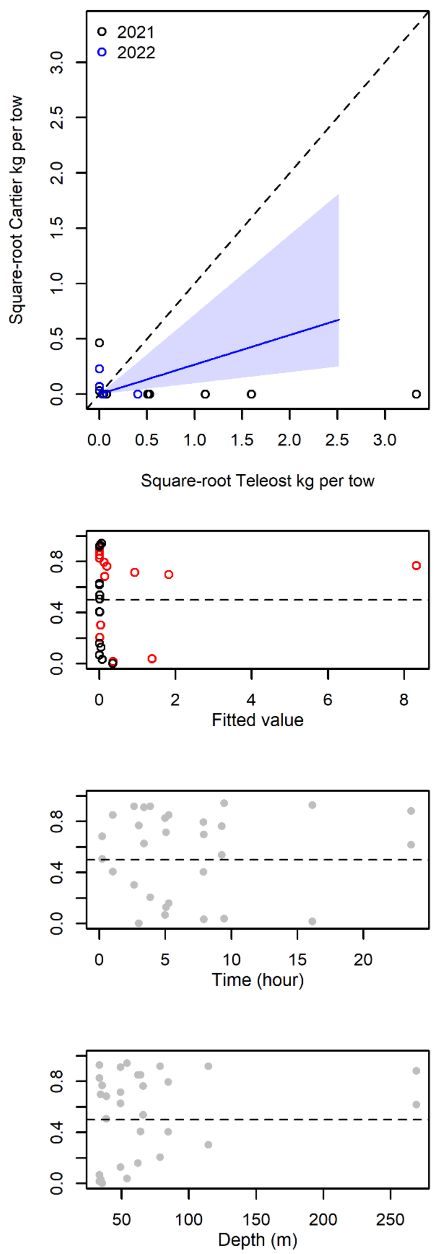

Figure 83. Visualisation of comparative fishing data, size-aggregated model predictions and residual plots for Leptasterias sp..

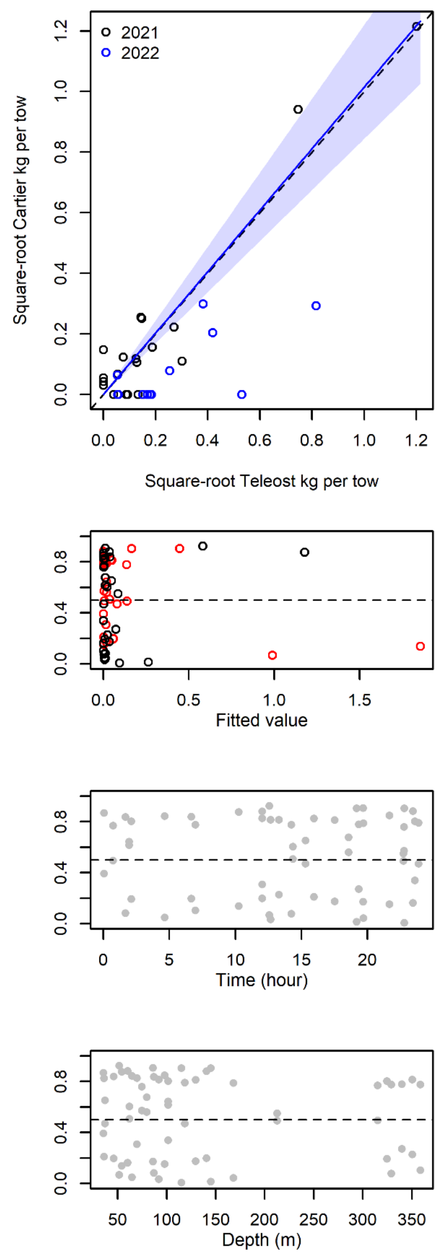

Figure 84. Visualisation of comparative fishing data, size-aggregated model predictions and residual plots for Ctenodiscus crispatus.

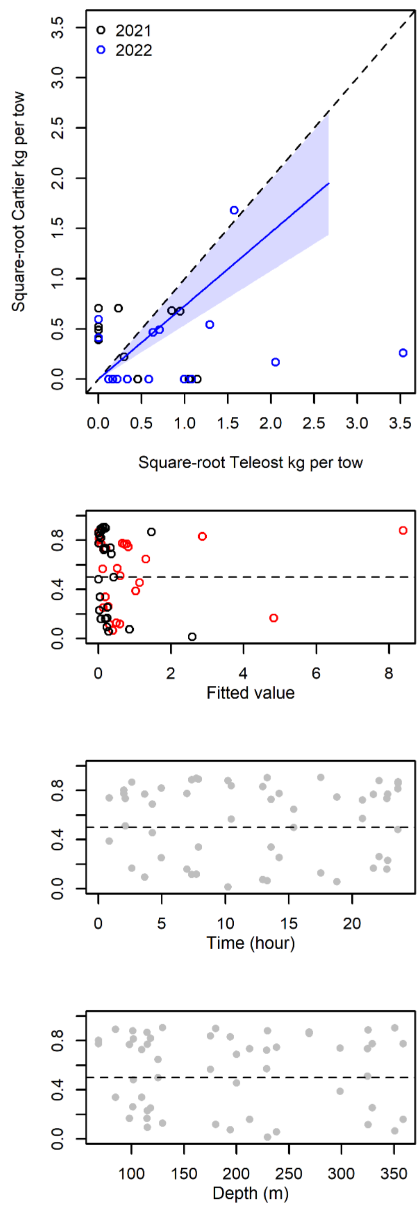

Figure 85. Visualisation of comparative fishing data, size-aggregated model predictions and residual plots for Hippasteria phrygiana*.*

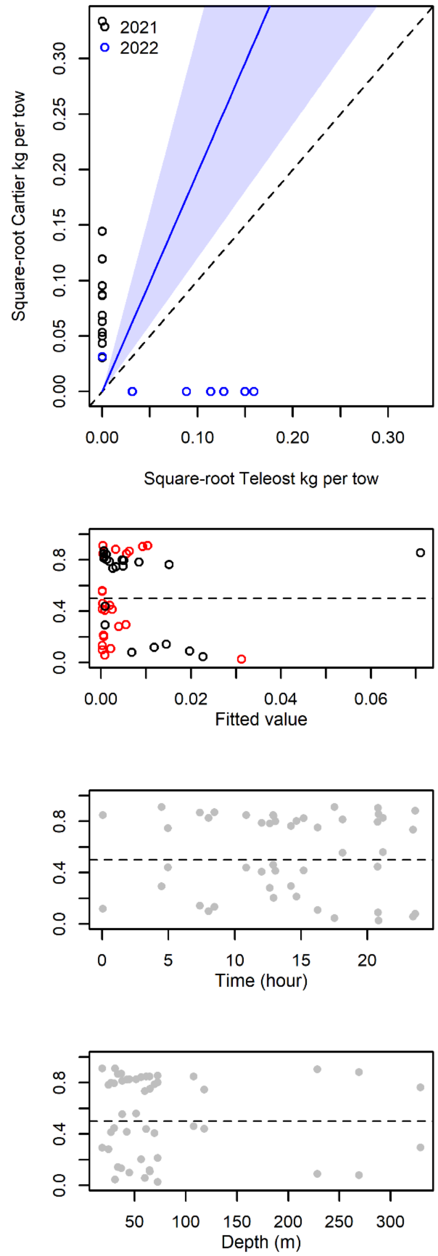

Figure 86. Visualisation of comparative fishing data, size-aggregated model predictions and residual plots for Henricia sp..

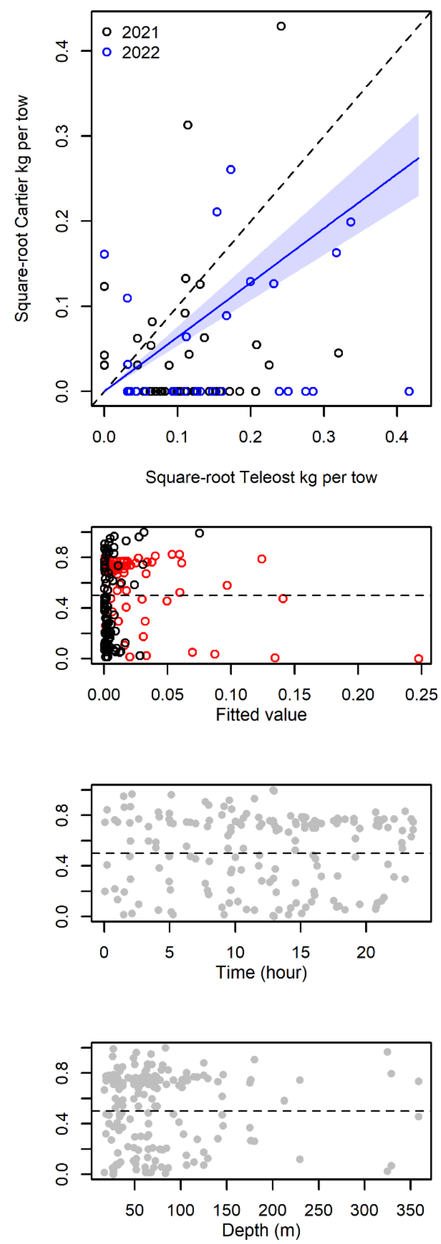

Figure 87. Visualisation of comparative fishing data, size-aggregated model predictions and residual plots for Henricia sanguinolenta*.*

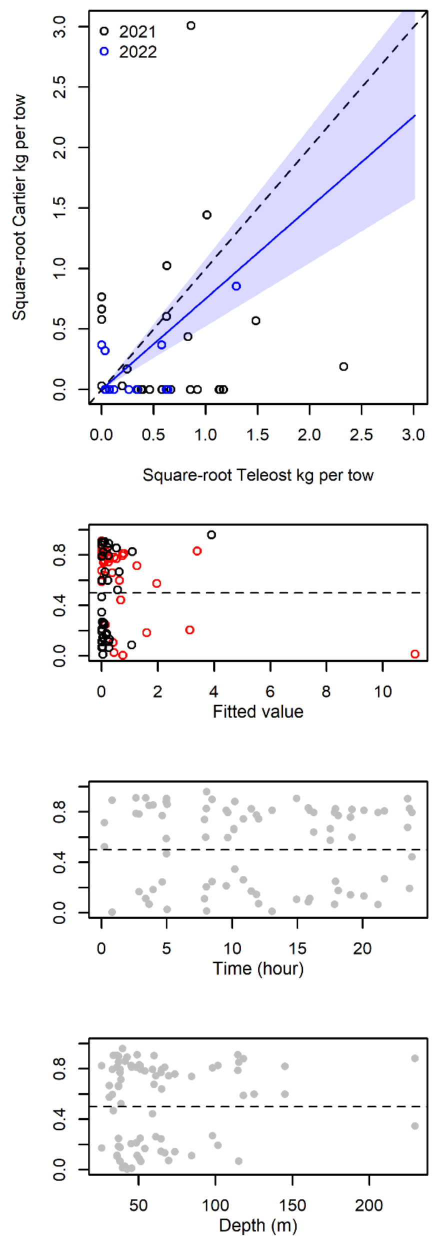

Figure 88. Visualisation of comparative fishing data, size-aggregated model predictions and residual plots for Solaster endeca*.*

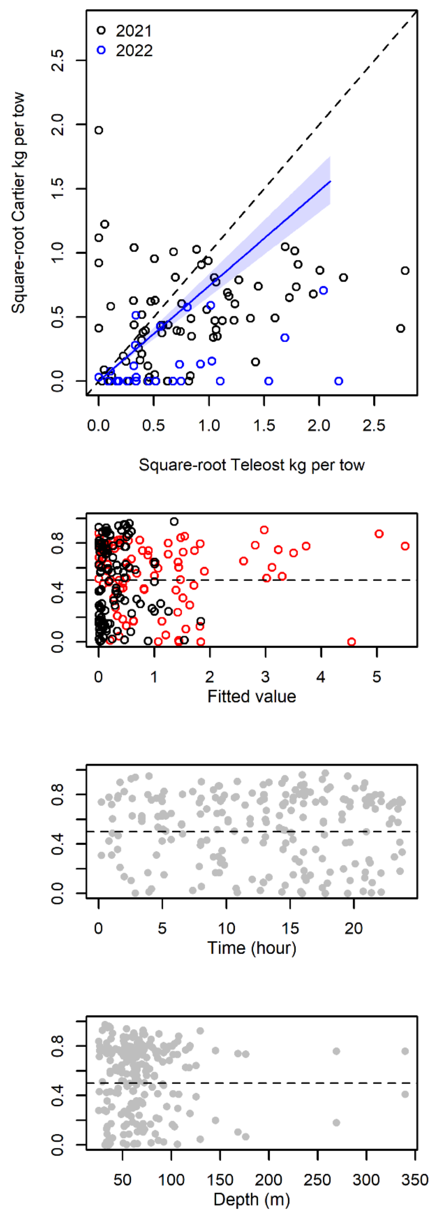

Figure 89. Visualisation of comparative fishing data, size-aggregated model predictions and residual plots for Crossaster papposus.

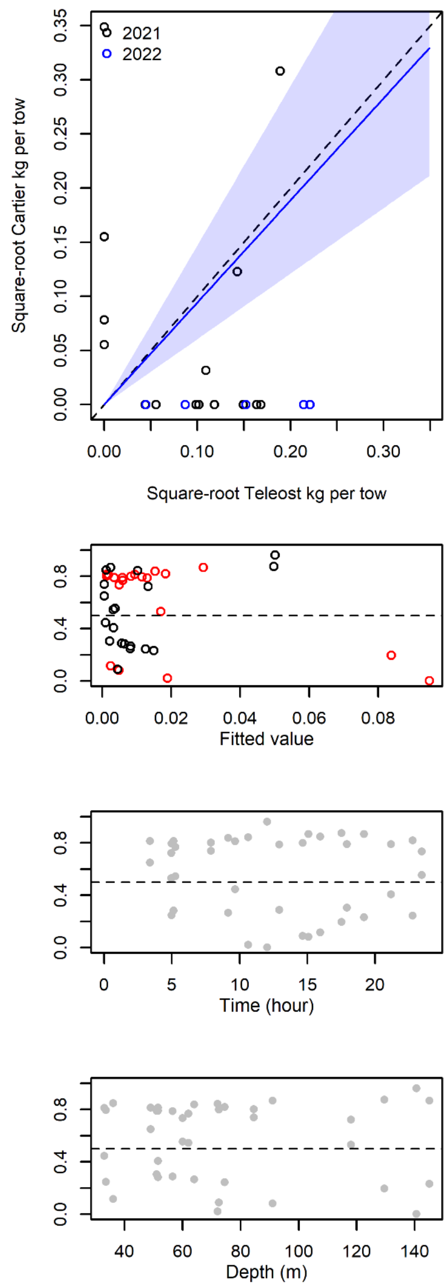

Figure 90. Visualisation of comparative fishing data, size-aggregated model predictions and residual plots for Pteraster militaris.

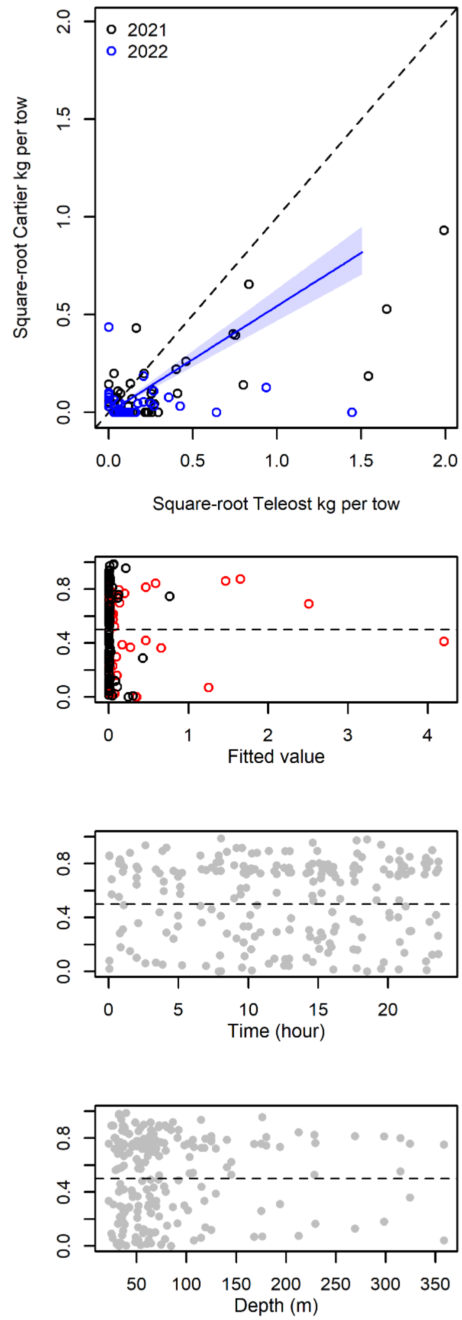

Figure 91. Visualisation of comparative fishing data, size-aggregated model predictions and residual plots for Ophiuroidea (c.).

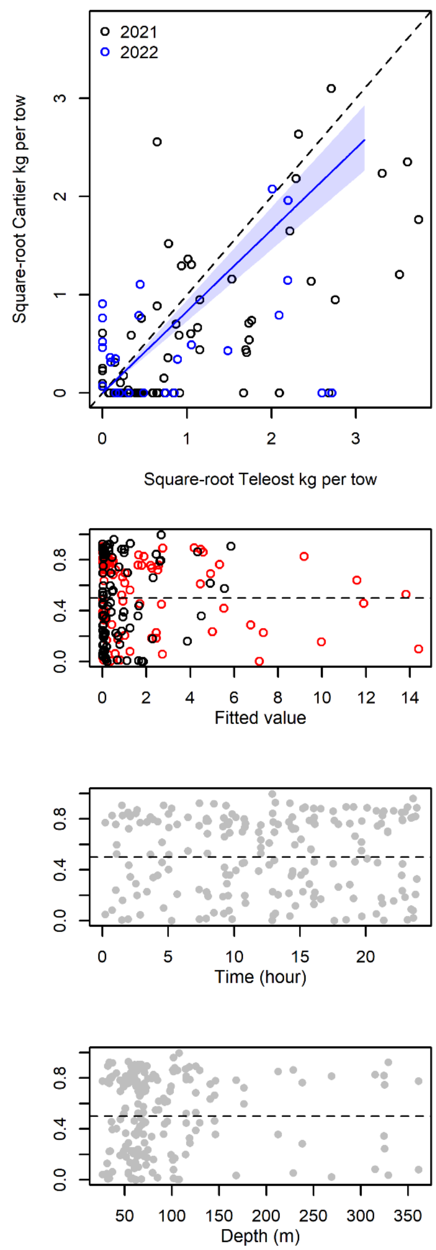

Figure 92. Visualisation of comparative fishing data, size-aggregated model predictions and residual plots for Euryalida (f.).

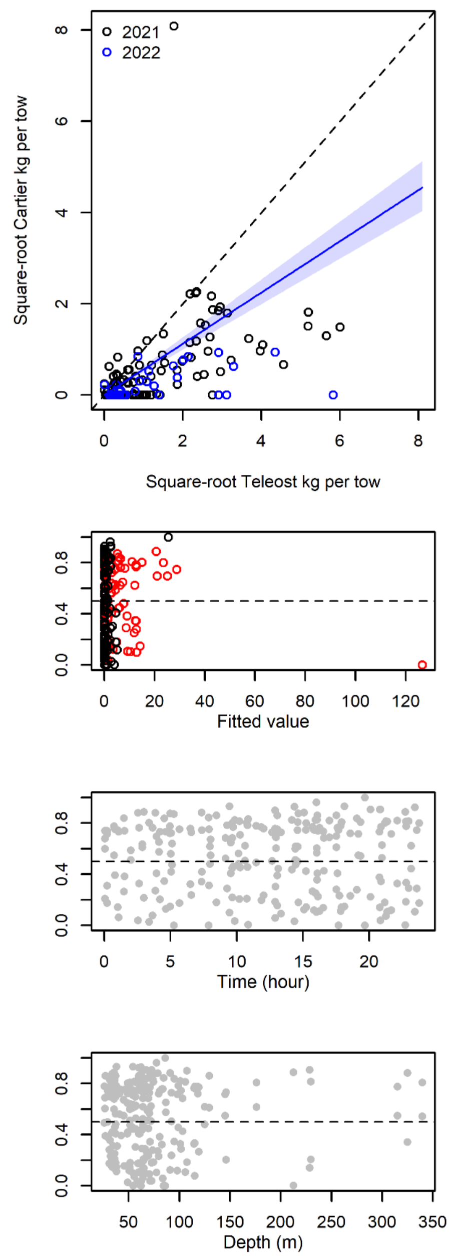

Figure 93. Visualisation of comparative fishing data, size-aggregated model predictions and residual plots for Strongylocentrotus sp..

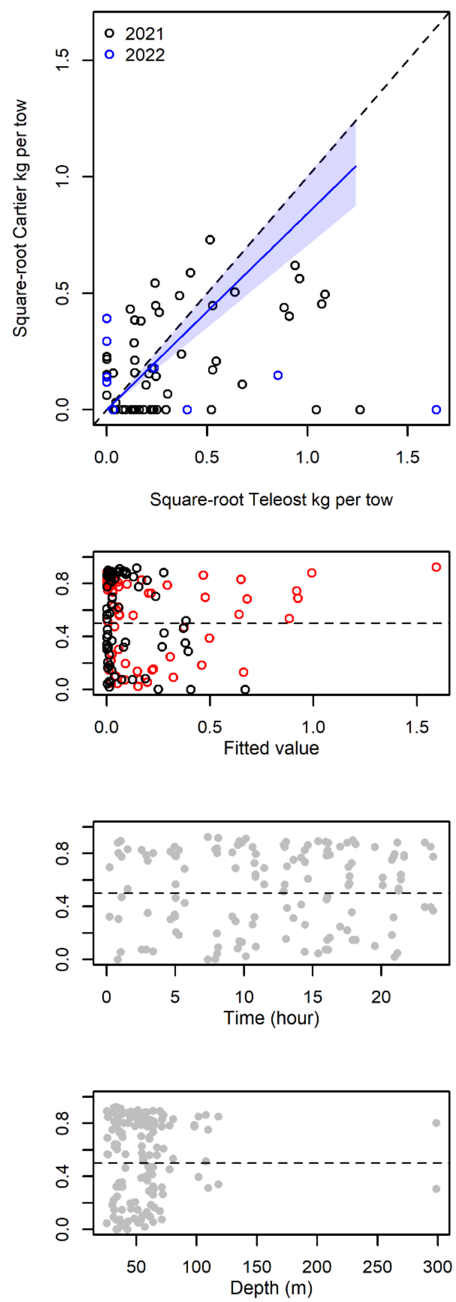

Figure 94. Visualisation of comparative fishing data, size-aggregated model predictions and residual plots for Clypeasteroida (o.).

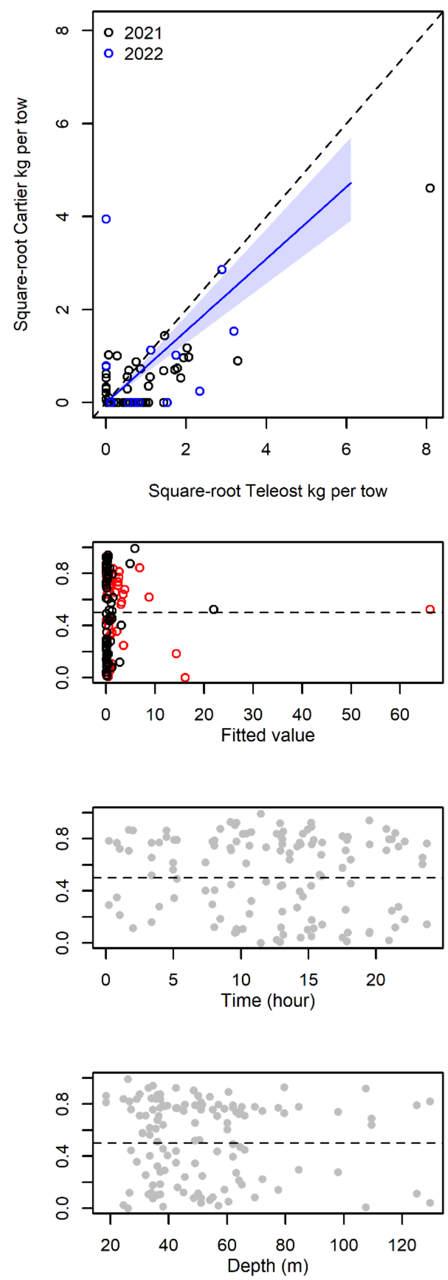

Figure 95. Visualisation of comparative fishing data, size-aggregated model predictions and residual plots for Holothuroidea (c.).

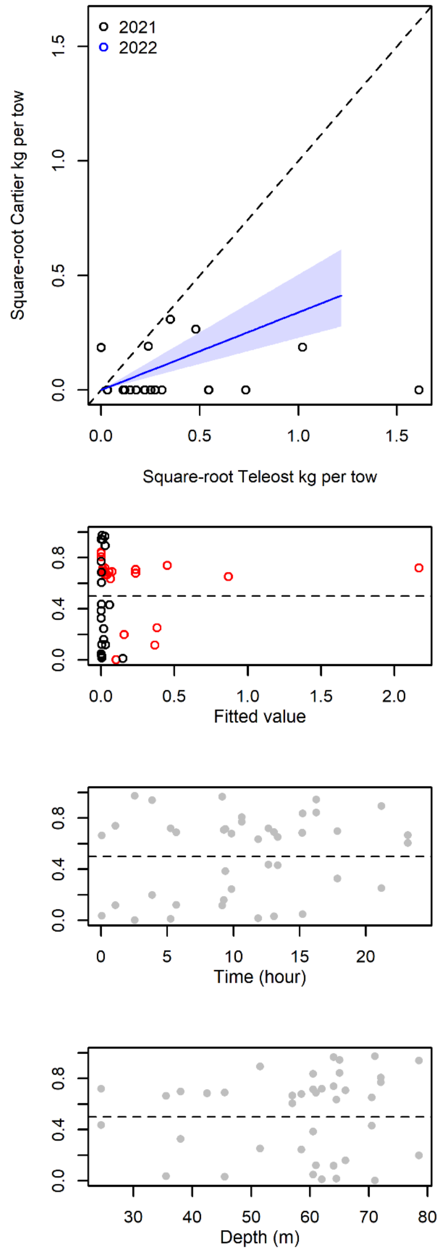

Figure 96. Visualisation of comparative fishing data, size-aggregated model predictions and residual plots for Psolus fabricii.

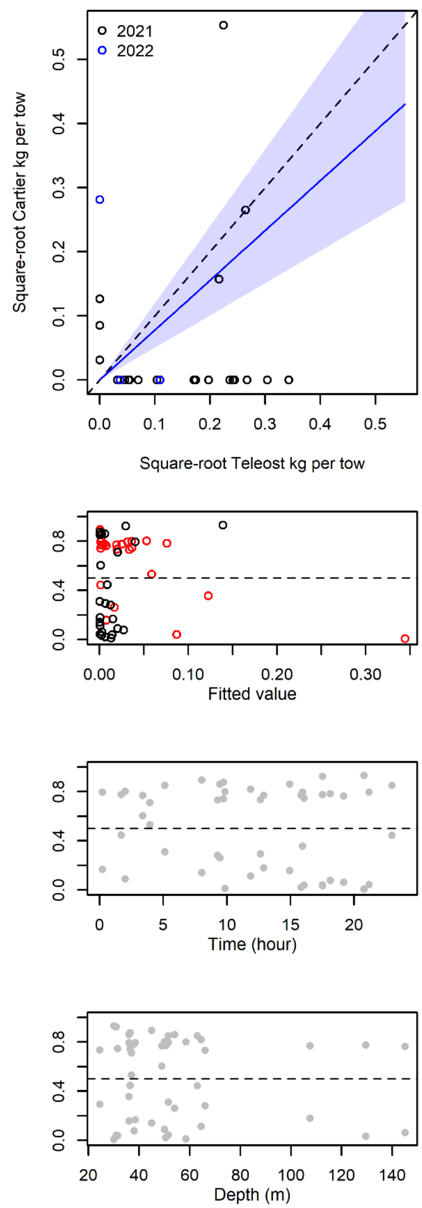

Figure 97. Visualisation of comparative fishing data, size-aggregated model predictions and residual plots for Psolus phantapus.

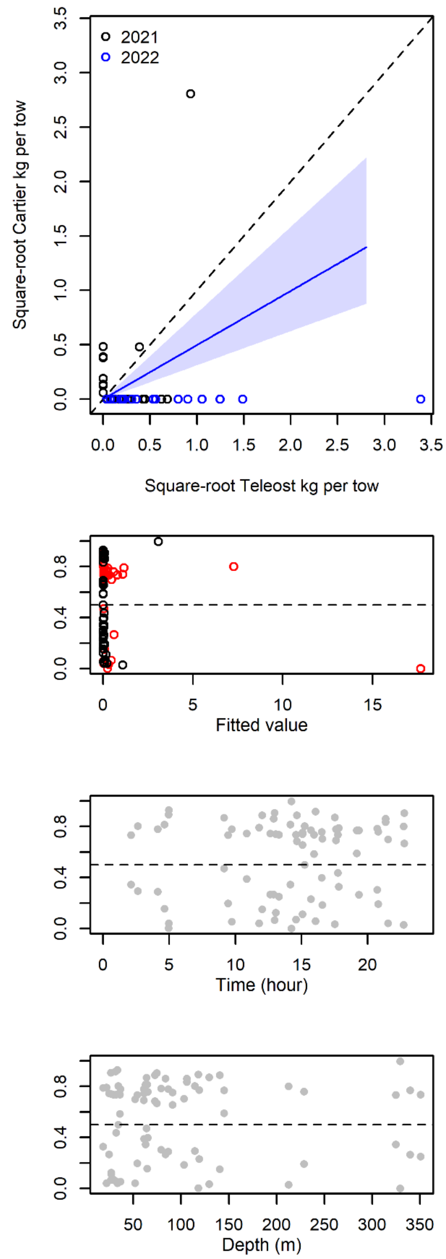

Figure 98. Visualisation of comparative fishing data, size-aggregated model predictions and residual plots for Actiniaria (o.).

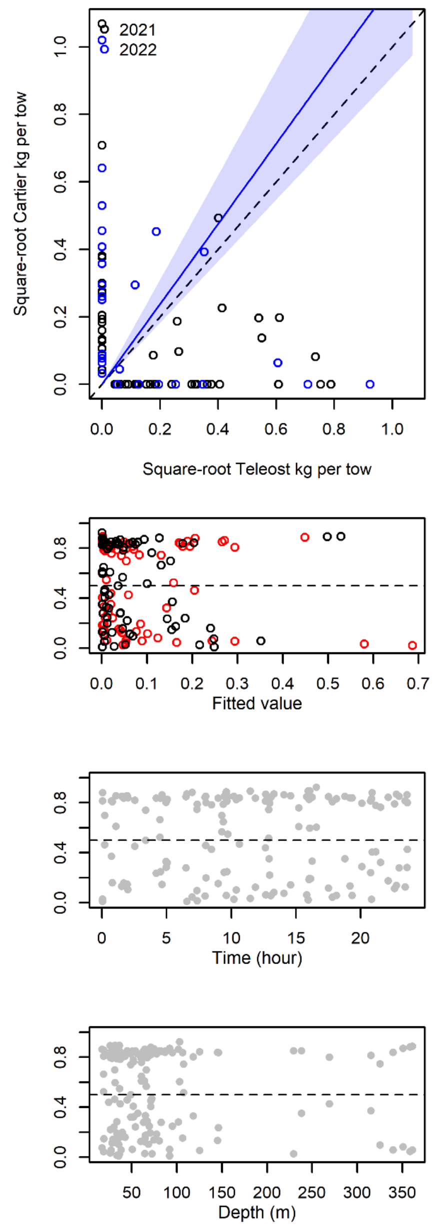

Figure 99. Visualisation of comparative fishing data, size-aggregated model predictions and residual plots for Anthozoa (c.).

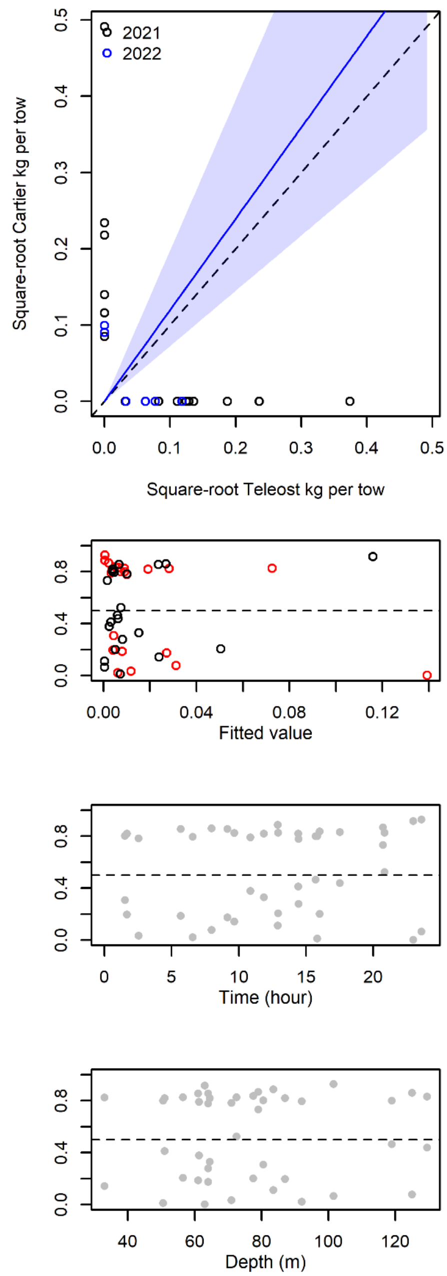

Figure 100. Visualisation of comparative fishing data, size-aggregated model predictions and residual plots for Stomphia coccinea.

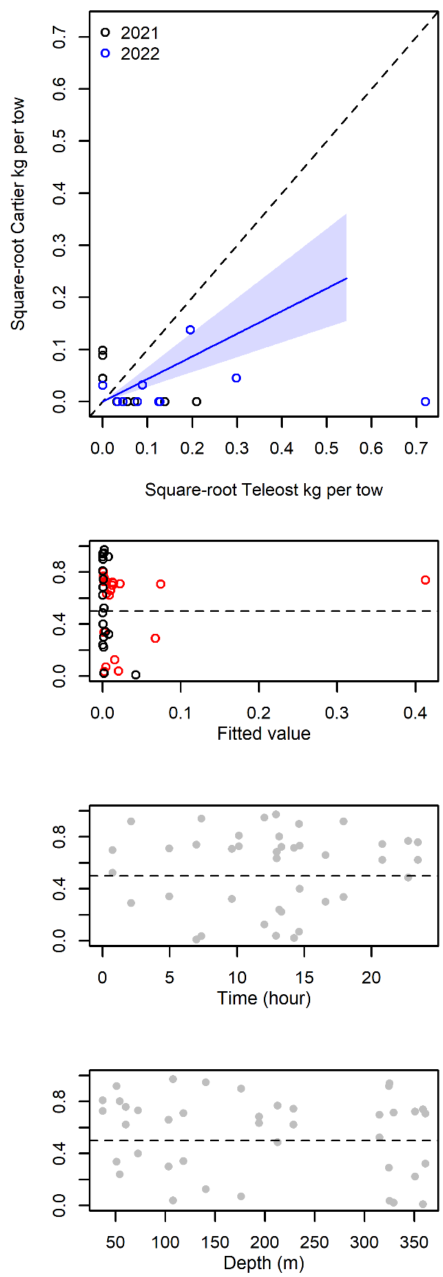

Figure 101. Visualisation of comparative fishing data, size-aggregated model predictions and residual plots for Pennatulacea sp..

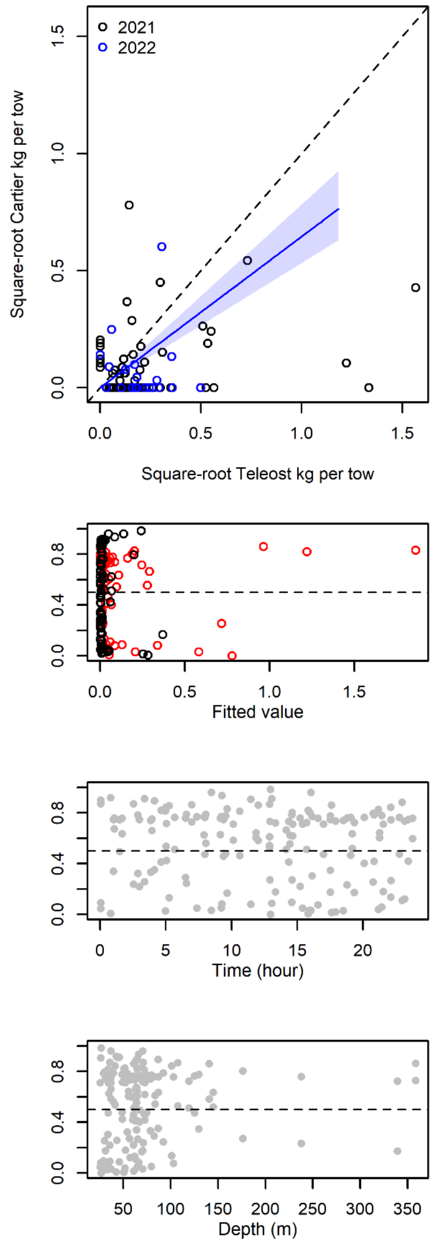

Figure 102. Visualisation of comparative fishing data, size-aggregated model predictions and residual plots for Gersemia rubiformis*.*

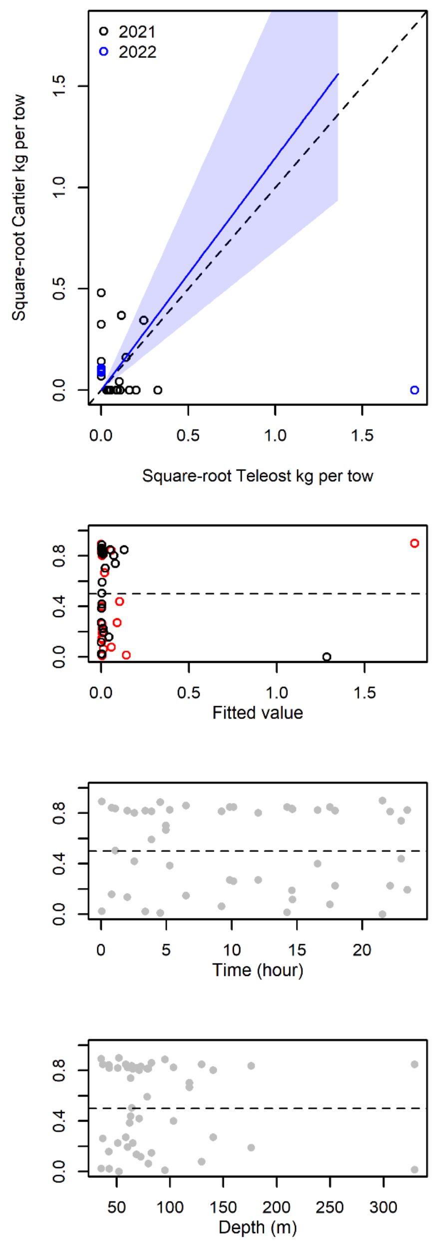

Figure 103. Visualisation of comparative fishing data, size-aggregated model predictions and residual plots for Soft coral unidentified.

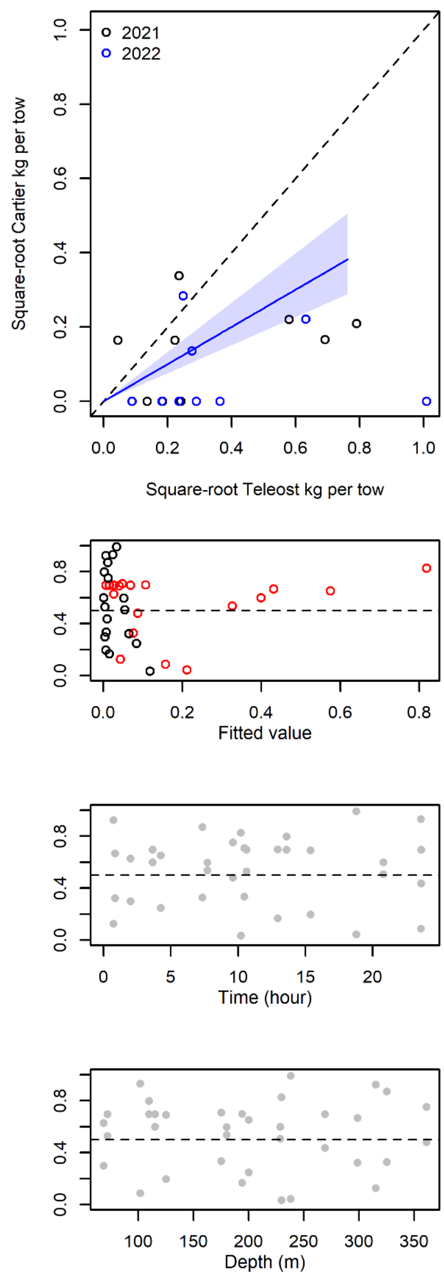

Figure 104. Visualisation of comparative fishing data, size-aggregated model predictions and residual plots for Pseudarchaster parelii*.*

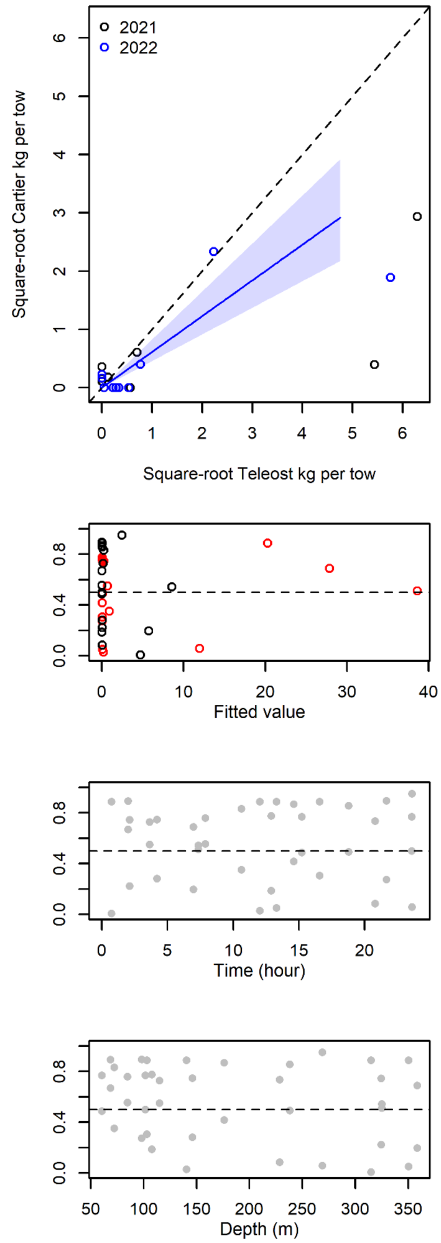

Figure 105. Visualisation of comparative fishing data, size-aggregated model predictions and residual plots for Ptilella grandis*.*

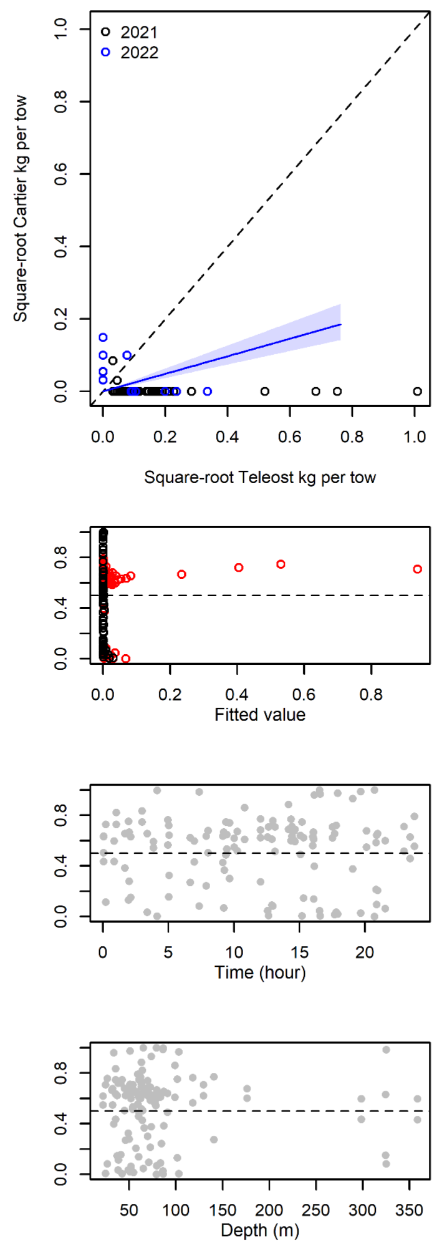

Figure 106. Visualisation of comparative fishing data, size-aggregated model predictions and residual plots for Hydrozoa (c.).

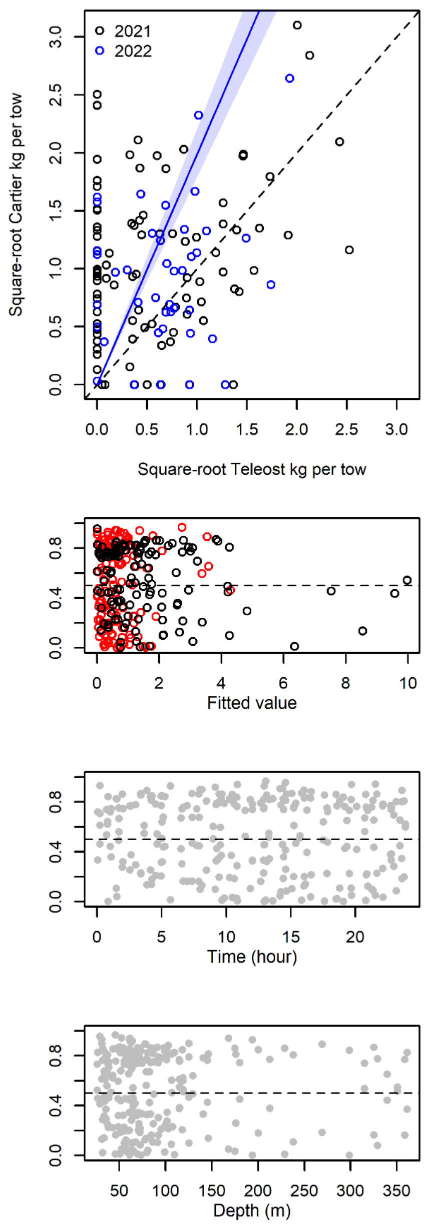

Figure 107. Visualisation of comparative fishing data, size-aggregated model predictions and residual plots for Scyphozoa (c.)*.*

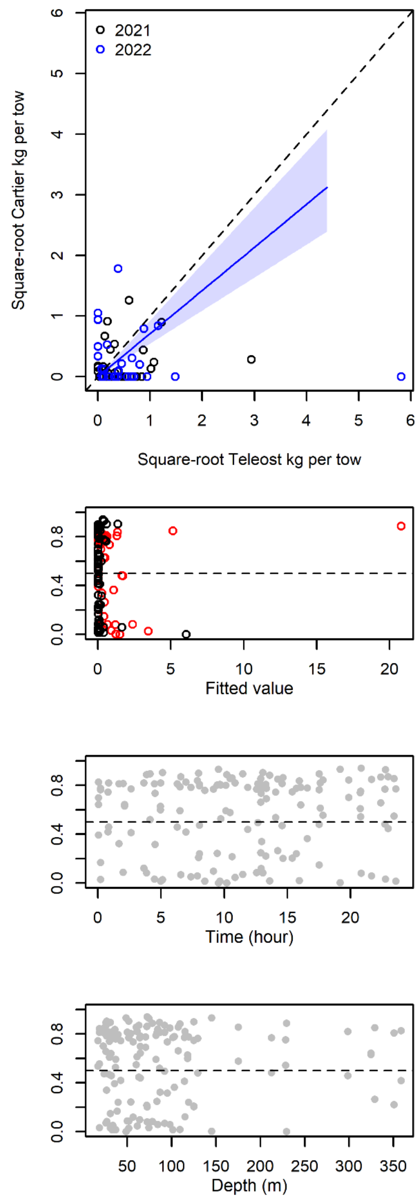

Figure 108. Visualisation of comparative fishing data, size-aggregated model predictions and residual plots for Porifera.

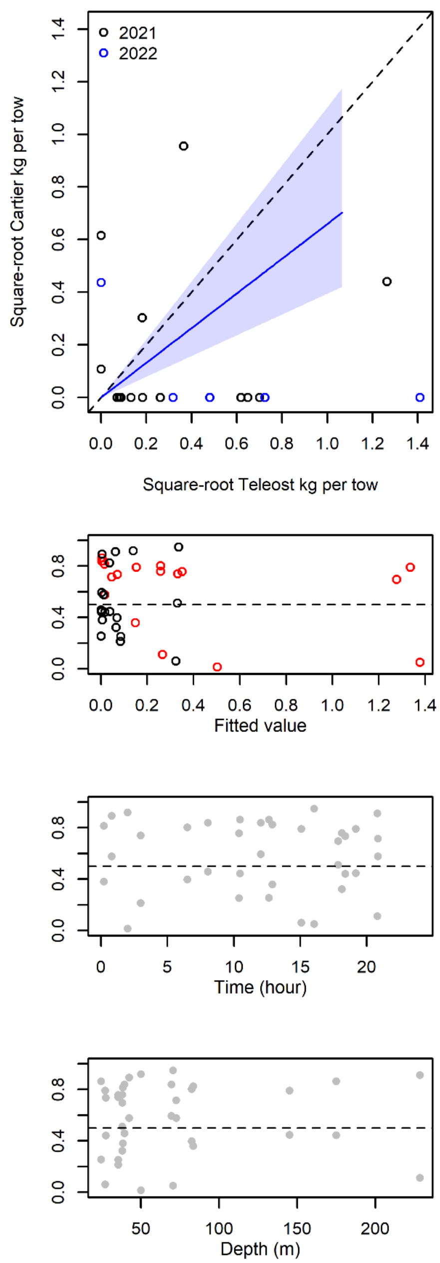

Figure 109. Visualisation of comparative fishing data, size-aggregated model predictions and residual plots for Suberites ficus.

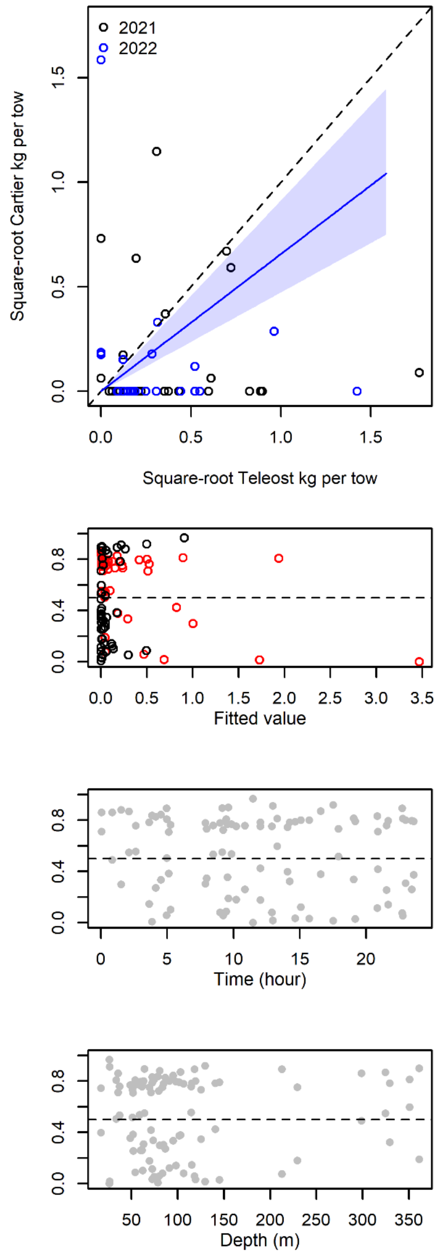

Figure 110. Visualisation of comparative fishing data, size-aggregated model predictions and residual plots for Mycale (Mycale) lingua*.*

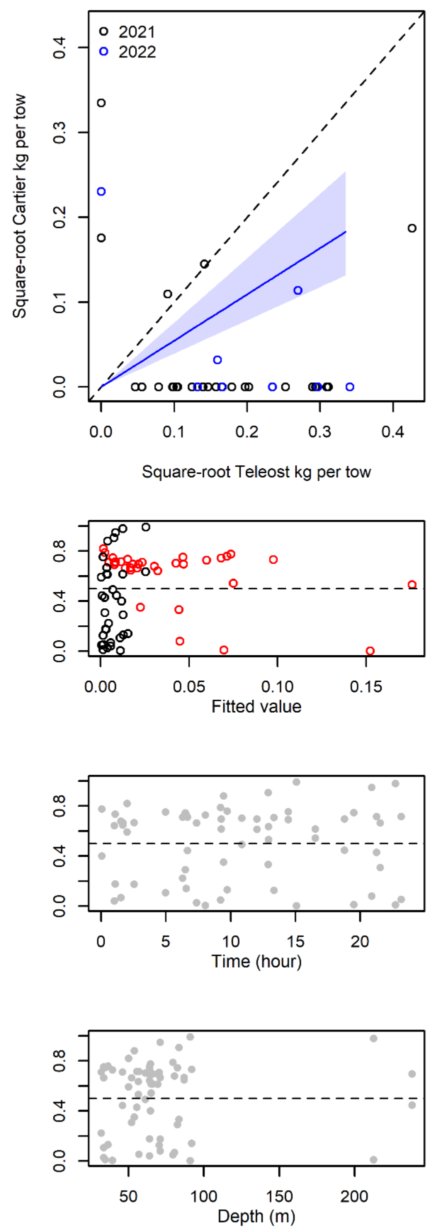

Figure 111. Visualisation of comparative fishing data, size-aggregated model predictions and residual plots for Cladocroce spatula*.*

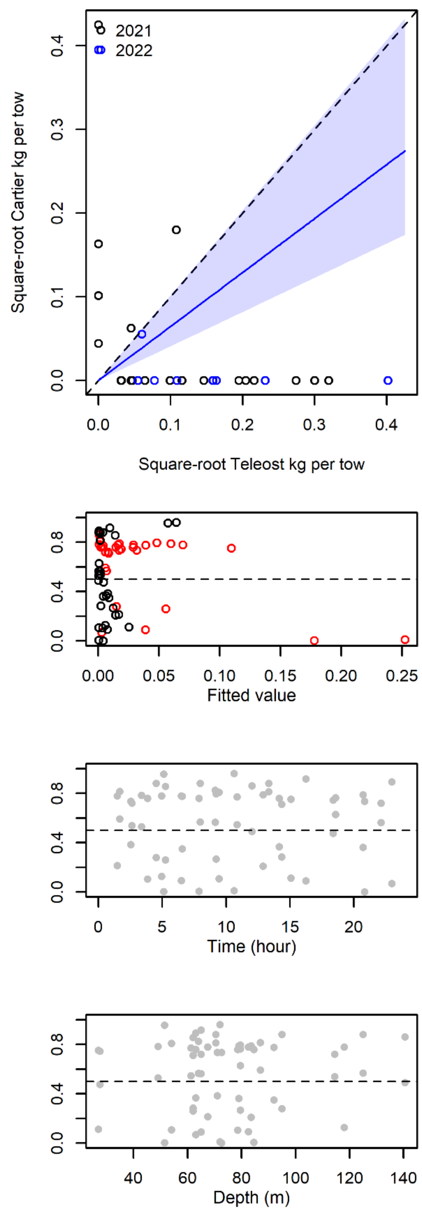

Figure 112. Visualisation of comparative fishing data, size-aggregated model predictions and residual plots for Semisuberites cribrosa*.*